

**IN-HOUSE PREPARED ^{99m}Tc -ETHYLENEDICYSSTEINE-
DEOXYGLUCOSE IN MICE, RABBITS AND BABOONS: TUMOUR,
LOCAL INFECTION/INFLAMMATION AND NORMAL
BIODISTRIBUTION**

by

J HORN-LODEWYK

submitted in fulfilment of the requirements for the degree

Philosophiae Doctor in Clinical Nuclear Medicine

(Ph.D. Clinical Nuclear Medicine)

in the

DEPARTMENT OF NUCLEAR MEDICINE

FACULTY OF HEALTH SCIENCES

UNIVERSITY OF THE FREE STATE

BLOEMFONTEIN

FEBRUARY 2015

STUDY LEADER: PROF. A.C. OTTO

CO-STUDY LEADER: PROF. J.R. ZEEVAART

DECLARATION

I hereby declare that the dissertation submitted by me is the result of my own independent research. Where help was sought, it was acknowledged. I further declare that this work is submitted for the first time at this university/faculty towards a Philosophiae Doctor degree in Radiographic Sciences and that it has never been submitted to any other university/faculty for the purpose of obtaining a degree.

.....
J Horn-Lodewyk

.....
2015-02-13

I hereby cede copyright of this product in favour of the University of the Free State.

.....
J. Horn-Lodewyk

.....
2015-02-13

I hereby cede copyright of this product in favour of the University of the Free State.

DEDICATION

To the memory of my father that was a great man and taught me never to give up.

To my mother whose love has no limits and has supported me every second of every day throughout my life.

To my husband, Reniël, for your unconditional love and support.

To my daughter, Nikita, your smile is as bright as the sun, may you always shine and never lose your loving spirit.

To my son, Reniël jnr., you are a blessing every day and whose constant love motivated me to complete this enormous task.

To Judith, that unknowingly inspires me every day to be a better mother and researcher.

ACKNOWLEDGEMENTS

I wish to express my sincere thanks and appreciation to the following:

- My promoter, Prof. A.C. Otto, previous Clinical Specialist of the Department of Nuclear Medicine, Faculty of Health Sciences, University of the Free State, for his incredible support, expert supervision and patience. I thank him for the time he took to share his extensive knowledge in the field of Nuclear Medicine with me and for his endless support for the research with the IHP ^{99m}Tc -EC-DG.
- My co-promoter, Prof. J.R. Zeevaart, I wish to express my sincerest gratitude who invited me to work in the field of pre-clinical radiopharmaceutical development. I gratefully acknowledge him for giving me the opportunity to complete this research and for his understanding towards my balancing act between work and home over the past five years.
- My co-researcher and official reviewer, Mrs J. Wagener I would like to thank for sharing her extensive knowledge in radiopharmaceutical chemistry and pre-clinical laboratory work performed on optimising the labelling methods for the IHP ^{99m}Tc -EC-DG. I would also like thank you for your valuable comments and language editing that also improved the quality of this dissertation, you are my "Friend in research forever".
- My co-researcher, Dr. M. Janse van Vuuren for her valuable help with data acquiring and analysis. Your endless support will never be forgotten.
- Biostatisticians, Prof. G. Joubert and Mr. F.C. Van Rooyen, Department of Biostatistics, Faculty of Healthy Sciences, University of the Free State, for their advice and management of the data analysis and other biostatistical aspects with insight and patience.
- The UFS Animal Research Center and their excellent pre-clinical research team. I would also in particular, like to thank Mr S. Lamprecht in particular for sharing his extensive knowledge and expertise on animal models for pre-clinical radiopharmaceutical development.

- Mrs B. van der Merwe is acknowledged for improving the language of this dissertation. Your friendship and never-ending support to me to complete this research will never be forgotten.
- My colleagues at the Department of Nuclear Medicine at Universitas Academic Hospital, Dr M.G. Nel and Dr G.H.J. Engelbrecht for their support and clinical diagnostic inputs.
- I wish to express my warmest thanks in particular to Mrs E. Wagenaar, Mrs M. Fikizolo and Mrs E. Ninham-Wunderatsch at the Department of Nuclear Medicine at Universitas Academic Hospital for their encouraging working environment during these years
- **I praise my Heavenly Father for giving me the strength to finish this research, you gave me wings when I could no longer walk.**

TABLE OF CONTENTS

CHAPTER 1: RESEARCH BACKGROUND

	<i>page</i>
1.1 INTRODUCTION	1
1.2 BACKGROUND	2
1.3 PRE-CLINICAL USE OF RADIOPHARMACEUTICALS	4
1.4 RADIOPHARMACEUTICALS USED IN THIS RESEARCH	4
1.4.1 ^{99m} Tc-EC-DG	5
1.4.1.1 ^{99m} Tc-EC-DG molecular formula and cellular uptake	5
1.4.1.2 Uptake mechanism of ^{99m} Tc-EC-DG in tumour cells	5
1.5 NUCLEAR MEDICINE MOLECULAR IMAGING MODALITIES	8
1.5.1 PET versus SPECT	8
1.6 ANIMAL MODELS USED IN THIS RESEARCH	8
1.7 PROBLEM STATEMENT	9
1.8 AIM	10
1.9 OBJECTIVES	10
1.10 SCOPE OF THE RESEARCH	11
1.11 SCIENTIFIC CONTRIBUTION OF THE RESEARCH	11
1.12 SIGNIFICANCE OF THE RESEARCH	12
1.13 PRE-CLINICAL ETHICAL CONSIDERATIONS OF RESEARCH	
PHASE ONE TO THREE	13
1.14 OUTLINE OF THE DISSERTATION	13

CHAPTER 2: LITERATURE REVIEW

2.1 INTRODUCTION	15
2.2 PHYSIOLOGY	15
2.2.1 Glycolysis	16
2.2.2 Glucose transporters	21
2.3 PATHOLOGY	22
2.3.1 Cancer	22
2.3.1.1 Tumours	23

	2.3.1.2 <i>Imaging</i>	23
2.3.2	Inflammation	24
2.3.3	Infection	24
	2.3.3.1 <i>Imaging</i>	28
2.4	PRE-CLINICAL RESEARCH	31
2.4.1	Animal research ethics	33
2.4.2	Athymic nude mice model	34
2.4.3	The rabbit model	35
	2.4.3.1 <i>IFI/IF rabbit model</i>	36
2.4.4	The baboon model	37
2.4.5	Interspecies differences	38
2.4.6	Animal biodistribution studies	38
2.4.7	Factors influencing animal biodistribution studies	41
2.5	RADIONUCLIDES AND RADIOPHARMACEUTICALS	41
2.5.1	Radiopharmacy	42
	2.5.1.1 <i>Methods of labelling</i>	42
	2.5.1.2 <i>Radiopharmaceutical quality control</i>	43
2.5.2	^{99m} Tc	44
	2.5.2.1 <i>Properties and production</i>	44
	2.5.2.2 <i>Uptake mechanism and clearance</i>	46
	2.5.2.3 <i>Imaging</i>	46
2.5.3	⁶⁷ Ga-citrate	46
	2.5.3.1 <i>Properties and production</i>	46
	2.5.3.2 <i>Uptake mechanism and clearance</i>	47
2.5.4	¹⁸ F-FDG	48
	2.5.4.1 <i>Properties and production</i>	48
	2.5.4.2 <i>Uptake mechanism and diagnostic imaging</i>	49
2.5.5	^{99m} Tc-EC-DG	51
	2.5.5.1 <i>Imaging and Properties</i>	51
	2.5.5.2 <i>^{99m}Tc-EC-DG radiation dosimetry and safety</i>	56
2.5.6	¹⁸ F-FDG versus ^{99m} Tc-EC-DG	57
	2.5.6.1 <i>Glycolysis targeting of glucose</i>	57
	2.5.6.2 <i>Uptake similarities and differences</i>	57
2.6	MOLECULAR IMAGING	61
2.6.1	PET/CT	64

2.6.1.1	<i>Principles</i>	64
2.6.1.2	<i>Positron-emitting radionuclides</i>	64
2.6.1.3	<i>Applications</i>	65
2.6.1.4	<i>¹⁸F-FDG - PET/CT gold standard</i>	66
2.6.2	SPECT/CT	66
2.6.2.1	<i>Principles</i>	66
2.6.2.2	<i>Single photon radionuclides</i>	67
2.6.2.3	<i>Applications</i>	67
2.6.3	Small-animal imaging systems	68
2.6.3.1	<i>Principles</i>	68
2.6.3.2	<i>Applications</i>	68
2.7	CONCLUSION	68

CHAPTER 3: METHODOLOGY

3.1	INTRODUCTION	70
3.2	MATERIALS, METHODS, RESULTS AND CONCLUSION OF PILOT STUDY	70
3.2.1	Introduction	70
3.2.2	Materials and methods	72
3.2.2.1	<i>Sample size</i>	72
3.2.2.2	<i>Animal handling and monitoring</i>	72
3.2.2.3	<i>Radiosynthesis of ^{99m}Tc-EC-DG (DL)</i>	73
3.2.2.4	<i>Gamma scintigraphy studies</i>	73
3.2.2.4.1	<i>Induced IFI/IF biodistribution</i>	73
3.2.3	Data analysis	74
3.2.3.1	<i>Quantitative analysis of the image of IFI/IF induced rabbits</i>	74
3.2.4	Results and discussion	75
3.2.4.1	<i>Radiosynthesis of ^{99m}Tc-EC-DG (DL)</i>	75
3.2.4.2	<i>In vivo biodistribution images</i>	75
3.2.4.3	<i>Quantitative analysis</i>	76
3.2.5	Conclusions and recommendations from pilot study	76

3.3	ETHICS, MATERIALS AND METHODS OF THE THREE PHASES RESEARCH	77
3.3.1	Ethics approvals	77
3.3.2	Materials and methods of the research	78
3.3.3	Animal models used in this research	80
	<i>3.3.3.1 Healthy and lung tumour-bearing nude mice model</i>	80
	<i>3.3.3.2 Healthy rabbit model</i>	80
	<i>3.3.3.3 IFI/IF rabbit model</i>	80
	<i>3.3.3.4 Healthy baboon model</i>	82
3.3.4	Animal handling and monitoring	83
	<i>3.3.4.1 Mice Model</i>	83
	<i>3.3.4.2 Rabbit Model</i>	84
	<i>3.3.4.3 Baboon Model</i>	85
3.3.5	IHP ^{99m}Tc-EC-DG	85
	<i>3.3.5.1 Physical appearance and chemical properties</i>	85
	<i>3.3.5.2 Handling and storage of EC-DG</i>	86
	<i>3.3.5.3 Labelling technique of IHP ^{99m}Tc-EC-DG (DL)</i>	86
	<i>3.3.5.4 Labelling technique of IHP ^{99m}Tc-EC-DG (KF)</i>	86
	<i>3.3.5.5 Physicochemical QC tests</i>	87
	<i>3.3.5.5.1 Determination of pH</i>	87
	<i>3.3.5.5.2 Determination of radiochemical purity</i>	87
3.3.6	Gamma scintigraphy	88
3.3.7	Instrumental calibration QC	88
3.4	RADIATION AND HEALTH SAFETY	88
3.4.1	External radiation dose to rabbits and baboons from CT of SPECT/CT	90
3.5	DATA ANALYSIS IN GENERAL	90
3.6	CONCLUSION	91

CHAPTER 4: RESEARCH PHASE ONE: THE MICE MODEL

4.1	INTRODUCTION	92
4.2	MATERIALS AND METHODS	94
4.2.1	Sample size	94

4.2.2	Radiosynthesis of ^{99m}Tc -EC-DG (DL)	96
4.2.3	Tissue distribution studies	96
4.2.4	Data analysis	97
4.3	RESULTS AND DISCUSSION	98
4.3.1	Healthy Mice Model	98
	4.3.1.1 Radiosynthesis of ^{99m}Tc -EC-DG (KF) and ^{99m}Tc -EC-DG (DL)	98
	4.3.1.2 <i>In vivo</i> normal tissue biodistribution IHP ^{99m}Tc -EC-DG (DL)	101
	4.3.1.3 Quantitative analysis of IHP ^{99m}Tc -EC-DG (DL)	101
4.3.2	Tumour Mice Model	105
	4.3.2.1 <i>In vivo</i> tumour tissue biodistribution IHP ^{99m}Tc -EC-DG (DL)	105
	4.3.2.2 Quantitative analysis of IHP ^{99m}Tc -EC-DG (DL)	105
	4.3.2.3 Comparison of IHP ^{99m}Tc -EC-DG (DL) in healthy and tumour-bearing mice	109
	4.3.2.4 Comparison of IHP ^{99m}Tc -EC-DG (DL) with ^{18}F -FDG in tumour-bearing mice	110
	4.3.2.5 Comparison of the biodistribution results of the IHP ^{99m}Tc -EC-DG (DL) with ^{18}F -FDG in lung tumour-bearing mice with literature results	116
4.4	CONCLUSION	119

CHAPTER 5: RESEARCH PHASE TWO: THE RABBIT MODEL

5.1	INTRODUCTION	121
5.2	MATERIALS AND METHODS	123
5.2.1	Sample size	123
5.2.2	Radiosynthesis of ^{99m}Tc -EC-DG (DL) and -(KF)	123
5.2.3	Gamma camera scintigraphy studies	124
	5.2.3.1 Normal biodistribution	124
	5.2.3.2 Induced IFI/IF biodistribution	126
5.2.4	Data analysis	126
	5.2.4.1 Quantitative analysis of images of healthy rabbits	126

5.2.4.2	<i>Quantitative analysis of images of septic and sterile IFI/IF rabbits</i>	128
5.2.4.3	<i>SQ and SQUAL analysis</i>	129
5.3	RESULTS AND DISCUSSION	130
5.3.1	Healthy Rabbit Model	130
5.3.1.1	<i>Radiosynthesis of ^{99m}Tc-EC-DG (DL)</i>	130
5.3.1.2	<i>In vivo normal biodistribution images</i>	131
5.3.1.3	<i>SQ and SQUAL analysis</i>	134
5.3.2	Healthy Rabbit Model	137
5.3.2.1	<i>Quantitative analysis of IHP ^{99m}Tc-EC-DG (DL) images</i>	137
5.3.2.2	<i>Comparison of IHP ^{99m}Tc-EC-DG (DL) with $^{99m}\text{TcO}_4^-$</i>	143
5.3.2.2.1	<i>In vivo normal biodistribution images</i>	143
5.3.2.2.2	<i>SQ and SQUAL analysis</i>	147
5.3.2.2.3	<i>Comparison of the quantitative analysis</i>	151
5.3.3	Septic IFI/IF rabbit model	159
5.3.3.1	<i>Radiosynthesis of IHP ^{99m}Tc-EC-DG (DL)</i>	159
5.3.3.2	<i>In vivo biodistribution images</i>	159
5.3.3.3	<i>SQ and SQUAL analysis</i>	162
5.3.3.4	<i>Quantitative analysis</i>	164
5.3.4	Sterile IFI/IF rabbit model	166
5.3.4.1	<i>Radiosynthesis of IHP ^{99m}Tc-EC-DG (KF)</i>	167
5.3.4.2	<i>In vivo biodistribution images</i>	167
5.3.4.3	<i>SQ and SQUAL analysis</i>	169
5.3.4.4	<i>Quantitative analysis of images of sterile IFI/IF in rabbits</i>	170
5.4	KEY FINDINGS - HEALTHY AND IFI/IF RABBIT MODELS	173
5.4.1	Healthy rabbit model	173
5.4.2	IFI/IF rabbit models	173
5.5	SIDE-EFFECTS OF IHP ^{99m}Tc-EC-DG IN HEALTHY AND IFI/IF INDUCED RABBITS	175
5.6	DISCUSSION	175
5.7	CONCLUSION	176

CHAPTER 6: RESEARCH PHASE THREE: THE BABOON MODEL

6.1	INTRODUCTION	177
6.2	MATERIALS AND METHODS	178
6.2.1	Sample size	178
6.2.2	Radiosynthesis of ^{99m}Tc -EC-DG (DL) and - (KF)	179
6.2.3	Gamma scintigraphy studies	179
	6.2.3.1 <i>Normal biodistribution</i>	179
6.2.4	Data analysis	181
	6.2.4.1 <i>Quantitative analysis of the image of healthy baboons</i>	181
	6.2.4.2 <i>SQ and SQUAL analysis</i>	181
6.3	RESULTS AND DISCUSSION	182
6.3.1	Healthy Baboon Model	182
	6.3.1.1 <i>Radiosynthesis of ^{99m}Tc-EC-DG (KF) and ^{99m}Tc-EC-DG (DL)</i>	182
	6.3.1.2 <i>In vivo normal biodistribution images</i>	182
	6.3.1.3 <i>SQ and SQUAL analysis</i>	189
	6.3.1.4 <i>Quantitative analysis of IHP ^{99m}Tc-EC-DG (KF) images</i>	191
	6.3.1.5 <i>Comparison of IHP ^{99m}Tc-EC-DG (KF) with $^{99m}\text{TcO}_4^-$</i>	194
	6.3.1.5.1 <i>In vivo normal biodistribution images</i>	195
	6.3.1.5.2 <i>SQ and SQUAL analysis</i>	202
	6.3.1.5.3 <i>Comparison of the quantitative analysis</i>	203
	6.3.1.6 <i>Comparison of IHP ^{99m}Tc-EC-DG (KF) with IHP ^{99m}Tc-EC-DG (DL)</i>	208
	6.3.1.6.1 <i>In vivo normal biodistribution images</i>	208
	6.3.1.6.2 <i>SQ and SQUAL analysis</i>	216
	6.3.1.6.3 <i>Comparison of the quantitative analysis</i>	218
6.4	KEY FINDINGS - HEALTHY BABOON MODELS	225
6.5	SIDE-EFFECTS OF IHP ^{99m}Tc -EC-DG IN HEALTHY BABOONS	225
6.6	INTERSPECIES DIFFERENCES BETWEEN HEALTHY BABOONS AND RABBITS	226
6.7	CONCLUSION	226

CHAPTER 7: CONCLUSIONS AND RECOMMENDATIONS

7.1	INTRODUCTION	228
7.2	OVERVIEW OF THE STUDY	228
7.2.1	Research problem	228
7.2.2	Methods of investigation	229
7.2.3	Results and findings	229
	7.2.3.1 <i>Normal biodistribution</i>	229
	7.2.3.1.1 <i>Excretion routes</i>	229
	7.2.3.1.2 <i>Organ biodistribution</i>	230
	7.2.3.1.3 <i>Interspecies differences</i>	230
	7.2.3.2 <i>Tumour biodistribution</i>	231
	7.2.3.3 <i>IFI/IF biodistribution</i>	232
	7.2.3.4 <i>Synthesis</i>	232
	7.2.3.5 <i>Safety</i>	233
7.3	RECOMMENDATIONS FROM THIS RESEARCH	233
7.4	CONTRIBUTION AND SIGNIFICANCE OF THE RESEARCH	234
7.4.1	Advantages of IHP ^{99m}Tc-EC-DG	234
7.5	FUTURE RESEARCH	235
7.6	CONCLUSIONS	237
7.7	CONCLUSIVE REMARK	237

REFERENCES

239

APPENDIXES

APPENDIX A: Ionising Radiation Control Commission Committee approval letter

APPENDIX B: Universitas Academic Hospital approval letter

APPENDIX C: North-West University approval letter

APPENDIX D: University of the Free State Ethics Committee approval letter

APPENDIX E: Animal welfare score sheet - rabbits

APPENDIX F: Animal welfare score sheet - baboons

LIST OF FIGURES

	Page
CHAPTER 1:	
FIGURE 1.1	The characteristics of an ideal tumour or IFI/IF radiopharmaceutical
	2
FIGURE 1.2	The chemical structure of IHP ^{99m}Tc-EC-DG
	5
FIGURE 1.3	The unique mechanism of EC-DG to internalise the cell
	7
CHAPTER 2:	
FIGURE 2.1	A diagrammatic overview of the key literature review concepts
	15
FIGURE 2.2	Representation of the different enzymatic processes of glycolysis
	17
FIGURE 2.3	Step 1 of glycolysis
	18
FIGURE 2.4	Step 2 of glycolysis
	18
FIGURE 2.5	Step 3 of glycolysis
	18
FIGURE 2.6	Step 4 of glycolysis
	19
FIGURE 2.7	Step 5 of glycolysis
	19
FIGURE 2.8	Step 6 of glycolysis
	19
FIGURE 2.9	Step 7 of glycolysis
	20
FIGURE 2.10	Step 8 of glycolysis
	20
FIGURE 2.11	Step 9 of glycolysis
	20
FIGURE 2.12	Step 10 of glycolysis
	21
FIGURE 2.13	Illustration of an immune reaction to a bacterial infection
	25
FIGURE 2.14	The trend from 1997-2007 indicating the leading categories for the cause of death in RSA
	27
FIGURE 2.15	Molecular imaging research chain
	32
FIGURE 2.16	CT topogram demonstration of the anatomy of the rabbit
	36
FIGURE 2.17	Mathematical representation of a number of mathematical rays passing through an imaging subject
	39

FIGURE 2.18	^{18}F-FDG uptake and accumulation mechanism in the cell	50
FIGURE 2.19	A side by side representation of the uptake and metabolism of glucose and FDG in (A) normal and (B) tumour cell	50
FIGURE 2.20	Chemical structures of (A) ^{18}F-FDG, (B) DG, (C) glucose, (D) EC-DG, (E) $^{99\text{m}}\text{Tc}$-EC-DG and (F) IHP $^{99\text{m}}\text{Tc}$-EC-DG	59
FIGURE 2.21	The mechanism of cell uptake and accumulation of ^{18}F-FDG, $^{99\text{m}}\text{Tc}$-EC-DG and glucose	60
FIGURE 2.22	Anterior whole-body images of (A) ^{18}F-FDG in a healthy patient, (B) $^{99\text{m}}\text{Tc}$-EC-DG in a patient with NSCLC in the right upper lung at 2 hours post radiopharmaceutical administration and (C) $^{99\text{m}}\text{Tc}$-EC-DG in a patient with rheumatoid arthritis in the left knee at 2 hours post radiopharmaceutical administration	62
FIGURE 2.23	Illustration of cancer cell targets for imaging	63
FIGURE 2.24	Comparison of the sensitivity of different imaging modalities	64
FIGURE 2.25	A selected few PET radiopharmaceuticals used in imaging for cancer management	65
 CHAPTER 3:		
FIGURE 3.1	Research design of the pilot study	72
FIGURE 3.2	A schematic overview of the three research phases	79
 CHAPTER 4:		
FIGURE 4.1	Research design for phase one with nude mice as animal model	88
FIGURE 4.2	Two of the healthy nude athymic mice used for phase one	90
FIGURE 4.3	The HPLC-UV chromatogram of the EC-DG for phase 1A	94
FIGURE 4.4	The HPLC radiometric chromatogram for the IHP $^{99\text{m}}\text{Tc}$-EC-DG (DL) of research phase 1A	94

FIGURE 4.5	The HPLC-UV chromatogram of the EC-DG for phase 1B	95
FIGURE 4.6	The HPLC radiometric chromatogram for the IHP ^{99m}Tc-EC-DG (DL) of research phase 1B	95
FIGURE 4.7	Biodistribution of IHP ^{99m}Tc-EC-DG to different organs from <i>ex vivo</i> results. Mean % uptake of (A) liver, (B) kidneys, (C) intestines and (D) brain of healthy mice administered with IHP ^{99m}Tc-EC-DG	99
FIGURE 4.8	Biodistribution of IHP ^{99m}Tc-EC-DG (DL) (G2 & G5) and ¹⁸F-FDG (G3 & G6) to tumours of lung tumour-bearing mice is shown with time	102
FIGURE 4.9	Tumour-to-tissue biodistribution of the different groups administered with ¹⁸F-FDG and IHP ^{99m}Tc-EC-DG (DL) in lung tumour-bearing mice. The (A) tumour-to-blood ratio-, (B) tumour-to-muscle ratio-, (C) tumour-to-lung ratio and (D) tumour-to-brain ratio is shown with time	110
CHAPTER 5:		
FIGURE 5.1	Research design for phase two with healthy, septic- and sterile IFI/IF induced New Zealand White rabbits as animal models	122
FIGURE 5.2	Co-researcher (MRS. J.M. Wagener) holding one of the New Zealand White rabbits used during phase two	123
FIGURE 5.3	One of the rabbits that received a SPECT/CT during phase two	125
FIGURE 5.4	Biodistribution of IHP ^{99m}Tc-EC-DG (DL) in healthy rabbits at (A) 0.1-, (B) 0.5-, (C) 1-, (D) 2- and (E) 4 hours post administration	133
FIGURE 5.5	(A) IHP ^{99m}Tc-EC-DG fused SPECT/CT (transverse, sagittal and coronal) images at 2 hour post radiopharmaceutical administration	135

FIGURE 5.5	(B) IHP ^{99m}Tc-EC-DG fused SPECT/CT (transverse, sagittal, and coronal) images at 4 hour post radiopharmaceutical administration	136
FIGURE 5.6	Clearance profile of organs that showed the highest IHP ^{99m}Tc-EC-DG (DL) uptake in healthy rabbits	141
FIGURE 5.7	Clearance profile of organs that showed the lowest IHP ^{99m}Tc-EC-DG (DL) uptake in healthy rabbits	142
FIGURE 5.8	Clearance profile of IHP ^{99m}Tc-EC-DG excretion by kidneys into the bladder for healthy rabbits	142
FIGURE 5.9	ANT biodistribution images of IHP ^{99m}Tc-EC-DG (A-E) and $^{99m}\text{TcO}_4^-$ (F-J) in healthy rabbits at (A & F) 0.1-, (B & G) 0.5-, (C & H) 1-, (D & I) 2- and (E & J) 4 hour post administration	145
FIGURE 5.10	POST biodistribution images of IHP ^{99m}Tc-EC-DG (K-O) and $^{99m}\text{TcO}_4^-$ (P-T) in healthy rabbits at (K & P) 0.1-, (L & Q) 0.5-, (M & R) 1-, (N & S) 2- and (O & T) 4 hour administration	146
FIGURE 5.11	(A) $^{99m}\text{TcO}_4^-$ fused SPECT/CT (transverse, sagittal and coronal) images at 1 hour post radiopharmaceutical administration	148
FIGURE 5.11	(B) IHP ^{99m}Tc-EC-DG fused SPECT/CT (transverse, sagittal and coronal) and (C) $^{99m}\text{TcO}_4^-$ images at 2 hour post radiopharmaceutical administration	149
FIGURE 5.11	(D) IHP ^{99m}Tc-EC-DG fused SPECT/CT (transverse, sagittal and coronal) and (E) $^{99m}\text{TcO}_4^-$ images at 4 hour post radiopharmaceutical administration	150
FIGURE 5.12	Comparison of clearance of high biodistribution organs from the IHP ^{99m}Tc-EC-DG and $^{99m}\text{TcO}_4^-$ in healthy rabbits. Mean % biodistribution values for the (A) liver, (B) heart and (C) brain (only high 0.1h to 1 h) are shown with time	156
FIGURE 5.13	Comparison of clearance for the low biodistribution organs of IHP ^{99m}Tc-EC-DG and $^{99m}\text{TcO}_4^-$ in healthy rabbits. Mean % biodistribution values for the (A)	

	brain (only low 1h to 4h) and (B) stomach are shown with time	157
FIGURE 5.14	Clearance profile of IHP ^{99m}Tc -EC-DG and $^{99m}\text{TcO}_4^-$ excretion by kidneys into the bladder for healthy rabbits	158
FIGURE 5.15	ANT septic IFI/IF static images of IHP ^{99m}Tc -EC-DG (A-F) was obtained at (A) 0.1-, (B) 1-, (C) 2-, (D) 3-, (E) 4- and (F) 6 hour post administration. Arrow indicate increase radiopharmaceutical uptake in septic IFI/IF induced area	161
FIGURE 5.16	^{67}Ga -citrate static images were obtained at (A) 24- and (B) 48 hour post radiopharmaceutical administration. Arrows indicate increased radiopharmaceutical uptake in septic IFI/IF induced area	161
FIGURE 5.17	IHP ^{99m}Tc -EC-DG fused SPECT/CT (A) transverse, (B) sagittal and (C) coronal images with <i>E. coli</i> thigh muscle IFI/IF 4 hour post radiopharmaceutical administration	162
FIGURE 5.18	^{67}Ga -citrate fused SPECT/CT (A) transverse, (B) sagittal and (C) coronal images with <i>E. coli</i> thigh muscle infection (arrow) 48 hour POST radiopharmaceutical administration	162
FIGURE 5.19	ANT sterile IFI/IF static images of IHP ^{99m}Tc -EC-DG (KF) (A-F) at (A) 0.1-, (B) 1-, (C) 2-, (D) 3-, (E) 4- and (F) 6 hour POST administration. Arrows indicate increased radiopharmaceutical uptake in sterile IFI/IF induced area	168
FIGURE 5.20	ANT sterile IFI/IF static images of ^{67}Ga -citrate (A) 24- and (B) 48 hour POST administration. Arrows indicate increased radionuclide uptake in sterile IFI/IF induced area	168
FIGURE 5.21	(A) 4 hour IHP ^{99m}Tc -EC-DG fused SPECT/CT coronal images and (B) 48 hour ^{67}Ga -citrate fused SPECT/CT coronal images of the zymosan induced IFI/IF in the thigh muscle	169

FIGURE 5.22	T/NT ratios of IHP ^{99m}Tc-EC-DG and ^{67}Ga-citrate of septic- and sterile IFI/IF thigh muscles in rabbits at different time intervals	174
FIGURE 5.23	The schematic whole-body image of the anatomy and scintigraphic images provided by Irwin <i>et al.</i> (1988:1271) on the normal biodistribution of $^{99m}\text{TcO}_4^-$ in a New Zealand White rabbit	175
FIGURE 5.24	PET whole-body image of a New Zealand White Rabbit	176
CHAPTER 6:		
FIGURE 6.1	Research design for phase three with healthy baboons as animal model	178
FIGURE 6.2	One of the baboons used for phase three with two of the research personnel	179
FIGURE 6.3	One of the baboons that received a SPECT/CT during phase three	180
FIGURE 6.4	Biodistribution of IHP ^{99m}Tc-EC-DG (KF) in healthy baboons at (A) 0.1-, (B) 1- and (C) 2 hour post administration	184
FIGURE 6.5	SPECT/CT (A) transverse, (B) sagittal and (C) coronal images post IHP ^{99m}Tc-EC-DG (KF) administration acquired at 0.1 hour post radiopharmaceutical administration	186
FIGURE 6.6	Co-registered SPECT/CT at 1 hour (A) transverse, (B) sagittal and (C) coronal images of healthy baboons acquired post IHP ^{99m}Tc-EC-DG (KF) administration	187
FIGURE 6.7	SPECT/CT (A) transverse, (B) sagittal and (C) coronal images acquired at 2 hour post administration of IHP ^{99m}Tc-EC-DG (KF)	188
FIGURE 6.8	Clearance of highest uptake organs from <i>in vivo</i> results of IHP ^{99m}Tc-EC-DG (KF) in healthy baboons. Mean % biodistribution values for the liver and heart are shown with time	193

FIGURE 6.9	Clearance profile of IHP ^{99m}Tc-EC-DG (KF) excretion by kidneys into the bladder for healthy baboons	193
FIGURE 6.10	Clearance of lowest uptake organs from <i>in vivo</i> results of IHP ^{99m}Tc-EC-DG (KF) in healthy baboons. Mean % biodistribution values for the stomach, brain and skin are shown with time	194
FIGURE 6.11	ANT biodistribution whole-body images of $^{99m}\text{TcO}_4^-$ (A, C & E) and IHP ^{99m}Tc-EC-DG (KF) (B, D & F) in healthy baboons at (A & B) 0.1-, (C & D) 1- and (E & F) 2 hour post administration	196
FIGURE 6.12	POST biodistribution images of $^{99m}\text{TcO}_4^-$ (G, I & K) and IHP ^{99m}Tc-EC-DG (KF) (H, J & L) in healthy baboons at (G & H) 0.1-, (I & J) 1- AND (K & L) 2 hour post administration	197
FIGURE 6.13	$^{99m}\text{TcO}_4^-$ co-registered SPECT/CT (A) sagittal and (B) coronal images and IHP ^{99m}Tc-EC-DG (KF) SPECT/CT (C) sagittal and (D) coronal images at 1 hour post radiopharmaceutical administration	200
FIGURE 6.14	$^{99m}\text{TcO}_4^-$ co-registered SPECT/CT (E) sagittal and (F) coronal images and IHP ^{99m}Tc-EC-DG (KF) SPECT/CT (G) sagittal and (H) coronal images at 2 hour post radiopharmaceutical administration	201
FIGURE 6.15	Comparison of clearance from the stomach for IHP ^{99m}Tc-EC-DG (KF) and $^{99m}\text{TcO}_4^-$ in healthy baboons. Mean % uptake values for the stomach are shown with time	205
FIGURE 6.16	Comparison of clearance from the highest uptake organs of IHP ^{99m}Tc-EC-DG (KF) and $^{99m}\text{TcO}_4^-$ in healthy baboons. Mean % uptake values for the (A) liver and (B) heart are shown with time	206
FIGURE 6.17	Comparison from the lowest uptake organs of IHP ^{99m}Tc-EC-DG (KF) and $^{99m}\text{TcO}_4^-$ in healthy baboons. Mean % uptake values for the (A) brain and (B) skin are shown with time	207

FIGURE 6.18	ANT whole-body biodistribution images IHP ^{99m}Tc-EC-DG (DL) (A, C & E) and IHP ^{99m}Tc-EC-DG (KF) (B, D & F) in healthy baboons at (A & B) 0.1-, (C & D) 1- and (E & F) 2 hour post administration	211
FIGURE 6.19	POST biodistribution images IHP ^{99m}Tc-EC-DG (DL) (G, I & K) and IHP ^{99m}Tc-EC-DG (KF) (H, J & L) in healthy baboons at (G & H) 0.1-, (I & J) 1- and (K & L) 2 hour post administration	212
FIGURE 6.20	IHP ^{99m}Tc-EC-DG (DL) co-registered SPECT/CT (A) sagittal and (B) coronal images and IHP ^{99m}Tc-EC-DG (KF) SPECT/CT (C) sagittal and (D) coronal images at 0.1 hour post radiopharmaceutical administration	214
FIGURE 6.21	IHP ^{99m}Tc-EC-DG (DL) co-registered SPECT/CT (E) sagittal and (F) coronal images and IHP ^{99m}Tc-EC-DG (KF) SPECT/CT (G) sagittal and (H) coronal images at 2 hour post radiopharmaceutical administration	215
FIGURE 6.22	Comparison of clearance of the high uptake organs from the IHP ^{99m}Tc-EC-DG (KF) and IHP ^{99m}Tc-EC-DG (DL) in healthy baboons. Mean % uptake values for the (A) intestines and the (B) gallbladder are shown with time	222
FIGURE 6.23	Comparison of clearance of high uptake organs for IHP ^{99m}Tc-EC-DG (KF) and IHP ^{99m}Tc-EC-DG (DL) in healthy baboons. Mean % uptake values for the (A) lungs, (B) liver and (C) heart are shown with time	223

LIST OF TABLES

	Page
CHAPTER 1:	
TABLE 1.1	Summary of the differences in the amounts of EC-DG and SnCl₂ needed for the IHP ^{99m}Tc-EC-DG (DL) compared with ^{99m}Tc-EC-DG found in the literature
	12
CHAPTER 2:	
TABLE 2.1	Summary of the glucose transporters in mammals
	22
TABLE 2.2	Radionuclides and radiopharmaceuticals for IFI/IF imaging
	30
TABLE 2.3	Biodistribution parameters generated from imaging and biosampling data
	39
TABLE 2.4	The absorbed radiation dose for ^{99m}TcO₄⁻ in adults
	45
TABLE 2.5	The absorbed radiation dose for ¹⁸F-FDG in adults
	49
TABLE 2.6	List of publications on ^{99m}Tc-EC-DG and short summary
	53
TABLE 2.7	The absorbed radiation dose for ^{99m}Tc-EC-DG and ^{99m}Tc-MDP in adults
	56
CHAPTER 3:	
TABLE 3.1	Summary to indicate the biodistribution of IHP ^{99m}Tc-EC-DG and ⁶⁷Ga-citrate in rabbits to the area of induced septic IFI/IF
	75
TABLE 3.2	Count ratio of the RH versus LT thigh muscle of rabbits induced with <i>E. coli</i> administered with IHP ^{99m}Tc-EC-DG and ⁶⁷Ga-citrate
	76
TABLE 3.3	Environmental conditions of the healthy and lung tumour-bearing nude mice at the Animal Research Centre, NWU
	84
TABLE 3.4	Summary of the calibration performed on this nuclear medicine research instrumentation
	89

CHAPTER 4:

TABLE 4.1	Summary of the differences (variances) between data acquiring during research phase 1A and 1B	97
TABLE 4.2	Summary of the QC results of the IHP ^{99m}Tc-EC-DG (PHASE 1A/1B)	94
TABLE 4.3	Biodistribution (%ID/g) of IHP ^{99m}Tc-EC-DG (DL) in healthy athymic nude mice for G1 and G4	102
TABLE 4.4	Biodistribution (%ID/g) of IHP ^{99m}Tc-EC-DG in lung tumour-bearing mice	106
TABLE 4.5	Comparison of the biodistribution (%ID/g) results in lung tumour-bearing mice for G2 with G3 and G5 with G6	113
TABLE 4.6	Comparison of the biodistribution (%ID/g) results of G2 and G5 with ^{99m}Tc-EC-DG from the literature and G3 and G6 with ¹⁸F-FDG from the literature in lung tumour-bearing mice	117
TABLE 4.7	Comparison of the biodistribution (%ID/g) results of G2 and G5 with ^{99m}Tc-EC-DG from the literature and G3 and G6 with ¹⁸F-FDG from the literature in lung tumour-bearing mice	118

CHAPTER 5:

TABLE 5.1	Summary of radionuclide and radiopharmaceutical dosages administered to rabbits in phase two of the research	124
TABLE 5.2	Siemens SYMBIA T parameters for the SPECT imaging	125
TABLE 5.3	The SQ and SQUAL static- and SPECT/CT results of the biodistribution to the different organs/tissues of IHP ^{99m}Tc-EC-DG (DL) in healthy rabbits	138
TABLE 5.4	Biodistribution of IHP ^{99m}Tc-EC-DG (DL) in healthy rabbits (<i>n</i>=10)	139
TABLE 5.5	Comparison of the SQ and SQUAL static and SPECT/CT results of the biodistribution to the lungs	

	of IHP $^{99m}\text{Tc-EC-DG}$ (DL) and $^{99m}\text{TcO}_4^-$ in healthy rabbits	152
TABLE 5.6	Comparison of the biodistribution results of $^{99m}\text{TcO}_4^-$ and IHP $^{99m}\text{Tc-EC-DG}$ in healthy New Zealand White Rabbits at 0.1-, 0.5-, 1-, 2- and 4 hour post radiopharmaceutical administration	153
TABLE 5.7	Comparison of the SQ and SQUAL static and SPECT/CT results of the biodistribution to the septic IFI/IF of IHP $^{99m}\text{Tc-EC-DG}$ (DL) and $^{67}\text{Ga-citrate}$ in rabbits	164
TABLE 5.8	Percentage target and non-target biodistribution of IHP $^{99m}\text{Tc-EC-DG}$ (DL) and $^{67}\text{Ga-citrate}$ in rabbits induced ($n=5$) with septic IFI/IF	165
TABLE 5.9	Target-to-non-target ratios of IHP $^{99m}\text{Tc-EC-DG}$ (DL) and $^{67}\text{Ga-citrate}$ of septic IFI/IF thigh muscles in rabbits ($n=5$) at different time intervals	166
TABLE 5.10	Comparison of the SQ and SQUAL static and SPECT/CT results of the biodistribution to the sterile IFI/IF of IHP $^{99m}\text{Tc-EC-DG}$ (KF) and $^{67}\text{Ga-citrate}$ in rabbits	170
TABLE 5.11	%Non-target and %Target biodistribution of IHP $^{99m}\text{Tc-EC-DG}$ KF and $^{67}\text{Ga-citrate}$ in rabbits induced ($n=5$) with sterile IFI/IF	171
TABLE 5.12	T/NT ratios of IHP $^{99m}\text{Tc-EC-DG}$ and $^{67}\text{Ga-citrate}$ of sterile IFI/IF thigh muscles in rabbits ($n=5$) at different time intervals	172
CHAPTER 6:		
TABLE 6.1	Summary of radionuclide and radiopharmaceutical dosages administered to the healthy baboons in phase three	179
TABLE 6.2	Siemens SYMBIA camera parameters for the two-bed SPECT imaging	180

TABLE 6.3	The SQ and SQUAL planar whole-body- and SPECT/CT results of the biodistribution IHP ^{99m}Tc-EC-DG (KF) to the organs of healthy baboons	190
TABLE 6.4	Biodistribution of IHP ^{99m}Tc-EC-DG (KF) in healthy baboons	192
TABLE 6.5	Comparison of the SQ and SQUAL planar whole-body- and SPECT/CT results of $^{99m}\text{TcO}_4^-$ and IHP ^{99m}Tc-EC-DG (KF) biodistribution to organs of healthy baboons	202
TABLE 6.6	Comparison of the biodistribution of IHP ^{99m}Tc-EC-DG (KF) with $^{99m}\text{TcO}_4^-$ in healthy baboons	204
TABLE 6.7	Comparison of the SQ and SQUAL planar whole-body- and SPECT/CT results of the biodistribution to the organs of IHP ^{99m}Tc-EC-DG (DL) and IHP ^{99m}Tc-EC-DG (KF) in healthy baboons	217
TABLE 6.8	Comparison of the biodistribution of IHP ^{99m}Tc-EC-DG (DL) with IHP ^{99m}Tc-EC-DG (KF) in healthy baboons	219

LIST OF ACRONYMS

ALARA	:	As Low As Reasonably Achievable
Ar	:	Argon
ADP	:	Adenosine Di-Phosphate
ANT	:	Anterior
ATP	:	Adenosine Tri-Phosphate
β	:	Beta
BBB	:	Blood brain barrier
BD	:	Biodistribution
BVSc	:	Bachelor Veterinary Science
$^{\circ}\text{C}$:	Degrees Celsius
C	:	Carbon
CD	:	cluster of differentiation
CD11a/CD18	:	Integrins
CD40L	:	Cluster of Differentiation 40 (glycoprotein) Ligand
CD40R	:	Cluster of Differentiation 40 (glycoprotein) Receptor
Cl	:	Chlorine
cm	:	Centimetres
cm^3	:	Cubic centimetres
CI	:	Confidence Interval
^{57}Co	:	Cobalt-57
CT	:	Computer Tomography
CTDI	:	CT Dose Index
CXCR/CCR	:	Chemokine receptor
2-D-glucosamine	:	Two amino-deoxyglucose
DC	:	Dendritic cell
DCCT	:	Diagnostic Contrast-enhanced Computed Tomography
DG	:	Deoxyglucose
DL	:	Directly labelled/Direct labelling
DNA	:	Deoxyribonucleic Acid
DNM	:	Department of Nuclear Medicine
Dr	:	Doctor

DoH	:	Department of Health
EANM	:	The European Association of Nuclear Medicine
EC	:	Ethylenedicysteine
<i>E. coli</i>	:	<i>Escherichia coli</i>
EC-DG	:	Ethylenedicysteine-deoxyglucose
ERB	:	Endoplasmic Reticulum Binding
¹⁸ F	:	Fluorine-18
F-6-P	:	Fructose-six-phosphate
FDA	:	Food and Drug Administration
FDG	:	Flurodeoxyglucose
¹⁸ F-FDG	:	Fluorine-18-flurodeoxyglucose
¹⁸ F-FDG-6-P	:	Fluorine-18-flurodeoxyglucose-six-phosphate
Γ	:	Gamma
G1	:	Group 1
G2	:	Group 2
G3	:	Group 3
G4	:	Group 4
G5	:	Group 5
G6	:	Group 6
G-6-P	:	Glucose-six-phosphate
⁶⁷ Ga-citrate	:	Gallium-67-citrate
GADP	:	Glyceraldehyde 3-Phosphate
GBq	:	Gigabecquerel
GlcNAc	:	N-acetylglucosamine
GLP	:	Good Laboratory Practice
GLUT	:	Glucose transporter
Gy	:	Gray
⁶⁷ Ga-citrate	:	Gallium-67-citrate
GE	:	General Electric
GFAT	:	Fructose 6-phosphate amidotransferase
GLP	:	Good Laboratory Practices
g/mol	:	Gram per mol
G-6-P	:	glucose-six-phosphate
GM	:	Geometric mean
GMP	:	Good Manufacturing Practice

h	:	Hour
H	:	Hydrogen
H ₂ O	:	Water
HCl	:	Hydrochloric-acid
HCO ₃	:	Bicarbonate
HEPA	:	High Efficiency Particulate Air
HKI	:	Hexokinase isoforms
HMPAO	:	Hexamethylpropyleneamine
HPLC	:	High performance liquid chromatography
¹¹¹ In	:	Indium-111
IAEA	:	International Atomic Energy Agency
ID	:	Injected dose
IFI/IF	:	Infection/Inflammation
IHP	:	In-house prepared or In-house preparation
IL	:	Interleukin
IP-10	:	Interferon-gamma induced protein-10
IRS	:	Insulin Receptor Substrate
ITLC-SG	:	Instant Thin Layer Chromatography-Silica Gel
JAM	:	junctional adhesion molecule
K	:	Potassium
keV	:	Kiloelectron volt
kg	:	Kilogram
KF	:	Kit formulation
kVP	:	Kilovolt peak
LEHR	:	Low-energy high resolution parallel-hole
LFA	:	Lymphocyte function-associated antigen
LT	:	Left
LTB4	:	Leukotriene B4
M	:	Mole
Max	:	Maximum
MBq	:	Megabecquerel
MCC	:	Medicines Control Council
mCi	:	Millicurie
<i>Mdn</i>	:	Median
MEHR	:	Medium-energy high resolution

MeV	:	Mega electronvolt
mg	:	Milligram
MHC	:	Histocompatibility complex
MIBI	:	Methoxy isobutyl isocyanide
min	:	Minutes
Min	:	Minimum
MIP	:	Macrophage inflammatory protein
ml	:	Millilitre
⁹⁹ Mo	:	Molybdenum-99
Mr	:	Mister
MRCVS	:	Member of the Royal College of Veterinary Surgeons
mRNA	:	Messenger Ribonucleic Acid
M.Sc	:	Magister Scientiae
mSv	:	Millisievert
^m	:	Metastable
mg	:	Milligram
mGy	:	Milligray
ml/min	:	millilitre per minute
mmol	:	Micromole
MRC	:	Medical Research Council
Mrs	:	Mistress
Myc	:	Myelocytomatosis Oncogene Cellular Homolog
n	:	Neutron
N	:	Nitrogen
<i>n</i>	:	Subsample size
N ₂	:	Nitrogen
Na	:	Sodium
n/a	:	Not applicable
NAD	:	Nicotinamide Adenine Dinucleotide - Hydrogen
NADH	:	Nicotinamide Adenine Dinucleotide
Necsa	:	The South African Nuclear Energy Corporation
NECSA	:	The South African Nuclear Energy Corporation
NFAT	:	Nuclear factor of activated T cells
NH	:	Nitrogen and Hydrogen
nm	:	Nanometer

no.	:	Number
NRF	:	National Research Fund
NSCLC	:	Non-small-cell lung cancer
NWU	:	North-West University
O	:	Oxygen
O-GlcNAc	:	Oxygen-linked protein N-acetylglucosamine
OH	:	Oxygen and Hydrogen
OGT	:	Oxygen-linked N-acetylglucosamine (GlcNAc) Transferase
QC	:	Quality control
<i>P</i> -value	:	Calculated probability
ρ	:	Spearman's rank order correlation
p53	:	Tumour suppressor protein that protects from DNA damage
p67	:	Phosphoprotein
PECAM	:	platelet endothelial cell adhesion molecule
PEP	:	Phosphoenolpyruvic acid
PET	:	Positron Emission Tomography
PET/CT	:	Positron Emission Tomography and Computed Tomography
pH	:	Measure of acidity or basicity of an aqueous solution ($-\log[H^+]$)
Ph.D.	:	Philosophiae Doctor
PI-3	:	Phosphatidylinositol 3
PMN	:	Polymorphonuclear neutrophil
PolII	:	Polymerase II
Prof	:	Professor
PSGL	:	P-selectin glycoprotein ligand
Pty Ltd	:	Proprietary Limited
POST	:	Posterior
R	:	Rand
rad	:	Radiation absorbed dose
RANTES	:	Regulated on activation, normal T cell expressed & secreted (CCL5 chemokine)
RBC	:	red blood cell
RCP	:	Radiochemical purity
rem	:	Roentgen-equivalent man
RH	:	Right

ROI	:	Region of interest
ROIs	:	Regions of interest
RP	:	Radiopharmaceutical
RPO	:	Radiation Protection Officer
RRR	:	Replacement, Reduction, Refinement
RSA	:	Republic of South Africa
SBAH	:	Steve Biko Academic Hospital
<i>SEM</i>	:	Standard error of mean
SGLT	:	Sodium glucose transporters
SH	:	Sulfhydryl or thiol
s-Le-x	:	sialyl-Lewis X
Sn	:	Tin
SnCl ₂	:	Tin (II) chloride
Sp	:	Specificity protein
Sp1	:	Specificity protein one
SPECT	:	Single Photon Emission Computed Tomography
SPECT/CT	:	Single Photon Emission Tomography/Computed Tomography
SQual	:	Semi-qualitative
SQ	:	Semi-quantitative
S-S	:	Disulphate
S	:	Sulphur
SUVmax	:	Maximum standard uptake values
Sv	:	Sievert
T	:	Thymus
TB	:	Tuberculosis
Tc	:	Technetium
<i>t</i>	:	Student's t-test
^{99m} TcO ₄ ⁻	:	Technetium-99-metastable-pertechnetate
<i>t</i> _{1/2}	:	Physical half-life of radionuclides
^{99m} Tc-EC-DG	:	Technetium-99-metastable-pertechnetate ethylenedicysteine-deoxyglucose
^{99m} Tc- UBI	:	^{99m} Tc-ubiquitin
TLC	:	Thin Layer Chromatography
TNF α	:	Tumour necrosis factor alpha

UAH	:	Universitas Academic Hospital
UDP-GlcNac	:	Uridine diphospho-N-acetylglucosamine
UFS	:	University of the Free State
<i>W</i> +	:	Wilcoxon sign rank test
WHO	:	World Health Organisation
www	:	World Wide Web
⁶⁸ Zn	:	Zinc-68
ZAR	:	South African Rand
%	:	Percent/Percentage
%ID/g	:	Percentage of administered dose per gram of wet tissue weight
µg	:	Microgram
µl	:	Microliter
µm	:	Micrometre
.gov	:	Web domain name for government agencies
.net	:	Web domain name for network services
.org	:	Web domain name for non-profit organisations
>	:	Greater than
<	:	Less than

GLOSSARY

ALARA principles:

"ALARA is an acronym for "As Low As Reasonably Achievable". This is a radiation safety principle for minimizing radiation doses by employing all reasonable methods

Annihilation radiation:

The photons produced when an electron and a positron unite and then cease to exist. The annihilation of a positron-electron pair results in the production of 2 photons; each has an energy of 0.51 MeV

Antibody:

Protein of the immunoglobulin class produced in lymphoid cells in response to stimulation by immunogen and capable of combining *in vivo* with said antigenic substance as a defence mechanism, or of reacting *in vitro* for specific analysis of the antigen; or, a substance produced in response to an antigen that reacts specifically with that antigen

Antigen:

Any substance that can induce the formation of antibodies and that reacts specifically with the antibodies formed

Beta emission:

The release of high energy beta-particles by disintegration of certain radioactive nuclides

Cancer:

Any malignant tumour including carcinoma and sarcoma. It arises from the abnormal and uncontrolled division of cells that then invade and destroy the surrounding tissues

Carrier free:

A preparation of a radionuclide of "high isotopic abundance" that is, one containing no carrier

Collimator:

A device for confining the elements of a beam within an assigned solid angle

Cyclotron:

A device for accelerating charged particles in a spiral fashion to high energies by means of an alternating electric field between electrodes placed in a constant magnetic field

Deoxyribonucleic acid:

The genetic material of nearly all living organisms. DNA is a nucleic acid composed of two strands made up of units called nucleotides. The two strands are wound around each other into a double helix and linked together by hydrogen bonds between the bases of the nucleotides. The genetic information of the DNA is contained in the sequence of bases along the molecule; changes in the DNA cause mutations. The DNA molecule can make exact copies of itself by the process of replication, thereby passing on the genetic information to the daughter cells when the cells divide

Dose:

In competitive binding assay, the amount of test substance added to any given reference standard

Dose (dosage):

According to current usage, the radiation delivered to the whole body or to a specific area or volume

Enzyme:

The substance formed by living cells, having the capacity to facilitate a chemical reaction

Et al.

An abbreviated form of et alia, Latin for "and others"

Ex vivo:

Study of biological process in a living organism, samples are taken after death

Fibroblast:

A stellate or spindle-shaped cell with a large, oval, flattened nucleus and a thin layer of cytoplasm found in fibrous tissue

Gamma emitters:

Radioactive substances that release photons (electromagnetic waves) on disintegration

Glucosamine:

The amino sugar of glucose, i.e. glucose in which the hydroxyl group is replaced by an amino group. Glucosamine is a component of mucopolysaccharides and glycoproteins: for example, hyaluronic acid, a mucopolysaccharide found in synovial fluid, and heparin.

Glucose (dextrose): a simple sugar containing six carbon atoms (a hexose). Glucose is an important source of energy in the body and the sole source of energy for the brain.

Glycolysis:

The conversion of glucose, by a series of ten enzyme-catalysed reactions, to lactic acid. Glycolysis takes place in the cytoplasm of cells and the first nine reactions (converting glucose to pyruvate) form the first stage of cellular respiration. The process involves the production of a small amount of energy (in the form of ATP), which is used for biochemical work. The final reaction of glycolysis (converting pyruvate to lactic acid) provides energy for short periods of time when oxygen consumption exceeds demand; for example, during bursts of intense muscular activity.

Infection:

Invasion of the body by harmful organisms (pathogens), such as bacteria, fungi, protozoa, rickettsiae, or viruses

Inflammation:

The body's response to injury, which may be acute or chronic

In vitro:

Study of biological process in artificial conditions using e.g. tissue slides

In vivo:

Study of biological process in a living organism

Leucocyte (white blood cell):

Any blood cell that contains a nucleus. In health there are three major subdivisions: granulocytes, lymphocytes and monocytes, which are involved in protecting the body against foreign substances and in antibody production. In disease, a variety of other types may appear in the blood, most notably immature forms of the normal red or white blood cells.

Macrophage:

Phagocytic cell (not a leukocyte) belonging to the reticulo-endothelial system. It has the capacity for storing in its cytoplasm certain aniline dyse in the form of granules.

Nuclide:

A type of atom as characterised by its atomic number and its neutron number

Radionuclide:

A nuclide that is radioactive

Radiopharmaceutical:

Are radioactive drug composing of a radionuclide and a pharmaceutical that are prepared by a radio-pharmacist or specially trained nuclear medicine physician and used in a Nuclear Medicine department for the diagnostic or therapeutic purposes of human disease

Tumour:

Any abnormal swelling in or on a part of the body. The term is usually applied to an abnormal growth of tissue, which may be benign or malignant.

SUMMARY

Key terms: in-house prepared ^{99m}Tc -EC-DG; biodistribution; infection/inflammation; tumour; imaging

This thesis covers the research to evaluate the normal-, tumour- and infection/inflammation biodistribution properties of the in-house prepared ^{99m}Tc -Ethylenedicysteine-deoxyglucose (IHP ^{99m}Tc -EC-DG) in nude mice, New Zealand White rabbits and baboons (*Papio Ursinus*). In the South African context there is a need for a low cost, widely available, single photon emission glucose metabolism imaging agent that can detect cancerous tumours and infection/inflammation (IFI/IF), since health care funding is problematic in the country. Fluorine-18-fluorodeoxyglucose (^{18}F -FDG) comes close to the ideal tumour detection radiopharmaceutical, but has certain shortcomings e.g. short physical half-life (no late imaging possible), high cost and non-specific. Yet ^{18}F -FDG biodistribution to IFI/IF and tumours are similar and pose a differentiation limitation of these two specific diseases. In the search for the ideal radiopharmaceutical for tumour/IFI/IF detection, The South African Nuclear Energy Corporation (Necsa) developed two different labelling routes, of ethylenedicysteine-deoxyglucose (EC-DG) with ^{99m}Tc that could be locally prepared at the Department of Nuclear Medicine at the Universitas Academic hospital.

The summation of different diseases and physiological conditions present in humans can be replicated by the use of animal models for research. Three different species of animals were utilised to obtain the necessary research data that contributed to the evaluation of the diagnostic potential of the IHP ^{99m}Tc -EC-DG.

All three animal species showed increased biodistribution of the IHP ^{99m}Tc -EC-DG to the liver (critical organ) and heart. IHP ^{99m}Tc -ECDG demonstrated rapid clearance by the kidneys seen as a decrease in background activity in animals on the scintigraphic images. The IHP ^{99m}Tc -EC-DG images showed no biodistribution to the brain in the larger animal models. This is the greatest difference between the biodistribution of IHP ^{99m}Tc -EC-DG visually compared to clinical ^{18}F -FDG studies (in the literature) which shows high brain uptake. The conclusion can be made that the IHP ^{99m}Tc -EC-DG does not pass over the blood brain barrier (BBB) in accordance with earlier literature findings.

The IHP ^{99m}Tc -EC-DG showed similar uptake to ^{18}F -FDG in lung tumours induced in nude mice. There are similarities between the uptake of the IHP ^{99m}Tc -EC-DG and the ^{99m}Tc -EC-DG described in the literature by Yang *et al.* (2003:470-471). This includes biodistribution to lung tumours, biodistribution to the liver and heart and excretion by the kidney.

IHP ^{99m}Tc -EC-DG uptake in septic- (*Escherichia coli*) and sterile (zymosan) IFI/IF induced in New Zealand White rabbits was evaluated and compared to ^{67}Ga -citrate uptake. IHP ^{99m}Tc -EC-DG is dependent on a cellular response and mainly uses this mechanism for uptake in IFI/IF, whereas ^{67}Ga -citrate has multiple mechanisms of uptake. IHP ^{99m}Tc -EC-DG is taken up in low grade cellular IFI/IF. Early diagnosis of low grade- (zymosan) and bacterial IFI/IF is possible with IHP ^{99m}Tc -EC-DG.

The IHP ^{99m}Tc -EC-DG could be a much cheaper and more affordable diagnostic alternative than ^{18}F -FDG and ^{67}Ga -citrate for tumour and IFI/IF imaging. From the research covered in this thesis, there is no doubt that the IHP ^{99m}Tc -EC-DG exhibits promising detection characteristics for both IFI/IF and specific tumours thus warranting human clinical trials. Furthermore, IHP ^{99m}Tc -EC-DG's has future potential to improve diagnosis and prognosis, planning and monitoring of cancer treatment in humans and must be investigated further.

OPSOMMING

Sleuteltermes: in-huis voorbereide ^{99m}Tc -EC-DG; biodistribusie; infeksie/inflammasie; tumor; beelding

Hierdie tesis handel oor navorsing om die normale-, tumor- en infeksie/inflammasie biodistribusie eienskappe van in-huis voorbereide ^{99m}Tc -etileendisisteïen-deoksiglukose (IHP ^{99m}Tc -EC-DG) in naakte muise, Nieu-Seelandse wit konyne en bobbejane (*Papio Ursinus*) te evalueer. In die Suid-Afrikaanse konteks is daar 'n behoefte vir 'n lae koste, algemeen beskikbare, enkelfoton emissie glukosemetabolisme beeldingsmiddel wat kankeragtige tumors en infeksie/inflammasie (IFI/IF) kan waarneem, omdat die befondsing van gesondheidsdienste problematies is in die land. Fluor-18-fluorodeoksiglukose (^{18}F -FDG) is amper die ideale tumor deteksie radiofarmaseutiese middel, maar dit het sekere tekortkominge, bv. 'n kort fisiese halfleeftyd (geen laat beelding moontlik), hoë koste en dit is nie-spesifiek. Ook is ^{18}F -FDG biodistribusie na IFI/IF en tumors soortgelyk en dit veroorsaak 'n beperking op die vermoë om te onderskei tussen hierdie spesifieke siektetoestande. In die soektog na die ideale radiofarmaseutiese middel vir tumor/IFI/IF deteksie, het die South African Nuclear Energy Corporation (Necsa) twee verskillende merkingsroetes van etileendisisteïen-deoksiglukose (EC-DG) met ^{99m}Tc ontwikkel, wat plaaslik voorberei kon word by die Departement Kerngeneeskunde by die Universitas Akademiese Hospitaal.

Die samevoeging van verskillende siektes en fisiologiese toestande wat by mense voorkom kan gesimuleer word deur die gebruik van modeldiere vir navorsing. Drie verskillende spesies diere is gebruik om die nodige navorsingsdata te verkry wat bygedra het tot die evaluering van die diagnostiese potensiaal van die IHP ^{99m}Tc -EC-DG.

Al drie spesies diere het verhoogde biodistribusie van die IHP ^{99m}Tc -EC-DG na die lewer (kritiese orgaan) en hart gehad. IHP ^{99m}Tc -EC-DG is vinnig opgeklaar deur die niere, wat waargeneem is as 'n afname in agtergrondaktiwiteit in diere op die sintigrafiese beelde. Die IHP ^{99m}Tc -EC-DG beelde het geen biodistribusie na die brein gewys in die groter modeldiere nie. Dit is die grootste verskil in die biodistribusie van IHP ^{99m}Tc -EC-DG wanneer vergelyk word (met literatuur) met kliniese ^{18}F -FDG studies wat hoë opname in die brein toon. Die gevolgtrekking kan gemaak word dat die IHP ^{99m}Tc -EC-DG nie deur die

bloed brein skans (BBS) kan beweeg nie, in ooreenstemming met vroeëre bevindings in die literatuur.

Die IHP ^{99m}Tc -EC-DG het soortgelyke opname as ^{18}F -FDG in longtumors, wat geïnduseer is in naakte muise, getoon. Daar is ooreenkomste tussen die opname van IHP ^{99m}Tc -EC-DG en ^{99m}Tc -EC-DG beskryf in die literatuur deur Yang *et al.* (2003:470-471). Dit sluit die biodistribusie na longtumors, biodistribusie na die lewer en hart en ekskresie deur die niere in.

IHP ^{99m}Tc -EC-DG opname in septiese (*Escherichia coli*) en steriele (zymosan) IFI/IF wat geïnduseer is in Nieu-Seeland wit konyne, is geëvalueer en vergelyk met ^{67}Ga -sitraat opname. IHP ^{99m}Tc -EC-DG is afhanklik van 'n sellulêre respons en gebruik hoofsaaklik hierdie meganisme vir opname in IFI/IF, terwyl ^{67}Ga -sitraat verskeie meganismes vir opname het. IHP ^{99m}Tc -EC-DG word opgeneem in laegraadse sellulêre IFI/IF. Vroeë diagnose van laegraadse (zymosan) en bakteriële IFI/IF is moontlik met IHP ^{99m}Tc -EC-DG.

Die IHP ^{99m}Tc -EC-DG kan 'n veel goedkoper en meer bekostigbare diagnostiese alternatief wees as ^{18}F -FDG en ^{67}Ga -sitraat vir tumor en IFI/IF beelding. Uit die navorsing gedek in hierdie tesis is daar geen twyfel dat die IHP ^{99m}Tc -EC-DG belowende deteksie karakteristieke vir beide IFI/IF en spesifieke tumors het nie en dus is menslike kliniese proewe geregverdig. Verder het IHP ^{99m}Tc -EC-DG toekomstige potensiaal om diagnose en prognose te verbeter en beplanning en monitering van kankerbehandeling in mense moet verder ondersoek word.

IN-HOUSE PREPARED ^{99m}Tc -ETHYLENEDICYSSTEINE-DEOXYGLUCOSE IN MICE, RABBITS AND BABOONS: TUMOUR, LOCAL INFECTION/ INFLAMMATION AND NORMAL BIODISTRIBUTION

CHAPTER 1

RESEARCH BACKGROUND

1.1 INTRODUCTION

Radiopharmaceutical development combines three different fields, chemistry, physics and physiology (Williams 2011:5). The radiopharmaceuticals presently available in the field of nuclear medicine for tumour and/or IFI/IF imaging have both advantages and disadvantages. The ideal radiopharmaceutical for one to one mapping of radiopharmaceutical to disease is referred to many clinicians as the “magical bullet” (Williams 2011:xv). The blood circulatory system influences the subsequent success of the radiopharmaceutical as a targeting agent (Williams 2011:3). The reason being that, this radiopharmaceutical interacts with different organs/tissue on its passage through the living body and may be interrupted due to the biologically predestine clearance mechanism. It must therefore pass through several organs, via their circulation, before reaching the tumour and/ IFI/IF sites (Williams 2011:4). This feature makes it questionable that the “magical bullet” will ever be engineered. The search for an ideal (novel) radiopharmaceutical as a tumour or IFI/IF imaging agent is also an ongoing process because of above mentioned reason. The characteristics for an ideal tumour and IFI/IF radiopharmaceutical are presented in Figure 1.1 (Rennen *et al.* 2001:243).

D.J. Yang in conjunction with the M.D. Anderson Cancer Centre, in Houston Texas in America is doing research in the field of developmental targeted molecular imaging and ethylenedicysteine (EC) technology (Kim & Yang 2001:1-273). The role of Technetium-99-metastable-pertechnetate ($^{99m}\text{TcO}_4^-$) in EC technology is that it can be chelated with a variety of ligands for imaging purposes (Yang *et al.* 2004:444). Chelation can be defined as the process when an inorganic complex in which a ligand established a coordinated bond to a metal ion on two or more points, so that the formulation of a ring of atoms, includes the metal (Oxford 2004:122). EC is the chelator (cross-linker) that is employed as the labelling strategy to attach the

deoxyglucose to $^{99m}\text{TcO}_4^-$ (Yang *et al.* 2006:1). Worldwide research is performed in the search for a cheaper, more widely available, IFI/IF- and tumour-specific radiopharmaceutical (Chen *et al.* 2006:342). This research evaluated the biodistribution and uptake of IHP Technetium-99-metastable-pertechnetate ethylenedicysteine-deoxyglucose ($^{99m}\text{Tc-EC-DG}$) in different animal models to determine its place and significance in the spectrum of IFI/IF and tumour imaging radiopharmaceuticals.

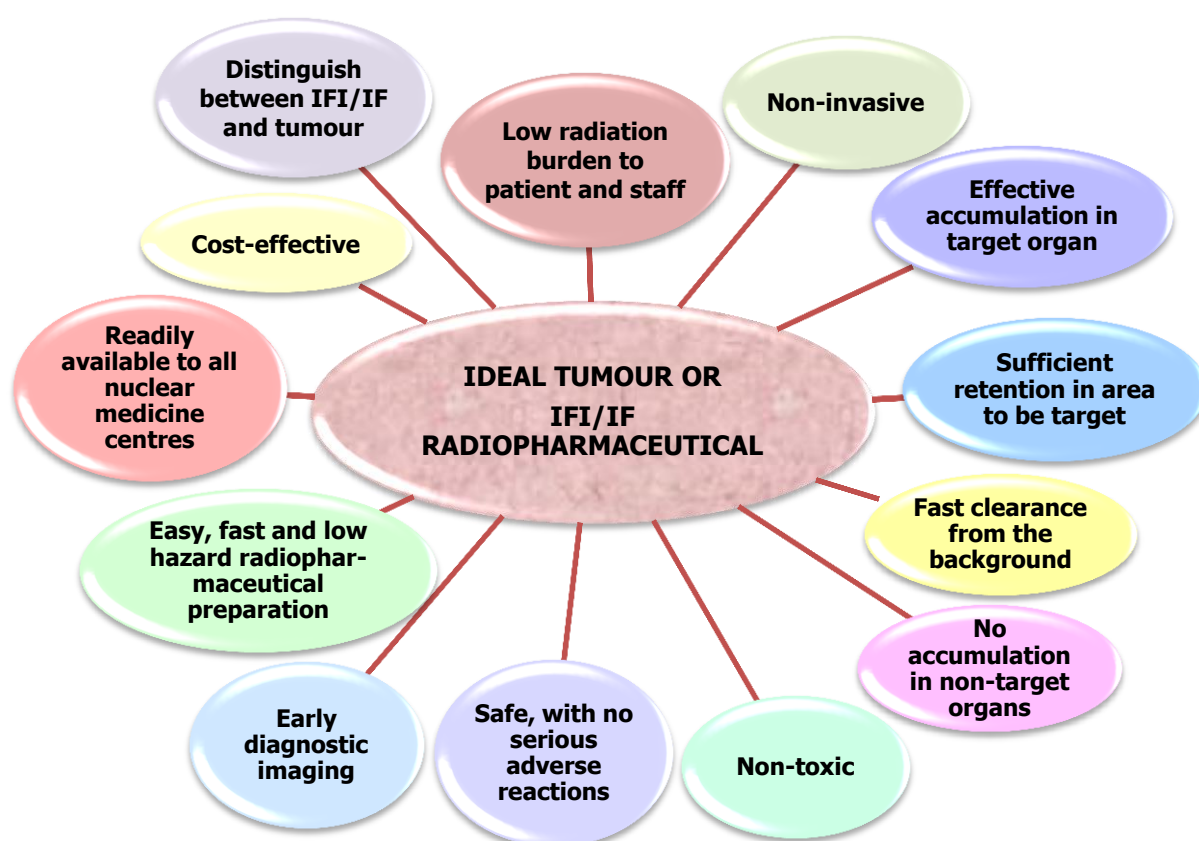


FIGURE 1.1: The characteristics of an ideal tumour or IFI/IF radiopharmaceutical (ADAPTED Rennen *et al.* 2001:243)

1.2 BACKGROUND

In order to understand what the ideal tracer in the Republic of South Africa (RSA) environment entails, a closer look was taken at the current financial Health Care situation in the RSA. The constitution of the RSA stipulates that it is the right of all citizens to have access to quality health care, nonetheless inequities still remain relating to the quality of healthcare services provided (Harris *et al.* 2011:102-103;

Taylor & Burns 2005:175). Over the past few years there has been a recurrence of the health care inflation rate substantially higher than the consumer price index to such an extent that only 17 percent (%) of the RSA population are able to afford private health care. The standard private health insurance (medical aids) principles have made it even more difficult for older and sick people to afford private health insurance (Taylor & Burns 2005:176). The results of research by independent health actuaries have shown a cost increase of 400% in the membership costs of a medical aid since 1980 (Good 2010:789).

In the RSA reasons such as unemployment and the high cost of living, forces more private health insurance members to become part of the national health care system (Govender 2005:39). The pressure on the national health care system to provide sustainable access to quality health service to the population, therefore increases annually (Dippenaar *et al.* 2005:37). The national health care budget must be managed in such a way to achieve the aim of providing quality health care to all citizens who require assistance. The Department of Nuclear Medicine (DNM) at Universitas Academic Hospital (UAH) also strives to achieve a budget that is cost-effective and still provides quality health care to all patients. One of the essential functions of the DNM at UAH is to provide accurate and early non-invasive detection of tumours and malignant diseases which play an important role in the diagnosis, staging, treatment and prognosis of a cancer patient (Chen *et al.* 2006:342).

In the search for the ideal diagnostic radiopharmaceutical for IFI/IF and/or tumour detection, the South African National Nuclear Energy Corporation (Necsa) has developed two different local radiolabelling routes, the first a direct labelling (DL) method and the second, a kit formulation (KF) of ethylenedicysteine deoxyglucose (EC-DG) for this purpose. Hence, this EC-DG can be labelled in-house with $^{99m}\text{TcO}_4^-$ at the DNM at UAH. In the text that will follow the synthesised ^{99m}Tc -EC-DG with the new labelling method will be referred to as the IHP ^{99m}Tc -EC-DG. Schechter *et al.* (2009:1583) concluded that ^{99m}Tc -EC-DG has adequate properties for a diagnostic glucose tumour-imaging agent. Controversies exist on whether ^{99m}Tc -EC-DG can differentiate IFI/IF from tumours (Case *et al.* 2012; Yang *et al.* 2005:32). Schechter *et al.* (2009:1583) also recommended that ^{99m}Tc -EC-DG should be further evaluated for its diagnostic potential. After *in-vitro* testing of new radiopharmaceuticals is completed, the next step is to evaluate the radiopharmaceutical as part of pre-clinical research phase (animals). The reason for this is that occasionally a

radiopharmaceutical can demonstrate satisfactory and promising characteristics, but *in vivo* results can be inadequate, e.g. fast clearance and unwanted accumulation in organs or tissue (Oyen *et al.* 2001:152). As the *in vitro* research on ^{99m}Tc -EC-DG (Yang *et al.* 2001:513-514) was completed with success, the mandatory next step was to evaluate the IHP ^{99m}Tc -EC-DG (developed at Necsa) biodistribution properties in healthy and disease-induced animals.

1.3 PRE-CLINICAL USE OF RADIOPHARMACEUTICALS

As this research was performed in the RSA this dissertation will focus more on the local regulations and legislation applicable to pre-clinical radiopharmaceutical development. International regulations and legislation related to pre-clinical use of radiopharmaceuticals will be discussed in more detail in Chapter 2. The Medicines Control Council (MCC) of RSA is the local controlling body of the production of drug products (medicines). The MCC published in 2004 the PIC/S Good Manufacturing Practice (GMP) guide version PE 009-2. The manufacture of radiopharmaceuticals (Medicines Control Council 2010:online), relative to clinical trials, but not for pre-clinical studies is addressed. Differences therefore exist between the terminology in-house manufactured and in-house prepared should be clearly defined. The term in-house preparation is defined in this dissertation as the non-industrial, non-commercial small-scale preparation of a radiopharmaceutical in a nuclear medicine department for in-house use for a pre-clinical and clinical study (European Association of Nuclear Medicine (EANM) Radiopharmacy Committee 2007:online; Elsinga *et al.* 2010:1051). The in-house manufacturing of radionuclides and radiopharmaceuticals was done in accordance with GMP for manufacturing on a small-scale. The European Association of Nuclear Medicine (EANM) provides general guidelines for current good radiopharmaceutical practices that include IHP of radiopharmaceuticals in the pre-clinical phase (EANM Radiopharmacy Committee 2007:online). This pre-clinical research was also performed within these prescribed guidelines given by the EANM.

1.4 RADIOPHARMACEUTICALS USED IN THIS RESEARCH

$^{99m}\text{TcO}_4^-$, Gallium-67-citrate (^{67}Ga -citrate) and Fluorine-18-fluorodeoxyglucose (^{18}F -FDG) were compared in different animal models with the investigative radiopharmaceutical

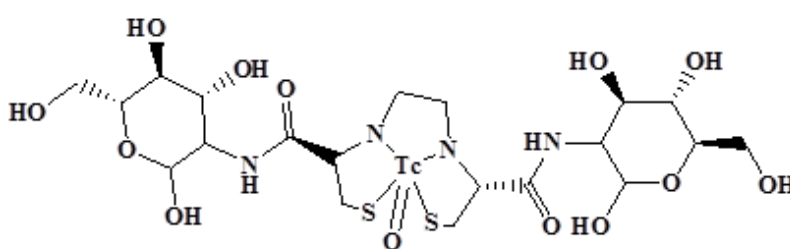
IHP ^{99m}Tc -EC-DG. Each of these comparative radionuclides and radiopharmaceuticals ($^{99m}\text{TcO}_4^-$, ^{67}Ga -citrate and ^{18}F -FDG) has advantages and disadvantages that make it unique and valuable for use in this research project. A summary of the characteristics $^{99m}\text{TcO}_4^-$, ^{67}Ga -citrate and ^{18}F -FDG is given in Chapter 2 with a full literature review on these specific radionuclides and radiopharmaceuticals.

1.4.1 ^{99m}Tc -EC-DG

In the next section molecular formula of ^{99m}Tc -EC-DG is given and the chemical structure of the IHP ^{99m}Tc -EC-DG. The principle of how ^{99m}Tc -EC-DG is metabolised by the cell that makes tumour imaging possible is also discussed.

1.4.1.1 ^{99m}Tc -EC-DG molecular formula and cellular uptake

Two amino-deoxyglucose (also known as 2-D-glucosamine) molecules (National Center for Biotechnology 2014:online) are conjugated to EC and can then be labelled with $^{99m}\text{TcO}_4^-$ (Xiong & Chen 2008:377). The molecular formula for IHP ^{99m}Tc -EC-DG is $\text{C}_{20}\text{H}_{34}\text{N}_4\text{O}_{12}\text{S}_2\text{Tc}$ and the chemical structure is illustrated in Figure 1.2. The molecular weight for ^{99m}Tc -EC-DG is 685.54 gram per mol (g/mol). ^{99m}Tc -EC-DG has an amino group at position two of the sugar (Yang *et al.* 2005:31).



(Tc=Technetium; H=Hydrogen; N=Nitrogen; NH=Nitrogen and Hydrogen; O=Oxygen; OH=Oxygen and Hydrogen; S=Sulphur)

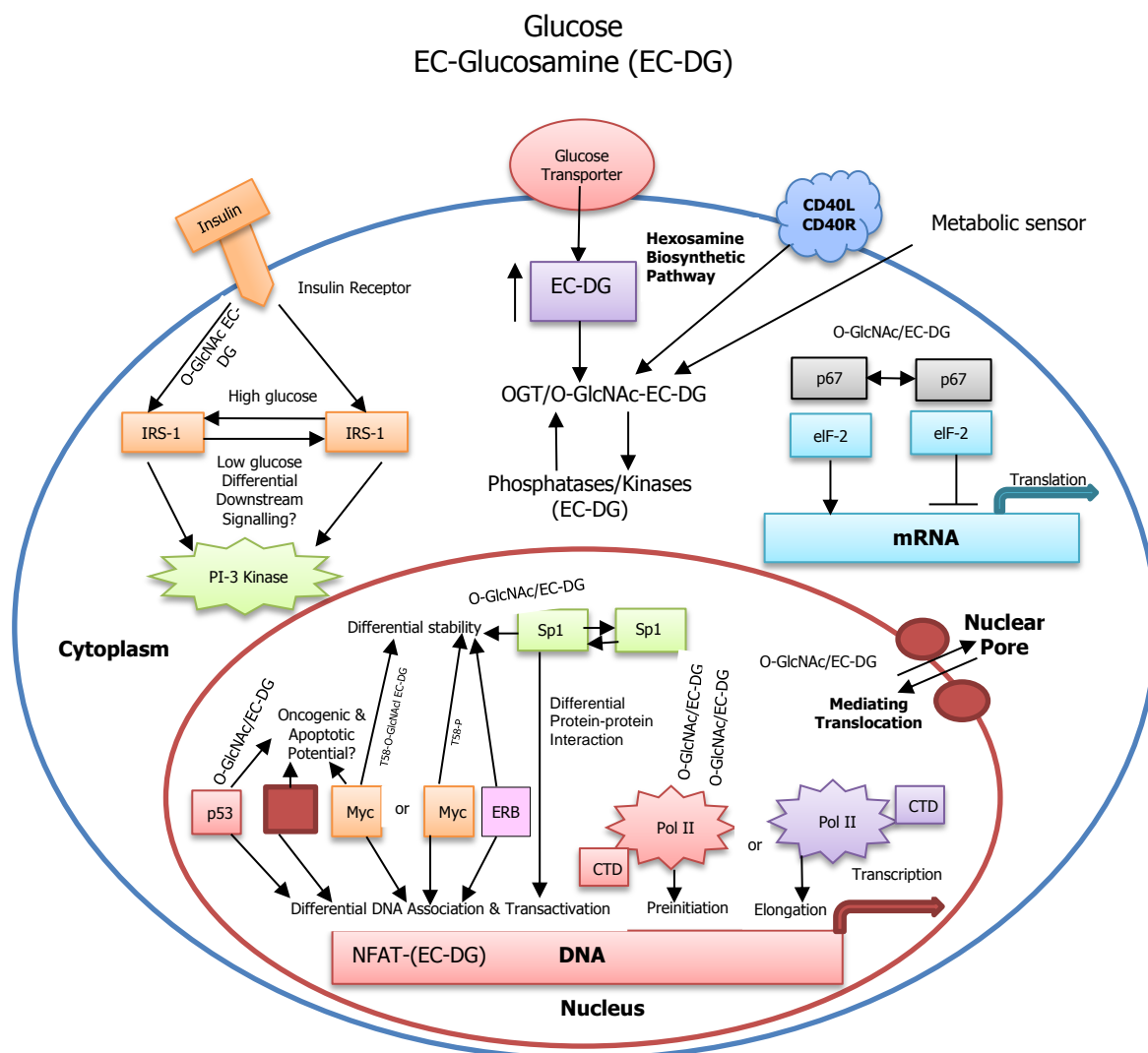
FIGURE 1.2: The chemical structure of IHP ^{99m}Tc -EC-DG (PROVIDED COURTESY OF Necsa)

1.4.1.2 Uptake mechanism of ^{99m}Tc -EC-DG in tumour cells

Tumour cells have increased proliferation and metabolic rates in order to meet the energy consumption requirement for their increased cellular growth

(Almeida & Barry 2010:129). ^{99m}Tc -EC-DG enters the cell using a glucose-mediated process (hexosamine biosynthetic pathway) via glucose transporters where it is phosphorylated illustrated in Figure 1.3 (Schechter *et al.* 2009:1584; Yang *et al.* 2005:31). The glucosamine-6-phosphate produce regulatory products that set in motion processes that include insulin activation, downstream signalling, and tumour growth (Zhang *et al.* 2012:2). Overexpression of glutamine: fructose 6-phosphate amidotransferase (GFAT) is activated by the upregulated glucose transporters during this glucose-mediated process. The explanation of ^{99m}Tc -EC-DG uptake in tumours through this glucose-mediate process may also lay in that EC-DG has significant structural positions (2 and 6) for D-glucosamine. Furthermore, EC has linkage positions at the two COO-arms and two thiol's (SH). Molecular modifications take place during the synthesis through the peptide linkage between position 2 of the sugar with EC and occurs at the two carboxy groups of EC (Yang *et al.* 2005:31).

A peptide bond linkage is created by EC with two SH's which can interact with glycoproteins in the lumen part of the cell membrane [like Oxygen-linked N-acetylglucosamine (O-GlcNAc)]. The EC-DG SH bonds, fix to cytosolic and transmembrane enzymes (Beta-N-acetylglucosaminidase and O-GlcNAc transferase) and membrane associated proteins (O-GlcNAc) and then forms EC-DG disulphate (S-S) protein linkages. Furthermore, this S-S bridge protein linkages then provides the necessary support for EC-DG to internalise the cell (Yang *et al.* 2005:31). Phosphorylated glucosamine takes place at two positions (1 and 6) and interacts with uridine diphosphate (UDP) then forms uridine diphospho-N-acetylglucosamine (UDP-GlcNAc) at those same positions (Yang *et al.* 2005:31; Zhang *et al.* 2012:2). This process also involves interaction between nuclear and cytosolic proteins. The O-GlcNAc takes part in hexosamine pathway and is abundant in all multicellular eukaryotes and cell nucleus activity. Glycosylation also plays a part of posttranslational modification and modifies a considerable number of nucleocytoplasmic proteins. Oxygen-linked N-acetylglucosamine (GlcNAc) Transferase (OGT) is sensitive to the concentrations of UDP-GlcNAc and UDP in the cell. The UDP-GlcNAc and UDP on the other hand is easily affected by glucose concentrations and other stimuli.



[CD40L = Cluster of Differentiation 40 (glycoprotein) Ligand; CD40R = Cluster of Differentiation 40 (glycoprotein) Receptor; DNA = Deoxyribonucleic Acid; ERB=Endoplasmic Reticulum Binding; IRS = Insulin Receptor Substrate; mRNA = Messenger Ribonucleic Acid; Myc = Myelocytomatosis Oncogene Cellular Homolog; NFAT = Nuclear factor of activated T cells; p53 = Tumour suppressor protein that protects from DNA damage; p67 = Phosphoprotein; PI-3 = Phosphatidylinositol 3; O-GlcNAc = Oxygen-linked protein N-acetyl-glucosamine; OGT = Oxygen-linked N-acetylglucosamine (GlcNAc) Transferase; PolII = polymerase II; SH = Thiol functional group; Sp1 = Specific protein 1]

FIGURE 1.3: The unique mechanism of EC-DG to internalise the cell (ADOPTED AND REDRAWN FROM Yang *et al.* 2005:32)

In the cell nucleus the O-GlcNAc also extensively modifies specific protein 1 (Sp1) that is a ubiquitous transcription factor. In response to the increased glucosamine or hyperglycemia, Sp1 becomes hyperglycosylated. Insulin is activated by the regulatory products of glucosamine-6-phosphate which initialises low glucose differential downstream signalling and translocation (Yang *et al.* 2004:444). The consequence is the up-regulation of messenger ribonucleic acid (mRNA) expression and tumour growth. Research has confirmed the involvement of O-GlcNacylation in transcription, signalling in the cytoplasm, implying that O-GlcNAc has protein and site-specific effects on the

biochemistry and metabolism in the cell (Schechter *et al.* 2009:1584). Subsequently, this specific characteristic involvement of ^{99m}Tc -EC-DG with O-GlcNAc in the hexosamine pathway and cell nuclei activity makes it an appealing radiopharmaceutical for differential diagnosis in tumours (Yang *et al.* 2005:31; Zhang *et al.* 2012:2). ^{99m}Tc -EC-DG accumulates in tumour cells and has a unique structure that is involved in cell nuclei activity (Yang *et al.* 2004:444; Zhang *et al.* 2012:2).

1.5 NUCLEAR MEDICINE MOLECULAR IMAGING MODALITIES

The results of in-depth analysis of the advantages, disadvantages and differences of PET, Single Photon Emission Computed Tomography (SPECT), SPECT/CT, PET/CT, PET/MRI and microPET/SPECT/CT as molecular imaging systems will be discussed in Chapter 2 of this dissertation. The microPET/SPECT/CT imaging modalities advantage is that functional and anatomical information can be obtained without sacrifice of the animal. Nuclear medicine imaging modalities used in animal research can also evaluate disease progression and the response to therapy (Koba *et al.* 2013:319). This advantage has led to reduction in animals needed to be sacrificed for research purposes (Koba *et al.* 2013:323). Two major molecular imaging modalities PET versus SPECT are discussed.

1.5.1 PET versus SPECT

SPECT and PET, as molecular imaging modalities and in combination with CT have different advantages when it comes to anatomical/physiological organ and tumour localisation. PET imaging demonstrates a two to three times greater sensitivity to detect emitted events compared to SPECT (Rahmim & Zaidi 2008:194) which can be attributed to its coincidence detection design (PET cameras also has no collimators). Even though SPECT cameras use collimators the image resolution is acceptable.

1.6 ANIMAL MODELS USED IN THIS RESEARCH

The summation of different diseases and physiological conditions present in humans can be replicated accurately by the use of animal models for research (Stout 2012:6). Research utilizing an *in vitro* technique with isolated cells or cell colonies does not

replicate the complex environment present in living animals as with the use of an *in vivo* technique. The proposed animal research with a limited budget included nude mice, rabbits and baboons as the three putative models for different parts of the research. The additional reason for choosing these three specific animal types was availability - rabbits and baboons are available at the University of the Free State (UFS) Animal Research Centre next to UAH reducing the logistical complications to obtain the research animals making this research easier to perform. The animal species selected for the research were also relatively easy to handle. All three of these different types of animal models were utilised to obtain different research data that contributed to the evaluation of the diagnostic potential of the IHP ^{99m}Tc -EC-DG.

Hence, the research evaluated the biodistribution of IHP ^{99m}Tc -EC-DG in healthy animals (mice, rabbits and baboons), lung tumour-bearing mice and rabbits induced with septic and sterile IFI/IF as part of the research with three different phases, to evaluate the diagnostic potential of IHP ^{99m}Tc -EC-DG. A characteristic of a cancer cell is that it usually has an accelerated metabolism, high glucose consumption, thus, an increased uptake of glucose (Chen *et al.* 2006:342). In order to understand the transport mechanism of a molecular glucose imaging agent into and out of cells, a background relating to the physiology of glucose transport of tumour-, infection and inflammation (distinctly) and healthy cells is discussed in Chapter 2.

1.7 PROBLEM STATEMENT

^{18}F -FDG is currently the gold standard in glucose metabolism imaging agents for tumours, but is not used by all nuclear medicine private practices and government nuclear medicine departments due to the following reasons:

- ^{18}F is cyclotron produced thus expensive for consumers that do not have their own cyclotron for production. Flight cost charges further increase the price if it has to be transported over long distances.
- Special motivations have to support ^{18}F -FDG PET/CT diagnostic studies to be performed in private practice, if the government department does not have their own PET camera.
- Not all medical aids provide funding for ^{18}F -FDG studies due to their high cost and patients cannot always afford to pay R18 000 – R25 000 for a diagnostic study.

- PET cameras are expensive and not all government or private practices can afford this equipment, especially if sold combined as hybrid devices (PET with CT).

There is also other limitations to ^{18}F -FDG e.g. short physical half-life (no late imaging can be performed), inability to distinguish between IFI/IF and tumours, high brain uptake (difficult to evaluate low grade tumours even with SUV). Since these impacts the use of ^{18}F -FDG negatively there is a need for a glucose metabolism imaging agent overcoming these challenges. The newly synthesised IHP $^{99\text{m}}\text{Tc}$ -EC-DG (also glucose analogue) has to be investigated for its IFI/IF and tumour imaging characteristics to define its application and place in the spectrum of diagnostic imaging radiopharmaceuticals.

1.8 AIM

The aim of the research was to evaluate the biodistribution pattern of IHP $^{99\text{m}}\text{Tc}$ -EC-DG in tumour- induced, septic and sterile- induced IFI/IF and specific healthy animals at various scintigraphic imaging time intervals using different animal models.

1.9 OBJECTIVES

Each phase in this research had a specific objective in order to be able to achieve the aim. In the next section the objective of each of the research phases will be shortly stated:

- **Phase one – mice study:** To determine whether there was a difference in the biodistribution patterns of IHP $^{99\text{m}}\text{Tc}$ -EC-DG and ^{18}F -FDG in healthy nude mice and tumour-bearing mice at different time intervals.
- **Phase two – rabbit study:** To determine whether there was a difference in the biodistribution pattern of $^{99\text{m}}\text{TcO}_4^-$ and IHP $^{99\text{m}}\text{Tc}$ -EC-DG in healthy rabbits and evaluate IHP $^{99\text{m}}\text{Tc}$ -EC-DG biodistribution in rabbits induced with septic- and sterile IFI/IF compared to ^{67}Ga -citrate.

- **Phase three – baboon study:** To determine whether there was a difference in the normal biodistribution patterns of $^{99m}\text{TcO}_4^-$ and IHP $^{99m}\text{Tc-EC-DG}$ at different time intervals in healthy baboons.

1.10 SCOPE OF THE RESEARCH

The research was conducted in the field of Clinical Nuclear Medicine in the area of diagnostic Nuclear Medicine Health Care. Nuclear Medicine Health Care provides a spectrum of diagnostic and therapeutic services which include the diagnosis and staging of cancer, infection and several other disease processes through the utilisation of scintigraphic procedures which demonstrates the relevant physiological or pathophysiological changes. The central theme for the research is the search for a cost-effective radiopharmaceutical (imaging agent or tracer) for future research in the diagnosis of cancer and IFI/IF.

1.11 SCIENTIFIC CONTRIBUTION OF THE RESEARCH

Ethylenedicysteine-deoxyglucose (EC-DG) in its pure form is very sensitive to light, temperature and humidity that complicates labelling with $^{99m}\text{TcO}_4^-$. $^{99m}\text{Tc-EC-DG}$ could not be effectively labelled for biodistribution studies from the techniques and methods described in the literature (Yang *et al.* 2003:466). A different direct labelling method was employed in this study to obtain a labelling efficiency of between 90-99% to produce the IHP $^{99m}\text{Tc-EC-DG}$. This was also compared with results of the direct labelling method of $^{99m}\text{Tc-EC-DG}$ described by Yang *et al.* (2003:466). The final steps of labelling the $^{99m}\text{TcO}_4^-$ with the EC-DG for the DL method of the IHP $^{99m}\text{Tc-EC-DG}$ contains additional buffering steps compared to the labelling technique described by Yang *et al.* (2003:466) in the literature. In Table 1.1 the difference in amounts of the two key chemical ingredients, EC-DG and SnCl_2 is given of that used in this research and in the literature by Yang *et al.* (2003:466). This validates that the IHP EC-DG when labelled with $^{99m}\text{TcO}_4^-$ is similar to that described in the literature, but differences in the amount of chemical ingredients used exist. This new approach managed to deliver reproducible labelling results which will make it easier to utilise in a clinical setting.

TABLE 1.1: Summary of the differences in the amounts of EC-DG and SnCl₂ needed for the IHP ^{99m}Tc-EC-DG (DL) compared with ^{99m}Tc-EC-DG found in the literature (ADAPTED FROM Yang *et al.* 2003:466)

Chemical compounds	IHP ^{99m} Tc-EC-DG	^{99m} Tc-EC-DG in the literature (Yang <i>et al.</i> 2003:466)
EC-DG	10 mg	80-100 mg
SnCl ₂	0.1 mg	0.1 mg

The biodistribution results obtained from the lung tumour-induced mice for IHP ^{99m}Tc-EC-DG is compared with data reported in literature (Yang *et al.* 2003:470). The comparison of the IHP ^{99m}Tc-EC-DG biodistribution with ⁶⁷Ga-citrate in rabbits with induced septic (*E. coli*) and sterile (zymosan) IFI/IF done with this study was not mentioned previously in the literature. The scientific contribution therefore will be to determine if the biodistribution of IHP ^{99m}Tc-EC-DG to the area of induced septic and sterile IFI/IF is superior to the IFI/IF biodistribution of ⁶⁷Ga-citrate.

Cell>Point (private biopharmaceutical company) situated in the United States of America with The University of Texas M.D. Anderson Cancer Centre has patented EC technology that includes ^{99m}Tc-EC-DG in various countries including China, Australia, Hong Kong, India, Israel, South Korea, Poland and Canada (Cell>Point 2015:online). Research with ^{99m}Tc-EC-DG has progressed to clinical trials phase three in the United States of America. The research that was performed with IHP ^{99m}Tc-EC-DG in this study will make a contribution to the existing data. Limited clinical experience with IHP ^{99m}Tc-EC-DG may be further enlightened by the publication of this research.

1.12 SIGNIFICANCE OF THE RESEARCH

The IHP ^{99m}Tc-EC-DG could be a more cost effective and more affordable diagnostic radiopharmaceutical compared to ¹⁸F-FDG for infection and tumour imaging. This research therefore forms the basis for future research in humans for the diagnostic potential of the IHP ^{99m}Tc-EC-DG as a tumour and IFI/IF imaging agent. The evaluation of the biodistribution patterns of IHP ^{99m}Tc-EC-DG in healthy animals, septic and sterile IFI/IF induced animals and lung tumour-bearing animals will establish the diagnostic potential of the IHP ^{99m}Tc-EC-DG as a scintigraphic IFI/IF and/or tumour imaging radiopharmaceutical in animals.

1.13 PRE-CLINICAL ETHICAL CONSIDERATIONS OF RESEARCH PHASE ONE TO THREE

Approval was obtained from:

- Ionising Radiation Control Commission Committee (Appendix A) for phase 1-3
- UAH (Clinical Services and DNM) – scintigraphic imaging of animal models phase 2 and -3 (Appendix B)
- NWU Ethics Committee – animal studies phase 1 (Appendix C)
- UFS Interfaculty Animal Ethics Committee phase 1-3 (Appendix D)

The research adhered to all relevant RSA legislation, Acts and regulations for the use of animals for scientific purposes and pre-clinical radiopharmaceutical development, this included the following documentation:

- Animal Protection Act No. 71 of 1962
- Animal Disease Act No. 35 of 1984
- Veterinary and Para veterinary Professions Act No. 19 of 1982
- Medicines and Related Substances Control Act No. 101 of 1965
- SANS 10386: 2008. The care and use of animals for scientific purposes

The research was also directed in accordance to the accepted protocol, with reference to Good Laboratory Practices (GLP). Primary considerations encompassed the wellbeing of the research animals, in addition to the ensuring that all research personnel involved adheres to the general rules for working with radionuclide and radiopharmaceuticals at laboratories and at the animal research facilities.

1.14 OUTLINE OF THE DISSERTATION

The following structure gives an overview of the entire dissertation. It aims to guide the reader through the initial examination of and background to the research question, the methodology used in obtaining data, the analysis, interpretation and discussion of results, the use and application of research findings and finally, providing answers to the initial aim of the study. The structure that the research followed was reported as follows:

- Chapter 1, **Research background** describes the problem statement in relation to the research questions, the overall goal, aims, scope and objectives.

Furthermore, an insight on the scientific contribution and the significance of this research was given.

- Chapter 2, **Literature review** provides a study of relevant national and international literature and documents consulted to generate the theoretical perspective that forms the basis of this research.
- Chapter 3, **Methodology**, is a description of the methodology relative to radiation safety, experimental work and analysis methods used in the research as well as the pilot study, the methods of investigation.
- Chapter 4, **Research phase 1: Mice model**, include the research design, methods, results and discussion of tumour and normal biodistribution in nude mice.
- Chapter 5, **Research phase 2: Rabbit model**, include the research design, methods, results and discussion of normal biodistribution, septic IFI/IF and sterile IFI/IF biodistribution in rabbits.
- Chapter 6, **Research phase 3: Baboon model**, include the research design, methods, results and discussion of normal biodistribution of baboons.
- Chapter 7, **Conclusion, recommendations and limitations** of the research will be provided. A summary of the observations made and further insights to possibilities for **future research** will also be presented.

CHAPTER 2

LITERATURE REVIEW

2.1 INTRODUCTION

The literature review includes the physiology and pathology in the relevant animal models studied, aspects on pre-clinical research, the targeting of glucose metabolism with radiopharmaceuticals to facilitate diagnosis using molecular imaging together with the relevant nuclear medicine instrumentation. A diagrammatic overview of these key concepts is outlined in Figure 2.1.

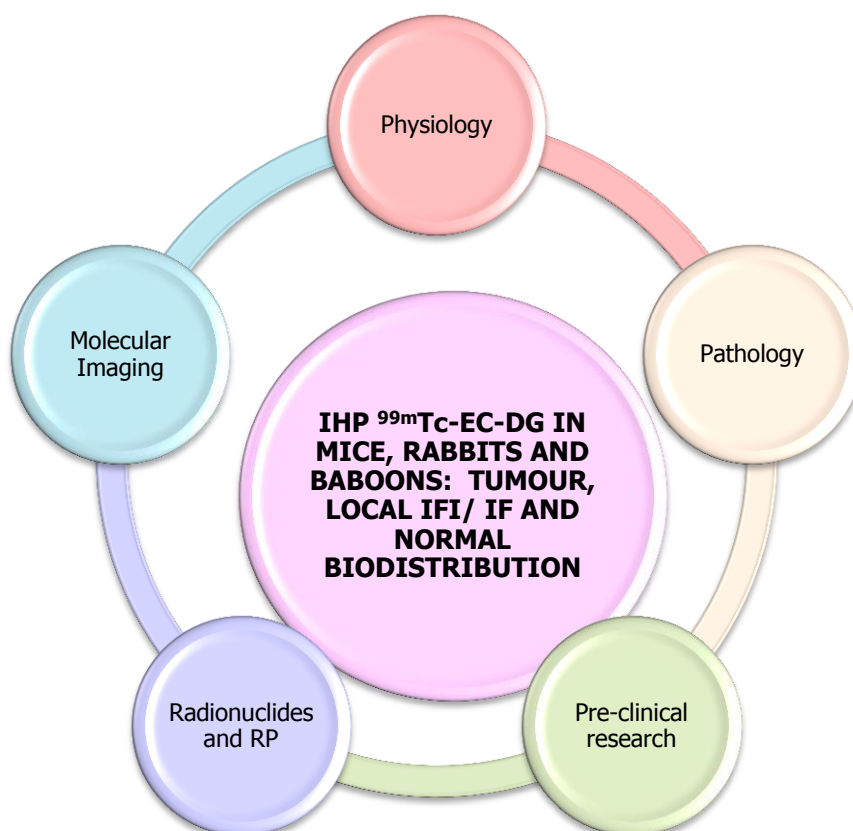


FIGURE 2.1: A diagrammatic overview of the key literature review concepts [Compiled by the Researcher, J. Horn-Lodewyk 2013]

2.2 PHYSIOLOGY

Radiopharmaceuticals can reflect different aspects of physiological-, proliferation-, morphological- and glucose metabolic changes (Velikyan 2014:49). ^{99m}Tc -EC-DG and

^{18}F -FDG are both glucose analogues that enter the cell with aid of glucose transporters and are phosphorylated via hexokinase. The physiological processes of the cell metabolism (glycolysis) and applicable transport of glucose, $^{99\text{m}}\text{Tc}$ -EC-DG and ^{18}F -FDG into the cell especially in normal and diseased conditions (IFI/IF and tumours) were included in the literature review.

2.2.1 Glycolysis

Adenosine Tri-Phosphate (ATP) is the key energy source of many other biochemical pathways and of the biological organism (Nelson & Cox 2004:23). Glycolysis, the source of ATP, is the metabolic reaction (pathway) that breaks down glucose ($\text{C}_6\text{H}_{12}\text{O}_6$) into pyruvate (Nelson & Cox 2004:704-719). The sequence of glycolysis is illustrated in Figure 2.2. Glycolysis does not require oxygen, hence is regarded as an anaerobic pathway that starts in the cytoplasm. It has ten steps in which enzyme catalysed reactions occur. The end products produced are four ATP's and two Nicotinamide Adenine Dinucleotides' (NADH) after completion of the multiple enzymatic reactions where glucose is broken down. Two ATP's are used during the preparatory phase. The key product of glycolysis, NADH, is formed by the 6th reaction to the enzyme dehydrogenase. NADH is an electron carrier with the potential to produce more ATP by a process called oxidative phosphorylation.

Glycolysis is divided into two phases:

- (a) The Preparatory phase:** This is the first five steps in the metabolic pathway from glucose to the formation of Glyceraldehyde 3-Phosphate (GADP). ATP (energy) is consumed (1st and 3rd steps) and turned into Adenosine Di-Phosphate (ADP), also known as the investment phase.
- (b) The Pay-off Phase:** The next five steps of glycolysis produces 4 ATP molecules when glyceraldehyde-3-phosphate (GADP) is converted to pyruvate. The energy restored during this phase is known as the Pay-off phase or the harvesting stage. ATP or energy is created either in the form of ATP alone or in the form of nicotinamide adenine dinucleotide – hydrogen (NADH) + H^+ which can be later converted to ATP via the electron transport chain.

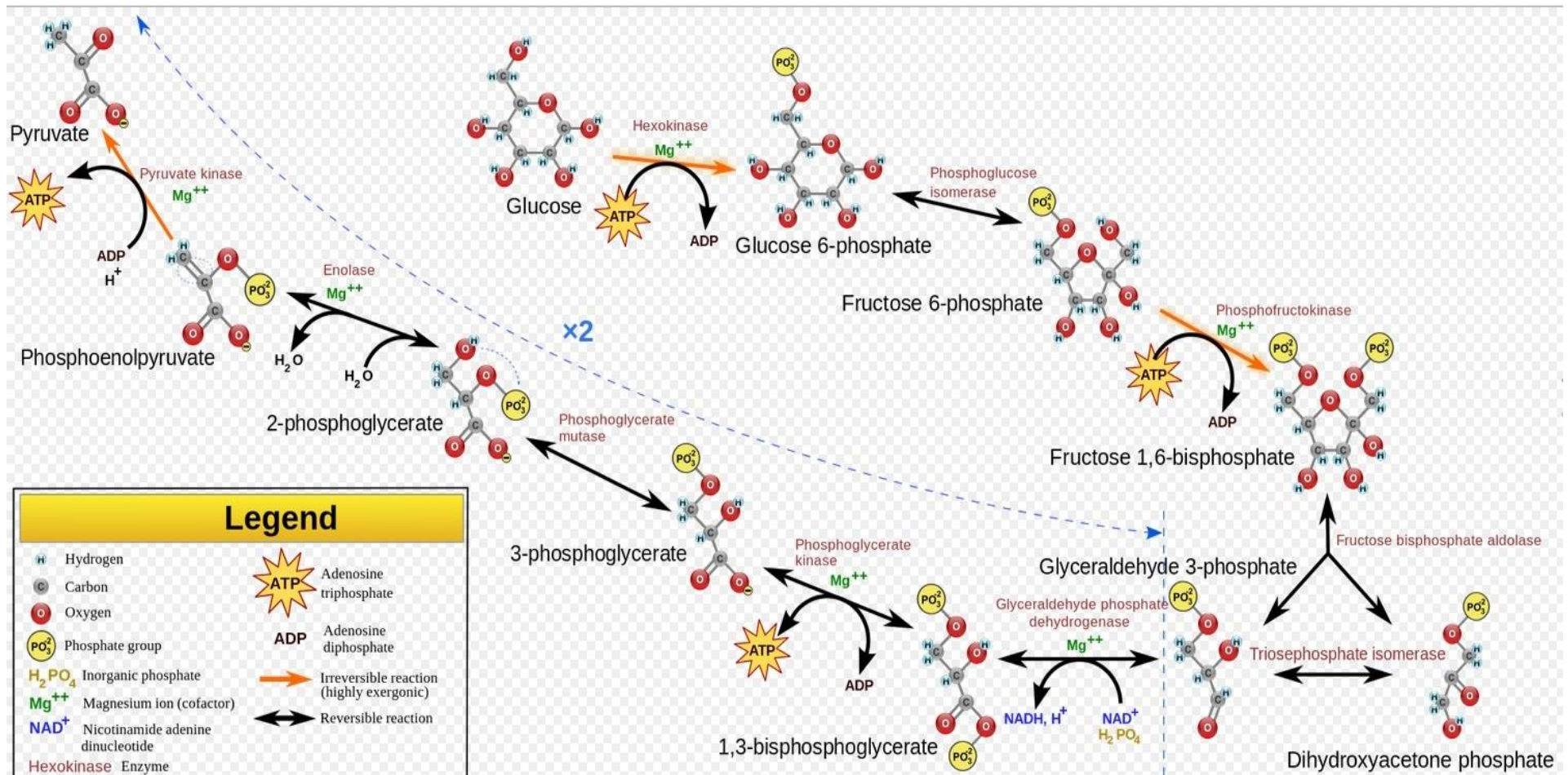


FIGURE 2.2: Representation of the different enzymatic processes of glycolysis (Adopted from Mrabet 2009:online)

Glycolysis consists of ten steps as illustrated in Figure 2.3 to Figure 2.12 (Alberts *et al.* 2002:124-125). Step 1: In the first step glucose is phosphorylated by the enzyme hexokinase, where a phosphate group from ATP is transferred to glucose to form glucose 6-phosphate (Figure 2.3). The glucose 6-phosphate is trapped inside the cell because the negative charge of the phosphate disables it to pass through the plasma membrane.

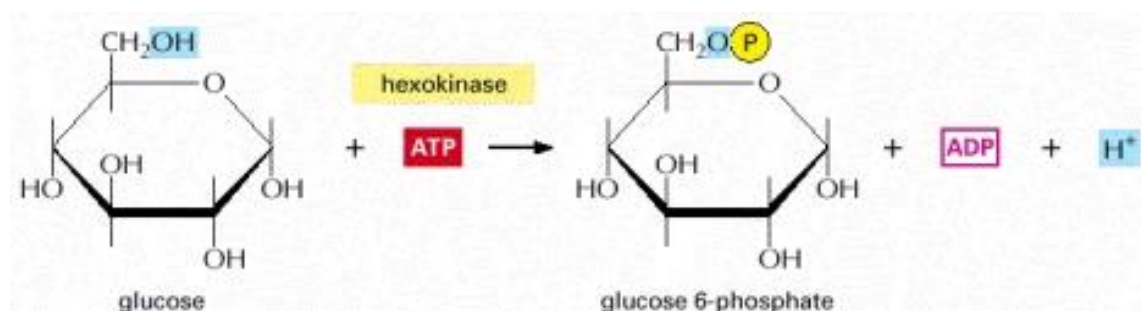


FIGURE 2.3: Step 1 of glycolysis (Adopted from Alberts *et al.* 2002:124)

Step 2: Glucose 6-phosphate is converted by the enzyme phosphoglucose isomerase to isomer fructose 6-phosphate. The carbonyl oxygen is therefore moved from carbon 1 to carbon 2 creating a ketose from an aldose sugar (Figure 2.4).

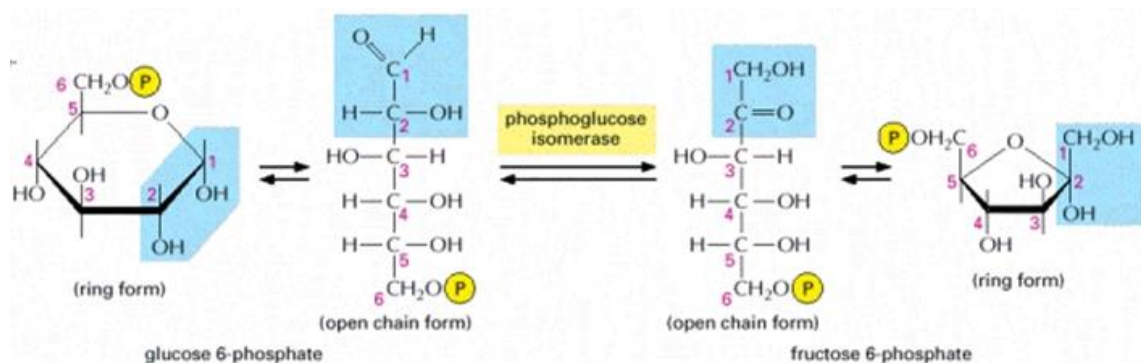


FIGURE 2.4: Step 2 of glycolysis (Adopted from Alberts *et al.* 2002:124)

Step 3: Figure 2.5 illustrates the process where the enzyme phosphofructokinase controls step 3. The ATP molecule moves a phosphate group to fructose 6-phosphate to create fructose 1,6-bisphosphate.

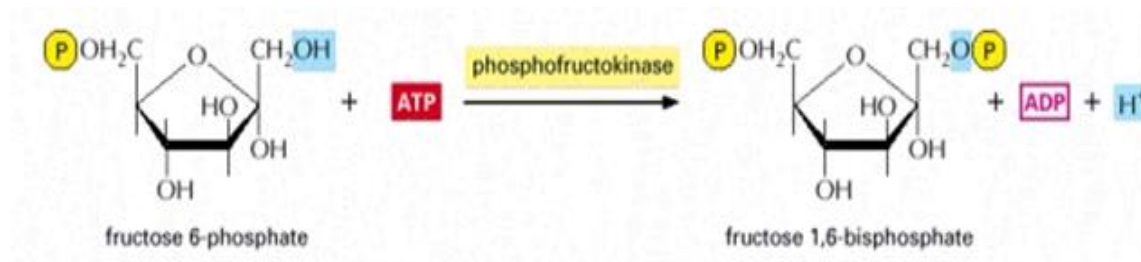


FIGURE 2.5: Step 3 of glycolysis (Adopted from Alberts *et al.* 2002:124)

Step 4: The enzyme aldolase cleaves fructose 1, 6-bisphosphate into two (Figure 2.6) and are called dihydroxyacetone phosphate and glyceraldehyde 3-phosphate. These two sugars are isomers of each other and are called dihydroxyacetone phosphate and glyceraldehyde 3-phosphate.

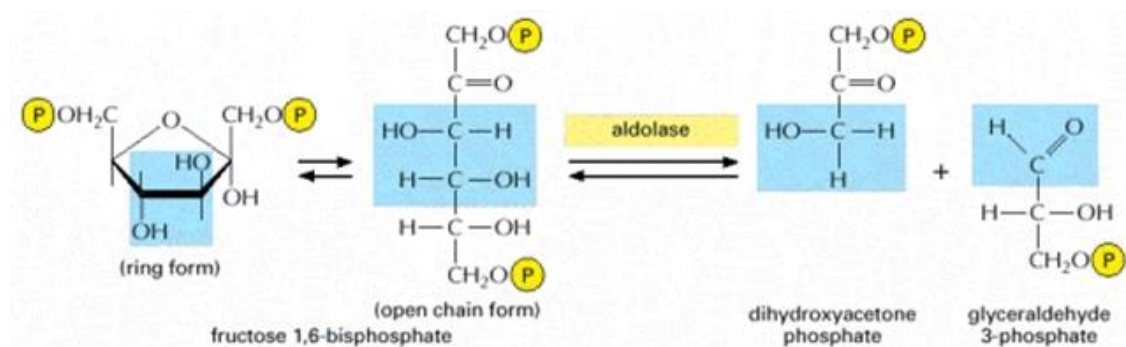


FIGURE 2.6: Step 4 of glycolysis (Adopted from Alberts *et al.* 2002:124)

Step 5: During this step the enzyme triose phosphate isomerase inter-converts the molecules dihydroxyacetone phosphate to form glyceraldehyde 3-phosphate (Figure 2.7).

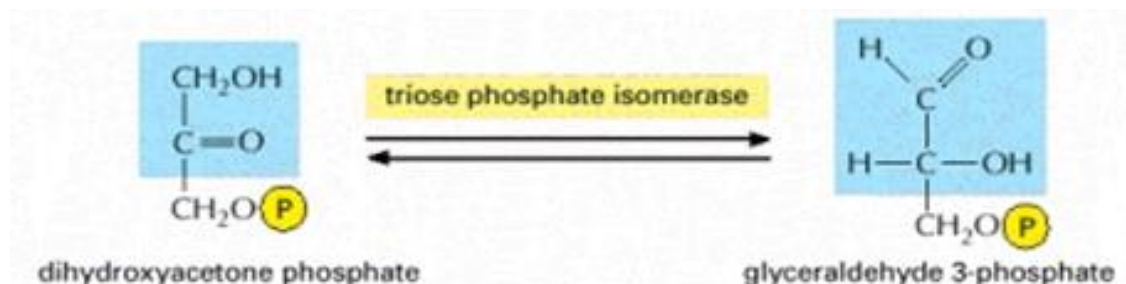


FIGURE 2.7: Step 5 of glycolysis (Adopted from Alberts *et al.* 2002:124-125)

Step 6: The enzyme triose phosphate dehydrogenase firstly transfers a hydrogen from glyceraldehyde phosphate (both molecules are oxidized) to the oxidizing agent nicotinamide adenine dinucleotide (NAD) to create NADH (Figure 2.8). Secondly this enzyme adds a phosphate from the cytosol to the oxidized glyceraldehyde phosphate to form 1, 3-bisphosphoglycerate.. The second phase of glycolysis starts at NADH.

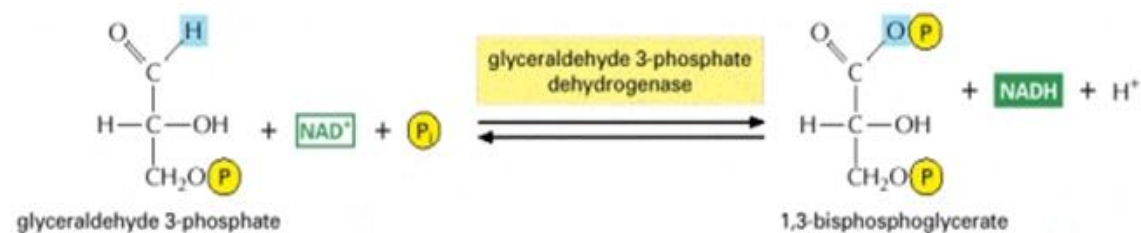


FIGURE 2.8: Step 6 of glycolysis (Adopted from Alberts *et al.* 2002:125))

Step 7: Figure 2.9 illustrates the mechanism of how the enzyme phosphoglycerokinase transfers a high-energy phosphate group from 1,3-bisphosphoglycerate to adenosine di-phosphate (ADP) to form ATP. This takes place for every molecule of 1,3-bisphosphoglycerate. The process produces two 3-phosphoglycerate molecules and two ATP molecules.

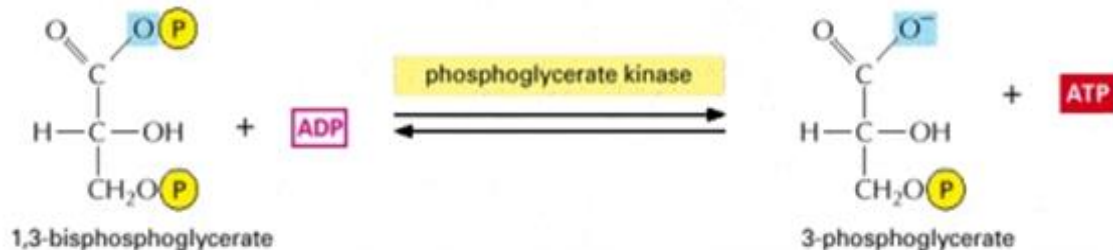


FIGURE 2.9: Step 7 of glycolysis (Adopted from Alberts *et al.* 2002:125)

Step 8: The enzyme involved in step 8 is phosphoglycerate mutase which relocates the remaining phosphate from 3-phosphoglycerate from the third carbon to the second carbon to form 2-phosphoglycerate (Figure 2.10).

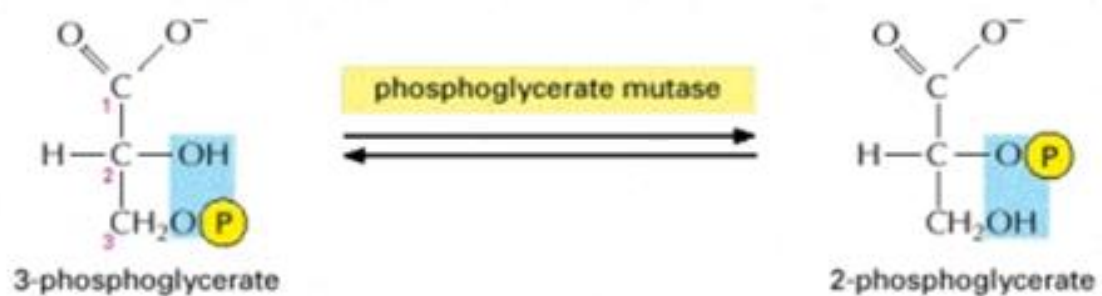


FIGURE 2.10: Step 8 of glycolysis (Adopted from Alberts *et al.* 2002:125)

Step 9: The enzyme enolase removes water from 2-phosphoglycerate to create a high energy enol phosphate linkage called phosphoenolpyruvic acid (PEP) and this is shown in Figure 2.11.

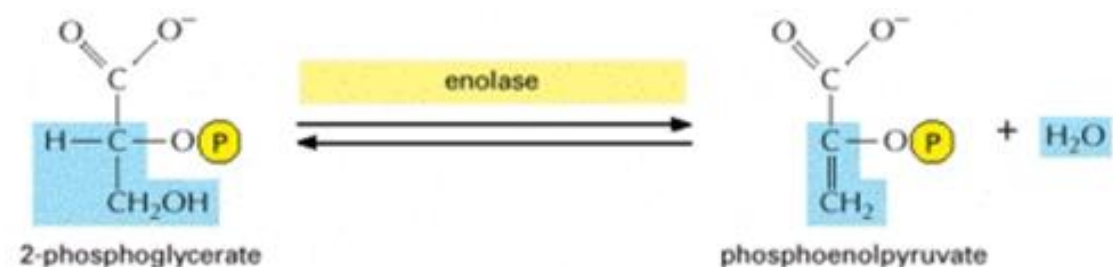


FIGURE 2.11: Step 9 of glycolysis (Adopted from Alberts *et al.* 2002:125)

Step 10: In the final step the enzyme pyruvate kinase transfers a high-energy phosphate group from PEP to ADP to create pyruvate (2 molecules yielded) and ATP (2 molecules yielded), completing the glycolysis pathway (Figure 2.12).

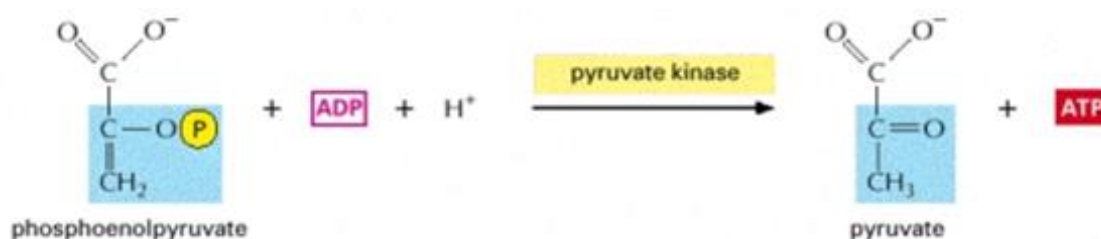


FIGURE 2.12: Step 10 of glycolysis (Adopted from Alberts *et al.* 2002:125)

2.2.2 Glucose transporters

Glucose transporters are unique heterogeneous glycosylated integral membrane proteins that facilitate transport of glucose in and out of the cell via the cell membrane (Pauwels *et al.* 1998:318). The glucose transporters can be divided into two different groups. Sodium glucose transporters (SGLT), SGLT1 and SGLT2 involved in secondary active transport (Brown 2000:237) and glucose transporters (GLUT), ranging from GLUT1 to GLUT13 (Barrett *et al.* 2012:434; Brown 2000:237). FDG- or glucose- or DG molecule in the circulation attaches to the outer part of the transporter protein on the outside of the cell membrane, after which the complex changes formation to move the FDG- or glucose- or DG molecule to the inside of the membrane (Pauwels *et al.* 1998:318). Subsequently the FDG- or glucose- or DG molecule is discharged into the cytoplasm and the transport protein returns to its original form in the membrane.

Transporter proteins are dispersed over the different kinds of tissues in mammals: GLUT 1 is present in ample amounts in erythrocyte cells, GLUT 2 is present in enterocytes and liver cells, GLUT 3 in the brain, GLUT 4 in the skeletal and heart muscle and GLUT 5 in the small intestines and kidneys and GLUT 7 presents primarily in hepatocytes (Pauwels *et al.* 1998:318-319). In Table 2.1 a broader summary of the glucose transporters present in major tissues is given. Under normal conditions glucose is transported in and out of cells via GLUT 1 and GLUT3 (Pauwels *et al.* 1998:319). Glucosamine and FDG's cellular uptake is via a glucose transporting mechanism, as both are glucose analogues. The glucose transporters utilized by ¹⁸F-FDG and ^{99m}Tc-EC-DG is different, ¹⁸F-FDG uses GLUT 1 and GLUT3, whereas ^{99m}Tc-EC-DG uses GLUT 1, GLUT 2 and GLUT 4 (Case *et al.* 2012; Zhang *et al.* 2012:7).

TABLE 2.1: Summary of the glucose transporters in mammals (Barrett *et al.* 2012:435)

	Function	Major sites of expression
Secondary active transport		
SGLT 1	Absorption of glucose	Small intestine, renal tubules
SGLT 2	Absorption of glucose	Renal tubules
Facilitated diffusion		
GLUT 1	Basal glucose uptake	Placenta, blood-brain barrier, brain, red cells, kidneys, colon, many other organs
GLUT 2	B-cell glucose sensor; transport out of intestinal and renal epithelial cells	B cells of islet, liver, epithelial cells of small intestine, kidneys
GLUT 3	Basal glucose uptake	Brain, placenta, kidneys, many other organs
GLUT 4	Insulin-stimulated glucose uptake	Skeletal and cardiac muscle, adipose tissue, other tissues
GLUT 5	Fructose transport	Jejunum, sperm
GLUT 6	Unknown	Brain, spleen and leucocytes
GLUT 7	Glucose 6-phosphate transporter in endoplasmic reticulum	Liver

Malignant cells have increased uptake of glucose and catabolize it to produce energy for glycolysis. The glucose transporters present in malignant cells have increased activity partially contributing to the increased uptake of glucose and glucose analogues into the cell. (Pauwels *et al.* 1998:280). Cancer cells have abundant levels of GLUT 1 and GLUT 3 compared to normal cells (Pauwels *et al.* 1998:319). The increased uptake of glucose in cancer has been attributed to the overexpression of GLUT 1 and GLUT 3 genes. The high GLUT-1 expression is abundant in inflammatory lesions (Mochizuki *et al.* 2001:1554).

2.3 PATHOLOGY

2.3.1 Cancer

Bowen & Orvig (2009:5077-5091) affirm that cancer tissue can be distinguished from normal tissue, as cancer cells have a decrease in oxidative phosphorylation and an increase in glycolysis. Cancer cells require a higher intake of glucose because of their ineffective metabolism as was first described by Warburg (1956:309-314). The characteristic feature of cancer cells to use more glucose than normal healthy cells to achieve the same energy production is also known as the "Warburg effect" (Bowen &

Orvig 2008:5077). The “Warburg effect” was incorporated into cancer research when developing new glucose targeting agents for diagnostic purposes.

2.3.1.1 Tumours

A tumour can be defined as an abnormal growth of tissue due to mutations or irregular activations of specific classes of normal genes that regulate the life cycle of the cell (Pauwels *et al.* 1998a:277). The transformation of normal cells to tumour cells can be caused by exposure to some environmental factors like pathogens (viruses and bacteria), certain chemicals and radiation (ultraviolet and ionizing) (Pauwels *et al.* 1998b:317). Tumours can be divided in two categories benign or malignant. Tumour cells undergo morphological differentiation that include gene modifications (cellular DNA), increased growth, altered cell-to-cell communications, change in cell morphology, modifications of the membrane properties and their receptors, and change in cell metabolism and can develop heterogeneous perfusion due to hypoxia present in certain tumours (Gilles *et al.* 1999:197). In this research we mainly focused on the characteristic of altered metabolism of tumour cells. Since IHP ^{99m}Tc -EC-DG is a glucose analogue and a change in cell metabolism may influence uptake and biodistribution to that cell.

2.3.1.2 Imaging

Cancer like lung-, tracheal-, bronchial cancer and infectious disease are under the top 25 leading causes of death in the RSA (Bradshaw *et al.* 2010:online). Nuclear Medicine as a diagnostic imaging modality plays an important role in the facilitation of early diagnosis of disease as this is where the value of treatment can make an impact on treatment success. The IHP ^{99m}Tc -EC-DG therefore can hold the possibility and affordable diagnostic imaging option to increase the early diagnosis of tumours and IFI/IF. As IFI/IF and tumour imaging forms a large part of Nuclear Medicine scintigraphy, a complete literature review is needed to give a complete background to the research “IHP ^{99m}Tc -EC-DG in rabbits, mice and baboons: normal, infection/inflammation and tumour biodistribution”.

2.3.2 Inflammation

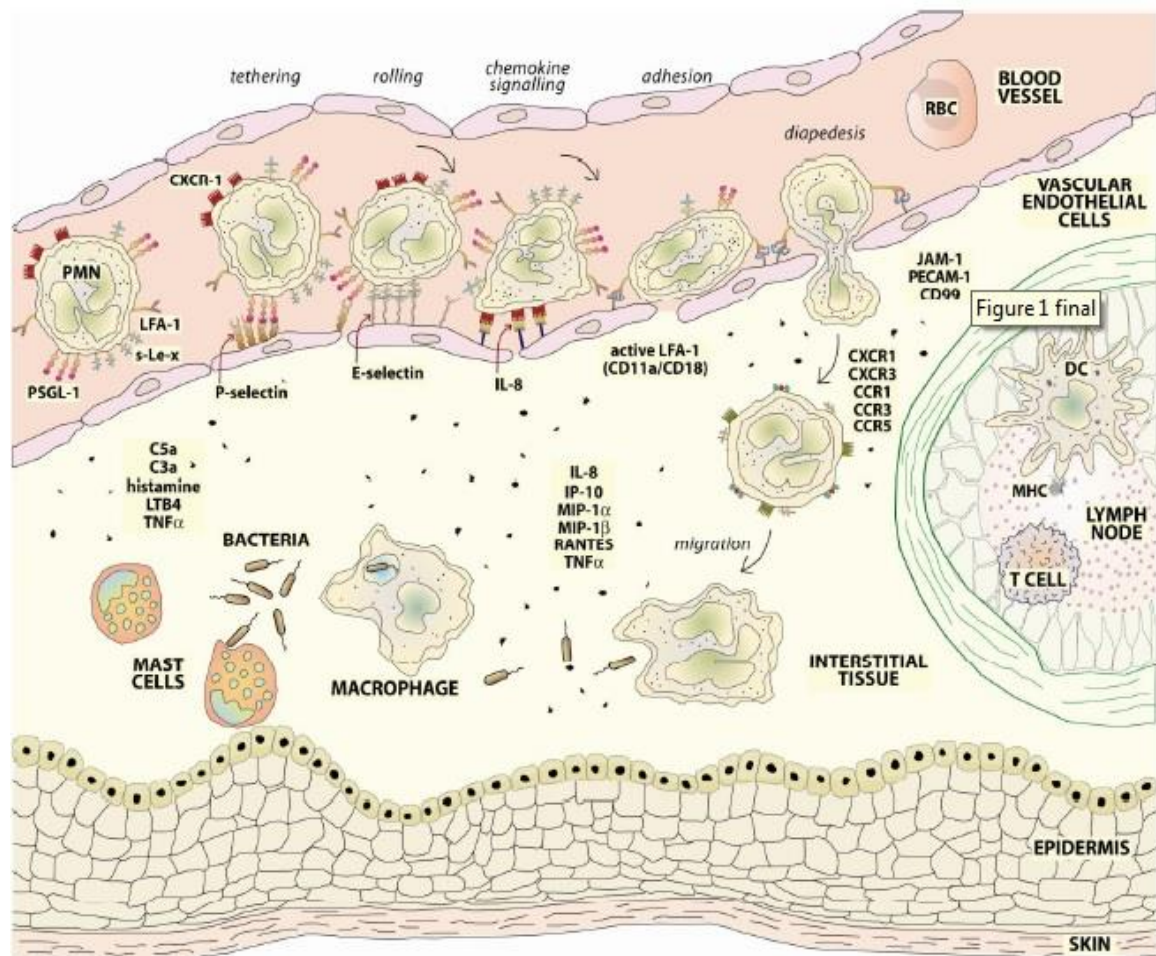
The Oxford Concise Medical Dictionary (2003:350) defines inflammation as the body's reaction to injury to initiate the healing steps, which can be acute (initial response) or chronic (prolonged inflammation). Inflammation and infection are two distinctive processes, even though inflammation can be present with infection. Inflammation can develop without the existence of micro-organisms and can develop from trauma, ischemia, neoplasm, autoimmune invasion or strikes by microorganisms (Petruzzi *et al.* 2009:115). Yet, the most common cause of inflammation is infection with pathogenic organisms. The clinical signs of inflammation include pain, heat, redness, swelling and loss of function of the area inflamed (Bleeker-Rovers *et al.* 2004:2936).

2.3.3 Infection

Infection (as cause of injury) is defined as the invasion of the body by harmful organisms (pathogens) such as bacteria, fungi, rickettsiae, or viruses (Oxford Concise Medical Dictionary 2002:350-351) and the resulting immunological response by the host. Rennen *et al.* (2000:241) outlined the symptomatic response to an acute IFI/IF as the following:

- Locally increased blood supply
- The area involved will display increased vascular permeability
- Increased transudation of plasma proteins
- Increased influx of leucocytes
- Leakage of a fluid

The immune system consists of a selection of specific biological structures and functional processes that aid the shielding of the host organism against disease (Tsopelas 2015:1). It can distinguish healthy tissue from other harmful agents like pathogens (bacteria, viruses, prions, viroids), micro-organisms or toxins. The dendritic cells internalize extracellular antigens to create major histocompatibility complex (MHC) molecules in response to the presence of foreign agents identify the antigen and communicate to other allied cells via pro-inflammatory cytokines (Tsopelas 2015:1).



[PMN = polymorphonuclear neutrophil; CXCR/CCR = chemokine receptor; s-Le-x = sialyl-Lewis X; LFA = lymphocyte function-associated antigen; PSGL = P-selectin glycoprotein ligand; IL = interleukin; CD = cluster of differentiation; CD11a/CD18 = integrins; RBC = red blood cell; JAM = junctional adhesion molecule; PECAM = platelet endothelial cell adhesion molecule; DC = dendritic cell; MHC = major histocompatibility complex; T cell = T lymphocyte; IP-10 = interferon-gamma induced protein-10; MIP = macrophage inflammatory protein; RANTES = regulated on activation, normal T cell expressed & secreted (CCL5 chemokine); TNF α = tumour necrosis factor alpha; C3a; C5a = complement component 3a, 5a; LTB4 = leukotriene B4]

FIGURE 2.13: Illustration of an immune reaction to a bacterial infection (Adopted from Tsopelas 2015:2)

The neutrophils are then initiated from the circulation to the infiltration area. Histamines are discharged by mast cells that then induce vasodilation. Neutrophils partake in the actions of rolling, adhesion and transmigration at the endothelial barriers to enter the area where the antigen is present (Tsopelas 2015:2).

The tethering, rolling, chemokine signalling, adhesion, diapedesis and attack actions that occur during the immunological response are demonstrated in Figure 2.13 and is shortly outlined below (Tsopelas 2015:2):

- Tethering: P-selectins fix to PSGL-1 and tether PMN;
- Rolling: P-selectins carry PMN close to E-selectins, slow rolling is initiated;
- Chemokine signalling: slow rolling permits IL-8 binding to CXCR1, followed by the activation signal to integrins by the internalized chemokine receptor;
- Adhesion: activated LFA-1 binds ICAM-1 or -2 for secure connection;
- Diapedesis: PMN initiates diapedesis by substituting close-fitting junction molecules with endothelial cells;
- Migration: PMN trails a gradient of inflammatory chemokines to pathogens;
- Attack: complement attacks the incoming pathogens, mast cells and macrophage phagocytose pathogens, toll-like receptor molecules activate inflammation, antigen presenting dendritic cells directs MHC molecules to stimulate T lymphocytes and to employ neutrophils.

Leucocytes (migrate from blood stream) are involved in a multifaceted system of intense cell signalling to recruit polymorphonuclear cells, as well as direct and indirect actions to control, damage and eliminate the antigen (Tsopelas 2015:2). Macrophages and T helper cells upon stimulation discharge inflammatory mediators, damaging enzymes (i.e.: myeloperoxidase, xanthine oxidase, etc.) and oxidizers (i.e.: superoxide anions, nitric oxide, hydrogen peroxide, N-chloro equivalents). The stimulated complement system partakes through an accelerated immunoglobulin generation and chemotactic mediators to acquire additional neutrophils. The healing phase starts after the antigen is eliminated by means of mast cells, T helper cells and basophils that discharge interleukin signals (Tsopelas 2015:2). Macrophages are stimulated into releasing tissue repair molecules and angiogenic growth agents. Fibroblast cell growth is activated which then gather at the wound location and multiply into myofibroblasts resulting in the activity of collagen deposition. T lymphocytes and monocytes are employed to this location. Macrophages change their reactions and angiogenesis is encouraged in the course of healing.

According to statistics reviewed in 2005 by the World Health Organisation (WHO) about the cause of deaths, the RSA ranked the lowest regarding quality of data available out of the 115 WHO countries (Bradshaw *et al.* 2010:online). The reason for RSA scoring so low was based on two leading factors, using a grouping of more than

20% of deaths being ill-defined deaths and fewer than 70% of deaths being registered. The quality of the cause of death statistics has improved since undertaken by the WHO, in terms of monitoring the health status of the nation and understanding the burden of disease (Bradshaw *et al.* 2010:online). However, there still remains an urgent need to improve the quality of cause of death certification to indicate direction of areas of diagnosis and treatment of specific treatment to improve mortality due to these high risk diseases. The statistics available from Statistic South Africa showed an increase in deaths due to infection (Figure 2.14) from 1997 to 2007 (Bradshaw *et al.* 2010:online).

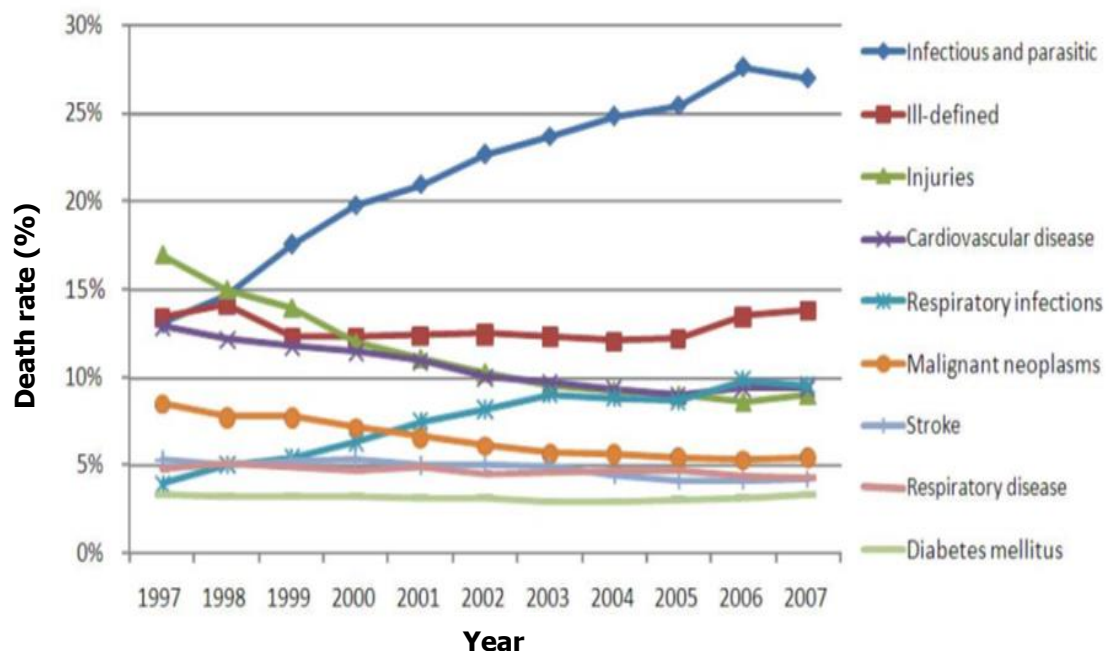


FIGURE 2.14: The trend from 1997-2007 indicating the leading categories for the cause of death in RSA (Courtesy of Bradshaw *et al.* 2010:online).

Diagnostic techniques for the identification of infection consist of clinical examination, laboratory tests (e.g. erythrocyte sedimentation rate, white-blood cell count & acute-phase proteins and cytokines), clinical and radiological tests (Diniz *et al.* 2005:89; Lambrecht *et al.* 2008:161). The disadvantages of some of these tests are that its time- and labor intensive, as well as having slow turnaround time for the results feedback which can influence the outcome of recovery from infection.

2.3.3.1 *Imaging*

The properties for an ideal radiopharmaceutical for the imaging of infection include the following:

- Fast localisation and favourable retaining at the site of infection
- High target-to-background ratio
- No uptake in sterile inflammation, specific to infection for the identification of infections caused by micro-organism
- The radiopharmaceutical uptake should be equivalent to the degree of infection
- No pharmacological consequence (side-effects) or immunological reaction to the radiopharmaceutical and safety should be established for repeated injection to different patients
- Labelling technique should be simple and easy to administer
- The uptake of the radiopharmaceutical should not be dependent on the leucocyte function of the host
- Lower cost than other diagnostic modalities and techniques combined to provide a diagnosis

Structural imaging techniques like MRI, CT and ultrasound are not the best diagnostic procedures for early identification and localisation of infection, as they detect morphological tissue alterations due to infection (Diniz *et al.* 2005:89). Nuclear medicine imaging can provide early non-invasive diagnosis as it is underlined by physiological and functional principles. Another advantage to scintigraphic imaging is that it can provide whole-body imaging, whereas CT and MRI concentrate on a section of the body. Different radiopharmaceuticals and radionuclides are available to localise infection tissue in any location in the body (Mettler & Guiberteau, 2012:397). The decision to use a specific radiopharmaceutical depends on factors like availability of radionuclide or radiopharmaceuticals, availability of a SPECT/PET camera in department, the clinical setting, patient clinical history, and the availability of funding.

The radionuclides and radiopharmaceuticals most frequently used for infection imaging include the following (Mettler & Guiberteau, 2012:397):

- Radiolabelled white blood cells for example ^{111}In labelled leucocytes and $^{99\text{m}}\text{TcCO}_4^-$ labelled with leucocytes
- ^{67}Ga -citrate
- ^{18}F -FDG
- Radiolabeled monoclonal antibodies and antibody fragments
- Radiolabelled peptides

The radiopharmaceuticals and radionuclides each have advantages and disadvantages as indicated in Table 2.2 and are chosen according to clinical indications of the patient and departmental situation. Radiopharmaceuticals for infection detection like $^{99\text{m}}\text{Tc}$ -ubiquitin ($^{99\text{m}}\text{Tc}$ -UBI) that is still in the early pre-clinical phases and are not used on a regular basis in nuclear medicine departments are not listed in Table 2.2. A patient referred to the DNM at UAH for IFI/IF imaging will undergo scintigraphy according to the patient's clinical history. A patient with a clinical history indicating localisation and detection of IFI/IF will undergo either a ^{67}Ga -citrate scintigram or leucocytes labelled with $^{99\text{m}}\text{Tc}$ -hexamethylpropyleneamine (HMPAO), also known as Ceretec scintigram. In RSA ^{67}Ga -citrate is cyclotron produced by iTHEMBA LABS and its availability is influenced by imminent shutdown of production. Indium-111 (^{111}In) is imported from producing countries and not produced in RSA, yet expensive and can only be ordered with special permission at UAH. ^{18}F -FDG as a diagnostic tool for the diagnosis of infection/inflammation is being promoted in the field of research and clinical practice (Buscombe 2013:1120). In RSA and many other countries the use of ^{18}F -FDG for the diagnosis of infection/inflammation has not yet fully been reimbursed, due to the high costs (Buscombe 2013:1120).

The volume of blood needed to label leucocytes *in-vitro* is large in order to ensure that enough white blood cells are obtained for labelling with $^{99\text{m}}\text{Tc}$ -HMPAO or ^{111}In . Rabbits are small animals and it is time-consuming and difficult to obtain large quantities of blood from them for effective leucocyte labelled studies. The marginal ear vein of the rabbits is also very small and that makes the drawing of blood difficult and jugular and cephalic veins rather

have to be used for this purpose. At UAH there is no PET camera available, therefore ^{18}F -FDG was not used as control radiopharmaceutical for the detection of IFI/IF tissue in rabbits.

TABLE 2.2: Radionuclides and radiopharmaceuticals for IFI/IF imaging (Adapted from Mettler & Guiberteau 2012:398; Tsopelas 2014:5-28)

Radionuclide/ Radiopharmaceutical	Indication	Advantages	Disadvantages
^{111}In white blood cells	<ul style="list-style-type: none"> • Vascular graft infections • Osteomyelitis 	<ul style="list-style-type: none"> • No interfering bowel/renal activity • Delayed imaging possible • Simultaneous $^{99\text{mTc}}$-sulfur colloid or $^{99\text{mTc}}$-diphosphonate bone imaging possible • Very sensitive 	<ul style="list-style-type: none"> • Less sensitivity for nonbacterial and nonpyogenic infections • ^{111}In label not ideal for imaging • Complex preparation –technical demanding • Difficult to draw enough blood from children to perform study • Thicker shielding – medium radiation burden
$^{99\text{mTc}}$ -white blood cells (HMPAO)	<ul style="list-style-type: none"> • Detect and localise site of infection • Osteomyelitis • Diabetic foot • Fever of unknown origin • Lung infections • Endocarditis • Infected prosthesis 	<ul style="list-style-type: none"> • Early imaging • Excellent early sensitivity • $^{99\text{mTcO}_4^-}$ labelling ideal with gamma camera imaging • Low radiation burden • $^{99\text{mTcO}_4^-}$ labelled with cells 	<ul style="list-style-type: none"> • Less sensitivity for nonbacterial and nonpyogenic infections • Delayed imaging not ideal • Early renal activity • Bowel activity after 1-2 h • Complex preparation • Long labelling time • Contamination of operator performing labelling procedure with blood (needle stick injuries)– high bio-burden • Risk of reinjecting back another patients blood if more than one study is performed • Difficult to draw enough blood from children to perform study • Need specialised equipment to label blood
^{67}Ga -citrate	<ul style="list-style-type: none"> • Aid in detecting some acute inflammatory lesions • Fever of unknown origin • Pulmonary and mediastinal inflammation/infection • Follow-up of active lymphocytic or granulomatous inflammatory disease such as sarcoidosis or tuberculosis • Vertebral osteomyelitis and/or disk space infection • Infections in immunocompromised patients • Retroperitoneal fibrosis 	<ul style="list-style-type: none"> • A variety of infections detected, including opportunistic • Do not have to label to radiopharmaceutical can be directly injected to patient • No blood cell labelling is involved – low risk contamination and bioburden 	<ul style="list-style-type: none"> • Interfering bowel and renal activity • Delayed imaging necessary usually over 48 h • ^{67}Ga not ideal for imaging, need also special equipment like medium energy collimator • Thicker shielding – higher radiation burden • Most often have to be ordered from an external suppliers and as cyclotron produced can have shut-down times with no or reduced availability
^{18}F -FDG	<ul style="list-style-type: none"> • For determining the location and extent of identification of regions of abnormal glucose metabolism associated • Inflammatory disorders like sarcoidosis, rheumatologic disease and vasculitis 	<ul style="list-style-type: none"> • Excellent spatial localisation • Very sensitive • Do not have to label to radiopharmaceutical can be directly injected to patient • No blood cell labelling is involved – low risk contamination • No biological burden 	<ul style="list-style-type: none"> • Not currently approved by the Food and Drug Administration (FDA) for infections • Non specific; also localises in tumours • Thicker shielding – higher radiation burden • Expensive as cyclotron produced • Non-specific • Special equipment needed – PET camera
$^{99\text{mTc}}$ -MDP (three phase bone studies)	<ul style="list-style-type: none"> • Skeletal imaging infections osteomyelitis 	<ul style="list-style-type: none"> • Sensitive for bone infections • Available in most nuclear medicine departments 	<ul style="list-style-type: none"> • Non-specific • Bone infections only • Need to use in conjunction with a specific infection imaging agent like

Radionuclide/ Radiopharmaceutical	Indication	Advantages	Disadvantages
		<ul style="list-style-type: none"> • $^{99m}\text{TcO}_4^-$ labelling no special equipment needed • Rapid labelling with kit • No blood cell labelling involved – no bio-burden 	^{99m}Tc -HMPAO
^{99m}Tc -Leukoscan	<ul style="list-style-type: none"> • Infection/inflammation in bone in patients with suspected osteomyelitis, including patients with diabetic foot ulcers 	<ul style="list-style-type: none"> • Fast localisation in infection within 1-9 hours • $^{99m}\text{TcO}_4^-$ labelling ideal with gamma camera imaging 	<ul style="list-style-type: none"> • Human anti-mouse antibody response
^{99m}Tc -Scintimun	<ul style="list-style-type: none"> • For determining the of IFI/IF in peripheral bone in adults with suspected osteomyelitis 	<ul style="list-style-type: none"> • Fast localisation in infection within 1-3 hours • $^{99m}\text{TcO}_4^-$ labelling ideal with gamma camera imaging 	<ul style="list-style-type: none"> • Anaphylactic reactions • Anaphylactoid reactions • Human anti-mouse antibody response
^{99m}Tc -Nanocoll	<ul style="list-style-type: none"> • Bone marrow imaging (hematopoietic activity) • Inflammation scanning (abdomen) 	<ul style="list-style-type: none"> • Fast localisation in inflammation area within 45-60 minutes • $^{99m}\text{TcO}_4^-$ labelling ideal with gamma camera imaging • Easily prepared • No labelling of cells involved 	<ul style="list-style-type: none"> • Hypersensitivity to active substance • Non-reactive to hepatitis B surface antigen • Non-reactive to antibodies towards the human immuno- deficiency virus • Non-reactive to hepatitis C virus • Nonspecific • Can not image infections outside the skeletal system
^{99m}Tc - or ^{111}In -labelled chemotactic peptides	<ul style="list-style-type: none"> • Imaging infection and inflammation 	<ul style="list-style-type: none"> • Can be synthesised chemically • Can handle severe chemical circumstances for alterations or radiolabelling • Less likely to induce an immunogenic response • Plasma clearance rapid 	<ul style="list-style-type: none"> • Can cause significant leucopenia at physiological concentration
^{99m}Tc - or ^{111}In -labelled Human Immunoglobulin (HIG)	<ul style="list-style-type: none"> • Imaging inflammatory- and infectious foci (bacterial infection, sterile inflammation and inflammatory tumours) 	<ul style="list-style-type: none"> • Excellent for the localisation of musculoskeletal IFI/IF • Pulmonary infection • IFI/IF in immunocompromised patients • Abdominal inflammation • Fever of unknown origin 	<ul style="list-style-type: none"> • Non-specific • Poor sensitivity for endocarditis • Poor sensitivity vascular lesions • Lengthy time passing between injection and final diagnosis (24-48 h)
^{99m}Tc - or ^{111}In -labelled liposomes	<ul style="list-style-type: none"> • Inflammation imaging 	<ul style="list-style-type: none"> • Early abscess imaging depending on the formulation used • Good correlation with the disease severity 	<ul style="list-style-type: none"> • Considerable amount of undesirable effects or adverse reactions • Difficult to prepare • Accumulate in liver and spleen • Non-specific for infection
Radiolabelled Antimicrobial agents e.g. ^{99m}Tc -Ciprofloxacin (Infecton)	<ul style="list-style-type: none"> • Localising IFI/IF 	<ul style="list-style-type: none"> • High target to background ratio • Images can be obtained at 1-, 4- and up to 24 h after administration • Simple to prepare and fairly low in cost • Does not involve handling patients' blood with the associated bio-hazards of blood borne infections • Is not influence by patient's white cell count 	<ul style="list-style-type: none"> • Non-specific binding to DNA of eukaryotic cells • Lack of bacterial uptake

2.4 PRE-CLINICAL RESEARCH

Clinical trials employed for radiopharmaceutical development are expensive (up to several million rand) (Williams 2011:51), and follow a well-defined research protocol using the outcomes of a pre-clinical trial to ensure the predicted outcomes. The animal model selection process for the pre-clinical research phase during this study

was influenced by the defined research end-points, its relationship to humans, the specific targets (IFI/IF and tumours) investigated, cost, animal types accessibility, welfare issues, equipment availability and tumour cell lines suitability.

Nuclear Medicine forms part of molecular imaging that can provide information about cell apoptosis, gene and nucleic acid-based approach, vascular angiogenesis, tumour hypoxia, cellular translational and transcriptional information (Schechter *et al.* 2007:1; Zhang *et al.* 2012:1). In order to clarify the research with IHP ^{99m}Tc -EC-DG a molecular imaging research chain figure is used (Figure 2.15). The four phases of the drug discovery process include in vitro, cellular-, preclinical and clinical imaging. The research with the IHP ^{99m}Tc -EC-DG is positioned as pre-clinical imaging in animal models (*in vivo* and *ex vivo*) in the molecular research chain (Fass 2008:116).

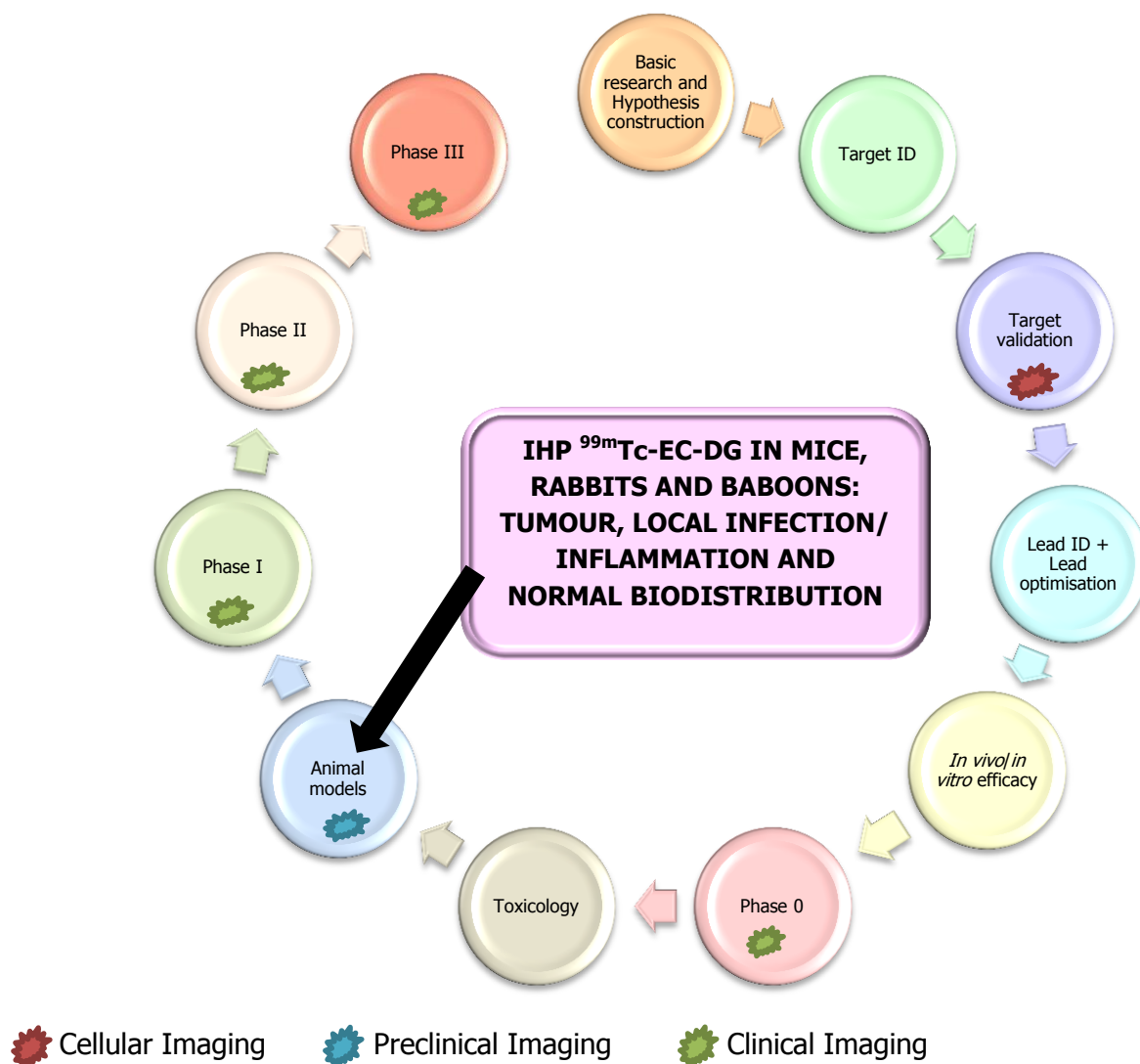


FIGURE 2.15: Molecular imaging research chain (Adapted and redrawn from Fass 2008:116)

2.4.1 Animal research ethics

Animal experiments form an indispensable branch of cancer research in order to comprehend the fundamental mechanisms underpinning malignancy, as well as to find enhanced techniques to counter, diagnose and treat cancer (Workman *et al.* 2010:1555). Ethically research starts at the pre-clinical research phase where the animal species is selected so that the research data can depict the clinical result (Williams 2011:24). Research comprising of the use of animals should be conducted with outstanding standards of animal care that are constant and in line with the conduct of high quality cancer research (Workman *et al.* 2010:1555).

Russell and Burch issued *The Principles of Humane Experimental Technique* in 1959 as a guideline for research protocols underpinning the three R's that include the following:

- replacement (of animals with alternative means),
- reduction (in the animals sample size used to accomplish the scientific goals) and
- refinement (of methods to limit and avoid animal distress) (Workman *et al.* 2010:1556).

The IHP ^{99m}Tc-EC-DG research with the different animals complied with the three "R's": i.e. replacement, reduction and refinement.

In RSA the legislation, Acts and regulations provides code of practices for the use of animals for scientific value and pre-clinical radiopharmaceutical development with the following documentation:

- Animal Protection Act No. 71 of 1962
- Animal Disease Act No. 35 of 1984
- Veterinary and Para veterinary Professions Act No. 19 of 1982
- Medicines and Related Substances Control Act No. 101 of 1965

The UFS Interfaculty Ethics Committee Constitution makes provision for the ethical handling and monitoring of animals for research purposes. The following documents were also used as ethical guidelines and protocol design for the research:

- SANS 10386:2008 The care and use of animals for scientific purposes
- American Veterinary Association Guidelines
- Canadian Council Care and Use Committee (Guidelines on the use of Farm Animals)
- NSPCA Humane endpoints Score Sheet
- NSPCA Animal Welfare Score Sheet

2.4.2 Athymic nude mice model

Mice are one of the most studied animals used in research and they are well understood regarding their anatomy, physiology and genetics. Over 95% (25 million per annum) of animal studies include mice models (Pomper & Lee 2005:3247). Mice are readily available, small in size that facilitate easy handling, less expensive to maintain than larger animals and have a fast reproduction rate (Workman *et al.* 2010:1555). Nude mice also have an absent thymus and therefore have an inhibited immune system due to the absence of the thymus (T) cells also known as T lymphocytes (Sharkey & Fogh 1984:341). The absence of T cells prevents nude mice from rejecting inoculated tumours (after inoculation referred to as xenografts) and therefore was one of the main motivations to use nude mice for this specific research. Research with human tumours transplanted into nude mice began as early as 1969 with great success (Rygaard & Povlsen 1969:758-760). In 1972 Giovanella *et al.* (1972:1531-1533) published the first article on tumour growth in nude mice resulting from the inoculation of cultured human melanoma cells.

A variety of factors can influence the frequency and the growth rate of the tumour transplants. For example the age, sex and genetic background of the nude mouse host, the tumour origin and the site of tumour inoculation (Sharkey & Fogh 1984:344). Sharkey & Fogh (1984:341) reported that different tumours can have different "take rates" according to their tissue origin, biological source (primary as compared to metastasis), doubling time, etc. (Sharkey & Fogh 1984:355). Malignant tumours generally grow quicker than benign tumours in nude mice, but it should also be emphasized that not all malignant tumours grow in nude mice when the decision is made to choose a tumour cell line. Sharkey & Fogh (1984:356) concluded that even though the *in vivo* nude mice model have certain technical problems, it still remains the model that offers the best advantages over other animal models to make it a useful tool for cancer research. The regulatory authorities like the MCC requires that new drugs first be tested in pre-clinical trials in animals before clinical trials in humans should be continued (Workman *et al.* 2010:1555). The nude mice were sacrificed, as the RSA does not have facilities to perform live small animal scans, microPET/CT and nanoSPECT/CT. The study with mice as animal model was performed *ex vivo* and the method of counting the radioactivity of the different body organs and the area of tumour growth of the nude mice was used to determine the biodistribution (section 4.2.4).

2.4.3 The rabbit model

Rabbits are classified under the family leporidae and order lagomorpha (Toutain, Ferran & Bousquet-Mélou 2010:22). They are herbivores, like the rabbits, rats and guinea pigs and have a distended functional caecum to break down the cellulose plant cell walls with a digestion process handled by micro-organisms (Hunter *et al.* 1995:331; Russell *et al.* 2011:1036). Rabbits are a useful option for a research model since they are phylogenetically closer to primates compared to rodents therefore assist in bridging the gap between small animal models and larger animal models required for translation research (Aly *et al.* 2015:12).

The rabbit has been used as an animal model for the following diseases:

- Infection and inflammation thigh model (Oyen *et al.* 2001:151-157) using for example: *S. aureus*, *E. coli*, *K. pneumonia*, *C. albicans*, Zymosan (sterile) and Turpentine (sterile)
- Acute colitis (Oyen *et al.* 2001:151-157)
- Tumours induced: VX2 tumours (Hamazawa *et al.* 1980:671) and amelanotic melanoma (Som *et al.* 1980:671).

The gallbladder is located deep within the abdominal cavity and excrete mostly biliverdin in their bile, contrary to bilirubin by majority mammalian species (Gonzaleza *et al.* 1983:67; Quesenberry & Carpenter 2011:no pagination). A CT topogram of the anatomy of the rabbit is provided in Figure 2.16.

The use of rabbits as an animal model have advantages; amongst them being, easy to handle and big enough for imaging on a SPECT gamma camera used for human scintigraphic imaging. Furthermore, rabbits are small enough for whole-body imaging to obtain complete quantification data and this was one of the reasons the decision was made to use rabbits as an animal model in this research.

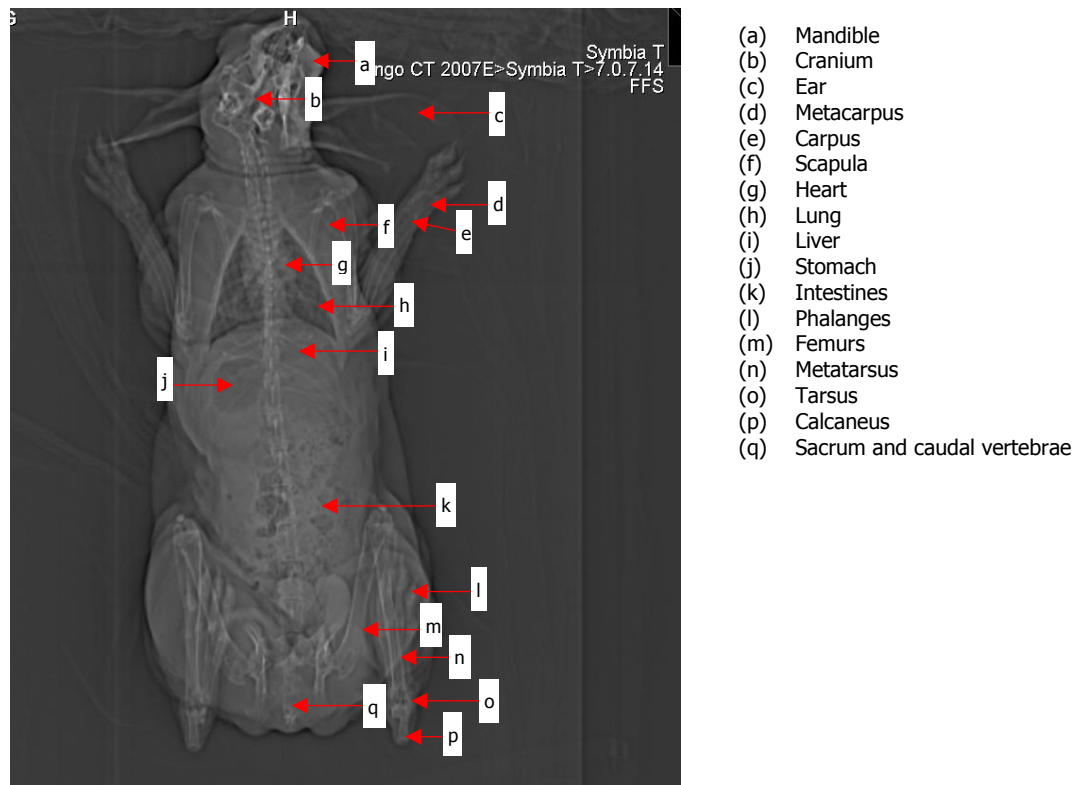


FIGURE 2.16: CT topogram demonstration of the anatomy of the rabbit (Courtesy of DNM, UAH)

2.4.3.1 IFI/IF rabbit model

The Oxford Concise Medical Dictionary (2003:350) defines inflammation as the body's response to injury and that inflammation can be acute or chronic. Infection is defined as the invasion of the body by harmful organisms (pathogens) such as bacteria, fungi, rickettsiae, or viruses (Oxford Concise Medical Dictionary (2003:350-351). Rennen *et al.* (2000:241) outlined the symptomatic response to an acute infection/inflammation as the following:

- Increased local blood supply
- The area involved will display increased vascular permeability
- Increased transudation of plasma proteins
- Increased influx of the leucocytes

The decision was made to induce *Escherichia coli* (*E. coli*) for this septic IFI/IF model rather than *Staphylococcus aureus* as the latter can cause sepsis and significant number of deaths especially in rabbit IFI/IF models (Oyen *et al.* 2001:153). Thus, assuming *E. coli* has a lower pathogenicity than the latter.

In accordance with the non-specific inflammatory accumulation characteristics of ^{67}Ga -citrate borne in mind, it was of value to determine what the difference in biodistribution of ^{67}Ga -citrate and IHP $^{99\text{m}}\text{Tc}$ -EC-DG is. Research has shown that ^{67}Ga -citrate accumulates in *E. coli* induced IFI/IF sites and therefore was used for the comparative purposes with the IHP $^{99\text{m}}\text{Tc}$ -EC-DG biodistribution (Rossouw *et al.* 2005: 394). The induction of *E. coli* in the rabbit model is referred to as the septic IFI/IF model (phase two) in this research. The rabbits in the research were not immune-compromised in order to obtain information about IHP $^{99\text{m}}\text{Tc}$ -EC-DG biodistribution in both healthy rabbits as well as then with *E. coli* local IFI/IF. The *E. coli* was used in the pilot study for the septic IFI/IF model and it was therefore decided to continue using this model for phase two.

Zymosan is a protein – polysaccharide complex extracted from the cell wall of yeast and can be induced in animal models to trigger an immune response (Erdő *et al.* 1993:137). Zymosan has been used in various kinds of induced animal IFI/IF models for example arthritis, paw edema, pleuritis, skin inflammation, peritonitis and air pouch inflammation. The zymosan induced as an IFI/IF is referred to in the dissertation as the sterile IFI/IF model (also part of phase two). A septic IFI/IF model with the *E. coli* produces a hyperemic lesion with granulocytes without major puss formation. Zymosan produces a granulocyte rich infiltration, whereas other sterile IFI/IF models for example with turpentine oil results in hyperaemia and increased vascular permeability with minor cellular infiltration (Oyen *et al.* 2001:153). Zymosan was chosen rather than turpentine oil in order to induce a sterile IFI/IF model to achieve a granulocyte rich IFI/IF area.

2.4.4 The baboon model

The baboon was first used in 1956 as an experimental animal (VandeBerg *et al.* 2009:xvii). The African or Arabian Old World Monkeys (*Catarrhini*) can be divided into two groups, namely baboons (genus *Papio*) and macaques (genus *Macaca*). There are five commonly recognised species or subspecies, but in this research the *Papio ursinus* (chacma baboon) was used. It is found in the RSA and southern parts of Africa (VandeBerg *et al.* 2009:xx). The baboon is chosen to be the ideal animal model for radiopharmaceutical biomedical research and can be used to measure all physiological

parameters measured in humans (Dormehl *et al.* 1992:109). *In-vivo* studies for this research were necessary to determine the physiological distribution of the IHP ^{99m}Tc -EC-DG. As the physiological characteristics of a baboon are very close to a human, any adverse reactions experienced by the baboons from the IHP ^{99m}Tc -EC-DG, would probably also be experienced by humans. The baboon as an animal model is therefore ideal for toxicity tests of new drugs or radiopharmaceuticals. The utilisation of a baboon model before the research and testing of the IHP ^{99m}Tc -EC-DG for human trials was a good quality assurance safety option. Baboons can also be imaged on the same nuclear medicine equipment used for humans, so no special additional equipment is needed to perform pre-clinical research on them. The SPECT/CT gamma camera used to collect the research data on the baboons is also used for human scintigraphic studies at the DNM at UAH.

2.4.5 Interspecies differences

Interspecies differences between animals exist e.g. the gallbladder of the baboons and the human especially relating to the bile viscosity, cholesterol, bilirubin, cholyglycine, sodium (Na), potassium (K), chlorine (Cl), bicarbonate (HCO_3), calcium and magnesium (Kobayashi *et al.* 1998:199). Varga (2013:123) reported that rabbits are better hepato-biliary excretors compared to dogs on a weight basis, whereas Theodorakis *et al.* (1980:584) classified rabbits, humans and primates as poor biliary excretors compared to dogs and rats. These two sources contradict each other and no other sources could clarify which one is the accurate. Interspecies differences relative to biochemistry, anatomy, physiology & behaviour (eating habits, fasting or non-fasting, type of food eaten) can influence the pharmacodynamics and pharmacokinetics of drugs (Toutain *et al.* 2010:19). Toutain (2010:45) concluded that no generalisation regarding different animal species used for research should be made as there are differences and the researchers should be aware of how these differences can impact the results that they will obtain.

2.4.6 Animal biodistribution studies

According to Williams (2011:39) animal biodistribution studies can utilize one or both of two different data recording methods: a direct bioassay via sacrifice used in this research for the tumour mice model (Chapter 4) and/or a sequence of scintigraphic images, used in rabbits- (Chapter 5) and baboon models (Chapter 6). The utilisation of

serial quantitative images enables the monitoring of the accumulation of the radiopharmaceutical in the tissues and organs over time. From the scintigraphic imaging and biosampling data a number of parameters can be generated relevant to the biodistribution; i.e. uptake, specific activity, activity and cumulated activity (Table 2.3).

TABLE 2.3: Biodistribution parameters generated from imaging and biosampling data (Adapted from Williams 2011:39)

Name of parameter	Units	Correction	Application
Uptake (μ)	%ID/g	For decay	Biodistribution
Specific activity (a)	%IA/g	none	Modelling of data
Activity	%IA	none	Modelling of data
Cumulated activity (\tilde{A})	%IA hours	none	Absorbed dose estimates

The parameter generated from the biosampling data was the μ value of IHP ^{99m}Tc -EC-DG in organs, tissue and lung tumours to determine the biodistribution of the IHP ^{99m}Tc -EC-DG (Williams 2011:39). The μ value's units in percent of injected dose/g (%ID/g) is used in the majority of radiopharmaceutical development literature in this decay-corrected format. The tumour- and organ μ of the IHP ^{99m}Tc -EC-DG is expressed in %ID/g and decay-corrected to determine the biodistribution of IHP ^{99m}Tc -EC-DG.

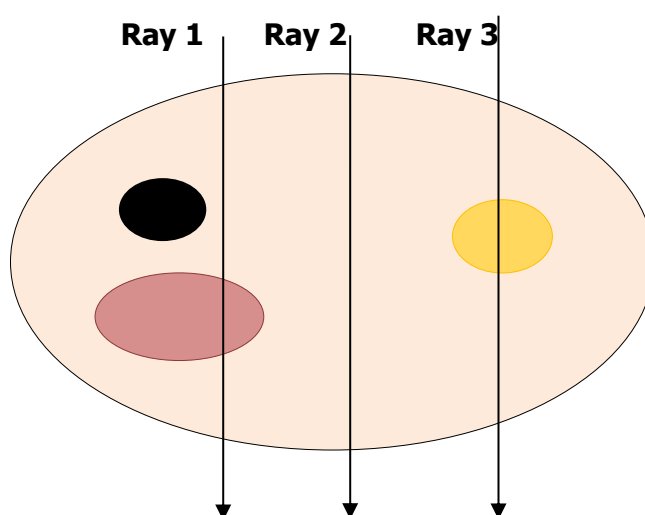


FIGURE 2.17: Mathematical representation of a number of mathematical rays passing through an imaging subject (Adapted from Williams 2011:111)

The gamma camera can be used to obtain images to also determine the activity in organs and tissue (Williams 2011:110). The geometric mean (GM) is a mathematical technique developed for this purpose. In Figure 2.17 a mathematical representation of the several rays passing through the imaging subject's anatomy is given.

Anterior (ANT) and posterior (POST) views are obtained from the imaging subject to determine the activity (Williams 2011:111). Important source organs are usually separated in an ANT to POST projection set. The geometric lines are drawn to pass through several points on the imaging subject's anatomy. The reason for obtaining multiple views is that it may be unclear which organ is along a particular direction from only a single nuclear projection. ANT and POST strong sources may be indicative of different tissues to confound the analysis (Ray 1). The number of counts recorded (N_a) on the ANT or POST projection of a geometric ray passing through an organ of interest can be determined by the following equation:

$$N_a = \Delta t \varepsilon A \exp(-\mu d_a) [1 - \exp(-\mu d_s)] / \mu d_s$$

Where ε is the camera detection efficiency

μ is the linear attenuation coefficient in the tissue

d_a is the thickness of the tissue over the source

d_s is the source thickness

Δt is the counting time

A is the activity (A) in the single tissue or organ imaged

The unknown factor is the activity (A) in the single tissue or organ imaged. The biodistribution of the IHP ^{99m}Tc -EC-DG was determined on the ANT and POST images of the rabbits and baboons by determining the A in the different organs by using the geometric mean method. The GM technique used for the calculation of the A of the IHP ^{99m}Tc -EC-DG in healthy rabbits and baboons were background corrected. This method has an uncertainty of 30% for animal models contributed by the overlapping of organs (Williams 2011:126). Whole-body planar images and static images were acquired with the IHP ^{99m}Tc -EC-DG from $t=0$ to the end of the study to obtain a sequence of geometric mean images.

2.4.7 Factors influencing animal biodistribution studies

Anaesthetic drugs like xylazine and ketamine have been found to reduce ^{18}F -FDG tumour uptake in mice (Lee *et al.* 2005:1531). Anaesthetic drugs can also influence glucose metabolism to other organs like the brain and the heart in animals and thus biodistribution of glucose analogue radiopharmaceuticals (Lee *et al.* 2012:246). As the duration of fasting of animals influences the glucose metabolism and consequently ^{18}F -FDG uptake, there is a high probability that can influence uptake results of the glucose analogue IHP $^{99\text{m}}\text{Tc}$ -EC-DG.

2.5 RADIONUCLIDES AND RADIOPHARMACEUTICALS

A radiopharmaceutical is a molecule that consists of two functional components (Kowalsky & Perry 1987:31-47; Saha 1998:81-323):

- A RP is a radionuclide that allows external tracking within the biological system since its emitting measurable radiation. This is detected with nuclear instruments with gamma- or positron cameras depending on the rays (positron- or gamma-) it emits; and
- A biological compound/ligand, that determines specificity and high concentrations localisation in the target organ. After entering the body, the radiopharmaceutical will accumulate in a specific organ or tumour tissue. The radionuclide attached to the targeting biological compound will undergo decay and produce specific amounts of radiation that can be used to diagnose or treat human diseases and injuries. The amount of radiopharmaceutical administered is carefully selected to ensure each patient's safety.

These radiopharmaceuticals "interrogate" cells and molecules. They are "molecular probes" designed to provide answers about healthy, normal biology, the biological process of disease, and even the molecular errors that cause disease. The radiation from the radionuclides make the body biochemically transparent and an essential part of radiopharmaceuticals.

2.5.1 Radiopharmacy

2.5.1.1 *Methods of labelling*

There are a number of scientific requirements that should be followed to when labelling chemistry is performed (IAEA 2009:22):

- Labelling yield should preferably be in the proximity or higher than 95%
- Limit or exclude purification procedures
- It must be extremely effective at low biomolecule concentration
- Possible toxic or unstable components are undesirable
- Bio-incompatible organic solvents are not allowed
- Applicable quality control tests such as high performance liquid chromatography (HPLC) and TLC to confirm labelled product
- No undefined labelling of the biomolecule ought to take place
- *In vivo* stability is vital

There are several methods available to label a radionuclide to a chemical agent. Iodination and chelation are the two types of labelling methods commonly used (Williams 2011:10). The chelator labelling method used for IHP ^{99m}Tc -EC-DG is where a distinct molecule is engineered to firmly hold a specific metal ion followed by a process where the chelator is attached to the relevant constructor molecule. This method usually consists of two steps:

- The attachment of the chelator (EC) to the component of interest (DG), and
- Labelling of the subsequent novel entity (EC-DG) by incubation with the chosen radio-metal (^{99m}Tc).

EC was used as the chelator to attach the $^{99m}\text{TcO}_4^-$ to the DG to achieve successful labelling of the IHP ^{99m}Tc -EC-DG.

Metastatic disease is a continuing problem not only in third world countries, but also in first world countries (Williams 2011:24). A possible approach would be to search different tumour sites with a radiolabelled specific tumour-targeting agent. This tumour-targeting agent can include gamma, beta- or alpha emitters can provide a specific targeted tumour treatment. Nano-engineering combined with multiple technologies can in future possibly provide

this solution. In Third World Countries these advanced technologies are not available yet and temporary low cost alternatives are considered. The pre-clinical research in this dissertation was to evaluate the IHP ^{99m}Tc -EC-DG as a possible future diagnostic targeted imaging agent.

2.5.1.2 Radiopharmaceutical quality control

Typical QC tests that the product must undergo before administration (Ziesmann *et al.* 2014:7) are divided into two categories (Saha 2003:151-174):

- Physicochemical Tests: to detect radionuclidic and radiochemical contaminations, to establish the pH, ionic strength, osmolality and physical nature of the sample
- Biological Tests: to ascertain the sterility, apyrogenicity and toxicity

Radiochemical purity (RCP) which is defined as the ratio, expressed as a percentage, of the activity of the radionuclide concerned which is present in the radiopharmaceutical preparation in the stated chemical form, to the total radioactivity of that radionuclide present in the radiopharmaceutical preparation. Factors that can influence radiochemical purity include insufficient labelling in the early steps, radiolysis, disintegration, pH fluctuations, light contact, or presence of oxidative or reducing agents. For most radiopharmaceuticals the lower limit of RCP is 95%, that is, at least 95% of the radioactive isotope must be attached to the ligand. RCP determination can be carried out by a variety of chromatographic methods:

- Paper and thin layer chromatography - Thin-layer chromatography is used when technetium is labelled with agents to assess the radiochemical purity of test radiopharmaceuticals and radiopharmaceuticals approved by regulatory commissions used on a daily basis. The quality insurance with technetium tests the presence of free pertechnetate and insoluble hydrolysed reduced technetium moieties (Ziesmann *et al.* 2014:8);
- High Performance Liquid Chromatography (HPLC) - TLC RCP methods may not be sufficient to identify all the compounds which are present in a product. HPLC has a higher sensitivity and resolving power than simple TLC methods. HPLC separation operates on the

hydrophilic/lipophilic properties of the components of a sample applied. Gamma emitters are detected using a well scintillation counter connected to a rate meter. Other detectors (ultraviolet or refractive index) can be connected in series allowing simultaneous identification of compounds. It should not be necessary to perform HPLC on radiopharmaceuticals reconstituted from licensed cold kits. It is useful to have techniques available for the purpose of eliminating a cause of any abnormal patient scan. For radiopharmaceuticals prepared 'in-house' or novel compounds for research purposes, an HPLC method for estimating radiochemical purity is essential. It should be noted that HPLC does not detect colloidal contaminants and that this should be estimated using TLC methods.

Radiochemical impurities can influence the biodistribution of radiopharmaceuticals negatively, degrading the image quality e.g. leading to background activity or undesirable uptake.

2.5.2 ^{99m}Tc

Segre and Seaborg discovered technetium as an element in 1937 (Wagner 2006:58). A ^{99}Mo (Molybdenum-99)- ^{99m}Tc generator was in use from the early as the 1960's and provides the short-lived radionuclide $^{99m}\text{TcO}_4^-$ on the principle that the parent radionuclide has a longer half-life than the daughter radionuclide (Saha 2006:51). The daughter radionuclide in a ^{99}Mo - ^{99m}Tc generator, $^{99m}\text{TcO}_4^-$ is separated from the parent radionuclide, ^{99}Mo through a chemical process. The ^{99}Mo - ^{99m}Tc generator is widely available and is easily transported to a nuclear medicine facility since it weighs only ± 14 kilograms. Subsequently, through the utilisation of a ^{99}Mo - ^{99m}Tc generator $^{99m}\text{TcO}_4^-$ will continuously be available to supply $^{99m}\text{TcO}_4^-$ on a daily basis to a nuclear medicine department. Thus, a nuclear medicine diagnostic imaging service can still be supplied by nuclear medicine departments without a cyclotron or reactor facilities (Saha 2006:51), resulting in better service delivery to government patients.

2.5.2.1 *Properties and production*

^{99m}Tc as a radionuclide has certain ideal imaging characteristics for a potential novel radionuclide if labelled to a glucose metabolism tracer. ^{99m}Tc is a

gamma-emitting radionuclide with a low energy of 140 keV that can be used for scintigraphic imaging using any standard gamma camera. The low energy, provides a low radiation dose (to patients and staff) that makes it advantageous, but still can effectively image tumours. The effective dose for ^{99m}Tc (0.048 rem/mCi, 0.013 mSv/MBq) is lower than that of ^{18}F -FDG (0.070 rem/mCi, 0.019 mSv/ MBq) (Table 2.4 and Table 2.5) (Saha 2003:201). It should be noted that ^{99m}Tc are a gamma emitting radionuclide, whereas ^{18}F is positron emitter (β^+) resulting in two 511 keV annihilation photons.

^{99m}Tc is also widely available, as the generator from which $^{99m}\text{TcO}_4^-$ is produced can be transported to any nuclear medicine department with safety and ease and $^{99m}\text{TcO}_4^-$ is not so expensive to produce (in bulk from fission), as compared to the dedicated production of ^{18}F by a cyclotron. This characteristic of ^{99m}Tc as a low cost radionuclide and wide availability makes it a very cost-effective radionuclide that can render a scintigraphic imaging service to oncology patients in the developing world and in the RSA (Uz ZaMan 2007:429). $^{99m}\text{TcO}_4^-$ (labelled and unlabelled) can account for about 85% of nuclear medicine procedures performed and worldwide roughly 40 million procedures per year is performed with $^{99m}\text{TcO}_4^-$ (Eckelman 2009:364). Additionally, these physical characteristics of $^{99m}\text{TcO}_4^-$ make it the preferred radionuclide for the labelling of radiopharmaceuticals. $^{99m}\text{TcO}_4^-$ as a radionuclide has certain ideal imaging characteristics as a potential novel radionuclide for the labelling with a glucose tracer. In the past, investigators and pharmacists have tried to label glucose with $^{99m}\text{TcO}_4^-$. $^{99m}\text{TcO}_4^-$ has an unstable chemical binding and investigators failed to achieve this goal, because of the inability to find a chemically stable chelate that could link the $^{99m}\text{TcO}_4^-$, with the glucose. Yet, the search and need for the development of a cheaper, more widely available tumour-specific radiopharmaceutical was continued (Chen *et al.* 2006:342).

TABLE 2.4: The absorbed radiation dose for $^{99m}\text{TcO}_4^-$ in adults (Saha 2003:201)

Organ	Dose
	(mGy/MBq)
Thyroid	0.0351
Upper large intestine	0.0324
Lower large intestine	0.0300
Stomach	0.0138
Ovaries	0.0081
Testes	0.0024
Gonads	0.0700

Silindir & Özer (2008:109) stated that adverse reactions due to $^{99m}\text{TcO}_4^-$ labelled radiopharmaceuticals are mostly mild and usually do not need any medical treatment. This advantage of technetium therefore makes it one of the most used radionuclides in nuclear medicine. Adverse events due to radiopharmaceuticals are rare as the dosages administered to patients are in diagnostic quantities and not in pharmacological treatment quantities (Silindir & Özer 2008:110). No complications due to the intravenous injection of $^{99m}\text{Tc-EC-DG}$ have been reported, except erythema (Schechter *et al.* 2003:470).

2.5.2.2 Uptake mechanism and clearance

$^{99m}\text{TcO}_4^-$ accumulates in the thyroid, salivary gland and stomach within 1 hour, with no concentration to the cerebrospinal fluid (Andros *et al.* 1965:1067). $^{99m}\text{TcO}_4^-$ is trapped in the thyroid, similar to iodide but is not organified or metabolised within the thyroid gland (Andros *et al.* 1965:1067). Thirty percent of $^{99m}\text{TcO}_4^-$ is excreted by the genitourinary system within 24 hours after administration.

2.5.2.3 Imaging

The uptake of unlabelled ^{99m}Tc in the stomach, salivary glands and thyroid in animal models for example mice, can be used as an indicative factor for insufficient labelling of the radiopharmaceutical (Franken *et al.* 2010:523). $^{99m}\text{TcO}_4^-$ unlabelled can be used for Meckel's diverticulum detection, salivary and thyroid gland scintigraphy, scrotal scan and heart flow studies (Levy *et al.* 1983:975; Ziesmann *et al.* 2014:6).

2.5.3 ^{67}Ga -citrate

2.5.3.1 Properties and production

Research with ^{67}Ga -citrate started in the 1960's and was initially developed as a bone-seeking radionuclide (Edwards & Hayes 1969:103; Ziessman *et al.* 2014:322). A closer look was taken at ^{67}Ga -citrate to validate the importance

of the comparison of the ^{67}Ga -citrate with IHP $^{99\text{m}}\text{Tc}$ -EC-DG in this research and to motivate other reasons for why it was used as control radiopharmaceutical for IFI/IF. ^{67}Ga -citrate is a cyclotron produced radionuclide that can be used for diagnostic imaging in its carrier-free state (Ziesmann *et al.* 2014:322). The characteristics of ^{67}Ga -citrate include a physical half-life of 78 h and a biological half-life of 2-3 weeks. ^{67}Ga -citrate has four photopeaks at 93- (41%), 185- (23%), 288- (18%) and 394 keV (4%) (Ziesmann *et al.* 2014:323). ^{67}Ga -citrate is still used today in nuclear medicine departments over the world and in RSA for the diagnosis of focal sites of IFI/IF, skeletal disorders (Rennen *et al.* 2001:243) and a variety of tumours. Limiting factors for its use include the need for a medium energy collimator to facilitate ^{67}Ga -citrate scintigraphic imaging and clinically the high degree of non-specific accumulation in both IFI/IF and tumours making differentiation between the two difficult. The diagnostic value of ^{67}Ga -citrate can be enhanced when combined with SPECT/CT in particular for diseases like lymphoma and IFI/IF (Jacene *et al.* 2008:75). Babich and Fischman (1999:244) emphasized the need for a more specific radiopharmaceutical to evaluate and distinguish between IFI/IF and tumours.

2.5.3.2 Uptake mechanism and clearance

^{67}Ga -citrate is handled as an analogue to ferric iron by the body (Ziesmann *et al.* 2014:322). This characteristic of ^{67}Ga -citrate enables it to bind to lactoferrin discharged from perishing leucocytes (Ziesmann *et al.* 2014:322). The IFI/IF uptake mechanism is also activated by binding to transferrin, bacterial siderophores, inflammatory proteins, and neutrophil cell membranes (Ziesmann *et al.* 2014:322). It localises in the inflammatory tissue by binding to the existing acid mucopolysaccharide (Ando *et al.* 1990:26). The site of IFI/IF is targeted within 12-24 h after administration (Ziesmann *et al.* 2014:322), but as a non-specific radionuclide it is limited in its ability to distinguish between infection and inflammation (Rennen *et al.* 2001:244). ^{67}Ga -citrate deposition in lysosomes plays a role in the different tumour uptake in animals and humans (Hammersley *et al.* 1980:274). ^{67}Ga -citrate is eliminated faster by the kidneys of rabbits compared to that found in humans (Sykes *et al.* 1987:98). Forty percent of the dose is excreted within 48 h from

rabbits as to twenty percent by humans. The greatest dissimilarity in biological behaviour of ^{67}Ga -citrate in rabbits to humans is the faster elimination of this radionuclide by the kidneys of rabbits.

2.5.4 ^{18}F -FDG

The strength of Positron Emission Tomography (PET) in oncology imaging is mainly due to the use of novel radiopharmaceuticals labelled with short-lived positron emitters. In most of the PET studies combined with Computed Tomography (CT), the radiopharmaceutical ^{18}F -FDG, glucose analogue is used. In the 1970's, ^{18}F -FDG was synthesised for the first time at the Brookhaven National Laboratory for clinical PET applications (Gatley 2003:1082). ^{18}F -FDG was first used in 1982 clinically for brain imaging (tumours) and the evaluation of liver metastasis (Fukuda, Kubota & Matsuzawa 2013:155). ^{18}F -FDG was first used in 1982 clinically for brain imaging (tumours) and the evaluation of liver metastasis (Fukuda, Kubota & Matsuzawa 2013:155).

2.5.4.1 *Properties and production*

^{18}F -FDG is currently the gold standard in metabolic tumour imaging, but has certain limitations including short half-life, high cost and non-specificity, as well as high brain uptake making it difficult to detect uptake of brain tumours. ^{18}F is produced by a cyclotron and has a short physical half-life ($T_{1/2}$ is 110 minutes). Since the $T_{1/2}$ of ^{18}F is relatively short, the PET/CT positron camera is required to be must optimally be close to a cyclotron. Because of this physical characteristic, the PET/CT should be situated as close as possible to a cyclotron which is often not possible. The cost of a PET/CT ranges from R14-25 million [(R) Republic of South African currency] and for a cyclotron from R20 million. Due to the high cost of the cyclotron, the PET/CT camera and cyclotron-produced radiopharmaceuticals, this modality is not readily accessible to Third World and developing countries. There are only four functional cyclotrons in The RSA, two in Pretoria and two in Cape Town. Yet, PET/CT has not only become popular in the first world private health practices, but also at national health care systems for tumour detection and localisation (Chen *et al.* 2006:342). Currently very few private practices in RSA have the

luxury of a PET/CT with a cyclotron close by. The result is that higher doses of ^{18}F -FDG have to be transported from a centre where there is a cyclotron to a centre that is equipped only with a PET/CT to compensate for the short physical half-life of ^{18}F .

In Table 2.5 the absorbed radiation dose of ^{18}F -FDG is provided.

TABLE 2.5: The absorbed radiation dose for ^{18}F -FDG in adults (Saha 2003:197-199)

Organ	Dose
	(mGy/MBq)
Brain	0.0189
Heart	0.0595
Bladder	0.1892
Spleen	0.0378
Ovaries	0.0170
Uterus	0.0230

2.5.4.2 Uptake mechanism and diagnostic imaging

^{18}F -FDG is a positron-emitting glucose analogue and is transported into the cells via glucose transporters (Imam 2005:166). FDG undergoes phosphorylation by hexokinase to convert to FDG-6-phosphate (Figure 2.18). This results in an alteration in the electrical charge and traps the FDG within the cell. It is theorised that FDG cannot undergo further metabolism because of the fluorine at the C-2 position of the ring, which prevents metabolism beyond the phosphorylation step (Southworth *et al.* 2003:494). FDG-6-phosphate due to low permeability undergoes almost no clearance from the cell (Pauwels *et al.* 1998:281). Southworth *et al.* (2003:494-502) used ^{19}F NMR spectroscopy in rats to indicate that FDG-6-P does not remain inactive within the cell as originally theorized, but 45% is subjected to further metabolism beyond this supposed "terminal metabolite". Further metabolism of FDG is tissue dependent and should be taken into account as it can affect accuracy of PET kinetic models and measurements of absolute glucose metabolism. ^{18}F -FDG can localise IFI/IF as neutrophils, macrophages and rapidly dividing cells have elevated uptake of this radiopharmaceutical (Kumar *et al.* 2006:104).

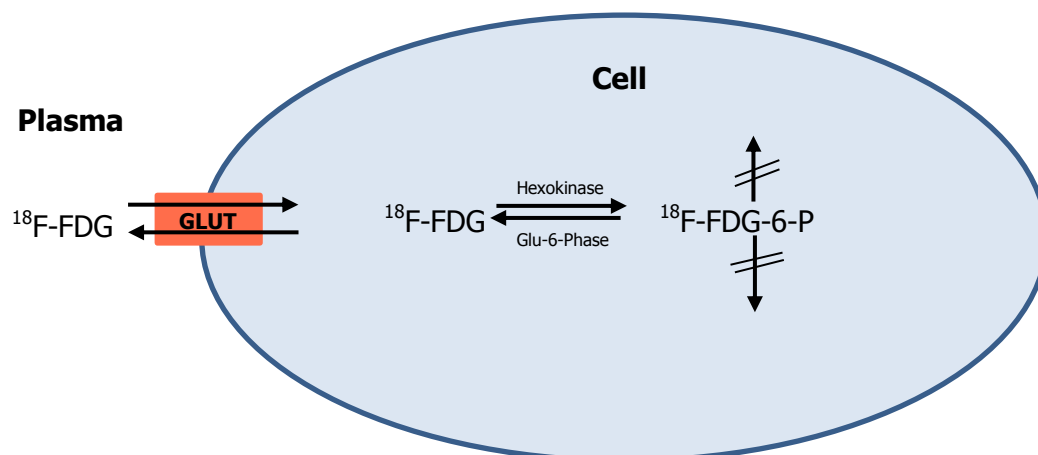


FIGURE 2.18: $^{18}\text{F-FDG}$ uptake and accumulation mechanism in the cell (Adopted and redrawn from Kim *et al.* 2012:42)

$^{18}\text{F-FDG}$ is used as a nuclear medicine imaging technique to evaluate the metabolic state of tumours (Pauwels *et al.* 1998:317). All cells metabolise glucose and take up FDG, yet FDG is not tumour specific and can give false/positive results with imaging (Pauwels *et al.* 1998:281). GLUT1 is overexpressed in cancer cells leading to a high uptake of FDG in cancerous cells (Imam 2005:166). FDG is in competition with glucose for the membrane transporters and with increased glucose in the blood FDG uptake is reduced in tumours (Figure 2.19).

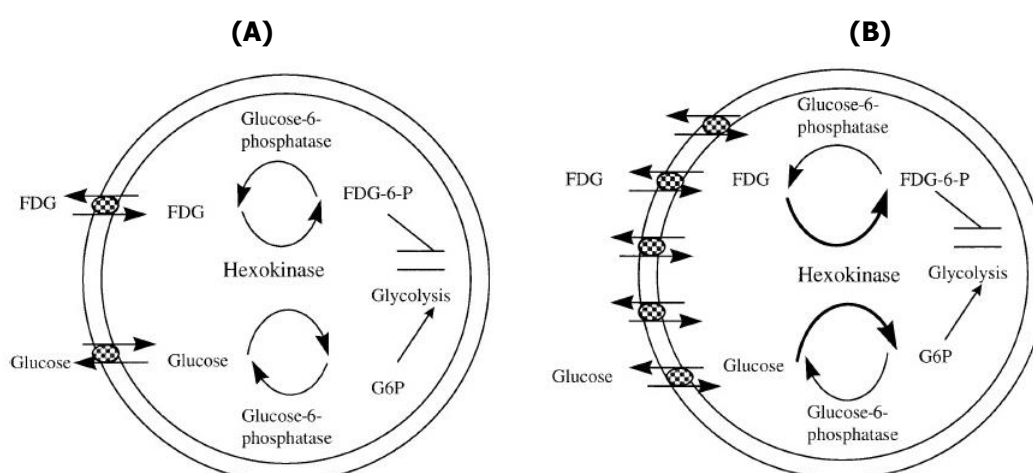


FIGURE 2.19: A side by side representation of the uptake and metabolism of glucose and FDG in (A) normal and (B) tumour cell (Adopted from Pauwels *et al.* 1998:281)

^{18}F -FDG has certain diagnostic limitations. Tumour with modest increase in metabolism, low-grade brain tumours and recurrent tumours (certain cases) is challenging to diagnose with ^{18}F -FDG due to the high physiological rate of glucose metabolism in the brain (Chen *et al.* 2006:904). Distinguishing between IFI/IF and certain malignancy with ^{18}F -FDG can pose difficulties. Maximum standard uptake values (SUVmax) can facilitate this problem to some extent, but in certain cases the SUVmax cannot be of assistance, as this can lead to false-positive reporting of malignant disease. Examples of situations that can lead to false-positive diagnostic reporting with ^{18}F -FDG, is with infection, inflammation, granulomatous disease, specifically Tuberculosis (TB) that also has enhanced ^{18}F -FDG uptake similar to malignancy (Sathekge *et al.* 2010:598). Other limiting factors of ^{18}F -FDG are its short $t_{1/2}$ (24 hour imaging acquisitions with ^{18}F -FDG not possible by means of same dose administration) and high cost (due to production cost and imaging equipment).

^{18}F -FDG also has advantages related to the imaging of disease. ^{18}F -FDG has a high uptake in most malignant tumours due to the high increase in the activity of hexokinase isoenzymes in these tumour cells (Chen *et al.* 2006:342). FDG therefore, has the characteristic to reflect the viability and proliferative activity of a tumour cell. ^{18}F -FDG can also facilitate the diagnosis of a variety of IFI/IF within two hours after administration. ^{18}F -FDG is the most widely used agent for the detection of hibernating myocardium and metabolically active cancer tissue. This research highlights this key aspect for the need of an ideal non-invasive, low cost, single photon emission glucose metabolism radiopharmaceutical (imaging agent) that can detect IFI/IF and/or tumours. Yet, ^{18}F -FDG as a radiopharmaceutical has certain advantages and disadvantages and has to be compared with other IFI/IF and tumour radiopharmaceuticals in the search for an ideal radiopharmaceutical.

2.5.5 $^{99\text{m}}\text{Tc}$ -EC-DG

2.5.5.1 *Imaging and Properties*

$^{99\text{m}}\text{Tc}$ -EC-DG is given different abbreviations and names in the literature for example $^{99\text{m}}\text{Tc}$ -EC-G, $^{99\text{m}}\text{Tc}$ -ECG, $^{99\text{m}}\text{Tc}$ -ECDG and $^{99\text{m}}\text{Tc}$ -Ethylenedicycysteine-Glucosamine. A summary of the published research on $^{99\text{m}}\text{Tc}$ -EC-DG is provided in Table 2.6.

The pre-clinical work performed with ^{99m}Tc -EC-DG in A549 human lung cancer xenografts (Yang *et al.* 2003:469) and VX-2 (squamous mammary) tumour bearing rabbits (Yang *et al.* 2004:447) showed promising results for the future detection of cancer in humans. The United States Food and Drug Administration (FDA) approved on the basis of these pre-clinical results, a clinical trials phase I in NSCLC (Schechter *et al.* 2009:1584). The Phase I clinical trial opened in January 2003 under supervision of Cell>Point and the Anderson Cancer Center (Houston, Texas) was completed in seven NSCLC patients. In four of the seven patients imaged with ^{99m}Tc -EC-DG, uptake in the primary lung lesion was observed on the planar whole-body scanning (Schechter *et al.* 2009:1591). In six of the seven patients the primary tumour was visualised with the ^{99m}Tc -ECDG SPECT scan at 4 h post injection. The closing date for Phase III clinical trials with ^{99m}Tc -ECDG in patients with NSCLC is at the end 2014. The diagnostic potential is accompanied by the low dose and low cost to be a good alternative for current glucose metabolism imaging agent for the detection of tumours (Schechter *et al.* 2009:1590).

Other literature worth mentioning performed with ^{99m}Tc -EC-DG included the evaluation of ^{99m}Tc -EC-DG in an inflammatory arthritis-induced rat model and it demonstrated significant uptake compared to ^{99m}Tc -Histidine-Core-Peptide and ^{99m}Tc -Histidine-Control (Kumar *et al.* 2007:10-13). Sixteen patients with rheumatoid arthritis or osteoarthritis that were imaged, showed accumulation in area of disease with ^{99m}Tc -EC-DG imaging (Angelides *et al.* 2014:655-665). The literature was also searched for evidence to determine whether ^{99m}Tc -EC-DG biodistributes to an area of induced IFI/IF compared to the IFI/IF biodistribution of ^{67}Ga -citrate, and no published literature could be found.

The normal biodistribution of ^{99m}Tc -EC-DG in baboons has not been described in the literature. Baboons are phylogenetically similar to humans Dormehl *et al.* (1992:109) and if any adverse reactions would occur in baboons, there would be a high probability that it would also occur in humans. The safety of the IHP ^{99m}Tc -EC-DG was established and confirmed and this could be used for motivation for future clinical trials in humans.

TABLE 2.6: List of publications on ^{99m}Tc -EC-DG and short summary

Year	Author	Journal name or Congress presented	Title	Achievement	Animal/human
2001	Yang, D. J., Azhdarinia, A., Yu, D.F., Kim, E.E., Podoloff, D.A.	Journal Labelled Cpd. Radiopharm. 44, Suppl. 1 (Symposium Abstracts)	^{99m}Tc -EC-Deoxyglucose: Synthesis, Cellular uptake, Biodistribution and Scintigraphic Imaging	Confirmed <i>in vitro</i> cellular uptake of ^{99m}Tc -EC-DG via d-glucose mechanism and is phosphorylated. Brain and heart uptake less than ^{18}F -FDG. Biodistribution of ^{99m}Tc -EC-DG to lung tumours (A549 cell line) confirmed. ^{99m}Tc -EC-DG could be better than ^{18}F -FDG for brain and chest tumours, due to less biodistribution to that areas compared with ^{18}F -FDG.	Breast-tumour bearing Fischer 344 rats and lung-tumour bearing nude mice.
2003	Yang, D.J., Kim, C.G., Schechter, N.R., Azhdarinia, A., Yu, D.F., Oh, C.S., Bryant, J.L., Won, J.J., Kim, E.E. & Podoloff, D.A.	<i>Radiology</i> 226(2):465-473	Imaging with ^{99m}Tc -ECDG Targeted at the Multifunctional Glucose Transport System: Feasibility Study with Rodents.	Tissue distribution and scintigraphic studies performed in animal models. EC-DG can be labelled with ^{99m}Tc without difficulty and with great yield and high radiochemical purity and stability. Greater uptake in tumours, lower uptake in brain and muscle tissue. Confirming possible use of ^{99m}Tc -EC-DG as metabolic imaging agent.	Breast tumour-bearing rats and lung tumour-bearing nude mice.
2004	Yang, D., Yukihiro, M., Yu, D.F., Ito, M., Oh, C.S., Kohanim, S., Azhdarinia, A., Kim, C.G., Bryant, J., Kim, E.E. & Podoloff, D.	<i>Cancer Biotherapy & Radiopharmaceuticals</i> 19(4):443-455.	Assessment of Therapeutic Response Using ^{99m}Tc -Ethylenedicysteine-Glucosamine.	^{99m}Tc -EC-DG imaging for the evaluation of therapeutic effect of chemotherapy on tumour-bearing nude mice. Tc-EC-DG uptake in pulmonary and mammary cancer tissues lower than prior to therapy based on tumour to muscle ratio. ^{18}F -FDG no significant difference.	Autoradiographs of nude mice bearing uterine sarcoma and scintigraphic imaging performed on rabbits inoculated with VX-2 cells. Mammary tumour-bearing rats underwent scintigraphic imaging for therapeutic assessment of ^{99m}Tc -EC-DG.

Year	Author	Journal name or Congress presented	Title	Achievement	Animal/human
2007	Bryant, J., Yang, D., Schechter, N. (Also published in 2009 as full article by Schechter et al. in <i>European Journal of Nuclear Medical Molecular Imaging</i>)	<i>Journal of Nuclear Medicine</i> 48:354P	Evaluation of ^{99m}Tc --EC-DG in lung cancer patients.	Assessed the safety, biodistribution, imaging and dosimetry of ^{99m}Tc -EC-DG in a limited population with lung small-cell lung cancer (NSCLC) up to 24 hours after administration of ^{99m}Tc -EC-DG. This article indicated that SPECT images could demonstrate all known primary tumours, pointing out the critical organs as the kidneys. Safety of the absorbed dose to the different organs established and ^{99m}Tc -EC-DG demonstrated reasonable dosimetric properties to evaluate NSCLC.	Seven patients with lung cancer
2007	Kumar, V., Ali, M., Angelides, S. and Manolios, N.	<i>ANZ Nuclear Medicine</i> 38(3)	Synthesis and characterisation of ^{99m}Tc -Glucosamine & ^{99m}Tc -His-CP and evaluation of their utility in imaging inflammatory arthritis.	^{99m}Tc -ECDG demonstrated significantly higher focal uptake in the area of inflammatory arthritis compared to ^{99m}Tc -His-CP and ^{99m}Tc -His-Con.	Rats induced with arthritis and a human volunteer.
2009	Schechter, N.R., Erwin, W.D., Yang, D.J., Kim, E.E., Munden, R.F., Forster, K., Taing, L.C., Cox, J.D., Macapinlac, H.A. & Podoloff, D.A.	<i>European Journal of Nuclear Medical Molecular Imaging</i>	Radiation dosimetry and biodistribution of ^{99m}Tc -ethylenedicysteine-deoxyglucose in patients with non-small-cell lung cancer.	^{99m}Tc -EC-DG is suggested to be safe on the ground of this research performed in humans. The dosimetric properties are satisfactory and ^{99m}Tc -EC-DG biodistribution properties are suggestive that it can be used as a diagnostic radiopharmaceutical in a clinical setting for the diagnosis of tumours.	Seven patients
2010	Rollo, D., Bryant, J., Yang, D. And Kim, E.	<i>Journal of Nuclear Medicine</i> 51(Supplement 2):117	Clinical results for ^{99m}Tc -ECDG as a target specific imaging agent for NSCL	^{99m}Tc -ECDG combined with SPECT can be used for the diagnosing and staging of NSCLC. ^{99m}Tc -EC-DG also showed promising results for the monitoring of the effectiveness of chemotherapy.	Seven patients with NSCLC

Year	Author	Journal name or Congress presented	Title	Achievement	Animal/human
2010	Zhang, Y., Oh, C.S., Yang, D., Yu, D.F., Kohanim, S., Mendez, R, Chanda, J.B. and Kim, E.	<i>Journal of Nuclear Medicine</i> 51(2):1529	EC-DG: A molecule suitable in theranostic in cancers.	Radiation exposure of ^{99m}Tc -EC-DG to the whole-body, organs and gonads were below annual limits.	Breast tumour-bearing rats, lung tumour-bearing mice and rabbits with squamous VX-2 tumours.
2012	Case, J.A., Bateman, T.M., Cullom, J.S., Siegmund, M., Robison, K. & Rollo, D.	Unpublished poster presentation at: <i>Seventeenth Annual Scientific Session of the American Society of Nuclear Cardiology</i> , September 6-9, 2012, Baltimore, United States of America.	Myocardial Uptake of a Novel Tc-99m Labeled Glucose Analog (Tc-99m EC-DG) in Normal and Ischemic Subjects during Rest and Exercise Stress Testing.	Uptake of ^{99m}Tc -ECDG was not seen in the normal myocardium at rest or as a result of induced stress exercise. ^{99m}Tc -EC-DG may have the potential to be used to diagnose ischemic heart disease, without induced stress exercise.	Thirteen research subjects
2012	Zhang, Y.H., Bryant, J., Kong, F.L., Yu, D.F., Mendez, R., Kim, E.E. & Yang, D.	<i>Journal of Biomedicine and Biotechnology</i> 2012:1-9	Molecular Imaging of Mesothelioma with ^{99m}Tc -ECG and ^{68}Ga -ECG.	This pre-clinical study established that ^{99m}Tc -ECG takes up in mesothelioma cancer. ^{99m}Tc -ECG can play a role in the diagnosis and monitoring of response to treatment of mesothelioma.	Mesothelioma-bearing rats.
2014	Angelides, S., El-Mashaleh, M., Anagnostou, M., Howe, G., Spencer, D., Kumar, V. & Manolios, N.	<i>Nuclear Medicine Communications</i> 35(6)	The role of ^{99m}Tc -labelled glucosamine (^{99m}Tc -ECDG) in the evaluation of rheumatic joint disease: a screening experience.	^{99m}Tc -ECDG takes up in rheumatic inflammatory diseased area and can distinguish between synovial and bone biodistribution. ^{99m}Tc -ECDG as a diagnostic imaging agent can be useful in the diagnosis of rheumatic conditions and monitoring the effectiveness of treatment.	

2.5.5.2 ^{99m}Tc-EC-DG radiation dosimetry and safety

Basic knowledge has been obtained about ^{99m}Tc-EC-DG including synthesis, cellular uptake, biodistribution and scintigraphic imaging of non-small-cell lung cancer (NSCLC) tumours in humans and compared with the research that Yang performed (Yang *et al.* 2003:465-473; Yang *et al.* 2004:443-455). Radiation dosimetry of ^{99m}Tc-EC-DG to different organs described by Schechter *et al.* (2009:1583-1591) illustrates that it has acceptable dosimetric properties for humans and therefore safe to be used as a diagnostic imaging agent (Table 2.7). Schechter *et al.* (2009:1590) reported the effective dose equivalent of ^{99m}Tc-EC-DG is similar to a ^{99m}Tc-MDP (Table 2.7) study which is performed on a daily basis in many Nuclear Medicine departments over the world.

TABLE 2.7: The absorbed radiation dose for ^{99m}Tc-EC-DG and ^{99m}Tc-MDP in adults (Helal 2012:156; Schechter *et al.* 2009:1587)

Organ	^{99m} Tc-EC-DG Dose (mGy/MBq) Mean	^{99m} Tc-MDP Dose (mGy/MBq) Mean
Adrenals	0.00330	0.000223
Brain	0.00150	0.000223
Breasts	0.00160	0.000223
Gallbladder	0.00340	0.000223
Lower large intestine	0.00330	0.000223
Small intestine	0.00290	0.000223
Stomach	0.00840	0.000223
Upper large intestine	0.00290	0.000223
Heart wall	0.00280	0.000223
Kidneys	0.01230	0.004590
Liver	0.00470	0.000223
Lungs	0.00560	0.000223
Muscle	0.00210	0.000223
Ovaries	0.00410	0.000223
Pancreas	0.00390	0.000223
Red marrow	0.00220	0.002480
Bone surfaces	0.00360	0.028800
Skin	0.00130	0.000223
Spleen	0.00450	0.000223
Testes	0.00670	0.000223
Thymus	0.00210	0.000223
Thyroid	0.00630	0.000223
Urinary bladder	0.02470	0.017300
Uterus	0.00530	0.000223
Total body	0.00240	0.000586
Effective dose equivalent (mSv/MBq)	0.00620	0.002640
Effective dose (mSv/MBq)	0.00590	0.00175

Schechter *et al.* (2009:1590) reported that none of the patients suffered a serious adverse event related to ^{99m}Tc -EC-DG. One patient developed slight erythema at the injection site which was self-resolved within an hour. No vital sign, electrolyte or electrocardiogram (ECG) irregularity was attributed to the administration of ^{99m}Tc -EC-DG. Schechter *et al.* (2009:1590) concluded in his research that imaging NSCLC patients with 925 MBq (25 mCi) ^{99m}Tc -EC-DG is achievable and safe. The effective dose equivalent for 740 MBq of ^{99m}Tc -MDP whole-body bone scan is 4.22 mSv (Bushberg *et al.* 2002) and therefore similar to the effective dose ^{99m}Tc -EC-DG that is 4.36 mSv for 740 MBq (Schechter *et al.* 2009:1590). Yet, significantly lower than the 7.03 mSv for a nominal 370 MBq of ^{18}F -FDG PET imaging.

2.5.6 ^{18}F -FDG versus ^{99m}Tc -EC-DG

2.5.6.1 *Glycolysis targeting of glucose*

Glucose is transported in and out through cell membranes with the aid of the protein family of glucose transporters as discussed in 2.2.2 (Brown 2000:237). ^{18}F -FDG and ^{99m}Tc -EC-DG makes use of glucose transporters to internalize the cells. ^{18}F -FDG use different glucose transporters than ^{99m}Tc -EC-DG, but both their chemical structures are analogous to glucose (Kumar *et al.* 2007:10). The chemical structures of ^{18}F -FDG, *D*-Glucosamine, EC-DG, ^{99m}Tc -EC-DG (literature used) and IHP ^{99m}Tc -EC-DG are illustrated in Figure 2.20. When the hydroxyl group of glucose is replaced with $-\text{NH}_2$ it becomes DG and when ^{18}F replaces the hydroxyl group in glucose it becomes ^{18}F -FDG. ^{99m}Tc -EC-DG and ^{18}F -FDG are glucose analogues and thus treated similarly to glucose by healthy and tumour cells (Figure 2.21). A closer look is taken at the advantages and disadvantages of ^{18}F -FDG for PET imaging, as it is currently considered the best available glucose bounded tumour and infection seeking radiopharmaceutical.

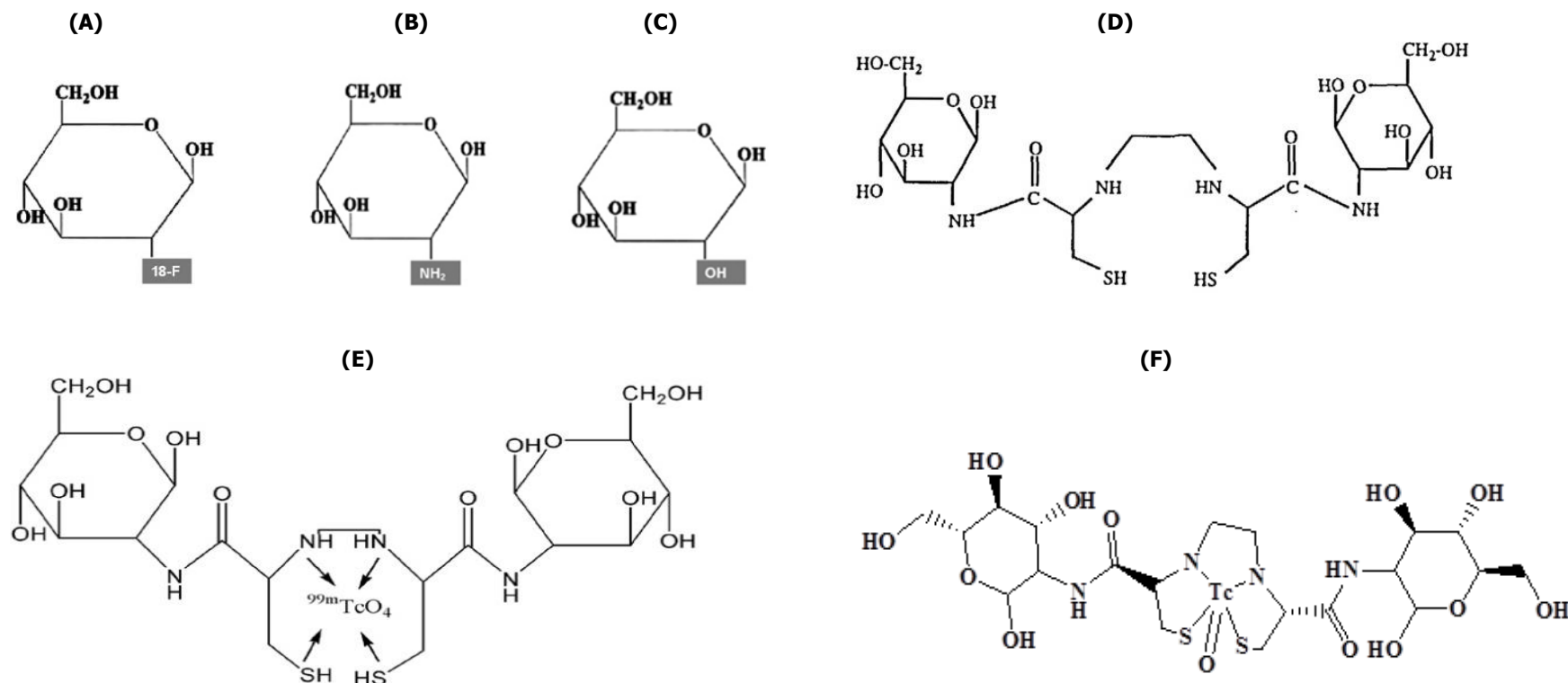
2.5.6.2 *Uptake similarities and differences*

^{99m}Tc -EC-DG is engaged in all three phases of the cell cycle and can assess cell nuclei activity (can transport across cell nuclei membrane) and tumour growth

(Yang *et al.* 2004:444). ^{18}F -FDG is “metabolically trapped,” assessing metabolic activity but cannot satisfactorily evaluate cell nuclei activity (Yang *et al.* 2004:452). FDG and DG corresponds with their chemical structure at position 2 of the sugar where they both have the fluorine and amino group (Yang 2004:444). ^{18}F -FDG and $^{99\text{m}}\text{Tc}$ -EC-DG utilizes different glucose transporters for passage into the cytoplasm of the cell. Glucose transport for ^{18}F -FDG is facilitated into the cell by GLUT 1 and GLUT 3, but for $^{99\text{m}}\text{Tc}$ -EC-DG GLUT 1, GLUT 2 and GLUT 4 become active (Case *et al.* 2012; Zhang *et al.* 2012:7).

There is not only chemical structure and cellular activity differences between ^{18}F -FDG and $^{99\text{m}}\text{Tc}$ -EC-DG, but also nuclear medicine imaging differences. ^{18}F -FDG nuclear medicine images demonstrate high brain uptake, but $^{99\text{m}}\text{Tc}$ -EC-DG demonstrate low brain uptake (Yang *et al.* 2004:452) in animals and humans. A possible explanation for this is that $^{99\text{m}}\text{TcO}_4^-$ is stabilised by the electrons from the nitrogen and sulphur part of EC and that the charge therefore limit the uptake of $^{99\text{m}}\text{Tc}$ -EC-DG across the blood-brain barrier (Yang *et al.* 2003:471). ^{18}F -FDG has no charge and can cross the blood brain barrier (BBB) compared to $^{99\text{m}}\text{Tc}$ -EC-DG. Schechter *et al.* (2009:1583-1591) elaborates that the multiple hydroxyl groups present in the chemical structure might also prevent $^{99\text{m}}\text{Tc}$ -EC-DG to cross the BBB, because of its hydrophilicity. ^{18}F -FDG is not ideal for the diagnosis of low grade tumours due to elevated uptake in the brain, but if the BBB is damaged $^{99\text{m}}\text{Tc}$ -EC-DG can possibly be a diagnostic imaging option for low grade tumours. No normal biodistribution images of $^{99\text{m}}\text{Tc}$ -EC-DG in healthy humans were available in the literature for comparison.

Normal physiological variants can be encountered and should be taken into account in the clinical setting when reporting on ^{18}F -FDG images and should be reported in conjunction with patient history and patient preparation. ^{18}F -FDG uptake differences can be seen on nuclear medicine images to the brain, myocardium, breast, liver, spleen, stomach, intestines, kidneys, urine, skeletal muscle, lymphatic tissue, bone marrow, salivary glands, thymus, uterus, testicles and brown fat (Boellaard *et al.* 2009:191).



(Tc=Technetium; H=Hydrogen; N=Nitrogen; NH=Nitrogen and Hydrogen; O=Oxygen; OH=Oxygen and Hydrogen; S=Sulphur)

FIGURE 2.20: Chemical structures of (A) ^{18}F -FDG, (B) DG, (C) glucose (Adopted from Kumar *et al.* 2007:10), (D) EC-DG (Adopted from Yang *et al.* 2001:514), (E) $^{99\text{m}}\text{Tc}$ -EC-DG (Adopted from Kumar *et al.* 2007:11) and (F) IHP $^{99\text{m}}\text{Tc}$ -EC-DG (Provided courtesy of Necsa)

FIGURE 2.21: The mechanism of cell uptake and accumulation of ^{18}F -FDG, $^{99\text{m}}\text{Tc}$ -EC-DG and glucose (Adopted and redrawn from Yang *et al.* 2005:32)

In Figure 2.22 (A) ^{18}F -FDG demonstrates high uptake to the brain, slight uptake in the myocardium, moderate-mild liver and bone-marrow uptake and radiopharmaceutical excretion through the kidneys to the bladder. In Figure 2.22 (B) and (C) the patients diagnosed with disease administered with $^{99\text{m}}\text{Tc}$ -EC-DG demonstrated moderate uptake to the liver and myocardium and less avid uptake to the skeletal muscles. No brain uptake of $^{99\text{m}}\text{Tc}$ -EC-DG was demonstrated at 2 hour post radiopharmaceutical administration. Good physiological $^{99\text{m}}\text{Tc}$ -EC-DG activity was also noted in the kidneys that were excreted to the urinary bladder, displaying the known renal excretion of this radiopharmaceutical.

2.6 MOLECULAR IMAGING

Nuclear medicine imaging techniques can pinpoint molecular activity in humans and animals, with this ability it can be used for early diagnosis of disease before anatomical changes occur in the diseased area. In order to detect tumour sites the mechanism existing in the cancer cell must be present in elevated levels in the tumour, but nonexistent or in low levels in normal tissue (Weissleder *et al.* 2010:1182). Cancer therapy on the other hand has a higher variety of potential targets for cancer imaging to guided therapy. The therapy type and the monitoring of treatment are influenced by the increased and decreased levels of the mechanism. Figure 2.23 depicts a variety of targets for tumour detection.

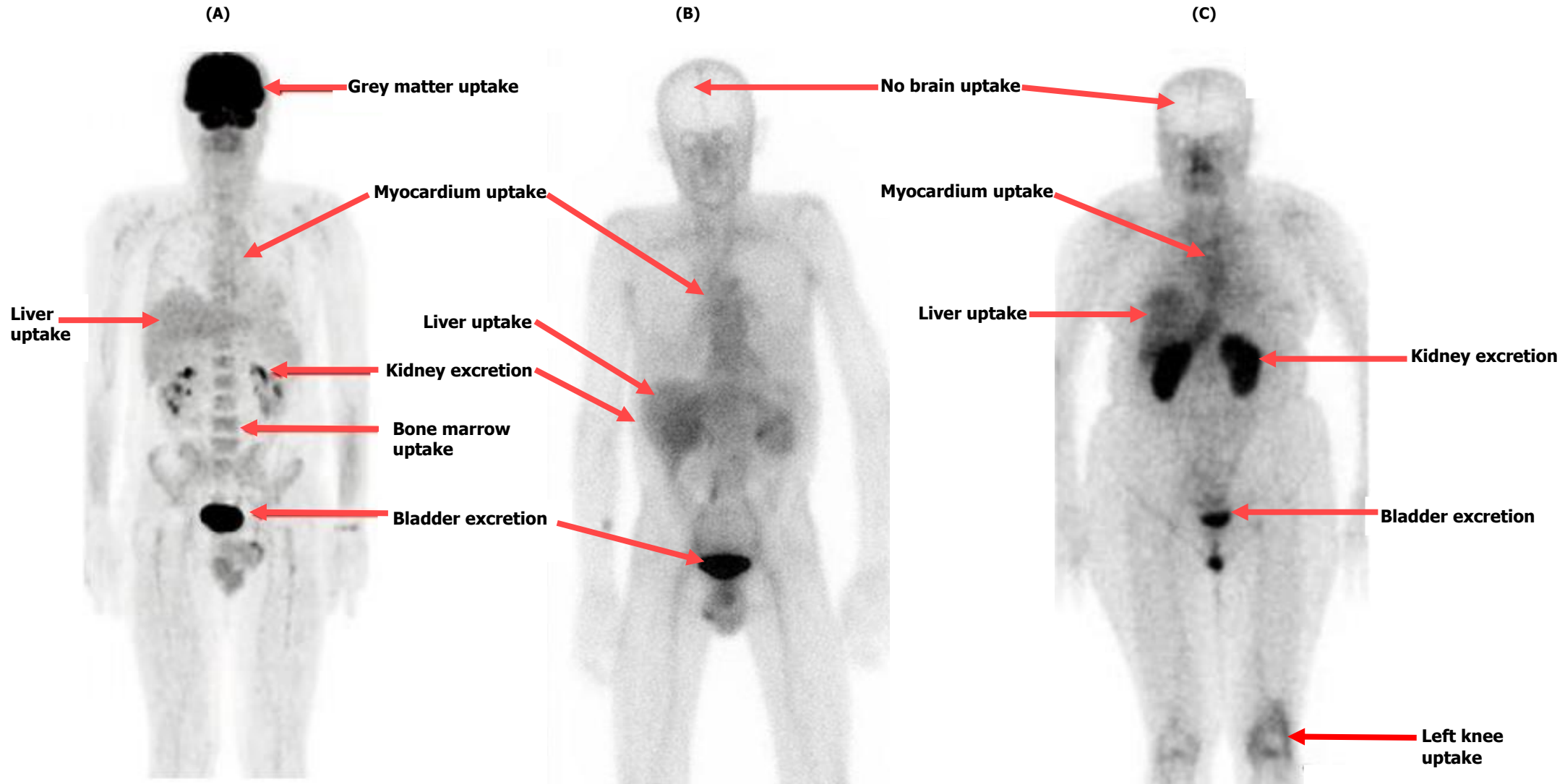


FIGURE 2.22: Anterior whole-body images of (A) ^{18}F -FDG in a healthy patient (Fanti *et al.* 2014:6), (B) $^{99\text{m}}\text{Tc}$ -EC-DG in a patient with NSCLC in the right upper lung at 2 hours post radiopharmaceutical administration (Schechter *et al.* 2009:1589) and (C) $^{99\text{m}}\text{Tc}$ -EC-DG in a patient with rheumatoid arthritis in the left knee at 2 hours post radiopharmaceutical administration (Kumar *et al.* 2007:13).

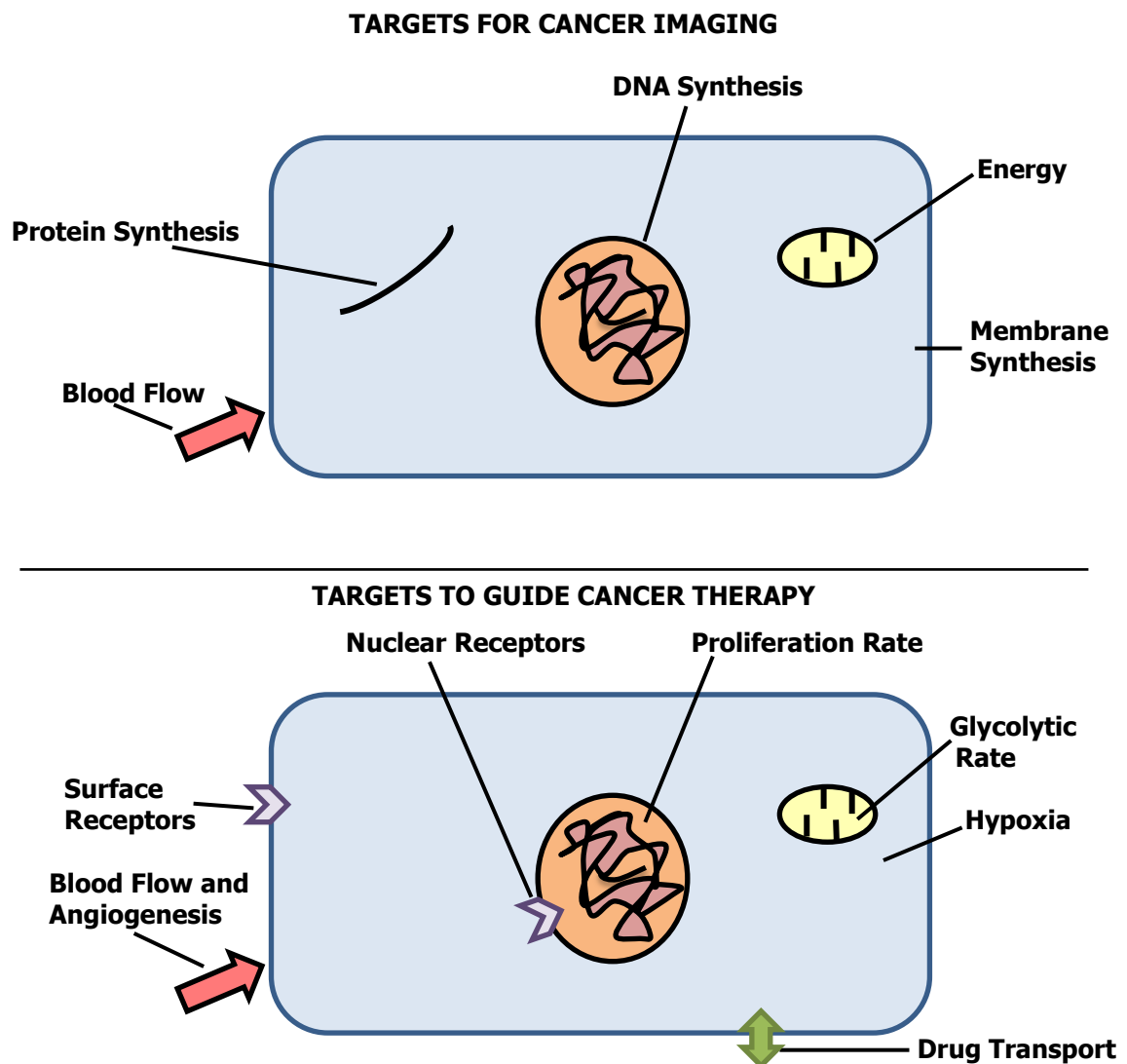


FIGURE 2.23: Illustration of cancer cell targets for imaging (Adapted and redrawn Weissleder *et al.* 2010:1182)

The different imaging modalities show variances in physical characteristics relating to the sensitivity, temporal and spatial resolution (Fass 2008:117). In comparison with other imaging modalities, PET and nuclear medicine studies are superior in sensitivity lying between nanomole/kg and picomole/kg, making them the most sensitive clinical imaging modalities (Fass 2008:117). CT, MRI and ultrasound can not provide cellular target information and have to be used in conjunction with nuclear medicine imaging modalities to overcome this limitation (Schechter *et al.* 2007:1). Physical properties of imaging modalities can vary in respective to sensitivity, temporal and spatial resolution and in Figure 2.24 the referring sensitivity of particular imaging technologies is depicted (Fass 2008:117).

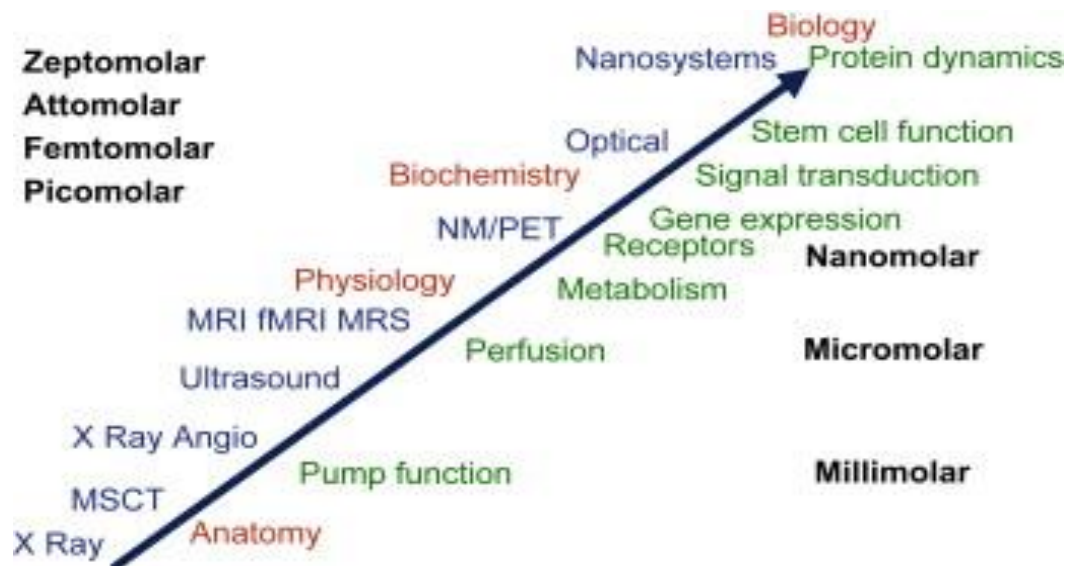


FIGURE 2.24: Comparison of the sensitivity of different imaging modalities (Adopted from Fass 2008:117)

2.6.1 PET/CT

2.6.1.1 Principles

PET/CT provides not only physiological parameters with superior spatial resolution, but also anatomical information that can improve diagnosis through localisation. The principle of PET still remains the same where gamma rays emitted from positron decaying radionuclide in opposing directions after interaction with tissue (Zanzonico 2004:87). The positron is annihilated by colliding with an electron and the atomic nuclei of the matter and combines with a free electron founding a positronium (Ziegler 2005:679). The positronium then decays through the activity of annihilation. A pair of gamma rays (511 keV) is created that progress in opposite directions, that can be detected by the scintillation detectors of a PET camera. The PET equipment detects these coincidence signals from several planes at the same time to provide at the end a three-dimensional image after the data is reconstructed (Zanzonico 2004:87).

2.6.1.2 Positron-emitting radionuclides

PET radionuclides that can be effectively used for nuclear medicine clinical studies (see Figure 2.25) included ^{18}F (tumour and IFI/IF), Carbon-11

(metabolism), Iodine-124, Yttrium-86, Oxygen-15 (perfusion agent), Copper-64. Nitrogen-13 (metabolism) and Gallium-68 (blood volume, IFI/IF) is accessible from radionuclide generators (Fass 2008:133; Ziesmann *et al.* 2014:9). A variety of diagnostic procedures can be provided with unique information to evaluate and monitor cardiac -, neurological, pulmonary disease and cancer. These radionuclides and radiopharmaceutical will not be discussed in detail as IHP ^{99m}Tc -EC-DG is compared as glucose analogue with ^{18}F -FDG and forms the focus of this dissertation.

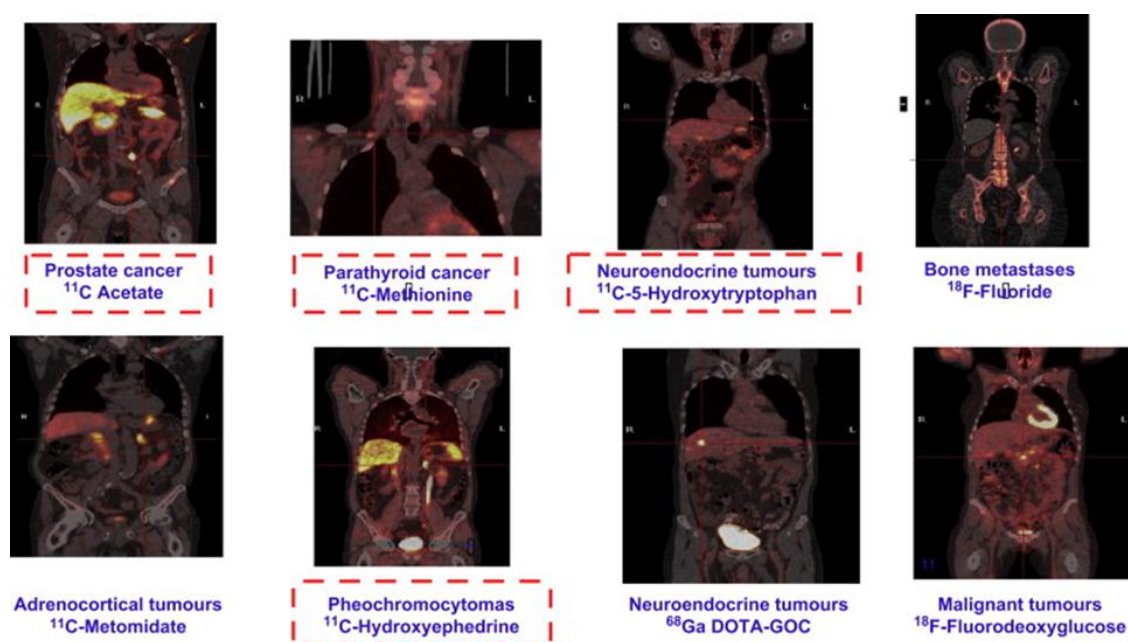


FIGURE 2.25: A selected few PET radiopharmaceuticals used in imaging for cancer management (Fass 2008:134)

2.6.1.3 Applications

PET imaging play a role in the diagnosis of cancer and especially in determining the cancer therapy success as a staging tool. The time point at which breast and lung cancer is detected can make a difference in the treatment management of a patient. ^{18}F -FDG is not ideal for the diagnostic screening of primary breast cancer, due to its high cost compared to mammography (Eubank & Mankoff 2005:85). ^{18}F -FDG PET/CT imaging plays an important supporting role with ^{99m}Tc -MDP bone scan and CT in the regulating, monitoring of cancer patients and detecting recurrent cancer.

2.6.1.4 ^{18}F -FDG PET/CT gold standard

PET combined with CT, has become more popular in private health practice for tumour detection and localization (Chen *et al.* 2006:342). In most of the PET/CT studies, the radiopharmaceutical ^{18}F -FDG a glucose analogue is used. The cost of a PET/CT ranges between 14-17 million rand and a cyclotron from 15 million rand. There are only three cyclotrons (producing ^{18}F -FDG) in RSA, two in Pretoria and one in Cape Town.

Very few private practices can afford the luxury of a PET/CT positron camera with its own cyclotron and furthermore, cannot be afforded by rural practices due to budget constraints. The result is that high doses of ^{18}F -FDG often have to be transported from a cyclotron to a distant PET/CT to compensate for the short half-life of ^{18}F . The high cost of a PET/CT centre with a cyclotron makes it an impossible dream for the primary health care system, as the constraints on the budget too high. ^{18}F as a radionuclide, therefore has certain advantages and disadvantages and has to be compared with other tumour radionuclides in the search for an alternative.

2.6.2 SPECT/CT

The gamma camera is the most shared and commonly used imaging system by nuclear medicine departments and was developed in the 1950s (Elgazzar 2011:2). Dynamic-, static-, whole-body and SPECT acquisitions can be obtained with a gamma camera. SPECT shows the three dimensional activity radionuclide and radiopharmaceutical uptake in organs and tissues with better contrast and improved delineation of pathology compared to whole-body planar imaging (Buck *et al.* 2008: 1305). SPECT provides poor anatomical information and the ideal is to combine it with CT to diminish this limitation. Hybrid SPECT/CT combines the best of both imaging modalities with SPECT's improved sensitivity and CT's high specificity.

2.6.2.1 Principles

Two-dimensional input data from the CT reconstruction consists of two-dimensional projection images taken at several angles around the body

(Naudé 1998:2.2). Back-projection works on the principle that counts from a single pixel of the planar projections are projected back through the computer space, each pixel of a projection establishing a trans-axial row for 360 degrees. The projection profiles for a single case of a point source of activity are taken into account. Every profile maps the position of the point source in the direction parallel to the projection profile and computers are then designed to use reconstruction algorithms to incorporate the statistical information for analysis of the image. Equal values are allocated to all points in the object plane contributing to the scan profile. The principles SPECT with image reconstruction is clearly outlined by Groch & Erwin (2000:233-244).

An advantage of SPECT is that it provides three dimensional improved target to non-target ratios compared to planar imaging, because it removes pointless information, both foreground and background (Early & Sodee 1995:291). A limitation that influences the SPECT/CT imaging is patient movement between sequential imaging of each modality (Williams 2011: 37). PET has up to three times higher sensitivity than SPECT cameras (Rahmim & Zaidi 2008:94). A variety of factors influence the resolution of images obtained by PET and SPECT cameras. The strengths, limitations and challenges of PET compared to SPECT were reviewed by Rahmim & Zaidi (2008:193-203).

2.6.2.2 *Single photon radionuclides*

$^{99m}\text{TcO}_4^-$ is the main single photon radionuclide used in nuclear medicine. Alternative single photon radionuclides that can be used for scintigraphy includes Iodine-123, Iodine-131 and Tallium-201 (Ziesmann *et al.* 2014:8-9).

2.6.2.3 *Applications*

SPECT combined with radionuclides and radiopharmaceuticals can provide improved physiological information on organs and tissue e.g. brain, thyroid, heart, pulmonary system, skeletal-, cardiac to evaluate for diagnosis of disease.

2.6.3 Small-animal imaging systems

2.6.3.1 *Principles*

Small-animal imaging systems have several advantages over clinical systems for RP animal research (Williams 2011:38). These advantages include improved spatial resolution that can be up to ten times more than a clinical system and easy transport between research centres due to their small size. The research performed with the IHP ^{99m}Tc -EC-DG in mice and rabbit models could not use these small- animal imaging systems as they were not available at Universitas Academic hospital. The baboon and rabbit model used the conventional clinical imaging system to evaluate IHP ^{99m}Tc -EC-DG biodistribution.

2.6.3.2 *Applications*

Dynamic acquisitions, planar static, planar whole-body, SPECT/CT and PET/CT can be used to obtain different information needed for pre-clinical research in small animals with radionuclides and radiopharmaceuticals (Pomper & Lee 2005: 3251). Nuclear medicine imaging modalities with small animals can be used to obtain pharmacokinetics-, pharmacodynamics-, gene expression-, cell tracking-, protein-protein interaction- and receptor-based imaging information for drug development.

2.7 CONCLUSION

^{18}F -FDG and ^{99m}Tc -EC-DG mimics each other in respect that they are both glucose analogues and can therefore provide information on metabolic changes that occur because of IFI/IF and tumours. The differences between these two radiopharmaceuticals include physical half-life, biodistribution, cost, production methods and equipment needed for imaging. There are a variety of that can be used for IFI/IF imaging, but not one specifically identifies infection over inflammation. Many radionuclides and radiopharmaceuticals are non-specific to distinguish between infection and inflammation. Usually it is possible to distinguish clinically (inflammatory signs red, heat, pain and loss of function) – uptake is dependent on the degree of

cellular infiltration. Cancer cells develop accelerated metabolism and because of the uptake mechanism of ^{18}F -FDG and $^{99\text{m}}\text{Tc}$ -EC-DG that is increased by increased metabolic activity and therefore localise in tumours. Factors like interspecies differences between themselves and humans, type of anaesthesia, fasting or non-fasting state of animal and holding conditions (passive or active) can influence the biodistribution of the test radiopharmaceutical. These factors should be closely looked at when designing the protocol for a pre-clinical study to ensure the success of the research. Mice, rabbits and baboons were chosen for their specific advantages as animal models to evaluate the normal-, tumour and IFI/IF biodistribution of IHP $^{99\text{m}}\text{Tc}$ -EC-DG. The literature review clarified that scintigraphic imaging and biosampling could be used to evaluate the biodistribution of IHP $^{99\text{m}}\text{Tc}$ -EC-DG in healthy, focal IFI/IF and tumour animal models.

CHAPTER 3

METHODOLOGY

3.1 INTRODUCTION

The biological animal model design is a known pre-clinical tool for the evaluation of molecular imaging radiopharmaceuticals for normal biodistribution and disease detection. The research design chosen involved an initial pilot study, followed by the research phases to evaluate the normal biological biodistribution, IFI/IF and tumour detection properties of the IHP ^{99m}Tc -EC-DG in different animal models. This research study consisted of three research phases to achieve the overall goal and aim. The radiation and health safety aspects of the research materials, scintigraphic equipment and the aspects relating to the experimental work with the DL technique and the KF of the IHP ^{99m}Tc -EC-DG used during the research will be discussed. The pilot study results are given since it was used to assist the research design of the three phases. Each of the three phases are described in separate chapters and include aspects like the materials and methods, sample, research design, results and data analysis.

3.2 MATERIALS, METHODS, RESULTS AND CONCLUSION OF PILOT STUDY

3.2.1 Introduction

The UFS Animal Research Centre does not house nude mice (xenografts) and therefore the decision was made to do a pilot study only on New Zealand White rabbits with IFI/IF. Economical, ethical and logistical considerations were taken into account with the research design of the different phases and therefore the scintigraphic imaging was done in the DNM at UAH with research animals obtained from the UFS Animal Research Centre. Additionally, rabbits were also used for the pilot study due to their availability and the cost implicative relative to baboons. Inoculation of the animals in the pilot study was done with *E. coli* rather than tumour cells since the Department of Micro-Biology at UAH supplied it without additional cost implications. Complementary to this, the IFI/IF cells also have an increased metabolism, (though lower than tumour cells) it was hypothesised that this raised metabolism of the targeted cells which would increase biodistribution of the IHP ^{99m}Tc -EC-DG to the induced IFI/IF area, making the

imaging possible. The aim of the pilot study was to determine whether there was any biodistribution of IHP ^{99m}Tc -EC-DG to a septic IFI/IF induced area in rabbits in comparison to ^{67}Ga -citrate.

Ethical approval for the pilot study protocol was obtained from the Ionising Radiation Control Committee of UAH and Pelonomi Hospital as well as the Interfaculty Animal Ethics Committee (UFS). Permission from the Head of Clinical Services at UAH and the Chief Specialist of the DNM at UAH were also obtained. The same protocol for the induction of septic IFI/IF in rabbits by Rossouw *et al.* (2005:390) was used for the pilot study. IHP ^{99m}Tc -EC-DG ($n=3$) was intravenously administered into the left (LT) ear vein of $n=3$ of the rabbits induced with septic IFI/IF and ^{67}Ga -citrate to two different rabbits. Labelling efficiency of direct labelling technique of the IHP ^{99m}Tc -EC-DG and biodistribution of IHP ^{99m}Tc -EC-DG DL to the area of induced septic IFI/IF compared to ^{67}Ga -citrate in rabbits were confirmed during this study.

Festing and Altman (2002:247) emphasized the importance of a pilot study to ensure optimal research design for statistical analysis. A pilot study does not have to be composed of a large sample size, but can even consist of a single animal to obtain the necessary information. The pilot study research design followed was two-fold and is illustrated in Figure 3.1. Firstly, a preliminary literature review was carried out relating to septic IFI/IF animal models, furthermore on ^{99m}Tc -EC-DG and ^{67}Ga -citrate and their radiopharmaceutical properties. Secondly, a prospective *in vivo* study was done on five male adult (± 3 kg) healthy immune-competent New Zealand White rabbits obtained from the UFS Animal Research Centre, an accredited supplier of animals used for pre-clinical research. Imaging was performed at the DNM, UAH. A qualified chief veterinary laboratory animal technician from the UFS Animal Research Centre sedated, administered the IHP ^{99m}Tc -EC-DG and monitored the rabbits.

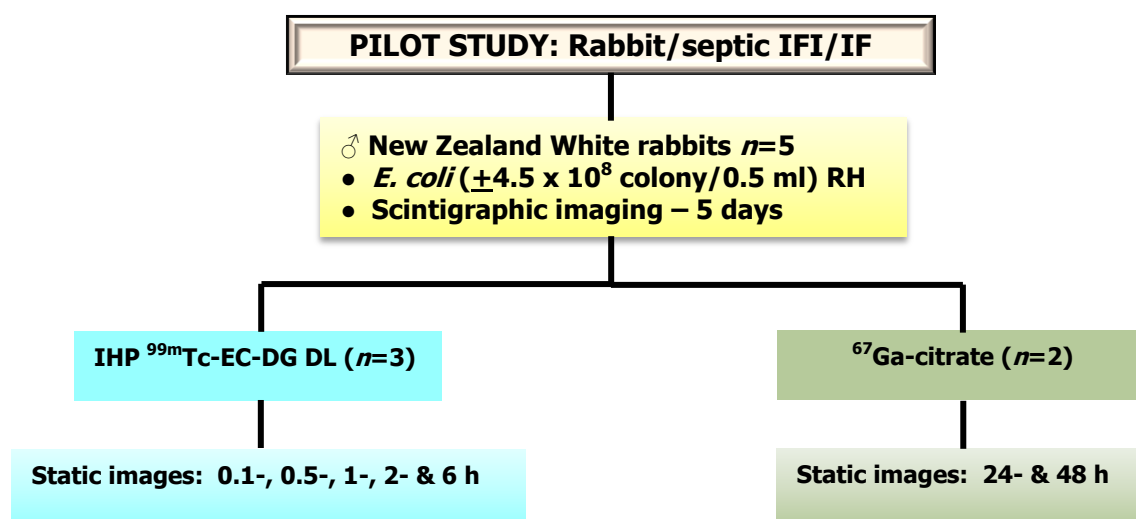


FIGURE 3.1: Research design of the pilot study

3.2.2 Materials and methods

3.2.2.1 Sample size

Five healthy immune-competent New Zealand White rabbits were used for the pilot study. Only adult (± 3 kg) male rabbits were available for this study, as the female rabbits at the UFS Animal Research Centre are used for breeding purposes only.

3.2.2.2 Animal handling and monitoring

The rabbits were monitored for side effects. An animal welfare score sheet was completed for each of the rabbits included in the research and the following parameters were monitored: mass of the rabbits, body temperatures, stools, general condition and abnormal behaviour. The rabbits administered with IHP $^{99m}\text{Tc-EC-DG}$ and $^{67}\text{Ga-citrate}$ were not fasting and kept separate from other rabbits in order to avoid radiation exposure to the other animals at the UFS Animal Research Centre that had not participated in the pilot study. The $t_{1/2}$ of $^{99m}\text{TcO}_4^-$ is 6 hours and of $^{67}\text{Ga-citrate}$ is 3.2 days. The rabbits administered with $^{99m}\text{TcO}_4^-$ were kept separate for 60 hours and the rabbits administered with $^{67}\text{Ga-citrate}$ for 32 days (ten times the $t_{1/2}$ of the radionuclide administered to the rabbits). The urine and faeces of the rabbits

were washed away as usual. The radio-activity administered to the rabbits was fairly low and no toxicity-, adverse and side-effects were experienced by the animals. The septic IFI/IF induced rabbits were given antibiotics until they were healthy.

3.2.2.3 Radiosynthesis of ^{99m}Tc -EC-DG (DL)

IHP ^{99m}Tc -EC-DG (DL) used was prepared according to the procedure described in section 3.3.5.3.

3.2.2.4 Gamma scintigraphy studies

3.2.2.4.1 Induced IFI/IF biodistribution

The technique described in the research by Rossouw *et al.* (2005:390) was used to induce the septic IFI/IF into five rabbits. A focal area of septic IFI/IF was induced with *E. coli* by intradermal administration of 0.5 milliliter (ml) of a suspension approximately 9×10^8 colony forming units per ml into the right (RH) thigh muscle of a rabbit. The septic IFI/IF was allowed to develop over a period of 120 hours (5 days). ^{67}Ga -citrate was ordered from iTemba LABS (Faure, Western Cape, RSA). The EC-DG was couriered from Necsa and was labelled with $^{99m}\text{TcO}_4^-$ at the DNM at UAH. The rabbits were sedated using a combination of ketamine (20 mg/kg) and medetomedine (0.3 mg/kg) as needed and the imaging of the IHP ^{99m}Tc -EC-DG and ^{67}Ga -citrate commenced 120 hours after induction of septic IFI/IF at specific time intervals post radiopharmaceutical administration (Rossouw et al. 2005:385). Eighty to ninety three MBq in 0.2 ml of the IHP ^{99m}Tc -EC-DG ($n=3$) was intravenously administered into the left (LT) ear vein of rabbits. Two different rabbits were administered with 10-13 MBq (0.2 ml) ^{67}Ga -citrate per animal into the LT ear vein.

A Siemens MultiSPECT 2 gamma camera (Multispect 2; Siemens Medical Solutions, Chicago, IL, USA) connected to a Siemens ICON acquisition and processing workstation was used for the scintigraphic acquisition and processing of the pilot study. The useful field of view is 53 cm x 38 cm. The intrinsic spatial resolution is 3.8 mm FWHM. The gamma camera was equipped with low-energy high resolution parallel-hole collimators (LEHR) for imaging with the IHP ^{99m}Tc -EC-DG. When imaging was performed with ^{67}Ga -citrate the gamma camera was equipped with medium-energy high resolution (MEHR) collimators. The New Zealand White rabbits were immobilised and positioned prone on the gamma camera imaging bed. Static planar ANT and POST whole-body images were collected with the stop conditions set at five minute recording times for the collection of count/whole-body over various time intervals. The matrix size was set at 256 x 256 and the zoom at 1 for the static images. The time intervals of imaging the IHP ^{99m}Tc -EC-DG were as follows for the pilot study: 0-, 0.5-, 1-, 2- and 6 h post administration. The scintigraphic imaging time intervals of imaging the ^{67}Ga -citrate were as follows: 24- and 48 h post administration. The images obtained with the IHP ^{99m}Tc -EC-DG and the ^{67}Ga -citrate was automatically transferred to the Siemens ICON workstation where all processing were performed.

3.2.3 Data analysis

3.2.3.1 *Quantitative analysis of the image of IFI/IF induced rabbits*

The uptake was expressed as a percentage of the count ratio between the ROIs drawn around the septic IFI/IF RH (target) versus the LT thigh muscle (non-target) on the ANT and POST static images. The counts in the ROIs drawn on the LT thigh muscle were considered to provide background counts (Rossouw *et al.* 2005:390). The mean \pm standard deviation was also calculated.

3.2.4 Results and discussion

3.2.4.1 Radiosynthesis of IHP ^{99m}Tc-EC-DG (DL)

IHP ^{99m}Tc-EC-DG (DL) was determined to have a radiochemical purity of 92.9% immediately after labelling which decreased to 90.9% after 3.25 h. No significant colloid formation was found (0.14%). A limit of 90% is suggested by Saha (1996:7) for "bound" Tc chelate and the labelling efficiency of IHP ^{99m}Tc-EC-DG (DL) was above this specification.

3.2.4.2 In vivo biodistribution images

The six hour delayed whole body static image of rabbit one, demonstrated a visible area of well-defined intense increased uptake in the region of the right hip (Table 3.1). The area of intense increased uptake matched the clinical details of the induced septic IFI/IF source. The six hour delayed whole-body static image of rabbit two, demonstrates a visible area of well-defined intense increased uptake in the region of the RH hip. The area of intense increased uptake matched the clinical details of the induced septic IFI/IF source. The two hour delayed images of rabbit three, demonstrated an area of increased uptake, varied in intensity compared to the urinary bladder, in the lower pelvis. The area of increased uptake can also be noted in the RH lower pelvis on the posterior view of the six hour delayed images, corresponding with the site of induction of septic IFI/IF source. Contamination was also seen in the lower pelvic area.

TABLE 3.1: Summary to indicate the biodistribution of IHP ^{99m}Tc-EC-DG and ⁶⁷Ga-citrate in rabbits to the area of induced septic IFI/IF

Radiopharmaceutical	Rabbit number	0 h	0.5 h	1 h	2 h	6 h	24 h	48 h
IHP ^{99m} Tc-EC-DG	1	x	x	x	x	√	#	#
	2	x	x	x	x	√	#	#
	3	x	x	x	√	√	#	#
⁶⁷ Ga-citrate	4	#	#	#	#	#	√	√
	5	#	#	#	#	#	√	√

Static image not acquired

x Uptake of radiopharmaceutical not visually noted on images in the area of interest

√ Uptake of radiopharmaceutical visually noted on images in the area of interest

3.2.4.3 Quantitative analysis

ROIs were drawn over the LT and RH thigh on the ANT and POST images of rabbit number one and -two administered with IHP ^{99m}Tc -EC-DG and rabbit number four and -five administered with ^{67}Ga -citrate. Rabbit number three administered with IHP ^{99m}Tc -EC-DG had to be excluded from the statistics as the area of urine contamination in the lower pelvic area of the rabbit influenced the count statistics.

TABLE 3.2: Count ratio of the RH versus LT thigh muscle of rabbits induced with *E. coli* administered with IHP ^{99m}Tc -EC-DG and ^{67}Ga -citrate

Radio-pharmaceutical	RH/LT count ratio at time points x 100						
	0 h	0.5 h	1 h	2 h	6 h	24 h	48 h
IHP ^{99m}Tc -EC-DG ^a	106 ± 10	103 ± 0.7	81 ± 7	82 ± 1	421 ± 77	#	#
^{67}Ga -citrate ^b	#	#	#	#	#	248±125	201±85

Data not acquired

^a Average of data obtained with two rabbits

^b Average of data obtained with two rabbits

The counts of the LT thigh were divided by the counts of the RH thigh and then multiplied by a 100 to obtain the RH/LT percentage and the mean ± standard deviation was calculated (Table 3.2).

3.2.5 Conclusions and recommendations from pilot study

The pilot study scintigraphic imaging reported results indicated biodistribution of the IHP ^{99m}Tc -EC-DG to a septic IFI/IF induced area. Scintigraphic findings also demonstrated biodistribution of the IHP ^{99m}Tc -EC-DG to the area of induced septic IFI/IF at six hour imaging time intervals on the whole-body static images. The uptake of IHP ^{99m}Tc -EC-DG at six hours post administration is similar to the uptake of 24- and 48 hour images of ^{67}Ga -citrate in areas of induced septic IFI/IF. IHP ^{99m}Tc -EC-DG could therefore be a cost effective and more affordable diagnostic radiopharmaceutical compared to ^{67}Ga -citrate for IFI/IF imaging and needed to be further investigated as a diagnostic imaging radiopharmaceutical.

The area of induced septic IFI/IF in the rabbits for the pilot study was the RH thigh area. Urine contamination with IHP ^{99m}Tc -EC-DG was seen with one of the rabbits in the area close to the RH thigh area of induced focal septic IFI/IF. The rabbits utilised for pilot study were not catheterized as the standard manual retrograde urinary catheterization can be a difficult procedure to perform (Uthamanthil *et al.* 2013:180). The full bladders of rabbits has an influence on the count ratio (statistics) of the area of induced IFI/IF of the IHP ^{99m}Tc -EC-DG and the ^{67}Ga -citrate. The recommendation was also made from the pilot study that methods and techniques should look at the micturition of the urinary bladders of the rabbits and to limit urine contamination. The suggestion was made that paediatric urine sample bags (U-bag) be attached around the area of the urethra of the rabbit to be used for the period of imaging in order to limit spread of urine contamination and this was incorporated in phase two of this research. The use of urine bags was implemented during phase two. This pilot study therefore forms the basis for the research framework of phase two that was designed to evaluate the potential of IHP ^{99m}Tc -EC-DG as an IFI/IF imaging agent though the evaluation of the biodistribution patterns of the IHP ^{99m}Tc -EC-DG in rabbits.

3.3 ETHICS, MATERIALS AND METHODS OF THE THREE PHASES RESEARCH

The research methods and design that were used in this research, to address the research questions are briefly elucidated on in the following section. Following the introductions of Chapter 4 – 6 additional details on the materials and methods used for each specific phase will be provided.

3.3.1 Ethical approvals

The research proposal was approved by the UFS Evaluation Committee for a Ph.D. in Clinical Nuclear Medicine. Permission was obtained from the Radiation Control Committee of Universitas/Pelonomi Hospitals (Appendix A). The head of clinical services of Universitas Academic Hospital also provided authorisation for this study to continue (Appendix B). Ethical Approval was obtained from the North-West University (NWU) Ethics Committee (Appendix C) and the UFS Interfaculty Animal Ethics Committee for this research (Appendix D).

3.3.2 Materials and methods of the research

Diseases and physiological conditions present in humans can very accurately be replicated and researched by the use of animal models. Three different species of animals were utilised to obtain the necessary research data to contribute to the evaluation of the diagnostic potential of the IHP ^{99m}Tc -EC-DG for molecular imaging of IFI/IF and tumours. The biodistribution of IHP ^{99m}Tc -EC-DG in lung tumour-bearing mice was compared to ^{18}F -FDG under the same circumstances to gain knowledge about the tumour biodistribution differences of these two glucose metabolism radiopharmaceuticals. With the IFI/IF accumulation characteristics of ^{67}Ga -citrate borne in mind, it was of value to determine what the difference in IFI/IF biodistribution of ^{67}Ga -citrate was when compared to that of IHP ^{99m}Tc -EC-DG. Research has shown that ^{67}Ga -citrate accumulates in *E. coli* induced IFI/IF sites and therefore was used for comparison purposes with the IHP ^{99m}Tc -EC-DG biodistribution. This research evaluated the biodistribution and diagnostic potential of IHP ^{99m}Tc -EC-DG in healthy animals (mice, rabbits and baboons), lung tumour-bearing mice and rabbits induced with septic and sterile IFI/IF with a three phase research design (Figure 3.2).

A quantitative approach was followed for this research design of all three phases of the research. First for phase one, the activity for the organs each of the sacrificed healthy and lung tumour-bearing mice were measured in a well-counter. Each of these sample tissues was calculated and expressed as the percentage of the administered (injected) dose per gram of tissue wet weight (%ID/g). Regions of interest (ROIs) were drawn around the organs of healthy rabbits (phase two) and baboons (phase three) administered with the IHP ^{99m}Tc -EC-DG or $^{99m}\text{TcO}_4^-$ in order to obtain quantifiable differences in relation to the whole-body for specific time intervals after radiopharmaceutical administration. ROIs were also drawn around the IFI/IF area and the opposite non-affected area to obtain quantifiable difference between the two regions of interest to compare IFI/IF uptake differences of ^{67}Ga -citrate and IHP ^{99m}Tc -EC-DG (phase two). Hence, these quantifications formed the basis for the discussion and clarification. The next section will outline the methods briefly.

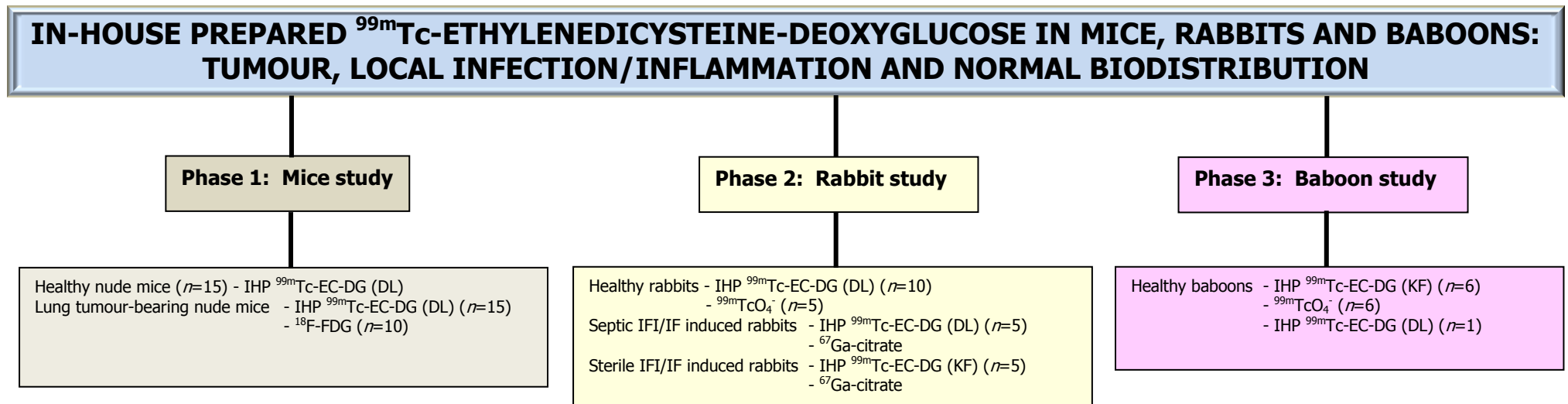


FIGURE 3.2: A schematic overview of the three research phases

3.3.3 Animal models used in this research

3.3.3.1 *Healthy and lung tumour-bearing nude mice model*

Mice are one of the most studied animals used in research and they are well understood regarding their anatomy, physiology and genetics. Nude mice also have an absent thymus and therefore have an inhibited immune system due to the absence of the thymus (T) cells also known as T lymphocytes (Sharkey & Fogh 1984:341). The absence of T cells prevents nude mice from rejecting inoculated tumours (after inoculation referred to as xenografts) and therefore was one of the main motivations to use nude mice for this specific research. The nude mice were sacrificed, as the RSA does not have facilities to perform live small animal scans, microPET/CT and nanoSPECT/CT. The study with mice as animal model was performed *ex vivo* and the method of counting the radioactivity of the different body organs and the area of tumour growth of the nude mice was used to determine the biodistribution (see 4.2.5). Male and female nude mice were used for phase one.

3.3.3.2 *Healthy rabbit model*

The use of rabbits as an animal model have advantages; amongst them being, easy to handle and big enough for imaging on a SPECT gamma camera used for human scintigraphic imaging. Furthermore, the rabbits are small enough for whole-body imaging to obtain complete quantification data to determine normal IHP ^{99m}Tc -EC-DG biodistribution in the healthy rabbits.

3.3.3.3 *IFI/IF rabbit model*

The Oxford Concise Medical Dictionary (2003:350) defines inflammation as the body's response to injury and that inflammation can be acute or chronic. Infection is defined as the invasion of the body by harmful organisms (pathogens) such as bacteria, fungi, rickettsiae, or viruses (Oxford Concise Medical Dictionary (2003:350-351). Rennen *et al.* (2000:241) outlined the symptomatic response to an acute infection/inflammation as the following:

- Increased local blood supply

- The area involved will display increased vascular permeability
- Increased transudation of plasma proteins
- Increased influx of the leucocytes

New Zealand rabbits induced with IFI/IF have been confirmed as the appropriate animal models for ^{67}Ga -citrate imaging for physiological biomedical research (Sykes *et al.* 1987:95) and therefore used as the control experiment in the IFI/IF rabbit model. The normal biodistribution of ^{67}Ga -citrate in rabbits is to the kidneys, skeleton, liver and spleen while in humans was found to be to the liver, spleen, marrow, skeleton, gastrointestinal and urinary tract. An inconsistent accumulation was also found in the breasts, nasopharynx, lacrimal- and salivary glands (Ziesmann *et al.* 2014:323).

The decision was made to induce *Escherichia coli* (*E. coli*) for this septic IFI/IF model rather than *Staphylococcus aureus* as the latter can cause sepsis and significant number of deaths especially in rabbit IFI/IF models (Oyen *et al.* 2001:153). Thus, assuming *E. coli* has a lower pathogenicity than the latter. In accordance with the non-specific inflammatory accumulation characteristics of ^{67}Ga -citrate borne in mind, it was of value to determine what the difference in biodistribution of ^{67}Ga -citrate and IHP $^{99\text{m}}\text{Tc}$ -EC-DG is. Research has shown that ^{67}Ga -citrate accumulates in *E. coli* induced IFI/IF sites and therefore was used for the comparative purposes with the IHP $^{99\text{m}}\text{Tc}$ -EC-DG biodistribution (Rossouw, Lötter, Du Raan, Jansen, Höhn & Burger 2005: 394). The induction of *E. coli* in the rabbit model is referred to as the septic IFI/IF model (phase two) in this research. The rabbits in the research were not immune-compromised in order to obtain information about IHP $^{99\text{m}}\text{Tc}$ -EC-DG biodistribution in both healthy rabbits as well as then with *E. coli* local IFI/IF. The *E. coli* was used in the pilot study for the septic IFI/IF model and it was therefore decided to continue using this model for phase two.

Zymosan is a protein – polysaccharide complex extracted from the cell wall of yeast and can be induced in animal models to trigger an immune response (Erdő, Török, Arányi & Székely 1993:137). Zymosan has been used in various kinds of induced animal IFI/IF models for example arthritis, paw edema, pleuritis, skin inflammation, peritonitis and air pouch inflammation. The

zymosan induced as an IFI/IF is referred to in the dissertation as the sterile IFI/IF model (also part of phase two). A septic IFI/IF model with the *E. coli* produces a hyperemic lesion with granulocytes without major puss formation. Zymosan produces a granulocyte rich infiltration, whereas other sterile IFI/IF models for example with turpentine oil results in hyperaemia and increased vascular permeability with minor cellular infiltration (Oyen *et al.* 2001:153). Zymosan was chosen rather than turpentine oil in order to induce a sterile IFI/IF model to achieve a granulocyte rich IFI/IF area. Information was obtained from uptake by the IHP ^{99m}Tc -EC-DG in this IFI/IF induced area. Zymosan was purchased from Davies Diagnostics Proprietary Limited (Pty Ltd).

3.3.3.4 Healthy baboon model

The motivation behind the use of a baboon as an animal model, was the numerous resemblances to the human physiology. Research that utilises a baboon model can use the same equipment that are used in human scintigraphic imaging and apply all parameters of the human physiology (Dormehl, Hugo & Beverley 1992:109). The SPECT/CT gamma camera used to collect the research data on the baboons is also used for human scintigraphic studies at the DNM at UAH.

In-vivo studies for this research were necessary to determine the physiological distribution of the IHP ^{99m}Tc -EC-DG. As the physiological characteristics of a baboon are very close to a human, any adverse reactions experienced by the baboons from the IHP ^{99m}Tc -EC-DG, would probably also be experienced by humans. The baboon as an animal model is therefore ideal for toxicity tests of new drugs or radiopharmaceuticals. The utilisation of a baboon model before the research and testing of the IHP ^{99m}Tc -EC-DG for human trials was a good quality assurance safety option. Formerly, Dormehl *et al.* (1992:109) also stated that the baboon is phylogenetically similar to humans and hence, enables the additional significant extrapolation of the results. The large size of the baboon was another advantage as the SPECT/CT gamma camera equipment used for this research is designed to accommodate whole-body imaging of a human being.

3.3.4 Animal handling and monitoring

3.3.4.1 Mice Model

The nude mice were housed at the Animal Research Centre at the Potchefstroom campus of the NWU under normal temperature, humidity and light conditions. The ethical guidelines outlined by Workman *et al.* (2010:1555-1577) were followed in order to comply with GLP and all RSA regulations for the scientific use of animals for research purposes (section 2.4.1). The PCDDP is an accredited supplier of animals and provided the healthy and tumour-induced athymic mice. The cancer cells used were also obtained from an accredited supplier, Biocom Biotech.

The nude mice were fed a standard pellet diet and water *ad libitum*. The Animal Research Centre at the Potchefstroom campus of the NWU was not registered for the $^{99m}\text{TcO}_4^-$ radionuclide research on site and hence research phase one were performed by experienced scientists at Necsa under the supervision of Prof. J.R. Zeevaart. Necsa has previously been used to conduct the pre-clinical laboratory studies. The cages in which the nude mice were transported, maintained HEPA filtration for their inlet air and met the required standards. Food and water were available to the nude mice *ad libitum* during the transport and care was taken to ensure only small changes in temperature occurred. No state veterinarian permit was required for the transport, as both Necsa and the PCDDP are in the North West Province. During phase one the exposure of the healthy and lung tumour-bearing nude mice to opportunistic pathogens was kept to a minimum. Although the animals were transported to Necsa for research phase one, environmental variables were kept constant as far as possible to ensure the optimum health of the sample (Table 3.3).

The nude mice were sacrificed at predetermined specific time intervals after the administration of the IHP ^{99m}Tc -EC-DG and the ^{18}F -FDG. The nude mice were transferred from their cages to a chamber containing Isoflurane to ensure painless sacrifice. The nude mice were also sacrificed to collect the desired organs (tissue).

TABLE 3.3: Environmental conditions of the healthy and lung tumour-bearing nude mice at the Animal Research Centre, NWU

Environmental parameter	Specification	Experimental conditions
Temperature	19 ± 2°C	21 ± 2°C
Relative humidity	55 ± 15%	55 ± 15%
Light intensity	350-400 lux one meter above floor level	350-400 lux one meter above floor level
Light period	12 hours light and 12 hours dark	12 hours light and 12 hours dark
Rate of ventilation	15-20 changes per minute	18 changes per minute

A veterinarian laboratory animal technician of the PCDDP observed for any signs of discomfort (chocking, vomiting or change in behaviour) experienced by the healthy and lung tumour-bearing nude mice during the study. In order to ensure complete anaesthesia and absence of pain during sacrifice, the nude mice were monitored using the foot-pinch method. Care was taken to ensure that the mice experienced as little as possible stress during the transport, handling and experimental procedures.

The tumour-bearing mice of research phase 1A were not fasted before the administration of ^{18}F -FDG and IHP $^{99\text{m}}\text{Tc}$ -EC-DG. It was found in literature that fasting of the tumour-bearing mice can improve biodistribution (uptake) of ^{18}F -FDG in the tumour (Fueger *et al.* 2006:999). Lee *et al.* (2005:1531) research concluded that the duration of fasting should also be taken into consideration when ^{18}F -FDG biodistribution studies are performed in animals. The lung tumour-bearing and healthy mice for research phase 1B were fasted for six hours. Due to the variances (fasting and non-fasting groups) between two research data sets of the results from research phase 1A and 1B had to be analysed separately.

3.3.4.2 Rabbit Model

The rabbits were monitored for side effects after administration of IHP $^{99\text{m}}\text{Tc}$ -EC-DG (DL) and ^{67}Ga -citrate. An animal welfare score sheet was completed for each rabbit that monitored specific parameters to evaluate the health status of the rabbits (Appendix E). The same radiation protection procedures that were used for the rabbits during the pilot study were used in phase two. The septic IFI/IF induced rabbits were given antibiotics until they were healthy again. The rabbits were not euthanized.

3.3.4.3 Baboon Model

After the research was completed, the baboons were monitored for toxicity-, adverse- and side effects. An animal welfare score sheet was completed for each baboon included in the research and the following parameters were monitored: mass, body temperatures, stools, general condition and abnormal behaviour (Appendix F). The baboons administered with $^{99m}\text{TcO}_4^-$ and IHP $^{99m}\text{Tc-EC-DG}$ was kept separate from other baboons in order to avoid radiation exposure to the non-administered animals in the Animal Research centre. The urine and faeces of the baboons were washed away as usual.

3.3.5 IHP $^{99m}\text{Tc-EC-DG}$

The IHP $^{99m}\text{Tc-EC-DG}$ contains 10 mg ECDG compared to the 80-100 mg required by Yang *et al.* (2003:466) in the original $^{99m}\text{Tc-EC-DG}$ labelling technique. The IHP $^{99m}\text{Tc-EC-DG}$ therefore does not potentially pose any extra side-effects or adverse events. The labelling of a radiopharmaceutical is dependent on several factors, e.g., the reactivity of the $^{99m}\text{TcO}_4^-$, and the chemical structure of the target compound and the selected solvent (Hung *et al.* 1996:208-210). In the next section the ideal physical appearance and chemical properties as well as the handling and storing of EC-DG will be discussed. The DL technique of the IHP $^{99m}\text{Tc-EC-DG}$, the labelling of the IHP $^{99m}\text{Tc-EC-DG}$ KF and the quality control (QC) that was performed on the IHP $^{99m}\text{Tc-EC-DG}$ will also be outlined.

3.3.5.1 Physical appearance and chemical properties

The physical and chemical properties of IHP $^{99m}\text{Tc-EC-DG}$ are described shortly below:

- Appearance: small, pale-yellow particles that are hygroscopic.
- Odour: slight sulphurous odour.
- Solubility: highly soluble in water.
- Stability: EC-DG before labelling with $^{99m}\text{TcO}_4^-$ is stable under dark, cold inert conditions preferably at 4°C. After labelling, the IHP $^{99m}\text{Tc-EC-DG}$ is stable at room temperature.

- Hazardous decomposition products: will not occur.
- Hazardous polymerisation: will not occur.
- Incompatibilities with other materials: none reasonably foreseeable.

3.3.5.2 Handling and storage of EC-DG

The ideal storage conditions for EC-DG in powder form was found in previous research done by Necsa, to be at $\leq 4^{\circ}\text{C}$ in darkness and under a nitrogen atmosphere. The EC-DG that was couriered from Necsa in Pretoria to DNM at UAH for the research was freeze-dried and/or under Argon (Ar). The EC-DG was also stored at 4°C prior to reconstitution with $^{99\text{m}}\text{TcO}_4^-$. After reconstitution, the shielded vial was stored between 4°C to 25°C and discarded after six hours from the time when labelling was completed. Handling devices such as syringe shields and tongs were used. Storage and disposal of the reconstituted, radioactive products were controlled in a manner that is in compliance with the appropriate regulations of the internal rules of the DNM at UAH and the Department of Health that authorised the license for the use of radionuclides.

3.3.5.3 Labelling technique of IHP $^{99\text{m}}\text{Tc}$ -EC-DG (DL)

The EC-DG that was received by DNM at UAH was labelled with $^{99\text{m}}\text{TcO}_4^-$ and specific materials in a laminar flow cabinet. The radiosynthesis of IHP $^{99\text{m}}\text{Tc}$ -EC-DG (DL) was achieved by adding the required weighed amount of EC-DG (9.8-10.2 mg) in solution to phosphate/citric acid buffer (pH 5.5). Finally tin (II) chloride (100 μg) in solution was added immediately followed by pertechnetate (1440 MBq per 0.5 ml). The solution was heated for 15 minutes for the reaction to complete.

3.3.5.4 Labelling technique of IHP $^{99\text{m}}\text{Tc}$ -EC-DG (KF)

In this procedure the one vial comprised of one or more sealed containers consisting of a freeze dried mixture of SnCl_2 and phosphate/citric acid buffer. The second vial contained the freeze dried EC-DG. The first vial was constituted and transferred to the second vial and constituted again, lastly the

radionuclide (in particular $^{99m}\text{TcO}_4^-$) was added. The reaction mixture was heated for 15 minutes for the reaction to complete.

3.3.5.5 Physicochemical QC tests

The physicochemical tests used, ensured the purity and integrity of the IHP ^{99m}Tc -EC-DG. In this study determination of the pH ($-\log[\text{H}^+]$) and radiochemical purity were required before administration.

3.3.5.5.1 Determination of pH

The pH criteria for a radiopharmaceutical entails that it should be in the physiologically acceptable range (5-8) and is optimised for the stability of the preparation. The pH was measured using Merck pH indicator test strips. The optimum labelling pH of IHP ^{99m}Tc -EC-DG should be a pH of 5.5-6, this is specified as an acceptable injectable pH for animals that will not lead to adverse effects.

3.3.5.5.2 Determination of radiochemical purity

QC testing for experimental work performed at Necsa during research phase one also included QC testing high performance liquid chromatography (HPLC system). The Varian ProStar series HPLC system consisted of an ultraviolet detector which was connected to a single sodium iodide crystal flow radioactivity detector (Raytest Gabi) using the Phenomenex Luna RP-C18 column (5 μm pore size, 250 mm length, id = 4.6). Elution was carried out at room temperature using 4.5% acetonitrile in 2 mmol ammoniumformate, the pH was adjusted with formic acid to pH 3 as the mobile phase for 35 minutes (min) at a flow rate of 1.0 ml/min and ultraviolet wavelength of 210 nm and 254 nm.

The stability of the IHP ^{99m}Tc -EC-DG over time was assessed at Necsa and was not part of this research. The radiochemical purity of the IHP ^{99m}Tc -EC-DG complex was assessed, in the DNM by instant thin

layer chromatography (ITLC) using a instant thin layer chromatography-silica gel (ITLC-SG) strip immediately after the labelling process were completed. The ITLC-SG strip were developed in a solution of 0.9% sodium chloride and Whatman No. 1 paper developed in acetone. After the development process, the strips were dried, cut in half and the activity of the origin and front were measured with the dose calibrator (Capintec CRC-15 BETA).

3.3.6 Gamma scintigraphy

The Siemens MultiSPECT 2 and Siemens Symbia T SPECT/CT dual-head gamma camera with LEHR or MEHR parallel-hole collimators were used during the rabbit (section 3.4.2.4 and 5.2.4) and baboon studies (section 6.2.4). The camera parameters and specifications used are explained in the appropriate sections.

3.3.7 Instrumental calibration QC

The calibration QC checks were performed on all instrumentation utilised in the research in order to ensure accurate and reproducible research performance of results. The instrumentation calibration (Table 3.4) was performed on the clinical radionuclide counting system (well-counter) and scintigraphic imaging instrumentation, as suggested by Zanzonico (2008:4-15).

3.4 RADIATION AND HEALTH SAFETY

The benefits of this research outweigh the disadvantages of the radioactive dosages that the different animal species would receive in the three phases. The reasons are:

- There is a real need for a low cost, glucose metabolism molecular imaging agent for the diagnosis of cancer and/or IFI/IF.
- The radioactive dosages the animal species received were very low and applicable literature were used to determine references of radiopharmaceutical dosages to be administered to animals, e.g. Yang *et al.* (2003:465-473). According to the literature (Silindir & Özer 2008:109) the intravenous injection of $^{99m}\text{TcO}_4^-$ labelled radiopharmaceuticals to humans can result in mild, reversible and non-severe adverse effects. The low probability of adverse reactions

occurring was also taken into account when the decision was made to use the IHP ^{99m}Tc -EC-DG as investigative agent in this research.

- The As Low As Reasonable Achievable (ALARA) radiation safety principle was applied continuously during the study to protect animals and research personnel.

TABLE 3.4: Summary of the calibration performed on this nuclear medicine research instrumentation (Adapted from Zanzonico 2008:4-15)
(Table continues on the next page)

Instrument	Annual	Quarterly or monthly	Weekly	Daily
HPLC	Calibration	n/a	n/a	Performance test
Dose calibrator	n/a	(a) Linearity (b) Accuracy (c) Precision (d) Geometry (e) High voltage supply	n/a	Consistency
Well counter	Efficiency (sensitivity)	n/a	n/a	(a) Energy peaking (b) Background (c) Constancy (energy resolution)
Siemens MultiSPECT 2	n/a	Uniformity for radionuclides performed with $^{99m}\text{TcO}_4^-$	(a) Spatial resolution (b) Planar uniformity (c) System sensitivity	(a) Energy peaking (b) Uniformity performed with $^{99m}\text{TcO}_4^-$
Siemens Symbia T	Dosimetry	(a) Laser alignment (co-registration for CT) (b) Image slice thickness (for CT) (c) Spatial resolution (d) Linearity (e) High-contrast resolution (for CT) (f) Low-contrast resolution (for CT) (g) Accuracy (h) CT-based attenuation corrections	n/a	(a) Energy peaking Uniformity (performed with $^{99m}\text{TcO}_4^-$) (b) Check-up (warming up of CT tube) (c) Tomographic uniformity (d) Accuracy of CT – number of water (e) Noise (for CT) (f) Registration between CT and SPECT

n/a = not applicable

3.4.1 External radiation dose to rabbits and baboons from CT of SPECT/CT

The external radiation that was received from the low dose SPECT/CT scans was difficult to determine because of the many factors involved (IAEA 2008b:online). The CTDI based on the scan parameters could be calculated and represents an index of radiation dose to a standard phantom. No literature could be found on the CTDI of baboons from SPECT/CT. CTDI reference values were given for different organs/body parts of humans for a range of kilovolt's by Hara *et al.* (2010:142-147) for external radiation exposure (x-ray). The CTDI was calculated by the scan parameters and were less for the baboon due to its body size in comparison to an adult human. The ALARA principle was followed in order to avoid unnecessary radiation exposure to the baboons.

3.5 DATA ANALYSIS IN GENERAL

Quantitative data analysis was used for all three phases of this research. Semi-quantitative (SQ) and semi-qualitative (SQUAL) data analysis and interpretation methods were also used for phase two and three. The Department of Medical Physics of the UFS was consulted for recommendations regarding the management of data and the processing of results. Analysis was performed by the Department of Biostatistics of the UFS. All values were expressed as the mean \pm standard error of the mean (*SEM*). Statistical need to be described paired/unpaired.

During the tissue biodistribution studies (phase one) for the non-parametric data of the groups of tumour-bearing mice the Wilcoxon test were calculated to determine the differences between the unpaired groups. Corrections were made for the background radiation and physical decay during counting. The activity in all organs and tissue samples was expressed as the percentage of the injected dose per gram (%ID/g) and presented as the mean \pm *SEM*. Statistical calculations on the data included the median- and the mean \pm *SEM* values, as well as *P* values.

Different areas of biodistribution were measured drawing ROIs around the whole body, injection site and major biodistribution tissues and organs on the scintigraphic images for data analysis of phase two and phase three. The ROIs were drawn on the anterior and posterior images for the different time intervals. The geometric mean of the

anterior and posterior counts was calculated for a specific organ/tissue at a specific time interval. Quantification was performed and % uptakes for a specific organ/tissue were obtained. A semi-quantitative (SQ) and semi-qualitative (SQUAL) data interpretation was done on the scintigraphic images by using the following indicative factors for biodistribution to specific organs, where a positive indicate an increase, a negative a decrease and doubtful when there is no clear increase or decrease. A further four-point grading scale was also included which is explained in detail in the applicable chapters.

3.6 CONCLUSION

An extensive literature review (Chapter 2) was done in order to facilitate the drafting of this specific research design. In Chapter 3 the reasons behind the specific design of the research was discussed, as well as the material and methods that was used. The research design was divided into three different phases in order to evaluate the biodistribution pattern of IHP ^{99m}Tc -EC-DG in tumour- induced, septic and sterile-induced IFI/IF and specific healthy animals at various scintigraphic imaging time intervals different animal models were used. The three different types of animals (mice, rabbits and baboons) are well established for the use of pre-clinical radiopharmaceutical research. In the next three chapters (Chapter 4-6), additional information on the materials and methods of each specific phase will be provided before the discussion of the results. The reasoning behind this specific chapter outline was to orientate the reader about the specific way each of the three phases were conducted.

CHAPTER 4

RESEARCH PHASE ONE: THE MICE MODEL

4.1 INTRODUCTION

The tumour bearing mice also called xenografts are the standard ethical way to prove that a specific radiopharmaceutical is selective for a specific cancer which it is intended to ultimately image in humans (Sharkey & Fogh 1984:356). Research phase one included the mice animal model, where normal- and tumour biodistribution of IHP ^{99m}Tc -EC-DG were obtained respectively in healthy athymic and NSCLC tumour-bearing nude mice. A comparison study with the gold standard, ^{18}F -FDG was also done on a third group of nude mice with lung tumours. The results obtained of the different experiments with tumour-bearing mice were also compared with the results of ^{18}F -FDG and ^{99m}Tc -EC-DG in the literature (Yang *et al.* 2003:470-472). The two studies, phase A and B, were completed and consisted each of three groups of nude mice (Figure 4.1). Statistical analysis was performed by the Department of Biostatistics of the UFS using SAS software. Corrections were made for the background radiation and physical decay during counting. The activity in all organs and tissue samples was expressed as the percentage of the injected dose per gram (%ID/g) and presented as the mean \pm SEM. For the non-parametric data of the groups of tumour-bearing mice the Wilcoxon test was calculated for the differences between the unpaired groups. P value <0.05 was considered statistical significant.

Normal biodistribution was obtained from healthy athymic nude mice administered with IHP ^{99m}Tc -EC-DG (DL) during research phase 1A and –1B for Group 1 (G1) and Group 4 (G4). The tumour biodistribution in lung tumour-bearing mice resulted from the administration of IHP ^{99m}Tc -EC-DG (DL) to Group 2 (G2) and Group 5 (G5) as well as using ^{18}F -FDG in Group 3 (G3) and Group 6 (G6). In order to quantify the biodistribution pattern more accurately, as well as to obtain statistics of the biodistribution in the mouse model, mice were sacrificed at regular predetermined time intervals after administration with IHP ^{99m}Tc -EC-DG and ^{18}F -FDG and the radioactivity of various tissue and organ samples were measured. The biodistribution of the agent to the lung tumour was indicative of the *in vivo* affinity of the agent for the specific tumour.

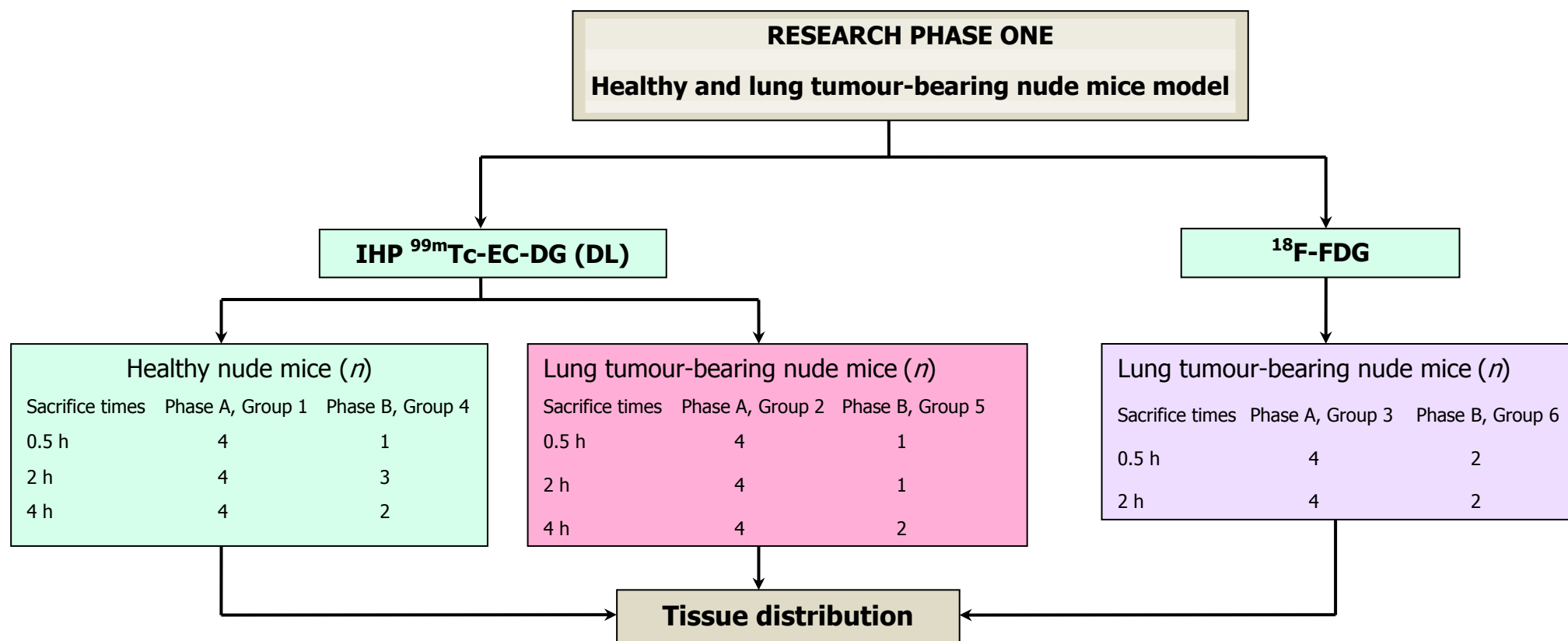


FIGURE 4.1: Research design for phase one with nude mice as animal model

QC plays a vital role in checking that the labelling efficiency of the developmental radiopharmaceutical is optimal for pre-clinical animal administration for testing. In the next section the materials and methods, including the QC results obtained from the IHP ^{99m}Tc -EC-DG (DL) will be provided. This is followed by the *ex vivo* biodistribution results of the healthy and tumour-bearing nude mice that was administered with IHP ^{99m}Tc -EC-DG and ^{18}F -FDG and sacrificed at predetermined time intervals.

4.2 MATERIALS AND METHODS

4.2.1 Sample size

The UFS Department of Biostatistics recommended a minimum of six athymic nude mice per time interval of sacrifice for the pre-clinical *ex vivo* research with ^{18}F -FDG and the IHP ^{99m}Tc -EC-DG in order to obtain statistical meaningful results. Festing & Altman (2002:244-258) also made recommendations that the smallest number of animals should be utilised to reach the scientific objective without losing biological significant effects. Yang *et al.* (2003:468) in the literature utilised three nude mice per time interval of sacrifice, to obtain information relating to the tissue distribution of ^{99m}Tc -EC-DG compared with ^{18}F -FDG.

In Figure 4.1 the complete summary is given of n , the number of sacrificed healthy and tumour-bearing nude mice used in research phase 1A and 1B. In phase A only four healthy and lung tumour-bearing mice per time interval for the different radiopharmaceuticals were studied. Therefore an additional research phase 1B was done in order to improve the significant sample size per time for statistical data analysis. The final sample used, included 47 adult (7-8 weeks) athymic nude mice that were randomly selected from the breeding colony at DST/NWU Pre-clinical Drug Development Platform (PCDDP).



FIGURE 4.2: Two of the healthy nude athymic mice used for phase one

Mostly female nude mice were used in research phase 1A and 1B due to the availability which may not be optimal since the female hormones can influence the results (Figure 4.2). Considering that Yang *et al.* (2003:468) also used primarily female athymic nude mice as xenografts for the feasibility study of ^{99m}Tc -EC-DG the sex of the athymic nude mice was viewed as a low impact factor on the results of the IHP ^{99m}Tc -EC-DG study.

Specific limiting factors that impacted on the statistical sample size of 6 mice per time interval:

- Premature death of healthy and lung tumour-bearing mice during the study.
- Complications due to the small tail veins used as the injection site for the radiopharmaceutical administration.
- Weak tumour growth - this can be contributed to the age of the nude mice, the number of cancer cells injected and the depth of injection of the cancer cells (Richmond & Su 2008:78). The conclusion was made that even though athymic nude mice are known for extra-thymic T-cell development, the viability of tumour growth in athymic nude mice does not mean tumourgenicity. The tumours sizes grown in the nude mice differed slightly in size for the two research sets. The tumours grown in the nude mice during research phase 1A were also smaller than the tumours grown in the nude mice during research phase 1B.

4.2.2 Radiosynthesis of ^{99m}Tc -EC-DG (DL)

The direct labelling technique was used as described in Chapter three (3.3.1.3) to achieve labelling of the IHP ^{99m}Tc -EC-DG for research phase 1A and -1B.

4.2.3 Tissue distribution studies

Thirty mice were anaesthetized with isoflurane gas and were inoculated subcutaneously with 0.2 ml suspension of A549 human lung cancer (3×10^6 cells per nude mice) at the lower middle dorsal region of the back with a 25-gauge needle. Research phase 1A and 1B were performed with tumours that reached a size of 0.6-0.8 cm in diameter (6-8 weeks after inoculation). The athymic nude mice were divided into three groups for research phase one as illustrated in Figure 4.1. The well-counter was calibrated with $^{99m}\text{TcO}_4^-$ and ^{18}F standards to ensure accuracy of radioactivity measurements.

The radioactivity that were administered for the tissue distribution of the IHP ^{99m}Tc -EC-DG and ^{18}F -FDG was 5-8 MBq per nude mouse and was administered through the tail vein. The mice were given an overdose of Isoflurane (or equivalent) and sacrificed at specific intervals. The time interval for sacrifice of the healthy and lung tumour-bearing nude mice after the administration of the IHP ^{99m}Tc -EC-DG was 0.5-, 2- and 4 h and for ^{18}F -FDG was 0.5- and 2 h. A 4 h time interval of the sacrifice after administration of ^{18}F -FDG was not obtained due to the short physical $t_{1/2}$ and the shortages in nude mice (healthy and tumour-bearing) due to the limiting factors (4.2.1). The number of nude mice per time interval sacrificed per time interval for phase 1A and -B is illustrated in Figure 4.1. The nude mice were dissected and the selected tissue or organs of interest were removed. The organs and tissues were weighed and counted in the well-counter at the specific allocated laboratory at Necsa. The organs included the following: brain, heart, lungs, liver, spleen, kidneys, thigh muscle, stomach (emptied), tumour tissue, gastro-intestinal tract, skeleton and bladder with urine and blood samples. The containers were weighed before the organ/tissues were placed inside and again after the organ/tissue were placed to determine the true weight of a specific organ. The radioactivity in each sample tissue (organ) was calculated as the %ID/g. Tumour-to-nontargeted tissue ratios were calculated from the corresponding values of administered dose per gram of tissue weight.

4.2.4 Data analysis

Statistical analysis of the data of research phase one was done by the Department of Biostatistics of the UFS. Numerical variables were summarised by the medians, means and standard errors. The Wilcoxon test was performed to compare the unpaired groups. The data of the two different research acquiring dates were not combined as certain conditions were changed due to improving the quality of the study as additional literature was found (Table 4.1). A third study was planned but the decision was made to not execute this study in order to adhere to the principle "reduction" (three R's) that is prescribed by Russel & Burch (1959:no pagination) as part of GLP in animal research. The results obtained will therefore answer the three research questions of phase one relating to the biodistribution of the IHP ^{99m}Tc -EC-DG and ^{18}F -FDG in healthy and lung tumour-bearing mice. An evaluation of the biodistribution comparison could be made between the ^{18}F -FDG and the IHP ^{99m}Tc -EC-DG to the organs and inoculated tumours. The nude mice sacrificed per time interval during the data acquiring in research phase 1A and 1B, therefore, answered the question indicating the clinical significance of the IHP ^{99m}Tc -EC-DG in lung tumours.

TABLE 4.1: Summary of the differences (variances) between data acquiring during research phase 1A and 1B

RESEARCH PHASE 1A	RESEARCH PHASE 1B
(a) Exercise were not restricted	(a) Exercise of mice restricted by removing exercise wheel
(b) Mice were not fasted	(b) Fasting of mice for 6 hours
(c) Tumours grown were small ± 0.6 cm	(c) Tumours grown were large ± 0.8 cm
(d) Dead time of counting statistics of tissue or organs counted in well-counter were between 10- and 20%	(d) Dead time of counting statistics of tissue or organs counted in well-counter were below 10%

The radioactive measurements of the organs and tissue samples were performed at Necsa laboratories. The weight of the organs and tissues the blood, lungs, liver, stomach, spleen, kidneys, thigh muscle, intestines (small and large), tumour (lung tumour-bearing nude mice only), brain, heart, tail, skeleton and bladder with urine were recorded. A $^{99m}\text{TcO}_4^-$ and ^{18}F calibration standard (4% of the administered dose) was also used to convert counts to % activity in MBq of administered dose per gram of sample (organ). The radioactive biodistribution of IHP ^{99m}Tc -EC-DG ($n=12$) in the organs and tissues of the healthy mice (control group) were compared with the biodistribution of the radioactive uptake of IHP ^{99m}Tc -EC-DG ($n=12$) in the organs and tissues of lung tumour-bearing mice. The IHP ^{99m}Tc -EC-DG ($n=12$) lung tumour-bearing mice were compared with the biodistribution of ^{18}F -FDG ($n=8$) as ^{18}F -FDG

biodistributes to lung cancer cells (Yang *et al.* 2003:465) for specific time intervals. In the literature, statistical analysis with ^{99m}Tc -EC-DG for feasibility and dosimetry was performed with three to four animals per time interval which resulted in meaningful statistical results (Yang *et al.* 2003:467; Yang *et al.* 2004:446).

4.3 RESULTS AND DISCUSSION

4.3.1 Healthy Mice Model

4.3.1.1 Radiosynthesis of ^{99m}Tc -EC-DG (KF) and ^{99m}Tc -EC-DG (DL)

The complexation of the EC-DG with freshly eluted $^{99m}\text{TcO}_4^-$ (1480 MBq in 0.5 ml) was carried out at pH 4 in a laminar flow cabinet in a Type B hot laboratory. The radiochemical purity of the directly labelled IHP ^{99m}Tc -EC-DG complex was assessed by TLC chromatography using ITLC-SC and Whatman No. 1 as described in section 3.3.5.3. QC was performed directly after the completion of the directly labelled ^{99m}Tc -EC-DG. The IHP ^{99m}Tc -EC-DG complex evaluated on the Whatman No 1 paper remained at the origin, however on ITLC-SC it migrated to the front solvent. The labelling efficiency was 91% and 87.8% respectively for IHP ^{99m}Tc -EC-DG (DL) used in phase 1A and 1B. The colloidal formation results were less than 3% for both labellings. The final labelling pH was between 5.5 and 6 (Table 4.2).

TABLE 4.2: Summary of the QC results of the IHP ^{99m}Tc -EC-DG (PHASE 1A/1B)

Parameter	Method	QC results	
		Phase 1A	Phase 1B
Labelling (%)	HPLC	94	85
	TLC	91	92
Radiochemical purity (%)	TLC	91	88
pH	pH strips	5.5	6

The HPLC-UV-chromatogram (Figure 4.3) of phase 1A also confirmed the presence of the ligand while the HPLC-UV-radiometric chromatogram (Figure 4.4) calculated from the area of the four radiometric peaks at the retention times between 6- and 14 minutes represent the radiometric labelling efficiency of 94%. The peaks at the retention time 2 to 5 min show 6% unbounded $^{99m}\text{TcO}_4^-$ is present in the product.

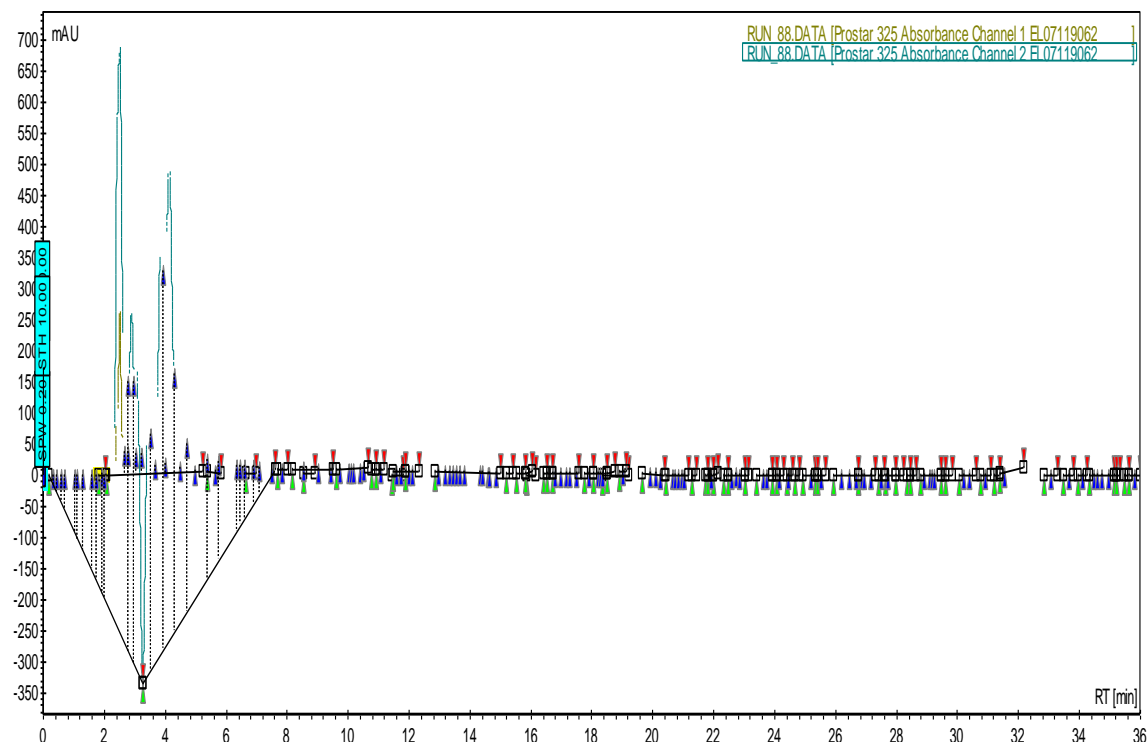


FIGURE 4.3: The HPLC-UV chromatogram of the EC-DG for phase 1A

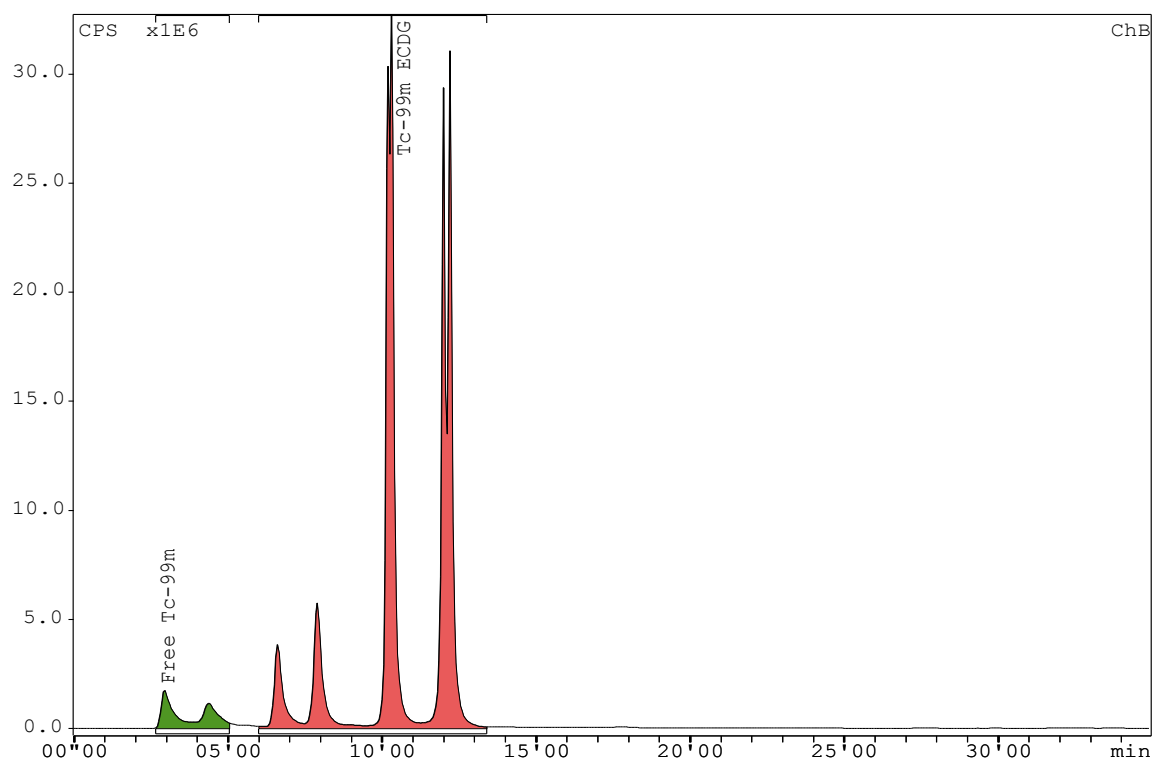


FIGURE 4.4: The HPLC radiometric chromatogram for the IHP ^{99m}Tc -EC-DG (DL) of research phase 1A

The HPLC-UV-chromatogram (Figure 4.5) of research phase 1B established the presence of the ligand while the HPLC-UV-radiometric chromatogram (Figure

4.6) showed a radiometric labelling efficiency of 85% with 15% unbound $^{99m}\text{TcO}_4^-$.

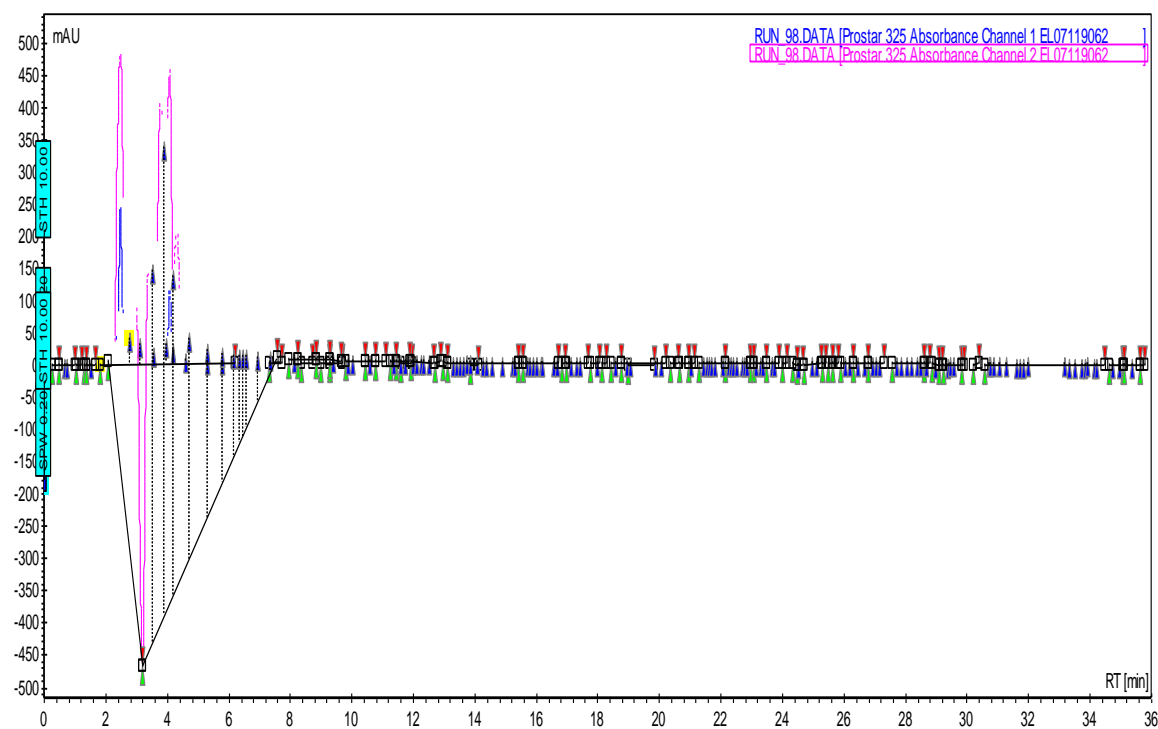


FIGURE 4.5: The HPLC-UV chromatogram of the EC-DG for phase 1B

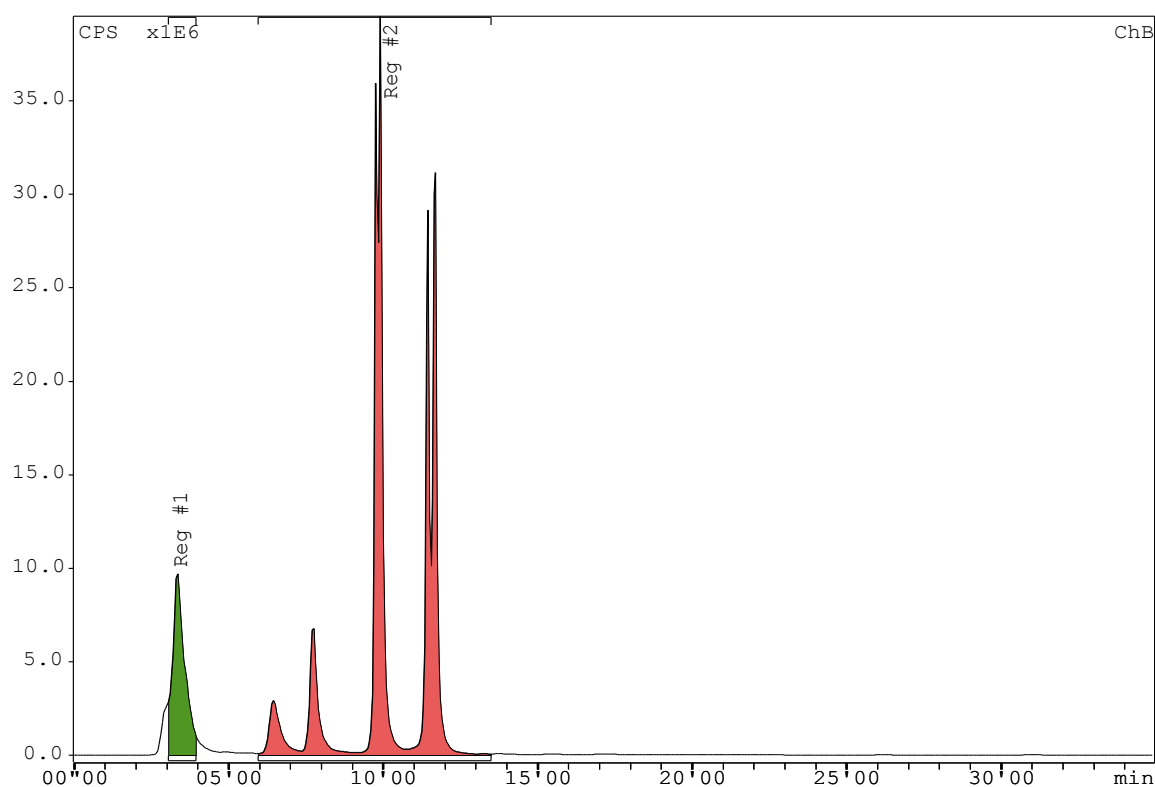


FIGURE 4.6: The HPLC radiometric chromatogram for the IHP ^{99m}Tc -EC-DG (DL) of research phase 1B

4.3.1.2 *In vivo* normal tissue biodistribution IHP ^{99m}Tc-EC-DG (DL)

Research phase 1A (G1) and research phase 1B (G4) evaluated the normal biodistribution pattern of the IHP ^{99m}Tc-EC-DG (DL), to the different organs in healthy nude mice by determining the activity in the organs. Healthy nude mice were administered with IHP ^{99m}Tc-EC-DG and sacrificed at 0.5-, 2- and 4 h post radiopharmaceutical administration. None of the nude mice showed signs of pain. No adverse effects were experienced before euthanization was performed. Corrections were made for background radiation and physical decay during counting.

In Table 4.3 the *ex vivo* biodistribution results of the IHP ^{99m}Tc-EC-DG at 0.5-, 2- and 4- post administration in healthy nude mice (G1 and G4) are given. The activity in all the organs and tissue samples is expressed as the percentage of the injected dose/tissue sample weight (%ID/g). All the data for each time point is expressed as the mean \pm SEM. The highest mean value of the two healthy mice groups for the three different time intervals are highlighted in bold and the lowest for each time interval in aqua. The median of the data for G1 and G4 is also provided in Table 4.3.

4.3.1.3 *Quantitative analysis of IHP ^{99m}Tc-EC-DG (DL)*

The mean %ID/g above 3% was considered significant for G1 and therefore used for reporting results. The uptake values for G1 at 0.5 h observed were as follow: blood (6.46 ± 0.52), lungs (5.55 ± 0.50), liver (11.15 ± 0.68), kidneys (21.09 ± 3.61), intestines (4.33 ± 0.38) and heart (3.77 ± 0.51) (Table 4.3). The SEM was higher than 1% at 0.5 h for the kidneys (3.61) and tail (2.30). An increase in uptake was only found for the intestines; (4.58 ± 0.35) at 2 h and (6.36 ± 1.14) at 4 h time intervals (G1). The uptake values decreased for the liver (6.51 ± 0.42 to 3.97 ± 0.64) and kidneys (7.70 ± 0.60 to 6.90 ± 1.70) respectively at 2h and 4 h. Muscle uptake (4.42 ± 4.13) above the set value of 3% was only found at 4 h. The SEM was higher than 1% at 4 h for the kidneys (1.70), muscle (4.13) and intestines (1.14). The mean \pm SEM of the %ID/g of tissue of

G1 indicated that the uptake in healthy nude mice was the highest to the kidneys, liver and intestines. The kidneys, liver and intestines showed the highest biodistribution of all the organs at the time interval 2h for G1. At the 4 h sacrifice time interval the three organs with the highest biodistribution in G1 was the kidneys, intestines and then liver. The lowest area of biodistribution for all three time intervals was to the brain (0.28 ± 0.02 ; 0.11 ± 0.01 ; 0.13 ± 0.04).

TABLE 4.3: Biodistribution (%ID/g) of IHP ^{99m}Tc -EC-DG (DL) in healthy athymic nude mice for G1 and G4

Organ/ Tissue	Time interval h	Median of G1	Median of G4	Mean \pm SEM of G1	Mean \pm SEM of G4
Blood	0.5	6.14	1.39	6.46 ± 0.52	1.39 ± 0.33
	2	0.86	0.20	0.87 ± 0.05	0.19 ± 0.01
	4	0.68	0.20	0.69 ± 0.07	0.20 ± 0.05
Lung	0.5	5.21	1.03	5.55 ± 0.50	1.04 ± 0.18
	2	0.91	0.18	1.45 ± 0.62	0.18 ± 0.01
	4	0.91	0.19	0.98 ± 0.23	0.19 ± 0.02
Liver	0.5	10.90	1.47	11.15 ± 0.68	1.47 ± 0.47
	2	6.42	1.41	6.51 ± 0.42	1.53 ± 0.13
	4	3.70	1.28	3.97 ± 0.64	1.28 ± 0.33
Stomach	0.5	2.45	0.75	2.24 ± 0.28	0.75 ± 0.20
	2	1.01	0.22	1.66 ± 0.76	0.30 ± 0.10
	4	0.96	0.33	1.36 ± 0.61	0.33 ± 0.20
Spleen	0.5	1.97	0.66	2.00 ± 0.17	0.66 ± 0.13
	2	0.63	0.15	0.83 ± 0.24	0.16 ± 0.04
	4	0.49	0.22	0.61 ± 0.19	0.22 ± 0.02
Kidneys	0.5	18.80	4.39	21.09 ± 3.61	4.39 ± 0.94
	2	7.75	1.74	7.70 ± 0.60	1.72 ± 0.09
	4	6.15	1.79	6.90 ± 1.70	1.79 ± 0.21
Muscle	0.5	2.28	0.72	2.19 ± 0.28	0.72 ± 0.30
	2	2.69	0.15	2.16 ± 0.60	0.14 ± 0.02
	4	0.35	0.18	4.42 ± 4.13	0.18 ± 0.07
Intestines	0.5	4.33	1.31	4.33 ± 0.38	1.31 ± 0.57
	2	4.80	0.54	4.58 ± 0.35	0.53 ± 0.25
	4	6.37	1.13	6.36 ± 1.14	1.13 ± 0.07
Brain	0.5	0.27	0.08	0.28 ± 0.02	0.08 ± 0.04
	2	0.11	0.05	0.11 ± 0.01	0.05 ± 0.00
	4	0.09	0.07	0.13 ± 0.04	0.07 ± 0.01
Heart	0.5	3.41	0.63	3.77 ± 0.51	0.62 ± 0.07
	2	0.64	0.14	0.61 ± 0.05	0.14 ± 0.01
	4	0.48	0.17	0.51 ± 0.07	0.17 ± 0.02
Tail	0.5	10.90	2.90	12.60 ± 2.30	2.90 ± 1.50
	2	0.70	0.20	0.80 ± 0.15	0.19 ± 0.01
	4	1.50	0.16	1.92 ± 0.44	0.16 ± 0.02
Skeleton	0.5	2.07	1.09	2.22 ± 0.25	1.09 ± 0.58
	2	3.25	0.18	2.72 ± 0.80	0.18 ± 0.01
	4	0.42	0.23	0.94 ± 0.60	0.23 ± 0.01

For G4 all mean uptake values above 1% are used. The mean uptake values observed included blood (1.39 ± 0.33), lung (1.04 ± 0.18), liver (1.47 ± 0.47), kidneys (4.39 ± 0.94) and intestines (1.31 ± 0.57) at 0.5 h post administration (Table 4.3). The *SEM* was higher than 1% at 0.5 h for G4 only in the tail (1.50). The kidney uptake decreased to (1.72 ± 0.09) at 2 h and minimal change at 4 h (1.79 ± 0.21). A slight increase was found for the liver (1.53 ± 0.13) at 2 h, followed by a decrease to (1.28 ± 0.33)

at 4 h. Uptake for the intestines (1.13 ± 0.07) was only found at 4 h. The *SEM* values were less than 1% at 2- and 4 h post administration of the IHP ^{99m}Tc -EC-DG for all the organs. The highest uptake for G4 for the 0.5 h time interval was observed in the kidneys and liver (Table 4.3). The kidneys, followed by the liver and then the intestines also showed the highest values at 2 h time interval for G4 compared to other organs. G4 at the 4 h time interval post IHP ^{99m}Tc -EC-DG administration indicated highest uptake to the kidneys, intestines and then liver. The organ with the lowest uptake for all three time intervals for G4 was the brain (0.08 ± 0.04 ; 0.05 ± 0.00 ; 0.07 ± 0.01).

The overall mean \pm *SEM* of IHP ^{99m}Tc -EC-DG uptake for G1 was higher than the mean \pm *SEM* for G4 in all the organs and different time intervals (Table 4.3). Analysis of the results primarily indicated that the uptake in healthy nude mice of the IHP ^{99m}Tc -EC-DG for all the time intervals was the highest to the kidneys (excretion), liver followed by the intestines (excretion) and with slight uptake to the heart. The slight uptake to the heart is probably due to glucose uptake by the myocytes. Highest excretion of IHP ^{99m}Tc -EC-DG was before 2 h after administration (Figure 4.7B). This high uptake of the IHP ^{99m}Tc -EC-DG by the kidneys at the three different time intervals is seemingly because the EC and EC-conjugates interact with renal tubules in the kidney (Zhang *et al.* 2012:6).

The three organs with the highest uptake and the organs with the lowest uptake of IHP ^{99m}Tc -EC-DG (DL) in healthy nude mice are illustrated in Figure 4.7. Liver uptake decreased over time (Figure 4.7A), but uptake of the IHP ^{99m}Tc -EC-DG to the intestines increased over time (Figure 4.7C). This event indicates possible excretion of the IHP ^{99m}Tc -EC-DG through the hepato-biliary system. Tail uptake was high due the point of administration through the tail vein, but decreased over time. The brain has the lowest IHP ^{99m}Tc -EC-DG uptake and a constant decrease in uptake is seen from 0.5-2 h, with a minimal increase between 2-4 h post radiopharmaceutical administration (Figure 4.7D). Low brain uptake of IHP ^{99m}Tc -EC-DG can be attributed to its hydrophilic characteristic that prevents it to cross the blood-brain barrier (Schechter *et al.* 2009:1590).

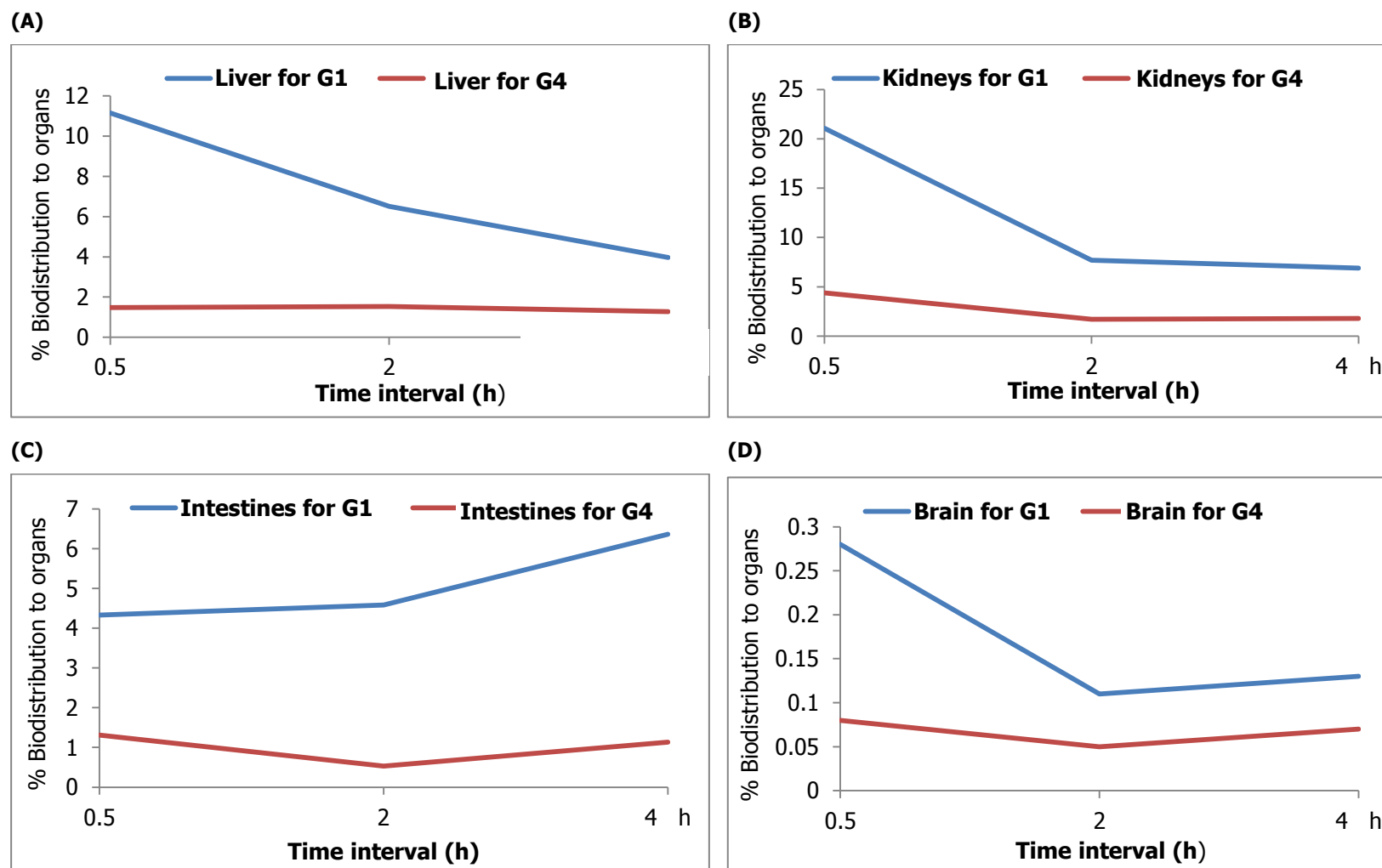


FIGURE 4.7: Biodistribution of IHP ^{99m}Tc -EC-DG to different organs from *ex vivo* results. Mean % uptake of (A) liver, (B) kidneys, (C) intestines and (D) brain of healthy mice administered with IHP ^{99m}Tc -EC-DG.

4.3.2 Tumour Mice Model

4.3.2.1 *In vivo tumour tissue biodistribution IHP ^{99m}Tc-EC-DG (DL)*

G2 and G5 consisted of lung tumour-bearing nude mice that was administered with IHP ^{99m}Tc-EC-DG and sacrificed at 0.5-, 2- and 4 h post radiopharmaceutical administration. The activity in all the organs and tissue samples is expressed as the percentage of the injected dose/tissue sample weight (%ID/g). All the data are expressed as the mean \pm SEM. In Table 4.4 uptake results for IHP ^{99m}Tc-EC-DG of G2 and G5 to the tissue/organs and tumours in lung tumour-bearing mice are given. The median and the mean \pm SEM of uptake of the of the two groups of tumour-bearing mice sacrificed at 0.5-, 2- and 4 h IHP ^{99m}Tc-EC-DG administration is also given in Table 4.4. The highest mean of the two groups for the different time intervals are highlighted in bold.

4.3.2.2 *Quantitative analysis of IHP ^{99m}Tc-EC-DG (DL)*

The mean %ID/g was higher in Phase 1A than Phase 1B and therefore it was decided to use uptake values above 3% for phase 1A and 1% for phase 1B to report results. The uptake values for G2 at 0.5 h observed were as follow: blood (7.27 \pm 0.90), lung (6.21 \pm 0.71), liver (14.35 \pm 1.16), kidneys (22.98 \pm 1.69), intestines (5.87 \pm 0.73), tumour (5.77 \pm 1.06), heart (3.61 \pm 0.43), skeleton (4.48 \pm 1.38) and tail (8.64 \pm 0.72) and the mean of the tumour-to-muscle (3.23 \pm 1.69) ratio and tumour-to-brain tissue ratio (18.63 \pm 1.49) (Table 4.4). The SEM of G2 was higher than 1% at 0.5 h for liver (1.16), kidneys (1.69) and muscle (2.77). Uptake decreased for the liver (5.14 \pm 1.66 to 2.88 \pm 0.31), kidneys (7.89 \pm 1.49 to 3.72 \pm 1.16), intestines (4.64 \pm 0.39 to 4.06 \pm 0.46) and tumour (1.52 \pm 0.08 to 1.25 \pm 0.44), from 2 h to 4 h. Muscle uptake (4.42 \pm 4.13) above the set value of 3% was only found at 4 h. The SEM was higher than 1% at 4 h for the kidneys (1.70), muscle (4.13) and intestines.

TABLE 4.4: Biodistribution (%ID/g) of IHP ^{99m}Tc-EC-DG in lung tumour-bearing mice

Organ/ Tissue	Time interval h	Median of G2	Median of G5	Mean \pm SEM of G2	Mean \pm SEM of G5	P-value of G1 with G2	P-value G4 with G5
Blood	0.5	6.91	0.92	7.27 \pm 0.90	0.92*	0.56	0.17
	2	0.90	0.14	0.90 \pm 0.14	0.14*	0.77	0.08
	4	0.50	0.30	0.49 \pm 0.01	0.30 \pm 0.11	0.02	0.45
Tumour	0.5	5.33	0.87	5.77 \pm 1.06	0.87*	×	×
	2	1.50	0.30	1.52 \pm 0.08	0.30*	×	×
	4	0.82	0.20	1.25 \pm 0.44	0.20 \pm 0.02	×	×
Lung	0.5	5.74	0.78	6.21 \pm 0.71	0.78*	0.39	0.16
	2	0.87	0.17	0.81 \pm 0.08	0.17*	0.12	0.10
	4	0.45	0.23	0.46 \pm 0.03	0.23 \pm 0.00	0.04	0.12
Liver	0.5	14.29	1.75	14.35 \pm 1.16	1.75*	0.04	0.74
	2	6.28	0.27	5.14 \pm 1.66	0.27*	0.16	0.28
	4	2.59	1.04	2.88 \pm 0.31	1.04 \pm 0.08	0.08	1.00
Stomach	0.5	3.14	0.43	3.07 \pm 0.56	0.43*	0.24	0.30
	2	0.78	0.23	0.73 \pm 0.13	0.23*	0.09	0.10
	4	0.40	0.19	0.52 \pm 0.17	0.19 \pm 0.11	0.15	0.44
Spleen	0.5	2.25	0.37	2.22 \pm 0.21	0.37*	0.78	0.17
	2	0.48	0.11	0.48 \pm 0.06	0.11*	0.15	0.10
	4	0.36	0.23	0.34 \pm 0.04	0.23 \pm 0.05	0.25	1.00
Kidneys	0.5	22.25	3.43	22.98 \pm 1.69	3.43*	0.38	0.17
	2	6.93	1.47	7.89 \pm 1.49	1.47*	0.56	0.47
	4	4.46	1.48	3.72 \pm 1.16	1.48 \pm 0.02	0.39	0.12
Muscle	0.5	2.31	0.52	4.65 \pm 2.77	0.52*	0.37	0.22
	2	0.37	0.13	0.43 \pm 0.09	0.13*	0.08	0.10
	4	0.23	0.18	0.25 \pm 0.05	0.18 \pm 0.02	0.39	1.00
Intestines	0.5	5.99	0.48	5.87 \pm 0.73	0.48*	0.09	0.30
	2	4.78	0.82	4.64 \pm 0.39	0.82*	0.77	0.10
	4	3.91	0.94	4.06 \pm 0.46	0.94 \pm 0.16	0.08	0.44
Brain	0.5	0.29	0.14	0.30 \pm 0.03	0.14*	0.77	0.17
	2	0.10	0.05	0.10 \pm 0.01	0.05*	0.56	0.10
	4	0.07	0.06	0.07 \pm 0.01	0.06 \pm 0.01	0.04	0.44
Heart	0.5	3.30	0.42	3.61 \pm 0.43	0.42	0.78	0.17
	2	0.52	0.14	0.51 \pm 0.05	0.14*	0.14	0.10
	4	0.31	0.19	0.32 \pm 0.02	0.19 \pm 0.03	0.02	0.44
Tail	0.5	8.98	1.30	8.64 \pm 0.72	1.30*	0.08	0.37
	2	0.87	0.20	0.98 \pm 0.18	0.20*	0.52	0.10
	4	0.93	0.21	1.18 \pm 0.41	0.22 \pm 0.09	0.15	1.00
Skeleton	0.5	4.21	0.44	4.48 \pm 1.38	0.44*	0.23	0.17
	2	0.34	0.20	0.37 \pm 0.06	0.20*	0.04	0.08
	4	0.26	0.24	0.28 \pm 0.05	0.24 \pm 0.08	0.25	1.00
Tumour- to-blood	0.5	0.79	0.95	0.78 \pm 0.06	0.95*	×	×
	2	1.86	2.16	1.83 \pm 0.29	2.16*	×	×
	4	1.92	0.80	2.65 \pm 1.00	0.80 \pm 0.38	×	×
Tumour- to-muscle	0.5	2.29	1.69	3.23 \pm 1.69	1.69*	×	×
	2	4.04	2.30	3.88 \pm 0.52	2.30*	×	×
	4	3.67	1.14	5.45 \pm 2.21	1.14 \pm 0.23	×	×
Tumour- to-lung	0.5	0.93	1.12	0.91 \pm 0.07	1.12*	×	×
	2	1.88	1.72	1.93 \pm 0.18	1.72*	×	×
	4	2.11	0.87	2.92 \pm 1.18	0.87 \pm 0.10	×	×
Tumour- to-brain	0.5	18.25	6.35	18.63 \pm 1.49	6.35	×	×
	2	15.38	6.44	15.01 \pm 1.15	6.44	×	×
	4	14.70	3.20	18.78 \pm 6.75	3.20 \pm 0.05	×	×

*No SEM could be calculated, only one observation

*P-value could not be calculated as only one group had tumours

The mean values increased for the tumour-to-blood tissue ratio (1.83 \pm 0.29 to 2.65 \pm 1.00), tumour-to-muscle tissue ratio (3.88 \pm 0.52 to 5.45 \pm 2.21), tumour-to-lung

tissue (1.93 ± 0.18 to 2.92 ± 1.18) ratio and the tumour-to-brain tissue ratio (15.01 ± 1.15 to 18.78 ± 6.75) from the 2- to 4 h time points (Table 4.4). At 2 h for G2 the *SEM* was higher than 1% for the liver (1.66) and kidneys (1.49). At the 4 h time interval for G2 the mean \pm *SEM* was increased above 1% for the liver (2.88 ± 0.31), kidneys (3.72 ± 1.16), intestines (4.06 ± 0.46) and tumour (1.25 ± 0.44). The kidneys (1.16) were the only organ at 4 h that had a *SEM* higher than 1%. The mean \pm *SEM* of the %ID/g of tissue of G2 indicated that the uptake in healthy nude mice was the highest to the kidneys and liver. For G2 the 4 h time interval post IHP ^{99m}Tc -EC-DG administration and sacrifice indicated highest uptake to the kidneys, intestines, tumour and then liver.

To evaluate the imaging potential of the IHP ^{99m}Tc -EC-DG, the tumour-to-blood activity ratios of G2 was evaluated. As shown in Table 4.4, a decreasing IHP ^{99m}Tc -EC-DG tumour (Figure 4.8) and blood uptake were found, resulting in an increase of the tumour-to-blood ratios over time (Figure 4.9A). The decreasing tumour and muscle uptake of IHP ^{99m}Tc -EC-DG found for G2, also lead to increased tumour-to-muscle ratios over time (Figure 4.9B). Increased tumour-to-lung-, tumour-to-brain-, tumour-to-brain ratios over time was also found for G2 (Figure 4.9).

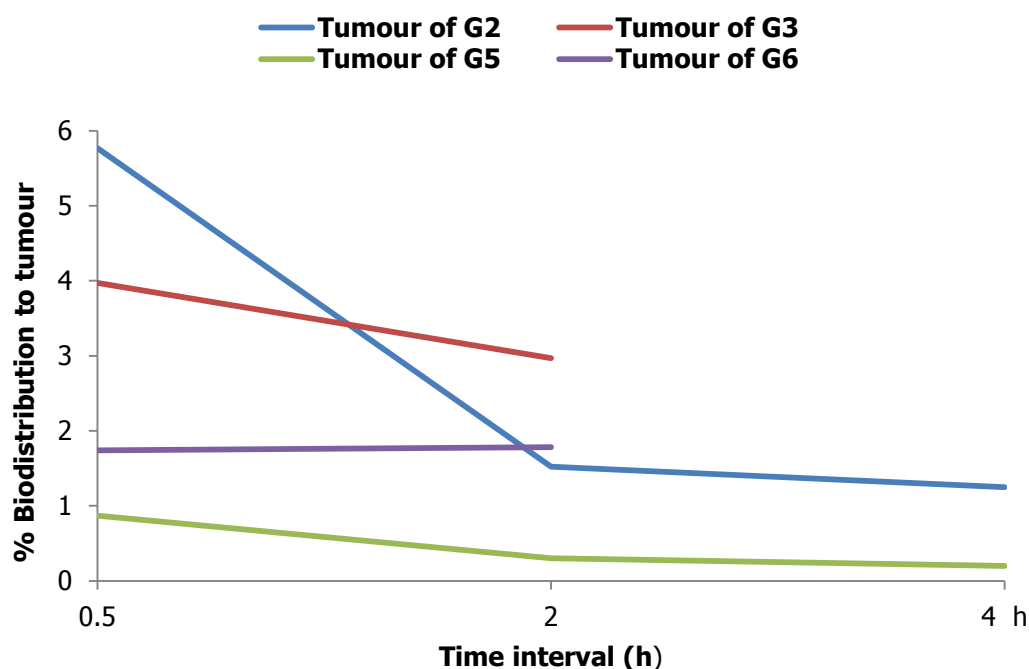


FIGURE 4.8: Biodistribution of IHP ^{99m}Tc -EC-DG (DL) (G2 & G5) and ^{18}F -FDG (G3 & G6) to tumours of lung tumour-bearing mice is shown with time.

Blood uptake (0.92) was only found at 0.5 h for G5, liver uptake (1.75, 1.04 ± 0.08) was found at 0.5- and 4 h. The uptake values of G5 decreased for the tumour (0.87, 0.30, 0.20 ± 0.02) and kidneys (3.43, 1.47, 1.48 ± 0.02) over the 0.5-, 2- and 4 h time points. Intestine uptake (0.82, 0.94 ± 0.16) was found at 2- and 4 h. The following organs showed significant uptake values only at 4 h: lung (0.23 ± 0.00), spleen (0.23 ± 0.05) and skeleton (0.24 ± 0.08). No *SEM* could be calculated for the sacrifice time interval at 0.5- and 2 h as G5 consisted of only $n=1$ tumour-bearing mouse for that specific time intervals. The mean of the tumour-to-muscle tissue ratio (1.69, 2.30, 1.14 ± 0.23) showed no trend over the time of the study, while the tumour-to-brain tissue ratio (6.35, 6.44, 3.20 ± 0.05) was high up to 2 h followed by a fast decrease at 4 h and the tumour-to-lung tissue ratio (1.12, 1.72) increased from 0.5- to 2 h time points (Table 4.4).

The *SEM* that was calculated for the $n=2$ mice of G5 at 4 h was found to be less than 1% for all the organs. The mean \pm *SEM* of the %ID/g of tissue of G5 indicated that the uptake in healthy nude mice was the highest to the kidneys, followed by the liver and intestines and then tumour at 0.5 h. Firstly the kidneys, intestines and then liver also showed the highest uptake for G5 at the time interval 2 h post IHP ^{99m}Tc -EC-DG administration. For G5 the 4 h time interval post IHP ^{99m}Tc -EC-DG administration and sacrifice indicated highest uptake to the kidneys, liver, intestines and then tumour.

To evaluate the imaging potential of the IHP ^{99m}Tc -EC-DG, the tumour-to-blood activity ratios of the G5 was evaluated. As shown in Table 4.4, there was a decreasing tumour uptake of IHP ^{99m}Tc -EC-DG (Figure 4.6) from 0.5- to 4 h and the blood uptake decreased from 0.5- to 2 h, followed by an increased from 2-4 h. This resulted in an increase of the tumour-to-blood ratios for IHP ^{99m}Tc -EC-DG at 2 h and a decrease tumour-to-blood ratio at 4 h. There was a decreasing tumour uptake of the IHP ^{99m}Tc -EC-DG from 0.5- to 4 h and the IHP ^{99m}Tc -EC-DG muscle uptake decreased from 0.5-2 h, but increased from 2- to 4 h time interval. Therefore the tumour-to-muscle ratios increased at 2 h and decreased at 4 h with time (Figure 4.9B). As shown in Table 4.5, there was decreasing tumour uptake of IHP ^{99m}Tc -EC-DG from 0.5-4 h and the blood uptake of IHP ^{99m}Tc -EC-DG decreased from 0.5-2 h, but increased again from 2-to 4 h time interval. This resulted in growing

tumour-to-lung ratios at 2 h and a decreasing tumour-to-lung ratio at 4 h with time (Figure 4.9C). Table 4.4 indicated a decreasing tumour uptake of IHP ^{99m}Tc -EC-DG for G5 from 0.5-4 h and an increasing brain uptake from 0.5-2h and then a decreasing brain uptake from the 2-4h time intervals. This resulted in growing tumour-to-brain ratios at 0-2 h and decreasing tumour-to-brain ratios from 2-4 h post IHP ^{99m}Tc -EC-DG administration with time (Figure 4.9D).

The mean \pm SEM of IHP ^{99m}Tc -EC-DG for G2 was higher than G5 for all the organs and tumours at the different time intervals of sacrifice (Table 4.4). The uptake of the IHP ^{99m}Tc -EC-DG of G2 and G5 indicated high uptake to the liver and excretion through the kidneys. Analysis of the results overall, indicated that for the research phase one, the IHP ^{99m}Tc -EC-DG uptake in lung tumour-bearing mice to the organs other than the tumour tissue for all the time intervals was the highest to the kidneys (excretion), liver and finally followed by the intestines (excretion).

Low brain uptake and high liver uptake was noted in G2 and G5 of the tumour-bearing mice administered with IHP ^{99m}Tc -EC-DG, similar results was found in these organs in the healthy nude mice. The results indicated uptake of the IHP ^{99m}Tc -EC-DG in both groups (G2 and G5) to the lung tumours, but G5 had the lower radiopharmaceutical uptake to the tumour. The tumour uptake in G5 was comparable to the blood uptake, thus not clinically significant.

4.3.2.3 Comparison of IHP ^{99m}Tc -EC-DG (DL) in healthy and tumour-bearing mice

Table 4.4 also gives the attained level of significance (P -value) to determine if there was statistical significant difference between the uptake to the different organs of healthy (G1 and G4) and tumour-bearing (G2 and G5) mice administered with IHP ^{99m}Tc -EC-DG. The P -value between the healthy and tumour-bearing mice was added in Table 4.5 to determine if there were any uptake differences between these two groups when administered with ^{99m}Tc -EC-DG. P value <0.05 was considered statistical significant (highlighted in red). P -value difference was noted between G1 and G2 at the 0.5 h time interval of the lungs, the 2 h time interval of the skeleton and the blood, lungs and brain at the 4 h time interval. No statistical significant differences were noted between the uptakes of IHP ^{99m}Tc -EC-DG of G4 with G5.

4.3.2.4 Comparison of IHP ^{99m}Tc -EC-DG (DL) with ^{18}F -FDG in tumour-bearing mice

In the last section of the results of phase one a comparison was made between the uptake results obtained with the IHP ^{99m}Tc -EC-DG and ^{18}F -FDG in lung tumour-bearing nude mice that were sacrificed at specific time intervals. G2 and G5 consisted of lung tumour-bearing nude mice that was administered with IHP ^{99m}Tc -EC-DG and sacrificed at is given for 0.5-, 2- and 4 h post radiopharmaceutical administration. G3 and G6 was administered with ^{18}F -FDG and sacrificed at 0.05- and 2 h post radiopharmaceutical administration. The activity in all the organs and tissue samples is expressed as the percentage of the injected dose/tissue sample weight (%ID/g). All the data are expressed as the mean \pm SEM. The median of the data for G2, G3, G5 and G6 is also provided in Table 4.5.

Table 4.5 compares the uptake results of G2 (IHP ^{99m}Tc -EC-DG) with G3 (^{18}F -FDG) and G5 (IHP ^{99m}Tc -EC-DG) with G6 (^{18}F -FDG) to the tissue/organs and tumours in lung tumour-bearing mice. A comparison is made for the median and the mean \pm SEM of uptake of the different groups in tumour-bearing mice for sacrifice at 0.5- and 2 h post radiopharmaceutical administration. Tumour-bearing mice were not sacrificed for time interval 4 h for G3 and G6, therefore no comparison could be made with G2 and G5 for 4 h after radiopharmaceutical administration and sacrifice. Data comparison for G3 with G6 is only made for the time intervals 0.5- and 2 h post radiopharmaceutical administration. The highest mean of the four groups of tumour-bearing mice were highlighted in bold (Table 4.5). The statistical significance ($P < 0.05$) was calculated from the results of the two sets of animal experiments, phase A and B for the two glucose analogue radiopharmaceuticals. A P value < 0.05 was considered statistical significant and highlighted in red (Table 4.6).

To evaluate the imaging potential of the IHP ^{99m}Tc -EC-DG with ^{18}F -FDG, the tumour-to-blood activity ratios of G2 were compared to G3. A decreased IHP ^{99m}Tc -EC-DG uptake pattern was indicated for the blood and tumour of G2 (Table 4.6). A decreased uptake of ^{18}F -FDG in the blood and tumour over time

was indicated for G3. This decreased RP uptake in the blood and tumour over time resulted in growing tumour-blood ratio for G2 and G3. To evaluate the imaging potential of the IHP ^{99m}Tc -EC-DG with ^{18}F -FDG, the tumour-to-muscle activity ratios of G2 was compared to G3. A decreased IHP ^{99m}Tc -EC-DG uptake pattern was indicated for the muscle and tumour of G2 over time. G3 indicated an increased ^{18}F -FDG uptake in the muscle uptake and decreased tumour uptake over time (Table 4.5). These differences in RP muscle uptake over time with tumour uptake resulted in a growing tumour-to-muscle ratio G2 and decreasing tumour-to-muscle ratio G3. The tumour-to-lung activity ratios of the G2 were also compared to G3. A decreased IHP ^{99m}Tc -EC-DG uptake pattern was indicated for the lung and tumour of G2 over time. G3 also indicated a decreased uptake of ^{18}F -FDG in the lungs and tumour uptake over time. This decreased uptake of the lung and tumour over time resulted in growing tumour-to-lung ratio for G2 and G3. In Table 4.6 G2 indicated a decreased tumour-to-brain tissue ratio over time and G3 indicated a slight increase over time from 0.5-2 h.

A decreased uptake pattern was indicated for the blood and tumour of IHP ^{99m}Tc -EC-DG for G5 over time (Table 4.5). G6 indicated a decreased blood uptake over time and an increased tumour uptake for ^{18}F -FDG. These differences between the tumour and blood uptake over time resulted in growing tumour-to-blood ratios for G5 and G6. Also, to provide additional information on the imaging potential of the IHP ^{99m}Tc -EC-DG with ^{18}F -FDG, an evaluation of the tumour-to-muscle activity ratios of G5 was compared to G6. A decreased IHP ^{99m}Tc -EC-DG uptake pattern was indicated for the muscle and tumour of G5 over time. G6 also indicated a decreased ^{18}F -FDG muscle uptake over time and tumour uptake slightly increased from 0.5-2 h after administration, as indicated in Table 4.5. This difference of the muscle uptake and tumour uptake over time resulted in growing tumour-to-muscle ratio for G5 and G6.

A decreased IHP ^{99m}Tc -EC-DG uptake pattern was indicated for the lung and tumour of G5 over time. G6 indicated a decreased ^{18}F -FDG lung uptake over time and an increased tumour uptake (Table 4.5). This decreased uptake of the lung and tumour over time resulted in growing tumour-to-lung ratio for G5 and G6 as shown in Table 4.5. Also, to evaluate the imaging potential of the IHP ^{99m}Tc -EC-DG with ^{18}F -FDG, the tumour-to-brain activity ratios of the G5 were compared with G6. A decreased uptake pattern was indicated for the brain and tumour of G5 over time, indicated in Table 4.5. G6 indicated a decreased ^{18}F -FDG brain uptake over time and an increased tumour uptake. This decreased uptake of IHP ^{99m}Tc -EC-DG in brain and tumour over time resulted in growing tumour-to-brain ratio for G5. The tumour-to-brain tissue of G6 also slightly increased as shown in Table 4.5.

A significant difference ($P < 0.05$) between G2 with G3 was found in blood, lung, liver, stomach, kidneys, intestines, brain, heart, tail and tumour-to-blood tissue ratio at 0.5 h and in blood, spleen, kidneys, muscle, intestines, tumour, brain, heart, skeleton, tumour-to-blood-, tumour-to-muscle-, tumour-to-lung ratio and tumour-to-brain tissue ratio at 2 h. Table 4.5 also indicates the P value for G5 with G6. No significant difference ($P > 0.05$) between G5 with G6 were found at 0.5– and 2 h for the regions of RP uptake.

TABLE 4.5: Comparison of the biodistribution (%ID/g) results in lung tumour-bearing mice for G2 with G3 and G5 with G6

Organ/ Tissue	Time interval h	Median of G2	Median of G3	Median of G5	Median of G6	Mean \pm SEM of G2	Mean \pm SEM of G3	Mean of G5	Mean \pm SEM of G6	P-value G2 with G3	P-value G5 with G6
Blood	0.5	6.91	0.67	0.92	0.74	7.27 \pm 0.90	0.82 \pm 0.19	0.92*	0.74 \pm 0.06	0.02	0.17
	2	0.90	0.35	0.14	0.62	0.90 \pm 0.14	0.34 \pm 0.03	0.14*	0.61 \pm 0.14	0.03	0.08
Tumour	0.5	5.33	3.14	0.87	1.74	5.77 \pm 1.06	3.97 \pm 0.98	0.87*	1.74 \pm 0.16	0.15	0.22
	2	1.50	3.16	0.30	1.51	1.52 \pm 0.08	2.97 \pm 0.30	0.30*	1.78 \pm 0.60	0.03	0.18
Lung	0.5	5.74	3.05	0.78	1.78	6.21 \pm 0.71	3.22 \pm 0.64	0.78*	1.78 \pm 0.05	0.02	0.17
	2	0.87	2.46	0.17	2.22	0.81 \pm 0.08	2.39 \pm 0.11	0.17*	2.77 \pm 0.72	0.12	0.10
Liver	0.5	14.29	1.31	1.75	1.42	14.35 \pm 1.16	1.38 \pm 0.24	1.75*	1.42 \pm 0.05	0.02	0.74
	2	6.28	1.15	0.27	1.04	5.14 \pm 1.66	1.13 \pm 0.03	0.27*	1.22 \pm 0.38	0.16	0.28
Stomach	0.5	3.14	1.39	0.43	0.96	3.07 \pm 0.56	1.34 \pm 0.14	0.43*	0.96 \pm 0.18	0.02	0.30
	2	0.78	1.51	0.23	1.60	0.73 \pm 0.13	1.51 \pm 0.18	0.23*	2.96 \pm 1.83	0.09	0.10
Spleen	0.5	2.25	2.01	0.37	1.73	2.22 \pm 0.21	2.21 \pm 0.38	0.37*	1.73 \pm 0.22	0.78	0.17
	2	0.48	1.62	0.11	1.62	0.48 \pm 0.06	1.69 \pm 0.22	0.11*	2.13 \pm 0.53	0.03	0.10
Kidneys	0.5	22.25	1.42	3.43	1.60	22.98 \pm 1.69	2.23 \pm 0.93	3.43*	1.60 \pm 0.12	0.02	0.17
	2	6.93	0.84	1.47	1.52	7.89 \pm 1.49	1.24 \pm 0.43	1.47*	1.43 \pm 0.33	0.03	0.46
Muscle	0.5	2.31	3.30	0.52	4.73	4.65 \pm 2.77	3.88 \pm 0.90	0.52*	4.73 \pm 0.94	0.37	0.22
	2	0.37	4.85	0.13	3.83	0.43 \pm 0.09	4.88 \pm 1.12	0.13*	4.47 \pm 2.06	0.03	0.10
Intestines	0.5	5.99	1.33	0.48	1.90	5.87 \pm 0.73	1.44 \pm 0.24	0.48*	1.90 \pm 0.56	0.02	0.30
	2	4.78	1.06	0.82	1.41	4.64 \pm 0.39	1.26 \pm 0.24	0.82*	1.85 \pm 0.45	0.03	0.10
Brain	0.5	0.29	5.86	0.14	6.49	0.30 \pm 0.03	5.95 \pm 0.21	0.14*	6.49 \pm 1.56	0.02	0.17
	2	0.10	3.65	0.05	4.24	0.10 \pm 0.01	3.41 \pm 0.40	0.05*	4.05 \pm 0.32	0.03	0.10
Heart	0.5	3.30	19.92	0.42	13.96	3.61 \pm 0.43	20.13 \pm 2.07	0.42*	13.96 \pm 8.82	0.02	0.17
	2	0.52	36.42	0.14	10.65	0.51 \pm 0.05	37.22 \pm 3.07	0.14*	19.49 \pm 9.24	0.03	0.10
Tail	0.5	8.98	1.57	1.30	2.73	8.64 \pm 0.72	1.57 \pm 0.11	1.30*	2.73 \pm 0.41	0.02	0.37
	2	0.87	1.07	0.20	1.34	0.98 \pm 0.18	1.08 \pm 0.25	0.20*	2.10 \pm 0.94	0.52	0.10
Skeleton	0.5	4.21	3.79	0.44	2.91	4.48 \pm 1.38	3.89 \pm 0.60	0.44*	2.91 \pm 0.06	0.23	0.17
	2	0.34	2.56	0.20	5.06	0.37 \pm 0.06	3.17 \pm 0.76	0.20*	4.55 \pm 1.47	0.04	0.08
Tumour-to-blood	0.5	0.79	4.78	0.95	2.38	0.78 \pm 0.06	4.84 \pm 0.29	0.95*	2.38 \pm 0.43	0.02	0.22
	2	1.86	8.22	2.16	2.54	1.83 \pm 0.29	8.81 \pm 1.41	2.16*	3.02 \pm 0.90	0.03	0.66
Tumour-to-muscle	0.5	2.29	1.16	1.69	0.38	3.23 \pm 1.69	1.12 \pm 0.24	1.69*	0.38 \pm 0.04	0.38	0.22
	2	4.04	0.49	2.30	0.73	3.88 \pm 0.52	0.71 \pm 0.23	2.30*	0.56 \pm 0.19	0.03	0.18
Tumour-to-lung	0.5	0.93	1.24	1.12	0.98	0.91 \pm 0.07	1.22 \pm 0.12	1.12*	0.98 \pm 0.12	0.08	0.22
	2	1.88	1.33	1.72	0.68	1.93 \pm 0.18	1.25 \pm 0.15	1.72*	0.62 \pm 0.07	0.03	0.18
Tumour-to-brain	0.5	18.25	0.51	6.35	0.29	18.63 \pm 1.49	0.67 \pm 0.17	6.35*	0.43 \pm 0.12	0.02	0.22
	2	15.38	0.80	6.44	0.36	15.01 \pm 1.15	0.90 \pm 0.19	6.44*	0.29 \pm 0.10	0.03	0.18

*No SEM could be calculated

^{18}F -FDG showed markedly increased uptake to the brain and heart compared to the groups administered with IHP $^{99\text{m}}\text{Tc}$ -EC-DG. Radiopharmaceutical excretion by the kidneys was noted in all four groups. Similar radiopharmaceutical uptake to the lung tumours was noted for the groups administered with IHP $^{99\text{m}}\text{Tc}$ -EC-DG and ^{18}F -FDG. G2 and G5 administered with IHP $^{99\text{m}}\text{Tc}$ -EC-DG had a higher tumour-to-muscle tissue and tumour-to-brain tissue ratios as a function of time (Figure 4.9B and -D). In contrast G3 and G6 administered with ^{18}F -FDG had higher tumour-to-blood ratios (Figure 4.9A). G2 with G3 showed statistical significant differences for the tumour-to-blood-, tumour-to-lung- and tumour-to-muscle ratios (Table 4.5). There were no significant differences calculated for the tumour-to-tissue for G5 with G6.

^{18}F -FDG overall had higher tumour-to-blood tissue ratios compared to the IHP $^{99\text{m}}\text{Tc}$ -EC-DG. This can be attributed to the fact that a higher concentration of IHP $^{99\text{m}}\text{Tc}$ -EC-DG is present in the blood compared to ^{18}F -FDG concentration in the blood. Chemical modifications had to be made to synthesize the IHP $^{99\text{m}}\text{Tc}$ -EC-DG that can have an effect on the uptake kinetics resulting in increased blood circulation times (Yang *et al.* 2003:470). These chemical modifications can also effect the radiopharmaceutical flow to the kidneys and effect the IHP $^{99\text{m}}\text{Tc}$ -EC-DG uptake to tumours.

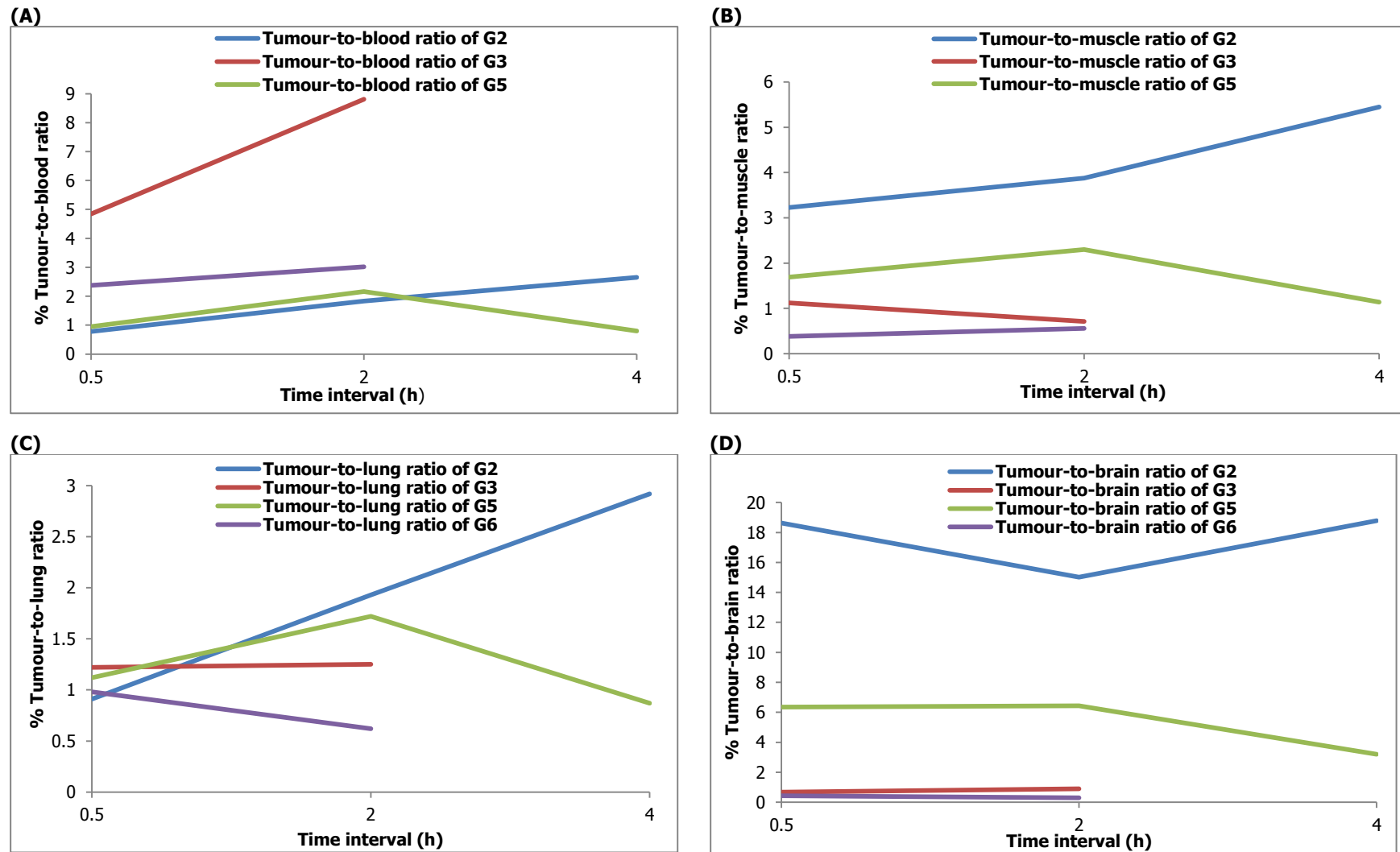


FIGURE 4.9: Tumour-to-tissue biodistribution of the different groups administered with ^{18}F -FDG and IHP $^{99\text{m}}\text{Tc}$ -EC-DG (DL) in lung tumour-bearing mice. The (A) tumour-to-blood ratio-, (B) tumour-to-muscle ratio-, (C) tumour-to-lung ratio and (D) tumour-to-brain ratio is shown with time.

4.3.2.5 Comparison of the biodistribution results of the IHP ^{99m}Tc -EC-DG (DL) with ^{18}F -FDG in lung tumour-bearing mice with literature results

The decision was made to determine if there is any difference between the uptake results from this research that were obtained with the IHP ^{99m}Tc -EC-DG and local produced ^{18}F -FDG administered to tumour-bearing mice with the results published by Yang *et al.* (2003:470-472) with ^{99m}Tc -EC-DG and ^{18}F -FDG. Table 4.6 compares the mean \pm SEM of uptake of the G2, G3, G5 (no SEM could be calculated for G5) and G6 in tumour-bearing mice for sacrificed at specific time intervals post radiopharmaceutical administration. Tumour-bearing mice were not sacrificed at time interval 4 h for G3 and G6, therefore no comparison could be made with the 4 h sacrifice time interval in the literature. Data comparisons were only made for G3 and G6 with ^{18}F -FDG results from the literature (Yang *et al.* 2003:472) for the time intervals 0.5- and 2 h post radiopharmaceutical administration. The highest mean value for the different groups for a specific organ for the time intervals is highlighted in bold. The highest mean values for most of the organs, except the spleen was obtained by G2 for the groups of tumour-bearing mice administered with ^{99m}Tc -EC-DG.

The highest tumour-to-blood, tumour-to-muscle, tumour-to-lung and tumour-to-brain were also achieved by G2 for the ^{99m}Tc -EC-DG. G6 had the lowest values for most of the organs, except the liver for the tumour-bearing mice administered with ^{18}F -FDG. ^{18}F -FDG for the literature had the highest values for the stomach, muscle, intestines and brain. G3 had the highest values for the blood, tumour, lung, spleen, kidneys and heart. ^{18}F -FDG from the literature had the highest tumour-to-blood value. G3 had the highest tumour-to-lung and tumour-to-brain value. G6 had the highest tumour-to-muscle value. This research had to evaluate the uptake pattern of IHP ^{99m}Tc -EC-DG synthesised compare to the golden standard ^{18}F -FDG for tumour induced in nude mice. G2 had the highest tumour uptake of ^{99m}Tc -EC-DG compared to G5 and the ^{99m}Tc -EC-DG tumour uptake in the literature. G3 had the highest tumour uptake of ^{18}F -FDG compared to G6 and the ^{18}F -FDG tumour uptake in the literature. G2 had overall the highest tumour uptake of the different

groups administered with ^{18}F -FDG and $^{99\text{m}}\text{Tc}$ -EC-DG. G2 had higher $^{99\text{m}}\text{Tc}$ -EC-DG uptake than the $^{99\text{m}}\text{Tc}$ -EC-DG uptake in the literature and G5 had slightly lower to similar $^{99\text{m}}\text{Tc}$ -EC-DG uptake in tumours. G3 had the highest ^{18}F -FDG tumour uptake compared to G6 and the mean value from the literature, but was not significant; this was confirmed in Table 4.7 with the CI.

TABLE 4.6: Comparison of the biodistribution (%ID/g) results of G2 and G5 with $^{99\text{m}}\text{Tc}$ -EC-DG from the literature and G3 and G6 with ^{18}F -FDG from the literature in lung tumour-bearing mice (Yang *et al.* 2003:270-272)

Organs/ Tissue	Time interval H	Mean \pm SEM of $^{99\text{m}}\text{Tc}$ -EC- DG in the literature	Mean \pm SEM of G2	Mean \pm SEM of G5	Mean \pm SEM of ^{18}F -FDG in the literature	Mean \pm SEM of G3	Mean \pm SEM of G6
Blood	0.5	1.61 \pm 0.39	7.27 \pm 0.90	0.92*	0.79 \pm 0.7	0.82 \pm 0.19	0.74 \pm 0.06
	2	0.98 \pm 0.27	0.90 \pm 0.14	0.14*	0.24 \pm 0.07	0.34 \pm 0.03	0.61 \pm 0.14
	4	0.79 \pm 0.15	0.49 \pm 0.01	0.30 \pm 0.11	0.20 \pm 0.06	0.20 \pm 0.06	0.20 \pm 0.06
Tumour	0.5	0.79 \pm 0.16	5.77 \pm 1.06	0.87*	2.23 \pm 0.15	3.97 \pm 0.98	1.74 \pm 0.16
	2	0.42 \pm 0.12	1.52 \pm 0.08	0.30*	1.70 \pm 0.17	2.97 \pm 0.30	1.78 \pm 0.60
	4	0.41 \pm 0.16	1.25 \pm 0.44	0.20 \pm 0.02	1.61 \pm 0.18	1.61 \pm 0.18	1.61 \pm 0.18
Lung	0.5	1.05 \pm 0.26	6.21 \pm 0.71	0.78*	2.49 \pm 0.21	3.22 \pm 0.64	1.78 \pm 0.05
	2	0.72 \pm 0.21	0.81 \pm 0.08	0.17*	2.22 \pm 0.14	2.39 \pm 0.11	2.77 \pm 0.72
	4	0.61 \pm 0.13	0.46 \pm 0.03	0.23 \pm 0.00	2.28 \pm 0.18	2.28 \pm 0.18	2.28 \pm 0.18
Liver	0.5	5.67 \pm 2.09	14.35 \pm 1.16	1.75*	1.05 \pm 0.06	1.38 \pm 0.24	1.42 \pm 0.05
	2	5.81 \pm 1.71	5.14 \pm 1.66	0.27*	0.59 \pm 0.04	1.13 \pm 0.03	1.22 \pm 0.38
	4	6.66 \pm 1.79	2.88 \pm 0.31	1.04 \pm 0.08	0.79 \pm 0.04	0.79 \pm 0.04	0.79 \pm 0.04
Stomach	0.5	0.54 \pm 0.11	3.07 \pm 0.56	0.43*	5.05 \pm 0.46	1.34 \pm 0.14	0.96 \pm 0.18
	2	0.44 \pm 0.14	0.73 \pm 0.13	0.23*	4.37 \pm 0.86	1.51 \pm 0.18	2.96 \pm 1.83
	4	0.54 \pm 0.12	0.52 \pm 0.17	0.19 \pm 0.11	2.28 \pm 0.46	2.28 \pm 0.46	2.28 \pm 0.46
Spleen	0.5	3.24 \pm 1.71	2.22 \pm 0.21	0.37*	1.82 \pm 0.20	2.21 \pm 0.38	1.73 \pm 0.22
	2	4.21 \pm 1.37	0.48 \pm 0.06	0.11*	1.90 \pm 0.14	1.69 \pm 0.22	2.13 \pm 0.53
	4	5.93 \pm 3.19	0.34 \pm 0.04	0.23 \pm 0.05	1.59 \pm 0.16	1.59 \pm 0.16	1.59 \pm 0.16
Kidneys	0.5	6.73 \pm 1.84	22.98 \pm 1.69	3.43*	1.14 \pm 0.12	2.23 \pm 0.93	1.60 \pm 0.12
	2	5.69 \pm 1.54	7.89 \pm 1.49	1.47*	0.55 \pm 0.104	1.24 \pm 0.43	1.43 \pm 0.33
	4	4.32 \pm 0.89	3.72 \pm 1.16	1.48 \pm 0.02	0.57 \pm 0.03	0.57 \pm 0.03	0.57 \pm 0.03
Muscle	0.5	0.26 \pm 0.07	4.65 \pm 2.77	0.52*	4.88 \pm 0.62	3.88 \pm 0.90	4.73 \pm 0.94
	2	0.15 \pm 0.04	0.43 \pm 0.09	0.13*	5.41 \pm 0.61	4.88 \pm 1.12	4.47 \pm 2.06
	4	0.15 \pm 0.02	0.25 \pm 0.05	0.18 \pm 0.02	4.74 \pm 0.61	4.74 \pm 0.61	4.74 \pm 0.61
Intestines	0.5	0.51 \pm 0.09	5.87 \pm 0.73	0.48*	2.32 \pm 0.54	1.44 \pm 0.24	1.90 \pm 0.56
	2	0.42 \pm 0.11	4.64 \pm 0.39	0.82*	2.76 \pm 0.50	1.26 \pm 0.24	1.85 \pm 0.45
	4	0.37 \pm 0.07	4.06 \pm 0.46	0.94 \pm 0.16	1.56 \pm 0.34	1.56 \pm 0.34	1.56 \pm 0.34
Brain	0.5	0.06 \pm 0.00	0.30 \pm 0.03	0.14*	6.56 \pm 0.39	5.95 \pm 0.21	6.49 \pm 1.56
	2	0.04 \pm 0.01	0.10 \pm 0.01	0.05*	3.11 \pm 0.13	3.41 \pm 0.40	4.05 \pm 0.32
	4	0.04 \pm 0.01	0.07 \pm 0.01	0.06 \pm 0.01	2.07 \pm 0.08	2.07 \pm 0.08	2.07 \pm 0.08
Heart	0.5	0.61 \pm 0.19	3.61 \pm 0.43	0.42	11.94 \pm 2.57	20.13 \pm 2.07	13.96 \pm 8.82
	2	0.34 \pm 0.08	0.51 \pm 0.05	0.14*	20.33 \pm 7.68	37.22 \pm 3.07	19.49 \pm 9.24
	4	0.32 \pm 0.07	0.32 \pm 0.02	0.19 \pm 0.03	19.35 \pm 8.29	19.35 \pm 8.29	19.35 \pm 8.29
Tumour- to-blood	0.5	0.50 \pm 0.02	0.78 \pm 0.06	0.95*	2.82 \pm 0.144	4.84 \pm 0.29	2.38 \pm 0.43
	2	0.42 \pm 0.02	1.83 \pm 0.29	2.16*	7.26 \pm 1.01	8.81 \pm 1.41	3.02 \pm 0.90
	4	0.50 \pm 0.12	2.65 \pm 1.00	0.80 \pm 0.38	8.93 \pm 1.97	8.93 \pm 1.97	8.93 \pm 1.97
Tumour- to-muscle	0.5	3.35 \pm 0.75	3.23 \pm 1.69	1.69*	0.46 \pm 0.03	1.12 \pm 0.24	0.38 \pm 0.04
	2	2.75 \pm 0.12	3.88 \pm 0.52	2.30*	0.32 \pm 0.03	0.71 \pm 0.23	0.56 \pm 0.19
	4	2.80 \pm 0.98	5.45 \pm 2.21	1.14 \pm 0.23	0.35 \pm 0.05	0.35 \pm 0.05	0.35 \pm 0.05
Tumour- to-lung	0.5	0.77 \pm 0.05	0.91 \pm 0.07	1.12*	0.91 \pm 0.12	1.22 \pm 0.12	0.98 \pm 0.12
	2	0.59 \pm 0.05	1.93 \pm 0.18	1.72*	0.78 \pm 0.113	1.25 \pm 0.15	0.62 \pm 0.07
	4	0.64 \pm 0.12	2.92 \pm 1.18	0.87 \pm 0.10	0.72 \pm 0.11	0.72 \pm 0.11	0.72 \pm 0.11
Tumour- to-brain	0.5	1.30*	18.63 \pm 1.49	6.35*	0.34*	0.66 \pm 0.16	0.29 \pm 0.10
	2	1.24*	15.01 \pm 1.15	6.43*	0.55*	0.90 \pm 0.19	0.42 \pm 0.12
	4	1.28*	18.78 \pm 6.75	3.20 \pm 0.05	0.78*	0.78*	0.78*

* No SEM could be calculated

◇ No mean \pm SEM were calculated for the specific time interval

A 95% CI for the mean value was calculated for the groups (G2, G3, G5 & G6) to determine if results found by Yang et al. (2003:270-272) were within range. A comparison could not be achieved by using statistical significance as the number of animals differed from that used by Yang *et al.* (2003:270-272). If the ^{99m}Tc -EC-DG from the literature does not fall within the range of the groups obtained at a specific time interval of this research, it is marked in red.

TABLE 4.7: Comparison of the biodistribution (%ID/g) results of G2 and G5 with ^{99m}Tc -EC-DG from the literature and G3 and G6 with ^{18}F -FDG from the literature in lung tumour-bearing mice (Yang *et al.* 2003:270-272)

Organ/ Tissue	Time interval H	Mean \pm SEM of ^{99m}Tc -EC- DG in the literature	95% CI of the mean of G2	95% CI of the mean of G5	Mean \pm the SEM of ^{18}F - FDG in the literature	95% CI of the mean of G3	95% CI of the mean of G6
Blood	0.5	1.61 \pm 0.39	[4.40; 10.10]	*	0.79 \pm 0.7	[0.21; 1.43]	[-0.07; 1.54]
	2	0.98 \pm 0.27	[0.14; 3.18]	*	0.24 \pm 0.07	[0.27; 0.40]	[0.02; 1.21]
	4	0.79 \pm 0.15	[0.44; 0.52]	[-1.13; 1.74]	0.20 \pm 0.06		
Tumour	0.5	0.79 \pm 0.16	[2.35; 9.04]	*	2.23 \pm 0.15	[0.84; 7.08]	[-0.33; 3.79]
	2	0.42 \pm 0.12	[1.28; 1.76]	*	1.70 \pm 0.17	[1.67; 4.25]	[0.77; 4.34]
	4	0.41 \pm 0.16	[-0.13; 2.63]	[-2.71; 0.46]	1.61 \pm 0.18		
Lung	0.5	1.05 \pm 0.26	[3.90; 8.50]	*	2.49 \pm 0.21	[1.19; 5.24]	[1.15; 2.41]
	2	0.72 \pm 0.21	[0.57; 1.04]	*	2.22 \pm 0.14	[1.91; 2.85]	[0.33; 5.87]
	4	0.61 \pm 0.13	[0.41; 0.51]	[0.20; 0.24]	2.28 \pm 0.18		
Liver	0.5	5.67 \pm 2.09	[10.7; 18.00]	*	1.05 \pm 0.06	[0.59; 2.14]	[0.79; 2.05]
	2	5.81 \pm 1.71	[-0.14; 10.42]	*	0.59 \pm 0.04	[0.99; 1.26]	[-0.44; 2.87]
	4	6.66 \pm 1.79	[1.88; 3.85]	[0.05; 2.02]	0.79 \pm 0.04		
Stomach	0.5	0.54 \pm 0.11	[1.29; 4.82]	*	5.05 \pm 0.46	[0.89; 1.78]	[-1.42; 3.34]
	2	0.44 \pm 0.14	[0.32; 1.11]	*	4.37 \pm 0.86	[0.75; 2.26]	[-4.89; 10.81]
	4	0.54 \pm 0.12	[-0.01; 1.03]	[-1.22; 1.59]	2.28 \pm 0.46		
Spleen	0.5	3.24 \pm 1.71	[1.60; 2.90]	*	1.82 \pm 0.20	[0.98; 3.43]	[-1.06; 4.51]
	2	4.21 \pm 1.37	[0.29; 0.65]	*	1.90 \pm 0.14	[0.76; 2.60]	[-0.16; 4.42]
	4	5.93 \pm 3.19	[0.22; 0.46]	[-0.45; 0.91]	1.59 \pm 0.16		
Kidneys	0.5	6.73 \pm 1.84	[17.6; 28.30]	*	1.14 \pm 0.12	[-0.72; 5.19]	[0.11; 3.08]
	2	5.69 \pm 1.54	[3.13; 12.62]	*	0.55 \pm 0.10	[-0.60; 3.07]	[0.01; 2.84]
	4	4.32 \pm 0.89	[0.06; 7.38]	[1.12; 1.85]	0.57 \pm 0.03		
Muscle	0.5	0.26 \pm 0.07	[-4.10; 13.40]	*	4.88 \pm 0.62	[1.02; 6.72]	[-7.22; 16.68]
	2	0.15 \pm 0.04	[0.14; 0.72]	*	5.41 \pm 0.61	[0.02; 9.60]	[-4.37; 13.31]
	4	0.15 \pm 0.02	[0.08; 0.42]	[-0.02; 0.37]	4.74 \pm 0.61		
Intestines	0.5	0.51 \pm 0.09	[3.60; 8.10]	*	2.32 \pm 0.54	[0.66; 2.21]	[-5.19; 9.00]
	2	0.42 \pm 0.11	[3.41; 5.86]	*	2.76 \pm 0.50	[0.24; 2.27]	[-0.07; 3.76]
	4	0.37 \pm 0.07	[2.59; 5.25]	[-1.12; 3.00]	1.56 \pm 0.34		
Brain	0.5	0.06 \pm 0.00	[0.20; 0.40]	*	6.56 \pm 0.39	[5.28; 6.59]	[-13.37; 26.33]
	2	0.04 \pm 0.01	[0.08; 0.12]	*	3.11 \pm 0.13	[1.69; 5.12]	[2.65; 5.43]
	4	0.04 \pm 0.01	[0.05; 0.08]	[-0.04; 0.16]	2.07 \pm 0.08		
Heart	0.5	0.61 \pm 0.19	[2.30; 4.90]	*	11.94 \pm 2.57	[13.53; 26.71]	[-98.08; 125.9]
	2	0.34 \pm 0.08	[0.36; 0.65]	*	20.33 \pm 7.68	[24.00; 50.39]	[-20.28; 59.26]
	4	0.32 \pm 0.07	[0.27; 0.36]	[-0.12; 0.51]	19.35 \pm 8.29		
Tumour-to- blood	0.5	0.50 \pm 0.02	[0.59; 0.97]	*	2.82 \pm 0.144	[3.93; 5.74]	[-3.08; 7.85]
	2	0.42 \pm 0.02	[0.19; 2.75]	*	7.26 \pm 1.01	[2.74; 14.87]	[-0.83; 6.86]
	4	0.50 \pm 0.12	[-0.54; 5.84]	[-3.96; 5.56]	8.93 \pm 1.97		
Tumour-to- muscle	0.5	3.35 \pm 0.75	[2.21; 8.60]	*	0.46 \pm 0.03	[0.34; 1.87]	[-0.13; 0.87]
	2	2.75 \pm 0.12	[2.21; 5.55]	*	0.32 \pm 0.03	[-0.28; 1.70]	[-0.24; 1.35]
	4	2.80 \pm 0.98	[-1.6; 12.40]	[-1.73; 4.02]	0.35 \pm 0.05		
Tumour-to- lung	0.5	0.77 \pm 0.05	[0.70; 1.10]	*	0.91 \pm 0.12	[0.85; 1.58]	[-0.55; 2.50]
	2	0.59 \pm 0.05	[1.34; 2.52]	*	0.78 \pm 0.113	[0.63; 1.87]	[0.34; 0.89]
	4	0.64 \pm 0.12	[-0.75; 6.57]	[-0.39; 2.12]	0.72 \pm 0.11		
Tumour-to- brain	0.5		[13.90; 23.30]	*		[0.14; 1.19]	[-0.92; 1.50]
	2		[11.30; 18.70]	*		[0.08; 1.73]	[-0.07; 0.92]
	4		[-2.70; 40.20]	[2.51; 3.89]			

* No SEM could be calculated

Part of the purpose of this research was to evaluate the uptake of IHP ^{99m}Tc -EC-DG to the tumour induced in nude mice, therefore the mean tumour values was of most importance. The mean tumour values of the ^{99m}Tc -EC-DG from the

literature falls within the range of that obtained by G2 at 4 hours and just out of the 4 h range of that obtained by G5. No *SEM* could be calculated or G5 as the animal sample were too small. It could be established with G2 and G5 that there were uptake of the IHP ^{99m}Tc -EC-DG in induced lung tumours, even though not exactly the same result could be achieved.

The evaluation of the tumour uptake of IHP ^{99m}Tc -EC-DG was successful. The mean values of the tumours ^{18}F -FDG from the literature fell into range of G3 and G6 for the 0.5 and 2 h animal sacrifice. Indicating similar results were obtained in the tumours of the tumour-bearing mice administered with ^{18}F -FDG.

4.4 CONCLUSION

The results from research phase 1A and 1B confirmed selectivity of the IHP ^{99m}Tc -EC-DG for A549 human lung cancer cells. Analysis of the results indicated that the biodistribution in healthy nude mice of the IHP ^{99m}Tc -EC-DG for all the time intervals was the highest to the kidneys (excretion), followed by liver then intestines (excretion) and with slight uptake to the heart. The slight uptake in the heart is due to glucose uptake by the myocytes. The highest excretion of IHP ^{99m}Tc -EC-DG by the kidneys was before 2 h after administration. This high uptake of the IHP ^{99m}Tc -EC-DG by the kidneys at the three different time intervals is likely due to the EC and EC-conjugates that interact with renal tubules in the kidney (Zhang *et al.* 2012:6).

IHP ^{99m}Tc -EC-DG biodistribution differences with relation to the lungs, skeleton, blood, lungs and brain were noted between the healthy (G1) and tumour-induced (G2) nude mice. These differences could be attributed to the tumour that can cause changes in metabolism throughout the body and thus affecting the uptake of these organs.

^{18}F -FDG showed markedly increased uptake to the brain and heart compared to the groups administered with IHP ^{99m}Tc -EC-DG as expected. Radiopharmaceutical excretion by the kidneys was noted in all four groups. Similar radiopharmaceutical uptake in the lung tumours was noted for the groups administered with IHP ^{99m}Tc -EC-DG and ^{18}F -FDG. ^{18}F -FDG overall had higher tumour-to-blood tissue ratio compared to the IHP ^{99m}Tc -EC-DG. This can be attributed to the fact that a higher concentration of IHP ^{99m}Tc -EC-DG is present in the blood (and clears slower from the blood) compared to ^{18}F -FDG concentration in the blood. Differences between IHP ^{99m}Tc -EC-DG and the

literature could be due to differences in the formulation and amounts of ECDG administered. As this is a new (experimental) radiopharmaceutical, procedures and optimum kit formulation has not been standardised between different laboratories.

IHP ^{99m}Tc -EC-DG had uptake in the lung tumours in nude mice, even though the results were not identical to the literature. Similar results were obtained in the tumours of the tumour-bearing mice administered with ^{18}F -FDG with that performed in the literature. IHP ^{99m}Tc -EC-DG had higher tumour-to-muscle ratios than ^{18}F -FDG but lower tumour-to-blood ratios than ^{18}F -FDG.

CHAPTER 5

RESEARCH PHASE TWO: THE RABBIT MODEL

5.1 INTRODUCTION

Research phase two comprised of prospective *in vivo* studies performed with 25 healthy New Zealand White rabbits that were divided into four different groups according to the radionuclide or radiopharmaceutical used (Figure 5.1). Normal- and infection biodistribution of IHP ^{99m}Tc -EC-DG respectively needed to be evaluated in healthy-, septic IFI/IF and sterile IFI/IF New Zealand White rabbits in order to achieve the aim. The biodistribution of IHP ^{99m}Tc -EC-DG to an area of induced IFI/IF (septic and sterile) in rabbits was compared to the biodistribution of ^{67}Ga -citrate to the same area of induced IFI/IF. ^{67}Ga -citrate was used due to the following reasons::

- Capability to detect a variety of infections/inflammations
- Availability of a medium-energy collimator at DNM, UAH for optimal imaging of this radionuclide.
- Affordability
- Accessibilty and availability of the radionuclide at DNM, UAH.

A comparison of IHP ^{99m}Tc -EC-DG with ^{67}Ga -citrate was performed as part of a control experiment to confirm sufficient induced septic- (*E. coli*) and sterile (zymosan) IFI/IF areas. Normal biodistribution of IHP ^{99m}Tc -EC-DG (DL) ($n=10$) was also compared to $^{99m}\text{TcO}_4^-$ ($n=5$) at specific time intervals. The uptake of IHP ^{99m}Tc -EC-DG (DL) in areas of septic- and sterile IFI/IF induced in rabbits was evaluated using induced IF/IF and control studies were performed using ^{67}Ga -citrate (Figure 5.1). The protocol that was designed, tried to limit the imaging time intervals to a minimum without losing statistical data in order to ensure as little as possible discomfort to rabbits by reducing anesthetic time.

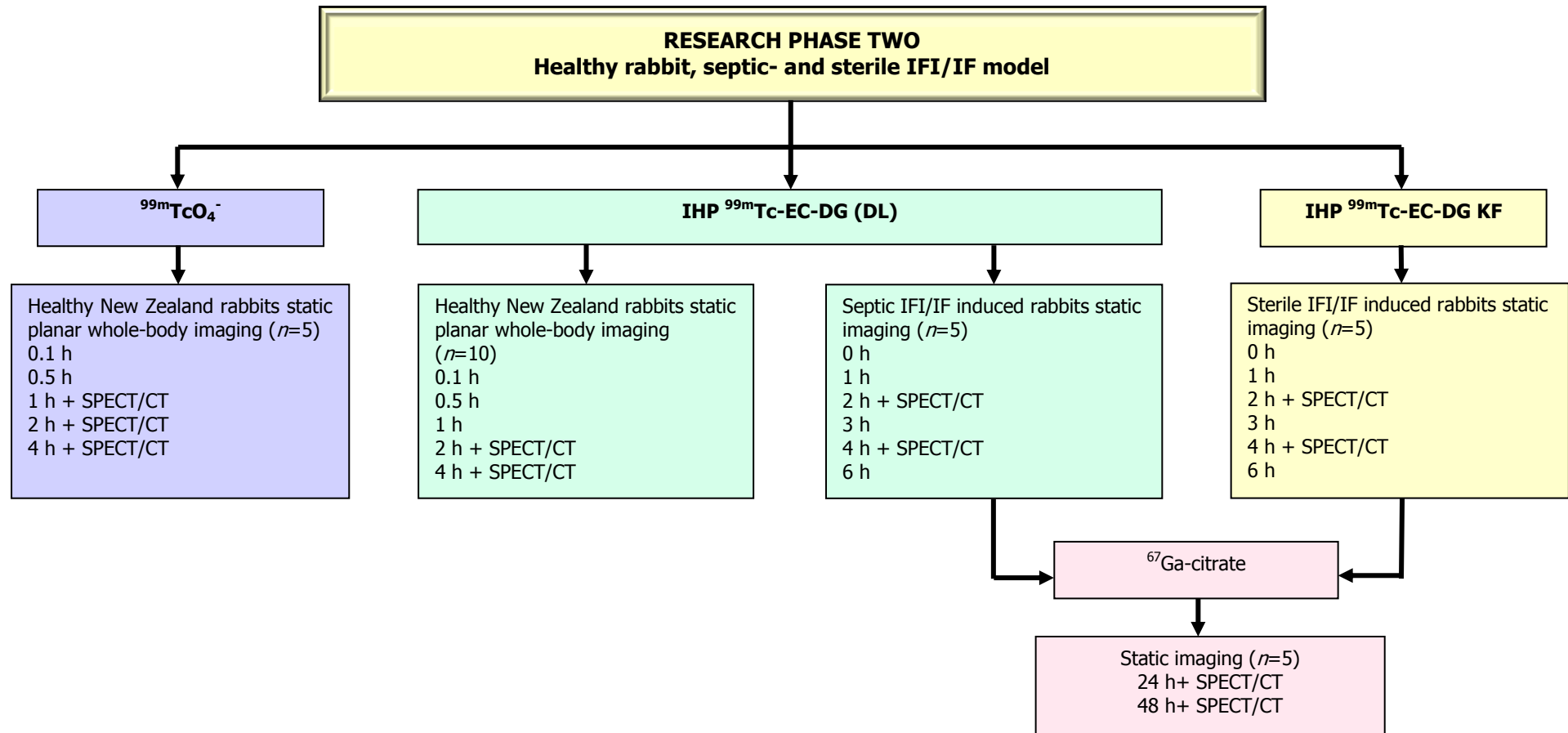


FIGURE 5.1: Research design for phase two with healthy, septic- and sterile IFI/IF induced New Zealand White rabbits as animal models

5.2 MATERIALS AND METHODS

5.2.1 Sample size

The sample size for phase two included 25 healthy immune-competent New Zealand White male rabbits (Figure 5.2). Only male rabbits were used since the female rabbits are exclusively used for reproduction purposes. The rabbits were housed at the UFS Animal Research Centre (accredited supplier of animals for research purposes) before, during and after the completion of the research. The Department of Biostatistics recommendations as well as cost implications were taken into consideration in the determination of the sample size.



FIGURE 5.2: Co-researcher (MRS. J.M. Wagener) holding one of the New Zealand White rabbits used during phase two

5.2.2 Radiosynthesis of ^{99m}Tc -EC-DG (DL) and -(KF)

The radiolabelling of IHP ^{99m}Tc -EC-DG (DL) used for the healthy and septic IFI/IF induced rabbits was performed according to the procedure described in section 3.3.5.3 (Chapter 3). The sterile IFI/IF induced rabbits were administered with IHP ^{99m}Tc -EC-DG (KF) that was radiolabelled as described in section 3.3.5.4.

5.2.3 Gamma camera scintigraphy studies

5.2.3.1 Normal biodistribution

In the gamma scintigraphy studies each group of healthy rabbits were injected intravenously in the ear with IHP ^{99m}Tc -EC-DG (DL) ($n=10$) and $^{99m}\text{TcO}_4^-$ ($n=5$) with 74 MBq radioactivity per animal (Table 5.1). Planar whole-body static images were obtained at 0.1-, 0.5-, 1-, 2- and 4 h after administration. One rabbit per group received low dose whole-body SPECT/CT. The one healthy rabbit administered with IHP ^{99m}Tc -EC-DG (DL) received a SPECT/CT at 2- and 4 h post injection and the one rabbit in the $^{99m}\text{TcO}_4^-$ group received a SPECT/CT at 1-, 2- and 4 h post radionuclide administration (Figure 5.3). The reason for the additional SPECT/CT at 1 h post $^{99m}\text{TcO}_4^-$ administration was to identify the thyroid tissue of the rabbit before washout of $^{99m}\text{TcO}_4^-$. The thyroid of the rabbit is small and can be missed on planar imaging and therefore the decision was made to do SPECT/CT. If thyroid uptake was to be identified on the IHP ^{99m}Tc -EC-DG images it could be indicative of poor labelling efficiency. The biodistribution was determined by using a SQ, SQUAL reporting system and radiopharmaceutical quantification technique that is discussed in detail in section 5.2.4.3.

TABLE 5.1: Summary of radionuclide and radiopharmaceutical dosages administered to rabbits in phase two of the research

Study group	Radionuclide/RP administered	Number of rabbits (n)	Injected dose MBq/rabbit
Healthy rabbits	IHP ^{99m}Tc -EC-DG (DL)	10	73.23 ± 2.4
	$^{99m}\text{TcO}_4^-$	5	71.74 ± 4.42
Rabbits induced with focal area of septic IFI/IF	IHP ^{99m}Tc -EC-DG (DL) ^{67}Ga -citrate	5	(a) 70.6 ± 4.27 (b) 11.07 ± 1.68
Rabbits induced with focal area of sterile IFI/IF	IHP ^{99m}Tc -EC-DG (KF) ^{67}Ga -citrate	5	(a) 71.97 ± 8.71 (b) 15.48 ± 1.15



FIGURE 5.3: One of the rabbits that received a SPECT/CT during phase two

The imaging of the rabbits of research phase two was performed using a Siemens Symbia T (Siemens Medical Solutions USA, Hoffman Estates, IL, USA) SPECT/CT dual-head gamma camera connected to the acquisition workstation. All the data were transferred and processed on a Siemens Syngo workstation. The gamma camera was equipped with LEHR parallel-hole collimators for the $^{99m}\text{TcO}_4^-$ and IHP $^{99m}\text{Tc-EC-DG}$. The collimator was changed to the MEHR parallel-hole collimator for the $^{67}\text{Ga-citrate}$ imaging. The useful field of view is 53 cm x 38 cm. The intrinsic spatial resolution is 3.8 mm. Static planar whole-body images were acquired with the stop conditions set at 5 minutes, the matrix size of 256 x 256 and the zoom at 1. The SPECT gamma camera parameters are summarised in Table 5.2.

TABLE 5.2: Siemens SYMBIA T parameters for the SPECT imaging

SPECT camera parameter	Setting
Window settings - $^{99m}\text{TcO}_4^-$	140 keV (15%)
Window settings - $^{67}\text{Ga-citrate}$	185 keV (15%), 92 keV (20%) and 300 keV (15%)
Matrix size	128 x 128
Degrees of Rotation per detector	180
Number of views per detector	32
Time per view in seconds	25
Orbit	Noncircular
Mode	Step and Shoot
Number of scans	1

5.2.3.2 Induced IFI/IF biodistribution

The same protocol as Rossouw *et al.* (2005:390) was used, where septic IFI/IF was induced by intradermal administration of 0.5 ml *E.coli* suspension (obtained from Microbiology, UAH) containing approximately 9×10^8 colony forming units per ml, in the RH hip (gluteus) muscle of the rabbit and developed over 120 h (5 days).

The sterile induced IFI/IF can be achieved with different percentages zymosan ranging from 1.0 - 7.5% (Handel & Hamel 2009:461). A 1 ml suspension of 2% zymosan (Davies Diagnostic Pty Ltd) was prepared and administered in RH hip muscle. The induced IFI/IF was developed for 168 h (7 days). The groups with septic IFI/IF ($n=5$) and sterile IFI/IF ($n=5$) were injected intravenously with IHP ^{99m}Tc -EC-DG (DL) or IHP ^{99m}Tc -EC-DG (KF) (74 MBq per animal) followed by ^{67}Ga -citrate (15 MBq per animal), after completion of the IHP ^{99m}Tc -EC-DG imaging (Table 5.1).

The scintigraphic images were also performed using the Siemens Symbia T camera. Static images for septic and sterile IFI/IF were obtained at 0.1-, 1-, 2-, 3-, 4- and 6 h post injection of IHP ^{99m}Tc -EC-DG. One rabbit also received a low dose SPECT/CT at 2- and 4 h. Directly after the 6 h IHP ^{99m}Tc -EC-DG static was acquired, ^{67}Ga -citrate was injected to the same group of rabbits. Static images ($n=5$) and SPECT/CT ($n=1$) were obtained at 24- and 48 h radionuclide administration. ^{67}Ga -citrate was used to confirm successful induction of a focal area of IFI/IF and to be compared to IHP ^{99m}Tc -EC-DG IFI/IF biodistribution images.

5.2.4 Data analysis

5.2.4.1 Quantitative analysis of images of healthy rabbits

The statistical analysis was performed by the Department of Biostatistics of the UFS. The activity in all organs and tissue samples was expressed as the percentage of the total body activity per organ and presented as the mean \pm SEM. The Wilcoxon Test

for unpaired data was calculated to determine the differences between the variables for the biodistribution of $^{99m}\text{TcO}_4^-$ and IHP $^{99m}\text{Tc-EC-DG}$. The total body counts of the healthy rabbits were determined by drawing the ROIs over the image of the entire rabbit. The biodistribution (counts) of the different radiopharmaceuticals in the different organs were determined by drawing ROIs over the organs of interest. The percentage of injected activity by these organs at various time intervals was calculated as: percentage biodistribution to organ = (organ counts at specific time/total body counts at that time) \times 100. Background correction and physical decay of radionuclides were taken into consideration.

The biodistribution of the IHP $^{99m}\text{Tc-EC-DG}$ and $^{99m}\text{TcO}_4^-$ in the organs of the healthy rabbits group was evaluated by comparing the ROIs of the specific organ to the image of the entire rabbit. The ROIs were drawn over the brain, liver, both kidneys (RH and LT separate ROIs), both lungs (RH and LT separate ROIs), skin (ROI drawn over ear that was not used for injection of radiopharmaceutical), muscle, stomach, knee joint, urinary bladder and the injection site in the images at different time points 0.1-, 0.5-, 1-, 2- and 4 h. The ROIs were drawn on the ANT and POST planar static images. At the time when adjacent organs were examined, the maximum display range was firstly set at low and was increased gradually until the organs could be well visualized and yet remain distinct. The percentage uptake of injected activity by these organs at various time intervals was calculated. One rabbit injected with IHP $^{99m}\text{Tc-EC-DG}$ and one rabbit injected with $^{99m}\text{TcO}_4^-$ received a low dose whole-body SPECT/CT at 2 h post administration. SPECT/CT provided additional anatomical and physiological information about the biodistribution of RP and was evaluated with a semi-quantitative (SQ) and semi-qualitative (SQUAL) data interpretation form.

For the quantitative analysis of the septic- and sterile induced IFI/IF (non-parametric data) the Wilcoxon test was used to calculate the

differences between the unpaired groups. To determine the IHP ^{99m}Tc -EC-DG or ^{67}Ga -citrate accumulation in the IFI/IF thigh the anterior and posterior images were selected. On all the ^{99m}Tc -EC-DG or ^{67}Ga -citrate images, an automatically adjusted ROI was drawn over the right thigh region (T) and a mirror image region was created over the contralateral normal thigh area (NT). Accumulation of the tracer (radionuclide or radiopharmaceutical) at the site of septic- or sterile IFI/IF was expressed as the ratio of counts in the target muscle to the counts in the non-target muscle (T/NT ratio). Statistical calculations were done on all the data which included the median and mean \pm SEM. A P value <0.05 was considered statistical significant.

5.2.4.2 *Quantitative analysis of images of septic and sterile IFI/IF rabbits*

The quantitative data analysis for the septic and sterile IFI/IF was performed using the same data analysis techniques. Quantitative analysis was used to determine the IHP ^{99m}Tc -EC-DG uptake in the septic or sterile IFI/IF thigh, reference images (0.1-, 1-, 2-, 3-, 4- and 6 h) were selected. The uptake of ^{67}Ga -citrate in IFI/IF area was also determined on the 24- and 48 h post administration images.

On all the reference images the ROIs were hand-drawn over the RH thigh region (target) and a mirror image was created over the contralateral normal thigh area (non-target). The Target (T) and Non-target (NT) ROIs were drawn on the ANT and POST planar static images. Biodistribution of the IHP ^{99m}Tc -EC-DG and ^{67}Ga -citrate at the site of septic or septic IFI/IF was expressed as the ratio of counts in the T muscle to the counts in the NT muscle (T/NT ratio). All values were expressed as the mean \pm Standard Error of the Mean (SEM) and the median was also calculated. ROIs were also hand-drawn around the accumulation of the IHP ^{99m}Tc -EC-DG

(DL) and ^{67}Ga -citrate to the area of septic IFI/IF on the SPECT/CT imaging for the different time intervals. Biodistribution ROIs were also hand-drawn over the biodistribution of the IHP $^{99\text{m}}\text{Tc}$ -EC-DG and ^{67}Ga -citrate at the site of septic IFI/IF on the SPECT/CT images and expressed as the ratio of counts in the T muscle to the counts in the NT muscle (T/NT ratio). All values were expressed as the mean \pm SEM. The results of the biodistribution around the area of septic or sterile IFI/IF on the different images were expressed as the mean \pm SEM for the different ROIs.

5.2.4.3 *SQ and SQUAL analysis*

Volumetrix software was not available at the DNM at UAH at the time of analysis of the SPECT/CT images. A SQ and SQUAL data interpretation form was designed and then used by a nuclear medicine physician for the scintigraphic static, whole-body and SPECT/CT images. The nuclear medicine physician that reported on the scintigraphic images had no knowledge on the biodistribution of $^{99\text{m}}\text{Tc}$ -EC-DG as described in the literature (blinded). The supervisor (Prof. A.C. Otto) of this thesis that is also a nuclear medicine physician confirmed the results that were found by the reporting nuclear medicine physician. Additional conclusions were drawn by using the information obtained for the image interpretation form and to confirm observations made from other quantitative results. The image interpretation form was used for the healthy rabbits administered with $^{99\text{m}}\text{TcO}_4^-$ and with IHP $^{99\text{m}}\text{Tc}$ -EC-DG that received static planar whole-body and a single rabbit that received SPECT/CT scintigraphic imaging at specific imaging time intervals. It was also used for the rabbits induced with septic- and sterile IFI/IF and imaged after administration with IHP $^{99\text{m}}\text{Tc}$ -EC-DG and ^{67}Ga -citrate at specific time intervals. The data interpretation form included a four-point grading scale (0 to 4) and a section to report any additional scintigraphic imaging observations.

The SQ and SQUAL indicative factors used for the reporting of the

scintigraphic images included the following:

- Positive (Post): *in vivo* biodistribution to the specific organ or focal area of IFI/IF is clearly increased
- Negative (Neg): *in vivo* biodistribution to the specific organ or focal area of IFI/IF is clearly decreased
- Background (Bkg): *in vivo* biodistribution to the specific organ or focal area of IFI/IF is not clearly increased or decreased

The four-point SQ and SQUAL grading scale included the following:

0 – Nil biodistribution, was defined as no increased/minimally increased radionuclide/radiopharmaceutical biodistribution to the specific organ or focal area of induced IFI/IF (biodistribution less than that of the neighbouring muscle tissue)

1 – Mild, radionuclide/radiopharmaceutical biodistribution that approximates that of the neighbouring muscle tissue

2 – Moderate, radionuclide/radiopharmaceutical biodistribution mildly greater than that of the neighbouring muscle tissue

3 – Severe, radionuclide/radiopharmaceutical biodistribution markedly greater than that of neighbouring muscle tissue

5.3 RESULTS AND DISCUSSION

5.3.1 Healthy Rabbit Model

5.3.1.1 Radiosynthesis of $^{99m}\text{Tc-EC-DG (DL)}$

Freshly eluted $^{99m}\text{TcO}_4^-$ (1480 MBq in 0.5 ml) was added to the chemicals in the measured quantities. The complexation was carried out at a pH of 6 in a laminar flow cabinet situated in a Type B radiological controlled laboratory. The radiochemical purity of the IHP $^{99m}\text{Tc-EC-DG (DL)}$ complex was assessed with TLC chromatography using ITLC-SC strips developed in saline and Whatman No. 1 developed in acetone. QC was performed directly after the completion of the $^{99m}\text{Tc-EC-DG (DL)}$. The IHP $^{99m}\text{Tc-EC-DG}$ complex evaluated

on the Whatman No. 1 paper remained at the origin, however on ITLC-SC it migrated to the front solvent. TLC analyses showed more than 98% radiochemical purity with less than 1% colloidal formation. The final pH was 7 for the IHP ^{99m}Tc -EC-DG directly labelled complex. The labelled compound therefore complied to the specification (radiochemical purity and pH) for use in the animal model. HPLC-QC could not be performed on the IHP ^{99m}Tc -EC-DG as used in research phase two, as the instrumentation necessary is not available at the DNM at UAH.

5.3.1.2 *In vivo normal biodistribution images*

Static ANT and POST whole-body images were acquired of the healthy rabbits administered with IHP ^{99m}Tc -EC-DG (DL) at 0.1-, 0.5-, 1-, 2- and 4 h post radiopharmaceutical administration (Figure 5.4). Specific organs of interest are indicated with different types and colour arrows. The bladder demonstrated intense increased IHP ^{99m}Tc -EC-DG (DL) activity due to the excretion by the kidneys, this was evident on the 0.1 h static image, increasing in size on the 1-, 2- and 4 h static images. No obvious biodistribution of IHP ^{99m}Tc -EC-DG (DL) was observed in the skin area (ear that was not used for RP administration). The earlier scintigraphic images before 1 h showed that no RP biodistribution could clearly be noted in the area of the intestines. An increasing intensity of activity over time (from 1-4 h) can be observed between the kidneys in the intestines. No biodistribution to the skeleton and joints were noted at any of the different imaging time intervals, due to low metabolic activity in the skeleton and joints. Increased blood pool activity was observed on the 0.1 and 0.5 h static views in the region of the lungs. The biodistribution activity noted in the lungs decreased to normal background activity on the 1-, 2- and 4 h static images, due to blood clearance of activity from the lungs. Intense increased biodistribution of IHP ^{99m}Tc -EC-DG (DL) was observed in the region of the brain on the 0.1 h and 0.5 h static images, because of the injection into the ear vein adjacent to the brain, this clears up completely along the last static images.

Visual assessment of the IHP ^{99m}Tc -EC-DG (DL) biodistribution in the region of the thyroid and salivary glands on the 1-, 2- and 4 h images indicating limited

amount of free $^{99m}\text{TcO}_4^-$ after clearance of the increased blood pool activity (0.1- and 0.5 h static images) due to RP administration. Intense increased blood pool activity was noted in the heart on the 0.1 h static images and on the 0.5-2 h images, biodistribution to the myocardium was evident which cleared towards the last static images at 4 h.

Notable intense increased IHP $^{99m}\text{Tc-EC-DG}$ (DL) biodistribution was present in the liver on the 0.1 h image, correlating with blood pool activity, which decreased towards the 4 h static image. Activity in the heart and liver thus represent mainly to be biodistribution (uptake), not blood pool activity.

No RP biodistribution could be observed in the region of the spleen, gallbladder and stomach on all the static views for the different imaging time intervals. Well-defined intense increased excretion of IHP $^{99m}\text{Tc-EC-DG}$ (DL) was observed in the kidneys on all the static image time points Background radiopharmaceutical activity was noted in the region of the muscles with no well-defined increased uptake. The rabbits were passive the day before the experiment and temperature regulated, this could have contributed to no significant muscle uptake. Muscle uptake can be seen as with animals/humans on glucose metabolism imaging agents like $^{18}\text{F-FDG}$ after exercise and cold temperature exposure, due to increased glucose consumption by muscles.

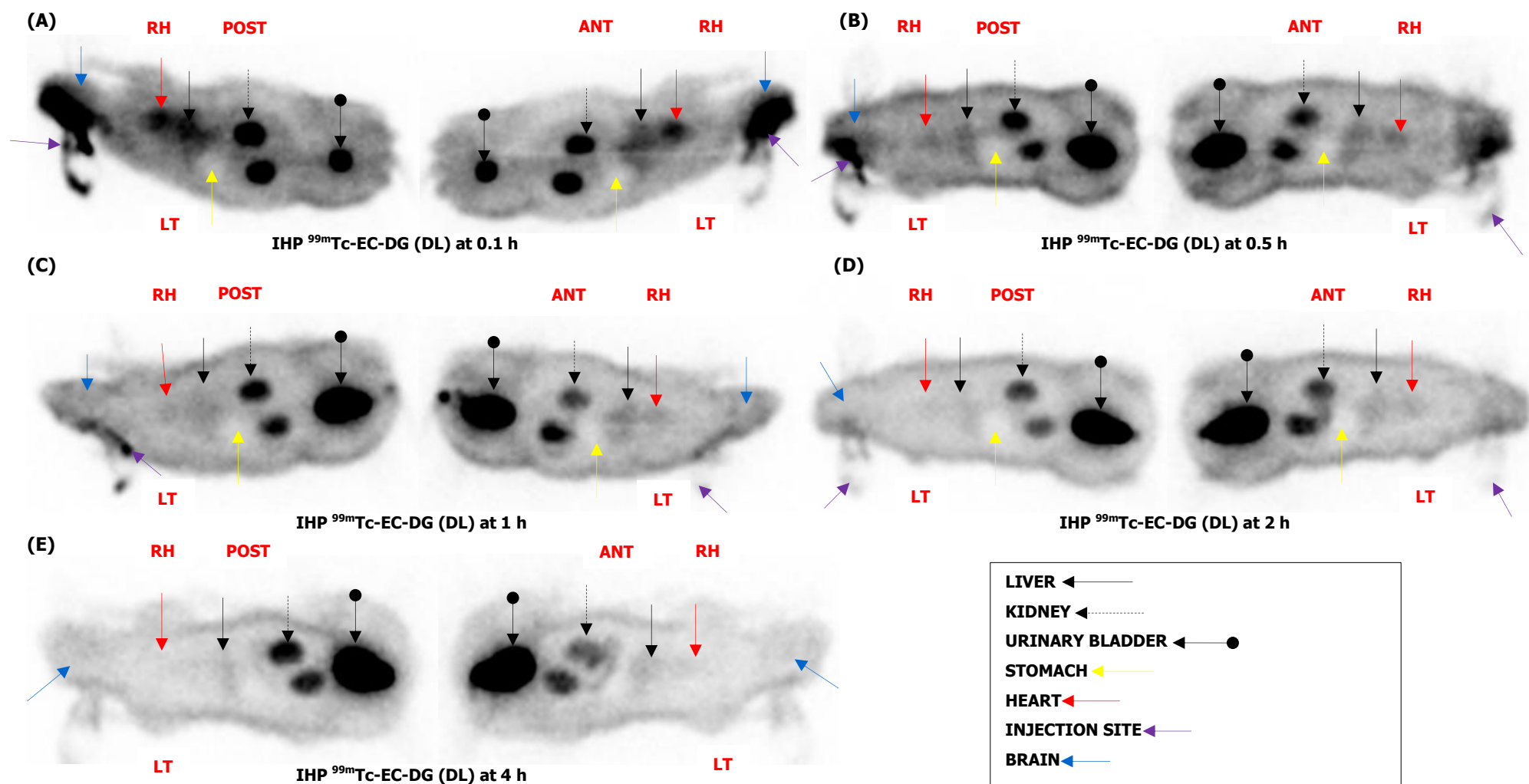


FIGURE 5.4: Biodistribution of IHP ^{99m}Tc -EC-DG (DL) in healthy rabbits at (A) 0.1-, (B) 0.5-, (C) 1-, (D) 2- and (E) 4 hours post administration. Liver (solid arrow), kidney (dashed arrow), urinary bladder (ball arrow), stomach (yellow arrow) and heart (red arrow) are well-outlined. The injection site (purple arrow) is also visible with no brain uptake (blue arrow).

Figure 5.5 (A & B) shows the IHP ^{99m}Tc -EC-DG SPECT/CT (transverse, sagittal and coronal) images at 2- and 4 h post administration. Organs of interest are indicated with arrows. The bladder demonstrated intense increased RP biodistribution on the 2- and 4 h SPECT/CT images. The skin (evaluated ear that was not used for RP administration) demonstrated no obvious IHP ^{99m}Tc -EC-DG biodistribution. IHP ^{99m}Tc -EC-DG biodistribution was noted to the intestines on both SPECT/CT imaging time points. No IHP ^{99m}Tc -EC-DG biodistribution was observed in the region of the skeleton and joints on all time points of the SPECT/CT views for the rabbits. The 2- and 4 h SPECT/CT images demonstrated no RP biodistribution to the lungs, small area of the brain in the field of view, stomach, gallbladder, spleen, thyroid and salivary glands. Mild increased RP activity was noted in the heart on the 2 h SPECT/CT, which has decreased in uptake on the 4 h SPECT/CT views. Well-defined increased biodistribution of the IHP ^{99m}Tc -EC-DG was observed in the liver on the 2- and 4 h SPECT/CT images. Intense increased RP biodistribution was noted in the kidneys on all three SPECT/CT time intervals. Background activity was observed in the muscles with no well-defined increased uptake.

5.3.1.3 SQ and SQUAL analysis

All images with the SQ and SQUAL indicative factors as described in section 5.2.4.3. A data interpretation form included a four-point grading scale (0 to 4) and additional scintigraphic imaging observations could be noted. These results were used to indicate and emphasise the quantitative results that determined the organs of the highest and lowest IHP ^{99m}Tc -EC-DG biodistribution in the healthy rabbits. These results of the normal biodistribution of the IHP ^{99m}Tc -EC-DG (DL) to the different organs found in the static whole-body and SPECT/CT images of the healthy rabbits, is summarised in Table 5.3.

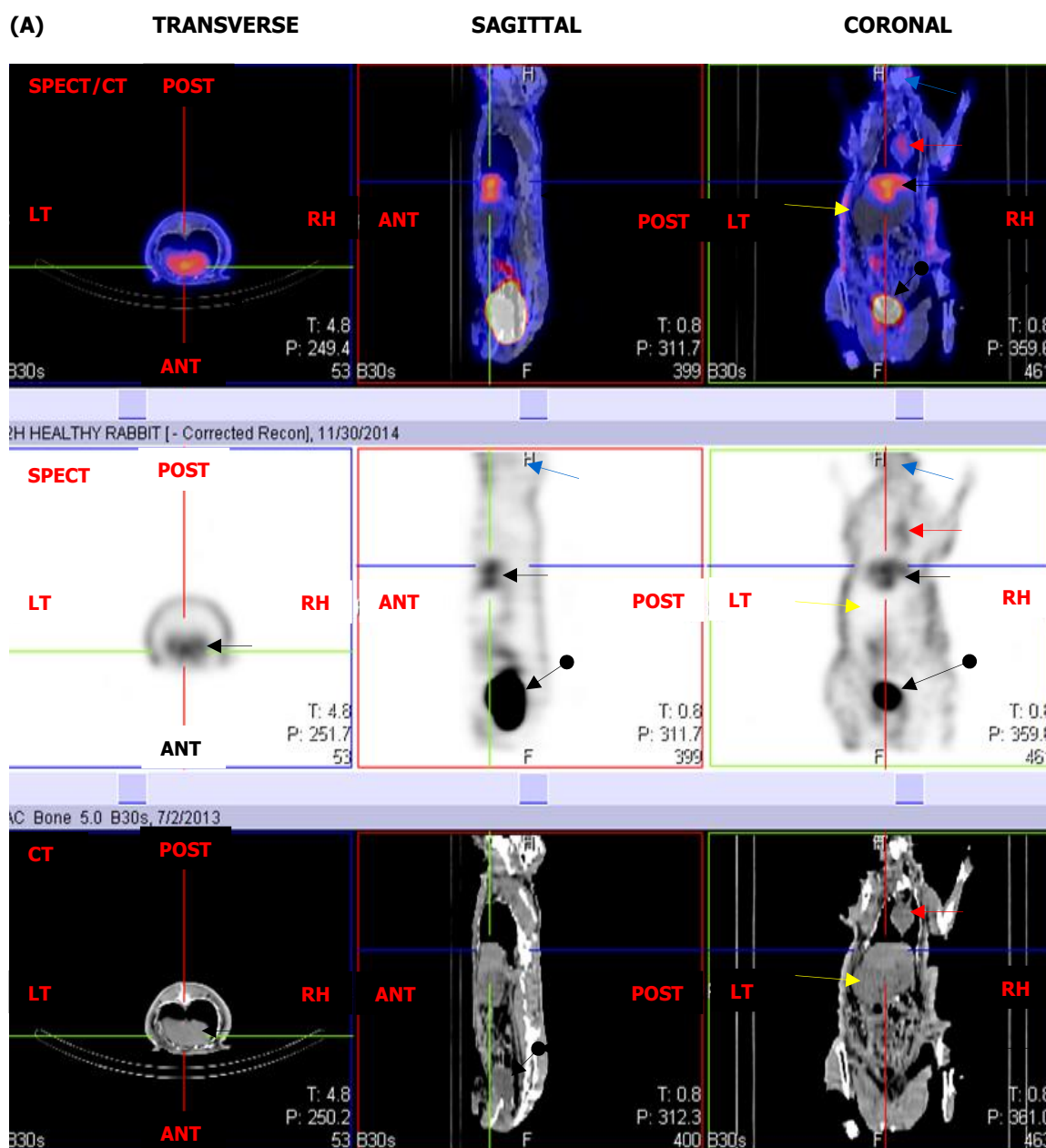


FIGURE 5.5: (A) IHP ^{99m}Tc-EC-DG fused SPECT/CT (transverse, sagittal and coronal) images at 2 hour post radiopharmaceutical administration. Liver (solid arrow), urinary bladder (ball arrow), stomach (yellow arrow) and heart (red arrow) are well-outlined. No visible brain uptake (blue arrow).

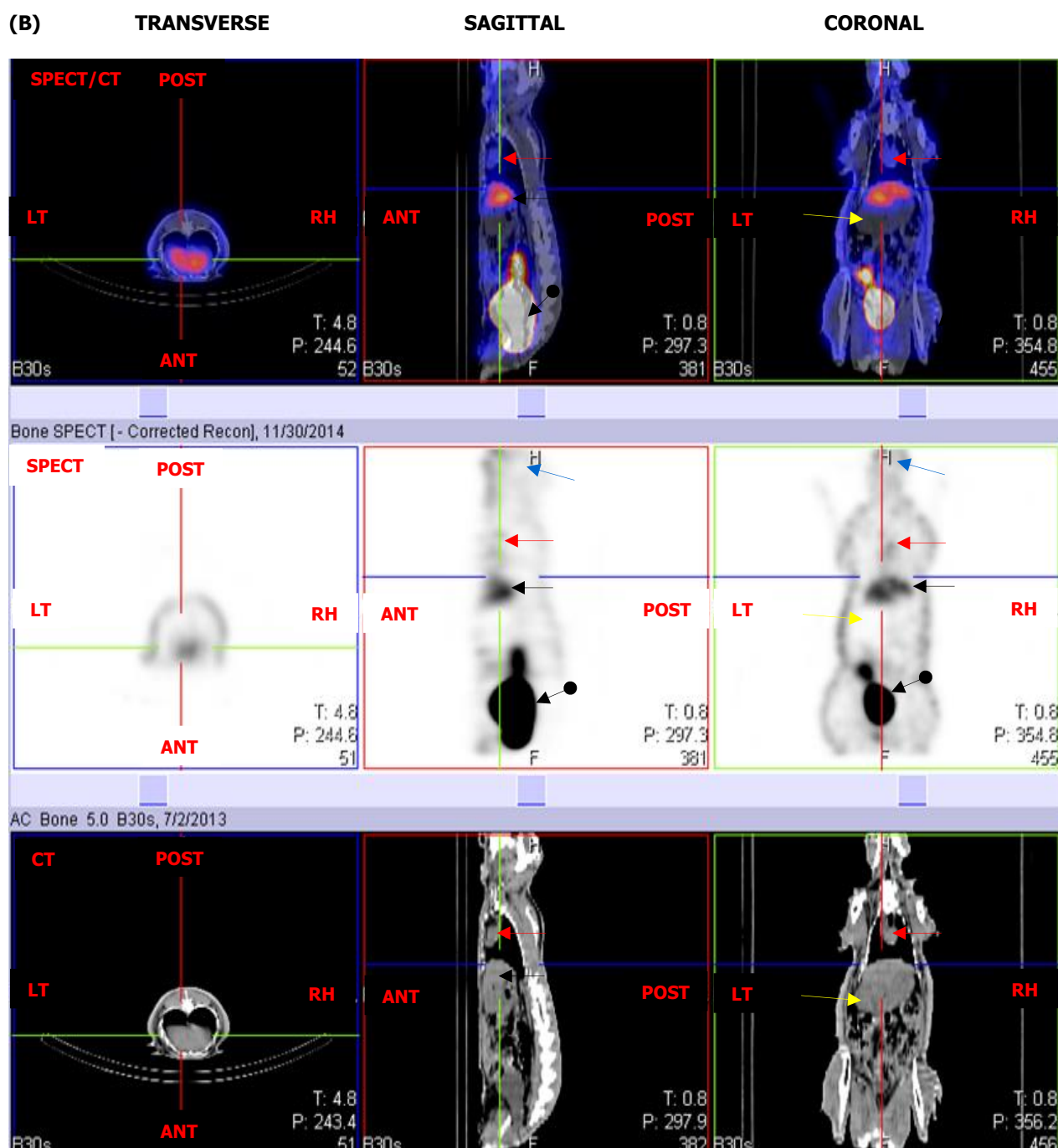


FIGURE 5.5: (B) IHP ^{99m}Tc -EC-DG fused SPECT/CT (transverse, sagittal, and coronal) images at 4 hour post radiopharmaceutical administration. Liver (solid arrow), urinary bladder (ball arrow), stomach (yellow arrow) and heart (red arrow) are well-outlined. No visible brain uptake (blue arrow).

According to the SQUAL results, background activity was mainly present in the lungs and the muscles for the different time intervals. Positive SQUAL results were obtained for the bladder, intestines, liver, kidneys and the early images of the heart. Negative SQUAL results were obtained for the stomach, spleen, thyroid, skin, brain (radioactivity present attributed to administration of IHP ^{99m}Tc -EC-DG in vein close to brain and not in brain), gallbladder, skeleton, joints and salivary glands. SQ values of 2-3 were allocated to the liver, bladder and heart, signifying that there were increased biodistribution to these organs in the healthy rabbit. A SQ value of 0 was assigned to the stomach, spleen, thyroid, muscle, brain, skin, gallbladder, skeleton, joints and salivary glands, indicating no increased biodistribution to these tissues and organs in the healthy rabbit.

5.3.2 Healthy Rabbit Model

5.3.2.1 Quantitative analysis of IHP ^{99m}Tc -EC-DG (DL) images

The activity in all organs and tissue was expressed as the percentage of the total body activity per organ and presented as the mean \pm SEM (for values obtained in $n=10$ rabbits), at 0.1-, 0.5-, 1-, 2- and 4 h post IHP ^{99m}Tc -EC-DG (DL) administration. All the data was decay corrected to the injection time of IHP ^{99m}Tc -EC-DG (DL). ROIs could not be drawn over the spleen and intestines accurately. The statistical calculation for the normal biodistribution of the IHP ^{99m}Tc -EC-DG (DL) is reported in Table 5.4. The median of the data for IHP ^{99m}Tc -EC-DG (DL) is also provided in Table 5.4. The mean is the sum of a set of data values divided by the number of data values, whereas the median is the middle value of the data set. In order to provide a complete summary of the data the median is provided and is not directly addressed in the data analysis. The organs are highlighted in different colors for the different scintigraphic imaging time intervals of IHP ^{99m}Tc -EC-DG (DL) image. The three organs with the highest biodistribution were indicated in bold and the three lowest biodistribution organs in blue. The kidneys and bladder are also highlighted (high values) but should be excluded as high uptake organs as they form part of excretion pathway of ^{99m}Tc -EC-DG.

TABLE 5.3: The SQ and SQUAL static- and SPECT/CT results of the biodistribution to the different organs/tissues of IHP ^{99m}Tc-EC-DG (DL) in healthy rabbits

Organ/ tissue	Time interval (h)	IHP ^{99m} Tc-EC-DG (DL)					
		Static			SPECT/CT		
		<i>n</i>	SQUAL	SQ	<i>n</i>	SQUAL	SQ
Lungs	0.1	10	Post	2	1	*	*
	0.5	10	Post	1		*	*
	1	10	Post	1		*	*
	2	10	Bkg	0		Bkg	0
	4	10	Bkg	0		Bkg	0
Stomach	0.1	10	Neg	0	1	*	*
	0.5	10	Neg	0		*	*
	1	10	Neg	0		*	*
	2	10	Neg	0		Neg	0
	4	10	Neg	0		Neg	0
Spleen	0.1	10	Neg	0	1	*	*
	0.5	10	Neg	0		*	*
	1	10	Neg	0		*	*
	2	10	Neg	0		Neg	0
	4	10	Neg	0		Neg	0
Kidneys	0.1	10	Post	3	1	*	*
	0.5	10	Post	3		*	*
	1	10	Post	3		*	*
	2	10	Post	3		Post	3
	4	10	Post	3		Post	3
Thyroid	0.1	10	Neg	0	1	*	*
	0.5	10	Neg	0		*	*
	1	10	Neg	0		*	*
	2	10	Neg	0		Neg	0
	4	10	Neg	0		Neg	0
Muscle	0.1	10	Bkg	0	1	*	*
	0.5	10	Bkg	0		*	*
	1	10	Bkg	0		*	*
	2	10	Bkg	0		Bkg	0
	4	10	Bkg	0		Bkg	0
Intestines	0.1	10	Neg	0	1	*	*
	0.5	10	Post	1		*	*
	1	10	Post	1		*	*
	2	10	Post	1		Post	2
	4	10	Post	1		Post	1
Brain	0.1	10	Neg	0	1	*	*
	0.5	10	Neg	0		*	*
	1	10	Neg	0		*	*
	2	10	Neg	0		Neg	0
	4	10	Neg	0		Neg	0
Bladder	0.1	10	Post	3	1	*	*
	0.5	10	Post	3		*	*
	1	10	Post	3		*	*
	2	10	Post	3		Post	3
	4	10	Post	3		Post	3
Skin	0.1	10	Neg	0	1	*	*
	0.5	10	Neg	0		*	*
	1	10	Neg	0		*	*
	2	10	Neg	0		Neg	0
	4	10	Neg	0		Neg	0
Gallbladder	0.1	10	Neg	0	1	*	*
	0.5	10	Neg	0		*	*
	1	10	Neg	0		*	*
	2	10	Neg	0		Neg	0
	4	10	Neg	0		Neg	0
Heart	0.1	10	Post	3	1	*	*
	0.5	10	Post	2		*	*
	1	10	Post	1		*	*
	2	10	Post	1		Post	1
	4	10	Post	1		Post	1
Skeleton	0.1	10	Neg	0	1	*	*
	0.5	10	Neg	0		*	*
	1	10	Neg	0		*	*
	2	10	Neg	0		Neg	0
	4	10	Neg	0		Neg	0
Joints	0.1	10	Neg	0	1	*	*
	0.5	10	Neg	0		*	*
	1	10	Neg	0		*	*
	2	10	Neg	0		Neg	0
	4	10	Neg	0		Neg	0
Salivary glands	0.1	10	Neg	0	1	*	*
	0.5	10	Neg	0		*	*
	1	10	Neg	0		*	*
	2	10	Neg	0		Neg	0
	4	10	Neg	0		Neg	0

TABLE 5.4: Biodistribution of IHP ^{99m}Tc -EC-DG (DL) in healthy rabbits ($n=10$)

Organ/Tissue	Time interval (h)	Median	Mean \pm SEM
LT Lung	0.1	1.99	2.01 \pm 0.12
	0.5	1.48	1.53 \pm 0.12
	1	1.13	1.13 \pm 0.11
	2	0.73	0.78 \pm 0.09
	4	0.37	0.38 \pm 0.04
RH Lung	0.1	2.19	2.21 \pm 0.10
	0.5	1.46	1.53 \pm 0.10
	1	1.12	1.15 \pm 0.10
	2	0.79	0.76 \pm 0.08
	4	0.33	0.37 \pm 0.04
Liver	0.1	3.95	4.05 \pm 0.22
	0.5	2.41	2.58 \pm 0.20
	1	1.92	1.92 \pm 0.14
	2	1.33	1.33 \pm 0.14
	4	0.73	0.73 \pm 0.06
Stomach	0.1	0.42	0.44 \pm 0.02
	0.5	0.40	0.42 \pm 0.04
	1	0.31	0.35 \pm 0.04
	2	0.24	0.23 \pm 0.02
	4	0.10	0.10 \pm 0.01
LT Kidney	0.1	4.28	4.53 \pm 0.24
	0.5	2.80	2.81 \pm 0.11
	1	2.36	2.44 \pm 0.10
	2	2.02	2.06 \pm 0.07
	4	1.63	1.69 \pm 0.08
RH Kidney	0.1	5.11	5.16 \pm 0.32
	0.5	3.06	3.06 \pm 0.11
	1	2.58	2.52 \pm 0.08
	2	2.13	2.14 \pm 0.10
	4	1.49	1.48 \pm 0.05
Brain	0.1	4.85	4.80 \pm 0.20
	0.5	2.94	2.97 \pm 0.26
	1	2.12	2.02 \pm 0.21
	2	1.36	1.38 \pm 0.11
	4	0.69	0.64 \pm 0.05
Heart	0.1	5.20	5.45 \pm 0.28
	0.5	3.23	3.24 \pm 0.18
	1	2.27	2.23 \pm 0.13
	2	1.59	1.51 \pm 0.09
	4	0.73	0.76 \pm 0.06
Skin	0.1	0.02	0.02 \pm 0.00
	0.5	0.03	0.03 \pm 0.00
	1	0.03	0.02 \pm 0.00
	2	0.02	0.02 \pm 0.00
	4	0.01	0.01 \pm 0.00
Muscle	0.1	0.31	0.32 \pm 0.04
	0.5	0.40	0.38 \pm 0.03
	1	0.29	0.29 \pm 0.02
	2	0.23	0.26 \pm 0.04
	4	0.12	0.13 \pm 0.02
Joint	0.1	0.26	0.29 \pm 0.02
	0.5	0.27	0.26 \pm 0.02
	1	0.20	0.22 \pm 0.02
	2	0.17	0.16 \pm 0.02
	4	0.08	0.07 \pm 0.01
Bladder	0.1	6.58	6.71 \pm 1.20
	0.5	22.82	23.58 \pm 2.58
	1	25.23	26.68 \pm 2.21
	2	34.70	34.70 \pm 1.28
	4	31.41	29.03 \pm 3.05

The three organ with the highest mean uptake values of IHP ^{99m}Tc -EC-DG were the heart (5.45 ± 0.28), liver (4.05 ± 0.22) and the brain (4.80 ± 0.20) (Table 5.4). The LT kidney (4.53 ± 0.24), RT kidney (5.16 ± 0.32) and bladder (34.70 ± 1.28) was excluded from this observation where the highest uptake was evaluated as the high uptake in the kidneys can be attributed to the excretion of the IHP ^{99m}Tc -EC-DG by the kidneys into the bladder. The heart (5.45 ± 0.28) also demonstrated high uptake results at 0.1 h imaging time interval. The stomach (0.10 ± 0.01), brain (0.64 ± 0.05) and skin (0.02 ± 0.00) demonstrated the lowest IHP ^{99m}Tc -EC-DG (DL) biodistribution in the healthy rabbits at 4 h post IHP ^{99m}Tc -EC-DG administration.

Analysis of the results primarily indicated that the biodistribution in the healthy rabbits administered with IHP ^{99m}Tc -EC-DG, for all the time intervals was the highest to the kidneys (excretion into the bladder), liver and to the heart (Table 5.4). The high activity in the region of the brain area can be attributed to the IHP ^{99m}Tc -EC-DG injection by using the ear vein, the ear veins into which the radioactivity was administered runs close to the brain. The IHP ^{99m}Tc -EC-DG activity due to the injection only starts at 1 h post RP administration. The phenomena of the slow clearance of the IHP ^{99m}Tc -EC-DG from the injection site close to the brain could also have influenced the % uptake in the brain as the counts obtained from the ROI drawn on the brain was higher. The IHP ^{99m}Tc -EC-DG activity present due to the slow clearance of activity in the ear vein cleared by 2 h and 4 h post administration. The results of the 2 h and 4 h time points would therefore give a more accurate interpretation of what the brain uptake % of ^{99m}Tc -EC-DG in rabbits are. The high IHP ^{99m}Tc -EC-DG uptake in the kidneys was expected because the EC and EC-conjugates interact with renal tubules in the kidney (Zhang *et al.* 2012:6). The maximum uptake to the heart is probably due to glucose uptake by the myocytes. IHP ^{99m}Tc -EC-DG was mostly excreted before 0.5 h via the kidneys to the bladder (Figure 5.8), and explains the increase of uptake in the bladder to 2 h followed by a decrease as the bladder is emptied.

Liver uptake cleared slowly over the time points on which images were obtained (Figure 5.6). The brain (at 4 h) (Figure 5.7), skin and stomach had the lowest IHP ^{99m}Tc -EC-DG (DL) biodistribution and a constant decrease was seen in the brain and from 0.1 to 4 h (Figure 5.7). A minimal, slow decrease was seen in

the skin and stomach (Figure 5.7). As previously mentioned the high % brain uptake calculated before 2 h can be attributed to the slow clearance of the IHP ^{99m}Tc -EC-DG from the veins close to the brain after RP administration into the ear. The low brain uptake of IHP ^{99m}Tc -EC-DG at 2- and 4 h can be attributed to its hydrophilic characteristic of IHP ^{99m}Tc -EC-DG that prevents it to cross the blood-brain barrier (Schechter *et al.* 2009:1590), as well as relatively larger molecular weight/size.

The SPECT/CT and static images, SQ, SQUAL and quantitative results confirmed that the highest uptake of IHP ^{99m}Tc -EC-DG (DL) in the healthy rabbits was to the liver and that excretion was from the kidneys into the urinary tract. Early uptake to the heart was confirmed with all the results evaluation techniques. The lowest biodistribution was found in the brain, stomach and skin.

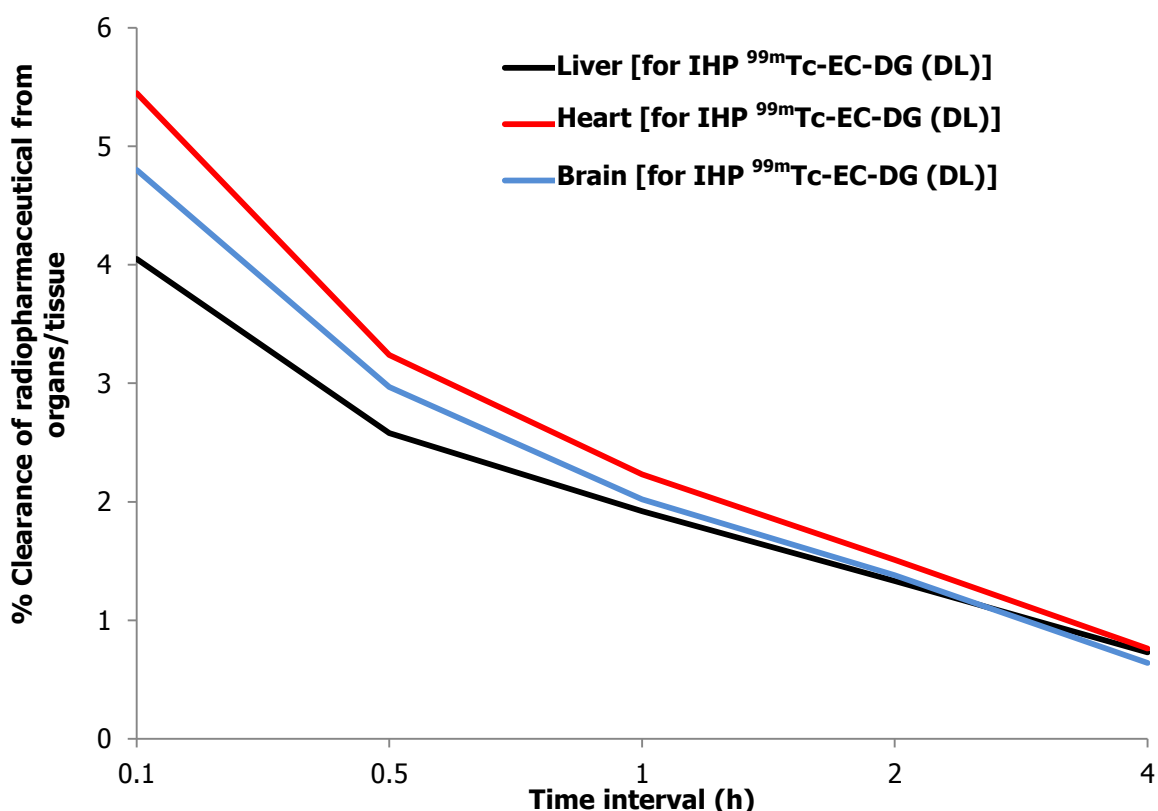


FIGURE 5.6: Clearance profile of organs that showed the highest IHP ^{99m}Tc -EC-DG (DL) uptake in healthy rabbits

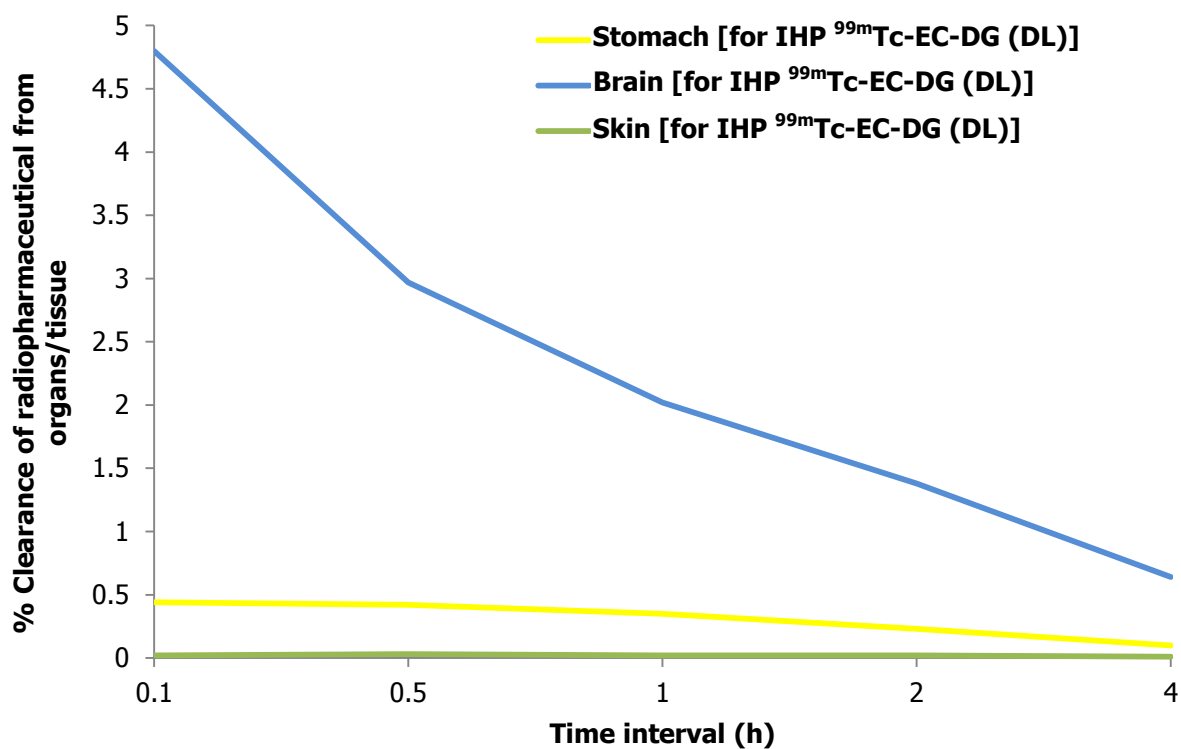


FIGURE 5.7: Clearance profile of organs that showed the lowest IHP ^{99m}Tc -EC-DG (DL) uptake in healthy rabbits

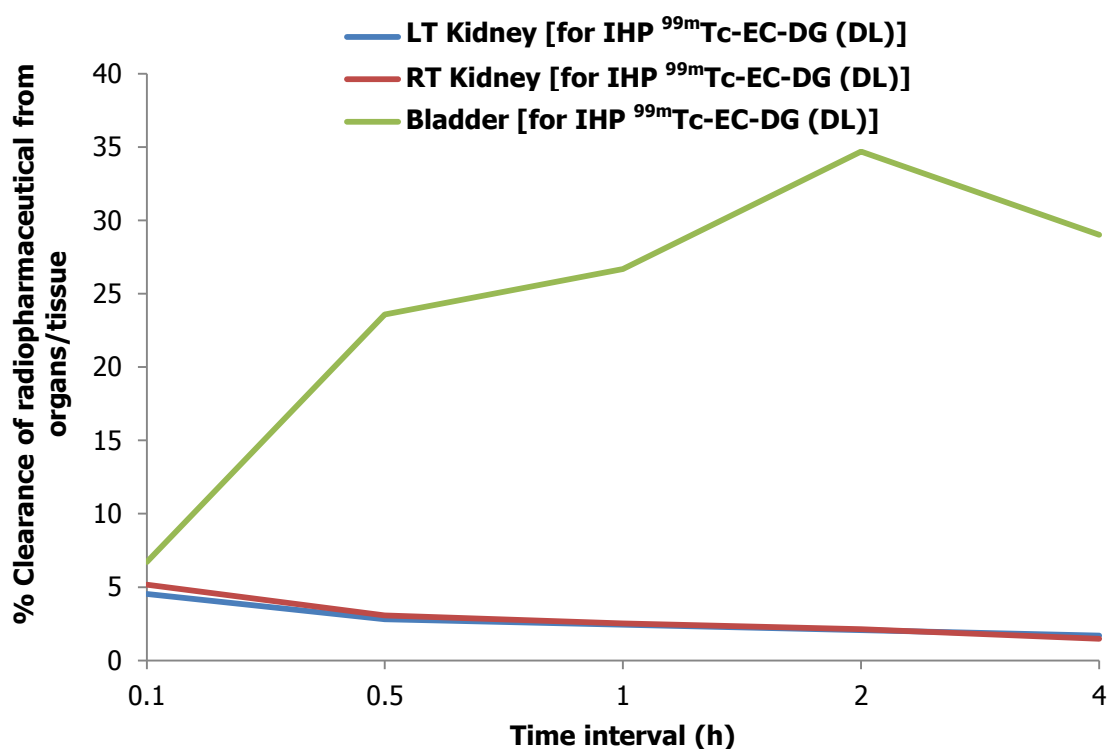


FIGURE 5.8: Clearance profile of IHP ^{99m}Tc -EC-DG excretion by kidneys into the bladder for healthy rabbits

5.3.2.2 Comparison of IHP $^{99m}\text{Tc-EC-DG (DL)}$ with $^{99m}\text{TcO}_4^-$

The results of the healthy rabbits ($n=10$) administered with IHP $^{99m}\text{Tc-EC-DG}$ (discussed in previous section) were compared to the results of rabbits ($n=5$) administered with $^{99m}\text{TcO}_4^-$. The rabbits used for these two experiments were non-fasting. The static and SPECT/CT images, statistical results, SQ and SQUAL analysis for IHP $^{99m}\text{Tc-EC-DG}$ and $^{99m}\text{TcO}_4^-$ were compared.

5.3.2.2.1 *In vivo normal biodistribution images*

Figure 5.9 and Figure 5.10 show the comparison of the ANT and POST scintigraphic images of the biodistribution of IHP $^{99m}\text{Tc-EC-DG}$ (DL) and $^{99m}\text{TcO}_4^-$ in healthy rabbits at 0.1-, 0.5-, 1-, 2- and 4 h post radiopharmaceutical administration. The bladder uptake was detected already at the 0.1 h static and SPECT images for IHP $^{99m}\text{Tc-EC-DG}$ and $^{99m}\text{TcO}_4^-$ (Figure 5.9, -5.10 and -5.11). $^{99m}\text{TcO}_4^-$ uptake to the bladder increased over time, with a slower excretion via the kidneys than IHP $^{99m}\text{Tc-EC-DG}$. Well-defined increased kidney uptake of $^{99m}\text{TcO}_4^-$ was observed from 0.1 h static images, decreasing dramatically thereafter with only mild increased radionuclide uptake on the later scintigraphic images. Low uptake is seen in the area of the intestines from 1 h to the 4 h imaging time interval. The static images demonstrated no uptake of $^{99m}\text{TcO}_4^-$ and IHP $^{99m}\text{Tc-EC-DG}$ to the skeleton. A slight increase uptake of $^{99m}\text{TcO}_4^-$ was seen in the region of the lungs on the 0.1 h static images due to normal blood pool activity, which decreased dramatically towards the 4 h static image to only background activity. No biodistribution of $^{99m}\text{TcO}_4^-$ was observed to the brain on all the imaging time intervals. Triangular shaped area of increased $^{99m}\text{TcO}_4^-$ uptake was observed in the region of the salivary glands on the 1-, 2- and 4 h static images and this was not seen on the IHP $^{99m}\text{Tc-EC-DG}$ images of the healthy rabbits (Figure 5.9 and Figure 5.10). Faint circular uptake of $^{99m}\text{TcO}_4^-$ is noted lower down in the neck area in the region of the thyroid and is well-defined on the 0.1-4 h ANT static images. This thyroid uptake was not observed on the IHP $^{99m}\text{Tc-EC-DG}$ static images.

Intense increased cardiac activity of $^{99m}\text{TcO}_4^-$ was noted in the region of the heart on the 0.1- and 0.5 h static images, due to blood pool activity which decreased with time to only background activity noted at the 4 h time interval. Intense increased blood pool activity of $^{99m}\text{TcO}_4^-$ was seen in the liver on the 0.1- and 0.5 h static views (Figure 5.9 and Figure 5.10).

The activity in the liver decreased mildly at the 4 h time imaging interval, but still demonstrated well-defined uptake relative to the background activity. The liver uptake of $^{99m}\text{TcO}_4^-$ is visually double that of the IHP $^{99m}\text{Tc-EC-DG}$ (DL) in healthy rabbits. The immediate 0.1 h static images demonstrated increased $^{99m}\text{TcO}_4^-$ uptake in the region of the spleen, which cleared completely at the 0.5 h image. $^{99m}\text{TcO}_4^-$ uptake was not observed in the stomach, gallbladder, muscles and joint area. IHP $^{99m}\text{Tc-EC-DG}$ (DL) also showed no stomach uptake (Figure 5.9 and Figure 5.10).

A SPECT/CT was performed for $^{99m}\text{TcO}_4^-$ at 1 h post administration (Figure 5.11A) to demonstrate early imaging or visibility of the thyroid. In Figure 5.11 (B-E) the SPECT/CT (transverse, sagittal and coronal) images of IHP $^{99m}\text{Tc-EC-DG}$ and $^{99m}\text{TcO}_4^-$ are compared at 2- and 4 h post administration. Thyroid uptake of $^{99m}\text{TcO}_4^-$ could be observed on all three SPECT/CT studies acquired at 1-, 2- and 4 h and increased over time. The skin, skeleton, joints, muscles, spleen and brain on the SPECT/CT images of $^{99m}\text{TcO}_4^-$ for the different time intervals demonstrated no uptake (Figure 5.11). Uptake of $^{99m}\text{TcO}_4^-$ in the region of the intestines could be observed from the 1 h SPECT/CT imaging time interval increasing to the 4 h above *in vivo* background activity. All three SPECT/CT studies of $^{99m}\text{TcO}_4^-$ acquired at the different time intervals, demonstrate well-defined uptake in the salivary glands. The SPECT/CT images of the $^{99m}\text{TcO}_4^-$ in the healthy rabbits demonstrate better delineation of the cardiac activity on the 1-, 2- and the 4 h SPECT/CT views than the static views due to the improved contrast obtained with SPECT images. Increased $^{99m}\text{TcO}_4^-$ uptake was seen in the region of the kidney areas.

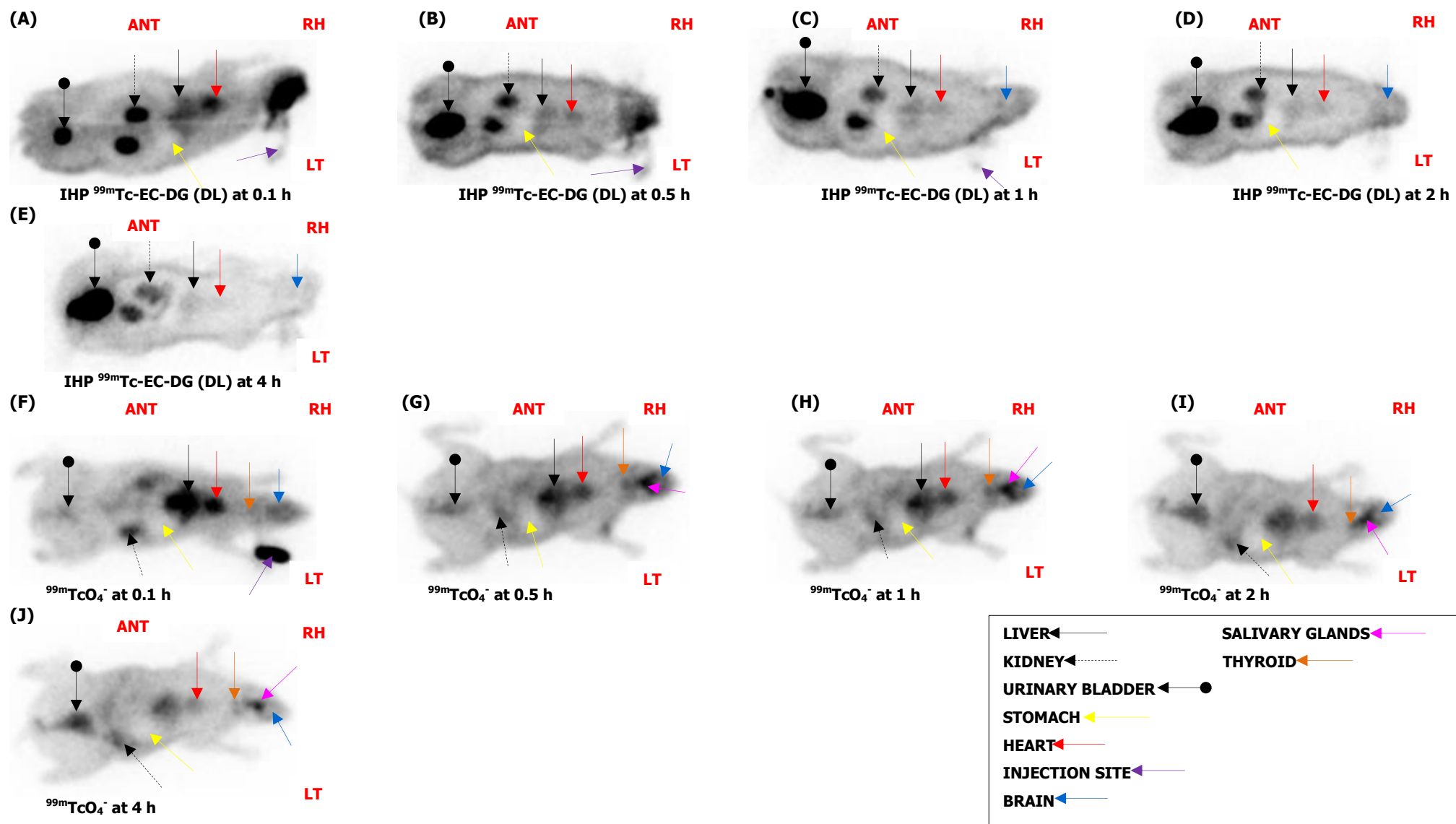


FIGURE 5.9: ANT biodistribution images of IHP ^{99m}Tc -EC-DG (A-E) and $^{99m}\text{TcO}_4^-$ (F-J) in healthy rabbits at (A & F) 0.1-, (B & G) 0.5-, (C & H) 1-, (D & I) 2- and (E & J) 4 hour post administration. Liver (solid arrow), kidney (dashed arrow), urinary bladder (ball arrow), stomach (yellow arrow), salivary glands (pink arrow), thyroid (orange) and heart (red arrow) are well-outlined. The injection site (purple arrow) is also visible and no brain uptake (blue arrow).

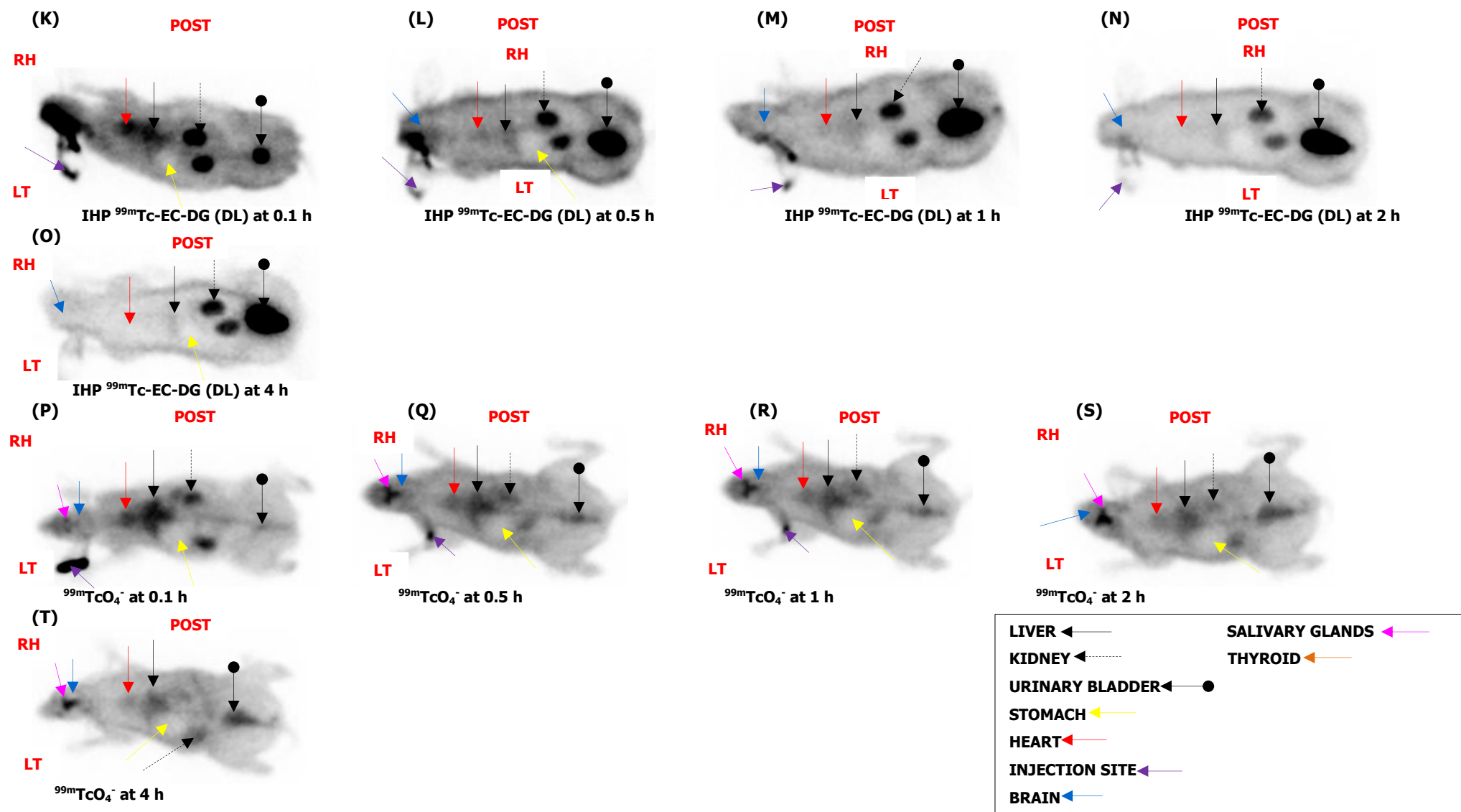


FIGURE 5.10: POST biodistribution images of IHP ^{99m}Tc -EC-DG (K-O) and $^{99m}\text{TcO}_4^-$ (P-T) in healthy rabbits at (K & P) 0.1-, (L & Q) 0.5-, (M & R) 1-, (N & S) 2- and (O & T) 4 hour administration. Liver (solid arrow), kidney (dashed arrow), urinary bladder (ball arrow), stomach (yellow arrow), salivary glands (pink arrow) and heart (red arrow) are well-outlined. The injection site (purple arrow) is also visible and no brain uptake (blue arrow).

The SPECT/CT and static images confirmed similar increased uptake of $^{99m}\text{TcO}_4^-$ and IHP $^{99m}\text{Tc-EC-DG}$ (DL) to the kidneys with excretion to the bladder, liver ($^{99m}\text{TcO}_4^-$ higher uptake) and early cardiac blood pool activity. No uptake was present on the SPECT/CT images of $^{99m}\text{TcO}_4^-$ and IHP $^{99m}\text{Tc-EC-DG}$ (DL) to the brain, muscle, joints, spleen and stomach in the healthy rabbits. Although a high liver uptake and delayed intestinal activity after administration with $^{99m}\text{TcO}_4^-$ and IHP $^{99m}\text{Tc-EC-DG}$ (DL) were found, the gallbladder could not be clearly visualised to confirm biliary excretion into the intestines. The high uptake to thyroid and salivary glands of the $^{99m}\text{TcO}_4^-$, was absent with IHP $^{99m}\text{Tc-EC-DG}$ (DL).

5.3.2.2.2 *SQ and SQUAL analysis*

The SQ and SQUAL biodistribution results of the IHP $^{99m}\text{Tc-EC-DG}$ (DL) and $^{99m}\text{TcO}_4^-$ was compared for the different organs in healthy rabbits in Table 5.5. According to the SQUAL results, background activity was mainly present in the muscles and lungs for the $^{99m}\text{TcO}_4^-$ and IHP $^{99m}\text{Tc-EC-DG}$ (DL). Positive SQUAL results were reported for the bladder, intestines, liver, kidneys and the early images of the cardiac $^{99m}\text{TcO}_4^-$. Similar SQUAL results were observed for the IHP $^{99m}\text{Tc-EC-DG}$ (DL) in these organs. Negative *in vivo* biodistribution was reported on to the stomach and brain for $^{99m}\text{TcO}_4^-$ and IHP $^{99m}\text{Tc-EC-DG}$ (DL). Positive *in vivo* activity was reported to the salivary glands and thyroid for the static and SPECT/CT images of the $^{99m}\text{TcO}_4^-$, but negative for the IHP $^{99m}\text{Tc-EC-DG}$ (DL). The SQ values for $^{99m}\text{TcO}_4^-$ between 2 and 3 were allocated to the liver, salivary glands, thyroid, heart, kidneys and bladder. A zero SQ value was assigned to the stomach, spleen, brain, skin, skeleton, gallbladder and muscles for the $^{99m}\text{TcO}_4^-$ biodistribution. Similarly, a zero SQ value was allocated to the stomach, spleen, brain (uptake due to slow clearance of radiopharmaceutical in veins close to the brain), skeleton and skin for the IHP $^{99m}\text{Tc-EC-DG}$ (DL) organ/tissue biodistribution. The conclusion may be made that the SQ and SQUAL is strongly influenced by visual interpretation due to poor contrast if a high activity organ (for example the thyroid) is in the close-by area.

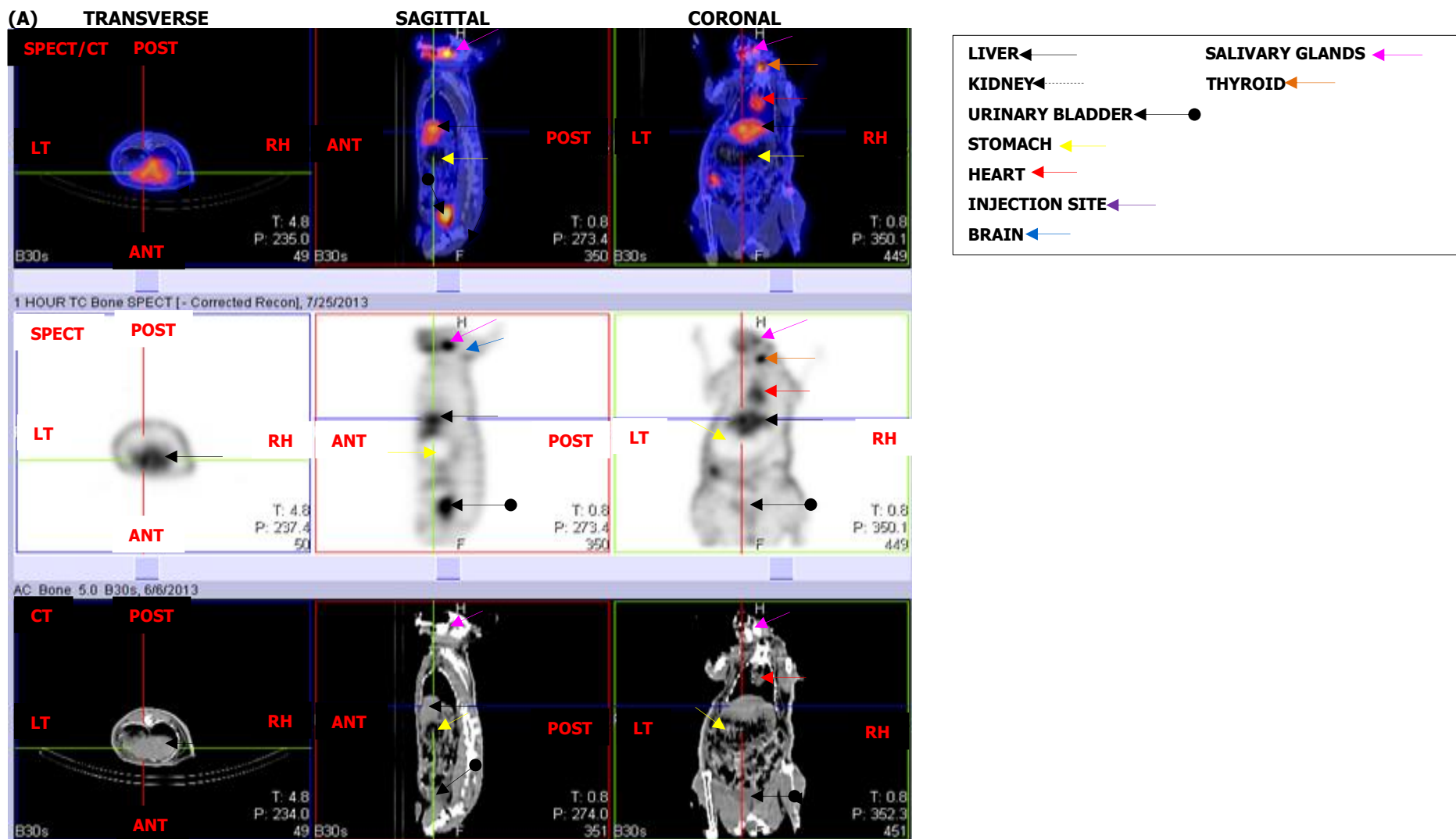


FIGURE 5.11: (A) $^{99m}\text{TcO}_4^-$ fused SPECT/CT (transverse, sagittal and coronal) images at 1 hour post radiopharmaceutical administration. Liver (solid arrow), urinary bladder (ball arrow), stomach (yellow arrow), salivary glands (pink arrow), thyroid (orange) and heart (red arrow) are well outlined. The injection site (purple arrow) is also visible with no brain uptake (blue arrow).

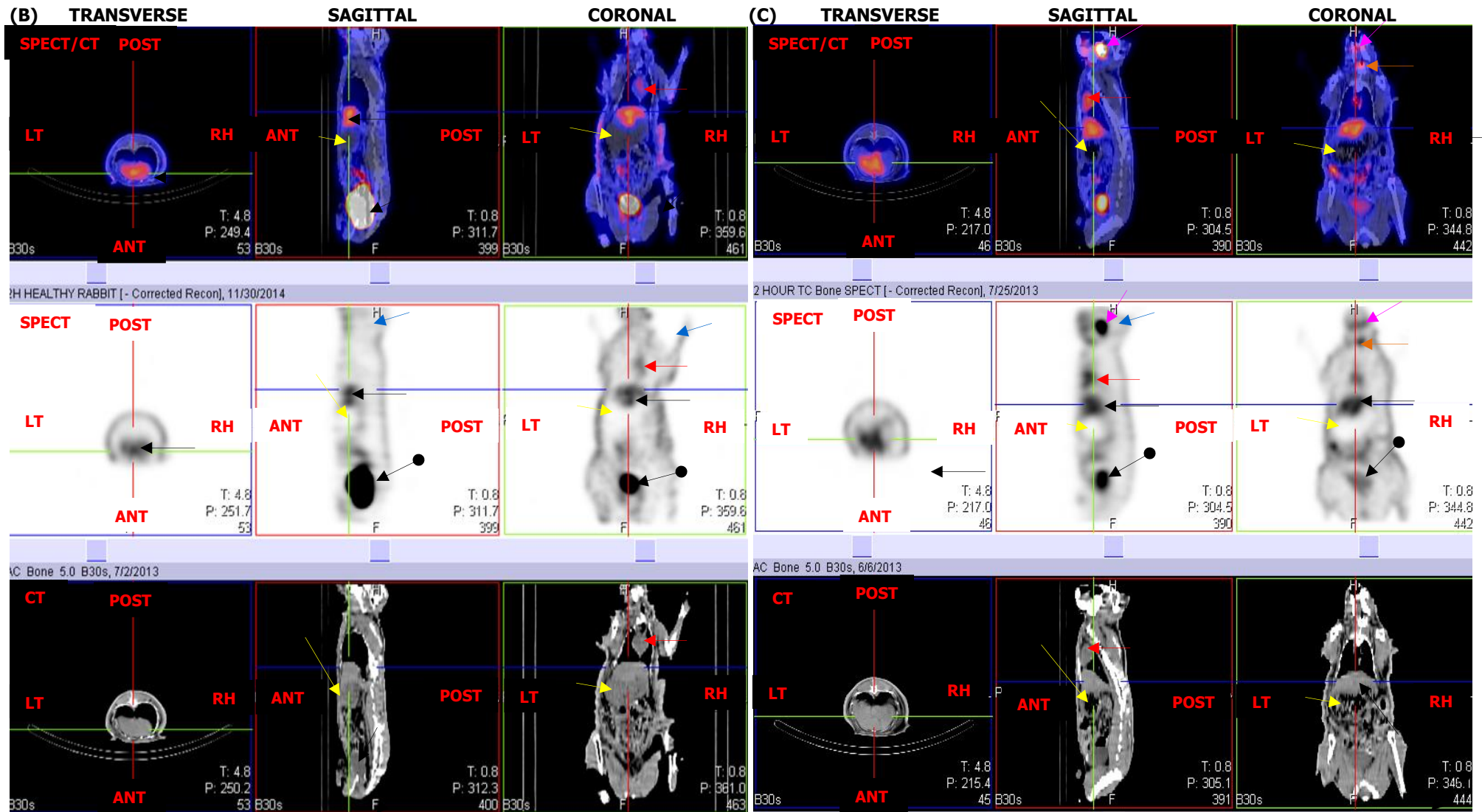


FIGURE 5.11: (B) IHP ^{99m}Tc -EC-DG fused SPECT/CT (transverse, sagittal and coronal) and (C) $^{99m}\text{TcO}_4^-$ images at 2 hour post radiopharmaceutical administration. Liver (solid arrow), urinary bladder (ball arrow), stomach (yellow arrow), salivary glands (pink arrow), thyroid (orange) and heart (red arrow) are well outlined. The injection site (purple arrow) is also visible and no brain uptake (blue arrow).

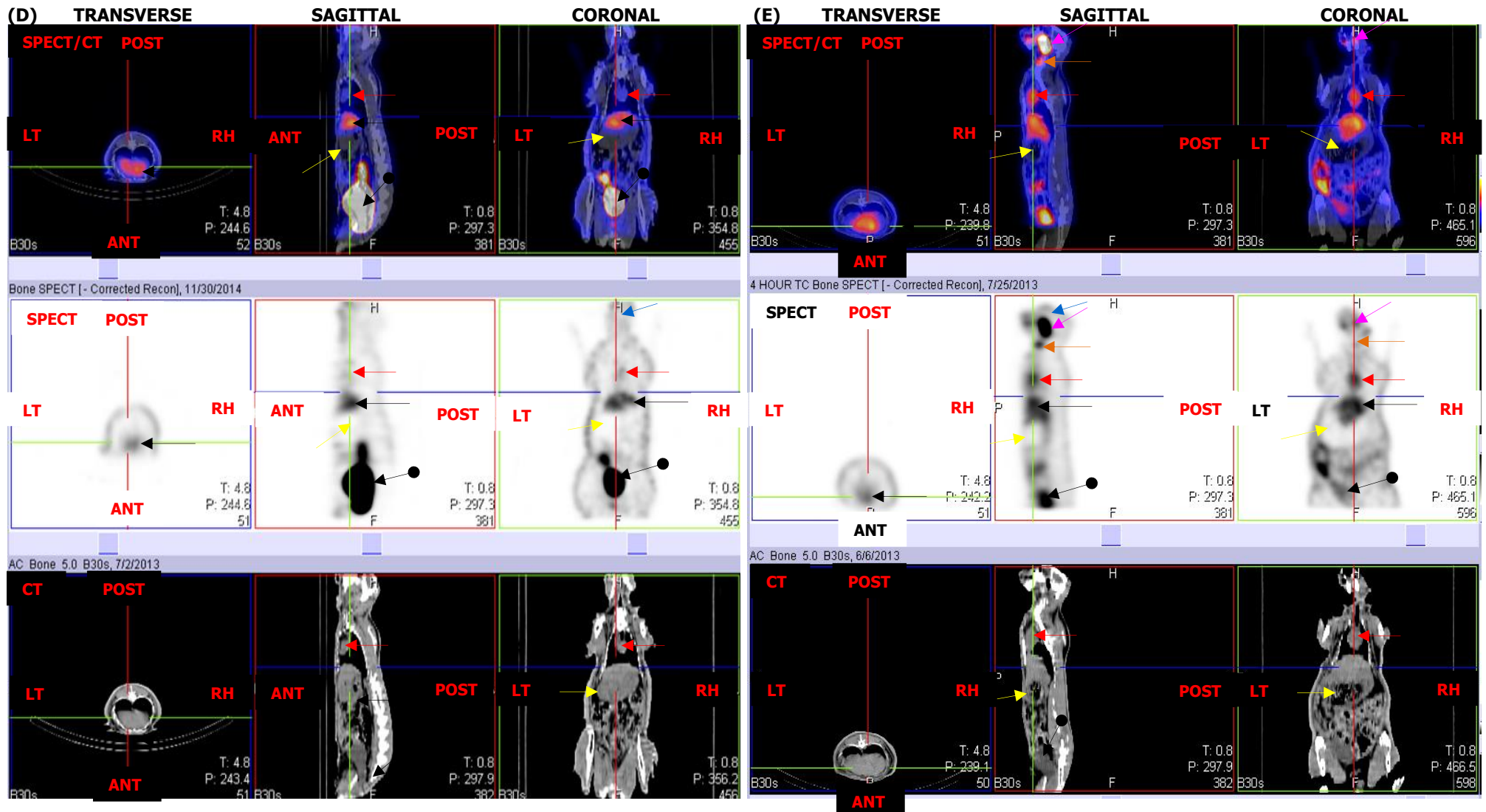


FIGURE 5.11: (D) IHP ^{99m}Tc -EC-DG fused SPECT/CT (transverse, sagittal and coronal) and (E) $^{99m}\text{TcO}_4^-$ images at 4 hour post radiopharmaceutical administration. Liver (solid arrow), urinary bladder (ball arrow), stomach (yellow arrow), salivary glands (pink arrow), thyroid (orange) and heart (red arrow) are well outlined. The injection site (purple arrow) is also visible and no brain uptake (blue arrow).

5.3.2.2.3 Comparison of the quantitative analysis

In Table 5.6 the IHP $^{99m}\text{Tc-EC-DG}$ (DL) biodistribution results were compared with $^{99m}\text{TcO}_4^-$ for different organs/tissues of healthy rabbits. The activity in all organs and tissue samples was expressed as the percentage of the total body activity per organ and presented as the mean \pm SEM, at 0.1-, 0.5-, 1-, 2- and 4 h post radiopharmaceutical administration. Statistical calculations of the median were also included in Table 5.6. The highest mean values for IHP $^{99m}\text{Tc-EC-DG}$ and $^{99m}\text{TcO}_4^-$ for each organ for all the time intervals is highlighted in bold and the lowest in blue. Table 5.6 also indicates the P value when comparing the IHP $^{99m}\text{Tc-EC-DG}$ (KF) with $^{99m}\text{TcO}_4^-$ distribution. A P value <0.05 was considered statistically significant (highlighted in red).

The mean uptake values of IHP $^{99m}\text{Tc-EC-DG}$ and $^{99m}\text{TcO}_4^-$ were the highest to the liver, LT kidney, RT kidney and bladder for the different imaging time intervals in the healthy rabbits (Table 5.6). The heart also demonstrated high increased uptake at 0.1 h. The % uptake in the brain of the rabbits administered with IHP $^{99m}\text{Tc-EC-DG}$ was high before 1 h after administration and was attributed to the slow clearance of RP from the veins after administration. The stomach, skeleton, joints, brain (at 4 h) and skin demonstrated the lowest IHP $^{99m}\text{Tc-EC-DG}$ (DL) and $^{99m}\text{TcO}_4^-$ uptake in the healthy rabbits for the different time intervals (Table 5.6).

TABLE 5.5: Comparison of the SQ and SQUAL static and SPECT/CT results of the biodistribution to the lungs of IHP $^{99m}\text{Tc-EC-DG}$ (DL) and $^{99m}\text{TcO}_4^-$ in healthy rabbits

Organ/ tissue	Time interval (h)	IHP $^{99m}\text{Tc-EC-DG}$ (DL)						$^{99m}\text{TcO}_4^-$					
		Static			SPECT/CT			Static			SPECT/CT		
		<i>n</i>	SQUAL	SQ	<i>n</i>	SQUAL	SQ	<i>n</i>	SQUAL	SQ	<i>n</i>	SQUAL	SQ
Lungs	0.1	10	Post	2	*	*	*	5	Bkg	1	*	*	*
	0.5	10	Post	1	*	*	*	5	Bkg	0	*	*	*
	1	10	Post	1	*	*	*	5	Bkg	0	*	*	*
	2	10	Bkg	0	1	Bkg	0	5	Bkg	0	1	Bkg	0
	4	10	Bkg	0	1	Bkg	0	5	Bkg	0	1	Bkg	0
Liver	0.1	10	Post	3	*	*	*	5	Post	3	*	*	*
	0.5	10	Post	2	*	*	*	5	Post	3	*	*	*
	1	10	Post	1	*	*	*	5	Post	2	*	*	*
	2	10	Post	1	1	Post	2	5	Post	2	1	Post	2
	4	10	Bkg	0	1	Post	2	5	Post	1	1	Bkg	0
Stomach	0.1	10	Neg	0	*	*	*	5	Neg	0	*	*	*
	0.5	10	Neg	0	*	*	*	5	Neg	0	*	*	*
	1	10	Neg	0	*	*	*	5	Neg	0	*	*	*
	2	10	Neg	0	1	Neg	0	5	Neg	0	1	Neg	0
	4	10	Neg	0	1	Neg	0	5	Neg	0	1	Neg	0
Spleen	0.1	10	Neg	0	*	*	*	5	Post	2	*	*	*
	0.5	10	Neg	0	*	*	*	5	Neg	0	*	*	*
	1	10	Neg	0	*	*	*	5	Neg	0	*	*	*
	2	10	Neg	0	1	Neg	0	5	Neg	0	1	Neg	0
	4	10	Neg	0	1	Neg	0	5	Neg	0	1	Neg	0
Kidneys	0.1	10	Post	3	*	*	*	5	Post	3	*	*	*
	0.5	10	Post	3	*	*	*	5	Post	2	*	*	*
	1	10	Post	3	*	*	*	5	Post	2	*	*	*
	2	10	Post	3	1	Post	3	5	Post	2	1	Post	2
	4	10	Post	3	1	Post	3	5	Post	2	1	Post	2
Thyroid	0.1	10	Neg	0	*	*	*	5	Post	1	*	*	*
	0.5	10	Neg	0	*	*	*	5	Post	3	*	*	*
	1	10	Neg	0	*	*	*	5	Post	3	*	*	*
	2	10	Neg	0	1	Neg	0	5	Post	3	1	Post	3
	4	10	Neg	0	1	Neg	0	5	Post	3	1	Post	3
Muscle	0.1	10	Bkg	0	*	*	*	5	Neg	0	*	*	*
	0.5	10	Bkg	0	*	*	*	5	Neg	0	*	*	*
	1	10	Bkg	0	*	*	*	5	Neg	0	*	*	*
	2	10	Bkg	0	1	Bkg	0	5	Neg	0	1	Neg	0
	4	10	Bkg	0	1	Bkg	0	5	Neg	0	1	Neg	0
Intestines	0.1	10	Neg	1	*	*	*	5	Post	1	*	*	*
	0.5	10	Post	1	*	*	*	5	Post	1	*	*	*
	1	10	Post	1	*	*	*	5	Post	1	*	*	*
	2	10	Post	1	1	Post	2	5	Post	1	1	Post	2
	4	10	Post	1	1	Post	2	5	Post	1	1	Post	1
Brain	0.1	10	Neg	0	*	*	*	5	Post	1	*	*	*
	0.5	10	Neg	0	*	*	*	5	Bkg	1	*	*	*
	1	10	Neg	0	*	*	*	5	Bkg	1	*	*	*
	2	10	Neg	0	1	Neg	0	5	Neg	0	1	Neg	0
	4	10	Neg	0	1	Neg	0	5	Neg	0	1	Neg	0
Bladder	0.1	10	Post	3	*	*	*	5	Post	2	*	*	*
	0.5	10	Post	3	*	*	*	5	Post	2	*	*	*
	1	10	Post	3	*	*	*	5	Post	3	*	*	*
	2	10	Post	3	1	Post	3	5	Post	3	1	Post	3
	4	10	Post	3	1	Post	3	5	Post	3	1	Post	3
Skin	0.1	10	Neg	0	*	*	*	5	Negative	0	*	*	*
	0.5	10	Neg	0	*	*	*	5	Neg	0	*	*	*
	1	10	Neg	0	*	*	*	5	Neg	0	*	*	*
	2	10	Neg	0	1	Neg	0	5	Neg	0	1	Neg	0
	4	10	Neg	0	1	Neg	0	5	Neg	0	1	Neg	0
Gallbladder	0.1	10	Neg	0	*	*	*	5	Neg	0	*	*	*
	0.5	10	Neg	0	*	*	*	5	Neg	0	*	*	*
	1	10	Neg	0	*	*	*	5	Neg	0	*	*	*
	2	10	Neg	0	1	Neg	0	5	Neg	0	1	Neg	0
	4	10	Neg	0	1	Neg	0	5	Neg	0	1	Neg	0
Heart	0.1	10	Post	3	*	*	*	5	Post	3	*	*	*
	0.5	10	Post	2	*	*	*	5	Post	3	*	*	*
	1	10	Post	1	*	*	*	5	Post	3	*	*	*
	2	10	Post	1	1	Post	1	5	Post	2	1	Post	2
	4	10	Post	1	1	Post	1	5	Post	2	1	Post	2
Skeleton	0.1	10	Neg	0	*	*	*	5	Neg	0	*	*	*
	0.5	10	Neg	0	*	*	*	5	Neg	0	*	*	*
	1	10	Neg	0	*	*	*	5	Neg	0	*	*	*
	2	10	Neg	0	1	Neg	0	5	Neg	0	1	Neg	0
	4	10	Neg	0	1	Neg	0	5	Neg	0	1	Neg	0
Joints	0.1	10	Bkg	1	*	*	*	5	Bkg	1	*	*	*
	0.5	10	Bkg	1	*	*	*	5	Bkg	1	*	*	*
	1	10	Bkg	1	*	*	*	5	Bkg	1	*	*	*
	2	10	Bkg	1	1	Bkg	1	5	Bkg	1	1	Bkg	1
	4	10	Bkg	1	1	Bkg	1	5	Bkg	1	1	Bkg	1
Salivary glands	0.1	10	Neg	0		*	*	5	Post	1		*	*
	0.5	10	Neg	0		*	*	5	Post	2		*	*
	1	10	Neg	0		*	*	5	Post	2		*	*
	2	10	Neg	0	1	Neg	0	5	Post	2	1	Post	2
	4	10	Neg	0	1	Neg	0	5	Post	2	1	Post	2

TABLE 5.6: Comparison of the biodistribution results of $^{99m}\text{TcO}_4^-$ and IHP $^{99m}\text{Tc-EC-DG}$ in healthy New Zealand White Rabbits at 0.1-, 0.5-, 1-, 2- and 4 hour post radiopharmaceutical administration

Organ/Tissue	Time interval (h)	Median		Mean \pm SEM		P-value
		IHP $^{99m}\text{Tc-EC-DG}$ (DL)	$^{99m}\text{TcO}_4^-$	IHP $^{99m}\text{Tc-EC-DG}$ (DL)	$^{99m}\text{TcO}_4^-$	
LT Lung	0.1	1.99	2.08	2.01 ± 0.12	1.88 ± 0.25	0.624
	0.5	1.48	1.76	1.53 ± 0.12	1.84 ± 0.15	0.142
	1	1.13	1.81	1.13 ± 0.11	1.79 ± 0.10	0.005
	2	0.73	1.47	0.78 ± 0.09	1.67 ± 0.23	0.002
	4	0.37	1.00	0.38 ± 0.04	0.98 ± 0.06	0.002
RH Lung	0.1	2.19	2.12	2.21 ± 0.10	1.86 ± 0.25	0.327
	0.5	1.46	2.16	1.53 ± 0.10	2.20 ± 0.15	0.007
	1	1.12	2.03	1.15 ± 0.10	2.05 ± 0.08	0.002
	2	0.79	1.61	0.76 ± 0.08	1.71 ± 0.17	0.002
	4	0.33	1.38	0.37 ± 0.04	1.34 ± 0.04	0.002
Liver	0.1	3.95	8.21	4.05 ± 0.22	8.85 ± 0.48	0.002
	0.5	2.41	7.39	2.58 ± 0.20	7.36 ± 0.36	0.002
	1	1.92	6.37	1.92 ± 0.14	6.55 ± 0.36	0.002
	2	1.33	6.37	1.33 ± 0.14	6.17 ± 0.29	0.002
	4	0.73	4.18	0.73 ± 0.06	4.25 ± 0.29	0.002
Stomach	0.1	0.42	1.55	0.44 ± 0.02	1.59 ± 0.07	0.002
	0.5	0.40	1.76	0.42 ± 0.04	1.78 ± 0.10	0.002
	1	0.31	1.78	0.35 ± 0.04	1.77 ± 0.07	0.002
	2	0.24	1.57	0.23 ± 0.02	1.54 ± 0.06	0.002
	4	0.10	1.29	0.10 ± 0.01	1.26 ± 0.09	0.002
LT Kidney	0.1	4.28	2.90	4.53 ± 0.24	2.91 ± 0.20	0.002
	0.5	2.80	2.76	2.81 ± 0.11	2.81 ± 0.08	0.624
	1	2.36	2.79	2.44 ± 0.10	2.78 ± 0.06	0.027
	2	2.02	2.65	2.06 ± 0.07	2.64 ± 0.03	0.002
	4	1.63	2.32	1.69 ± 0.08	2.30 ± 0.12	0.007
RH Kidney	0.1	5.11	3.16	5.16 ± 0.32	3.03 ± 0.22	0.002
	0.5	3.06	2.79	3.06 ± 0.11	2.78 ± 0.11	0.178
	1	2.58	2.65	2.52 ± 0.08	2.64 ± 0.05	0.462
	2	2.13	2.43	2.14 ± 0.10	2.43 ± 0.06	0.037
	4	1.49	2.02	1.48 ± 0.05	1.98 ± 0.08	0.003
Brain	0.1	4.85	1.51	4.80 ± 0.20	1.59 ± 0.17	0.002
	0.5	2.94	1.74	2.97 ± 0.26	1.65 ± 0.15	0.002
	1	2.12	1.25	2.02 ± 0.21	1.36 ± 0.13	0.037
	2	1.36	1.19	1.38 ± 0.11	1.51 ± 0.52	0.624
	4	0.69	0.82	0.64 ± 0.05	0.78 ± 0.05	0.066
Heart	0.1	5.20	4.01	5.45 ± 0.28	3.79 ± 0.26	0.002
	0.5	3.23	3.32	3.24 ± 0.18	3.21 ± 0.13	0.713
	1	2.27	2.82	2.23 ± 0.13	2.81 ± 0.09	0.020
	2	1.59	2.43	1.51 ± 0.09	2.48 ± 0.11	0.002
	4	0.73	1.81	0.76 ± 0.06	1.75 ± 0.07	0.002
Skin	0.1	0.02	0.04	0.02 ± 0.00	0.08 ± 0.03	0.014
	0.5	0.03	0.11	0.03 ± 0.00	0.15 ± 0.04	0.002
	1	0.03	0.12	0.02 ± 0.00	0.13 ± 0.02	0.002
	2	0.02	0.11	0.02 ± 0.00	0.11 ± 0.01	0.002
	4	0.01	0.07	0.01 ± 0.00	0.07 ± 0.01	0.002
Muscle	0.1	0.31	0.26	0.32 ± 0.04	0.26 ± 0.02	0.270
	0.5	0.40	0.32	0.38 ± 0.03	0.33 ± 0.03	0.221
	1	0.29	0.34	0.29 ± 0.02	0.34 ± 0.03	0.142
	2	0.23	0.31	0.26 ± 0.04	0.33 ± 0.03	0.142
	4	0.12	0.21	0.13 ± 0.02	0.24 ± 0.03	0.007
Joint	0.1	0.26	0.36	0.29 ± 0.02	0.36 ± 0.04	0.086
	0.5	0.27	0.48	0.26 ± 0.02	0.48 ± 0.03	0.002
	1	0.20	0.40	0.22 ± 0.02	0.38 ± 0.02	0.003
	2	0.17	0.37	0.16 ± 0.02	0.37 ± 0.02	0.002
	4	0.08	0.30	0.07 ± 0.01	0.29 ± 0.03	0.002
Bladder	0.1	6.58	1.95	6.71 ± 1.20	2.38 ± 0.53	0.028
	0.5	22.82	4.61	23.58 ± 2.58	4.70 ± 0.73	0.002
	1	25.23	5.36	26.68 ± 2.21	5.85 ± 0.73	0.002
	2	34.70	6.54	34.70 ± 1.28	7.22 ± 0.70	0.002
	4	31.41	8.01	29.03 ± 3.05	8.48 ± 0.82	0.014

Statistical significant differences were calculated for IHP ^{99m}Tc -EC-DG and $^{99m}\text{TcO}_4^-$ in LT lung at 1-4 h, RT lung at 0.5-4 h, LT kidney at 0.1 h and also at the 1-4 h time intervals. RH kidney between 2-4 h also indicated statistical significance between IHP ^{99m}Tc -EC-DG and $^{99m}\text{TcO}_4^-$. Statistical significance was also noted for the brain at 0.1-1 h and the heart at 0.1 h and 1-4 h. The skin and bladder demonstrated statistical significance at the imaging time intervals 0.1-4 h. The joints demonstrated statistical significance at the 0.5-4 h time intervals for the IHP ^{99m}Tc -EC-DG and $^{99m}\text{TcO}_4^-$.

In Figure 5.12 the *in vivo* clearance of the (A) liver, (B) heart, (C) brain (0.1 h to 1 h) with high uptake of $^{99m}\text{TcO}_4^-$ and IHP ^{99m}Tc -EC-DG (DL) are depicted. IHP ^{99m}Tc -EC-DG and $^{99m}\text{TcO}_4^-$ had the highest uptake to the liver before 0.1 h and constant clearance was seen from 0.1-4 h post administration. $^{99m}\text{TcO}_4^-$ had double the mean % uptake value to the liver compared to IHP ^{99m}Tc -EC-DG (Figure 5.12A). The IHP ^{99m}Tc -EC-DG (DL) and $^{99m}\text{TcO}_4^-$ uptake to the heart was the highest before 0.1 h and decreased constantly over time (Figure 5.12B). Before the 0.5 h time interval IHP ^{99m}Tc -EC-DG (DL) had the highest uptake to the heart, but from the 0.5-4 h time interval $^{99m}\text{TcO}_4^-$ had higher uptake to the heart. In Figure 5.12C can be seen that the brain clearance is fast from 0.1 h to 4 h post administration. The clearance of the IHP ^{99m}Tc -EC-DG (DL) and $^{99m}\text{TcO}_4^-$ from 2 h to 4 h is similar (Figure 5.12C). In Figure 5.13 the *in vivo* clearance of the (A) brain (only 2 h to 4 h show low uptake) and (B) stomach with low uptake of $^{99m}\text{TcO}_4^-$ and IHP ^{99m}Tc -EC-DG (DL) are depicted. $^{99m}\text{TcO}_4^-$ had constant low brain uptake. IHP ^{99m}Tc -EC-DG had higher brain uptake than $^{99m}\text{TcO}_4^-$ directly after radiopharmaceutical administration up to 2 hours after administration, but the mean % uptake values were low and a fast clearance of IHP ^{99m}Tc -EC-DG from the rabbit brain was seen to the 4 h time interval (Figure 5.13A). The uptake of IHP ^{99m}Tc -EC-DG to the stomach is higher than for the $^{99m}\text{TcO}_4^-$ (Figure 5.13B). Fast clearance of

the IHP $^{99m}\text{Tc-EC-DG}$ is seen before 0.5 h, to slightly higher uptake of that of $^{99m}\text{TcO}_4^-$ in the stomachs of the healthy rabbits.

The kidney clearance of $^{99m}\text{TcO}_4^-$ and IHP $^{99m}\text{Tc-EC-DG}$ (DL) was the fastest between 0.1-0.5 h post administration (Figure 5.14). The uptake of IHP $^{99m}\text{Tc-EC-DG}$ (DL) was higher than $^{99m}\text{TcO}_4^-$ to the kidneys. The radiopharmaceutical uptake of IHP $^{99m}\text{Tc-EC-DG}$ (DL) increased faster to the bladder and was also higher than that of $^{99m}\text{TcO}_4^-$ (Figure 5.14).

Characteristic biodistribution of $^{99m}\text{TcO}_4^-$ in the healthy rabbits was found to be the salivary glands and thyroid similar to humans (Harper, Lathrop, Jiminez, Fink & Gottschalk 1965:101), but no stomach uptake was found. The uptake of $^{99m}\text{TcO}_4^-$ to the liver of healthy rabbits is very high and can be confused to be that of the stomach, as stomach uptake in humans (Harper *et al.* 1965:101) and baboons are high (Chapter 6). These interspecies biodistribution differences of $^{99m}\text{TcO}_4^-$ to the liver and stomach were confirmed with SPECT/CT imaging in this dissertation. Fresh $^{99m}\text{TcO}_4^-$ eluent was used and no other radiopharmaceutical was labelled at the same time of this experiment and therefore could exclude these results as false positive/false negative. Good labelling efficiency of IHP $^{99m}\text{Tc-EC-DG}$ could be confirmed when compared to $^{99m}\text{TcO}_4^-$ static and SPECT/CT images as no salivary glands, or thyroid was visible, indicating no free $^{99m}\text{TcO}_4^-$. The normal excretory route of $^{99m}\text{TcO}_4^-$ in humans is by the urinary tract and this is also the case for rabbits (Figure 5.9B). $^{99m}\text{TcO}_4^-$ had slower kidney clearance than IHP $^{99m}\text{Tc-EC-DG}$ (DL). The SQ, SQUAL and quantitative results of the SPECT/CT and static images, confirmed high uptake to the liver, excretion from the kidneys into the urinary tract for the IHP $^{99m}\text{Tc-EC-DG}$ (DL) and $^{99m}\text{TcO}_4^-$ in the healthy rabbits.

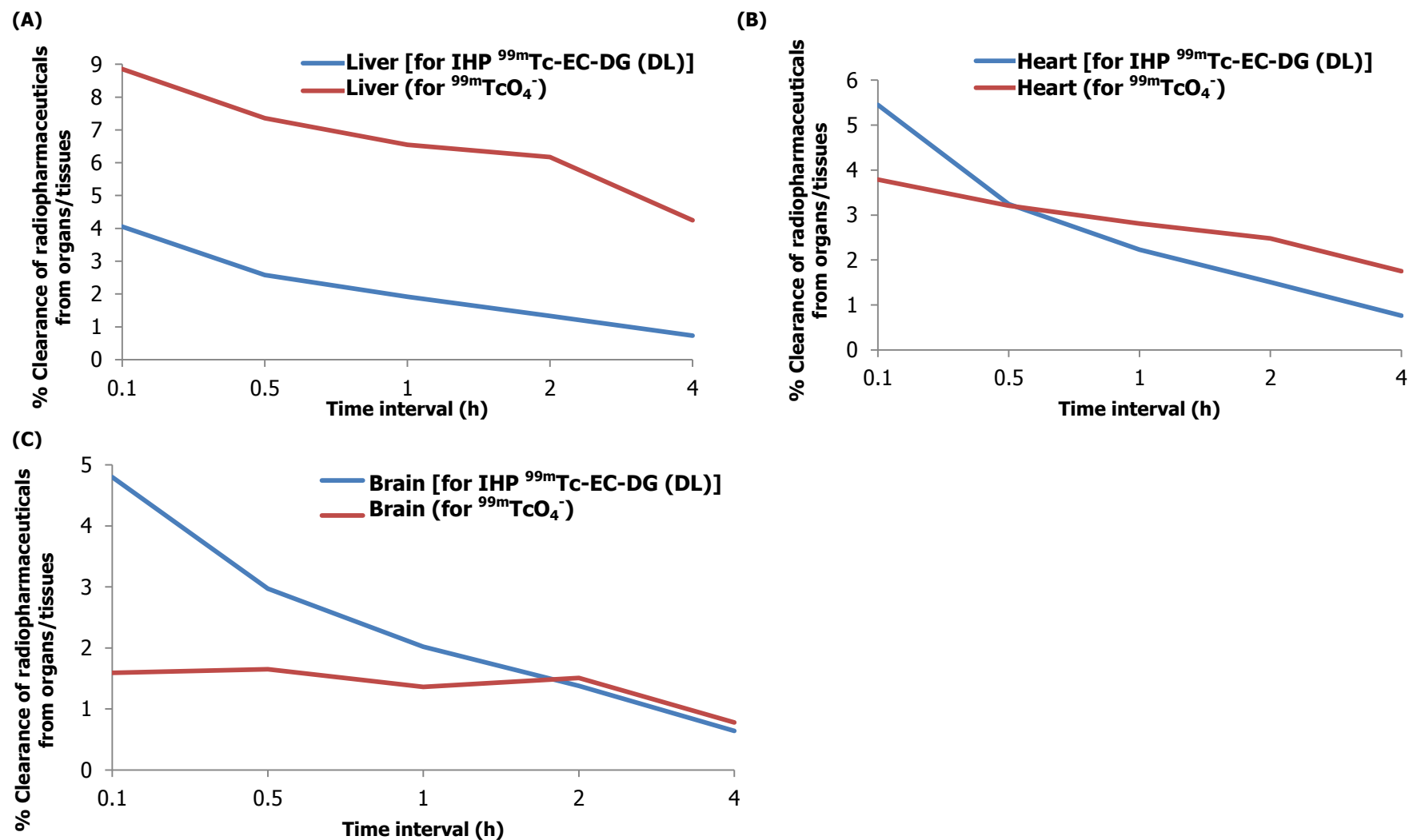


FIGURE 5.12: Comparison of clearance of high biodistribution organs from the IHP $^{99m}\text{Tc-EC-DG}$ and $^{99m}\text{TcO}_4^-$ in healthy rabbits. Mean % biodistribution values for the (A) liver, (B) heart and (C) brain (only high 0.1h to 1 h) are shown with time.

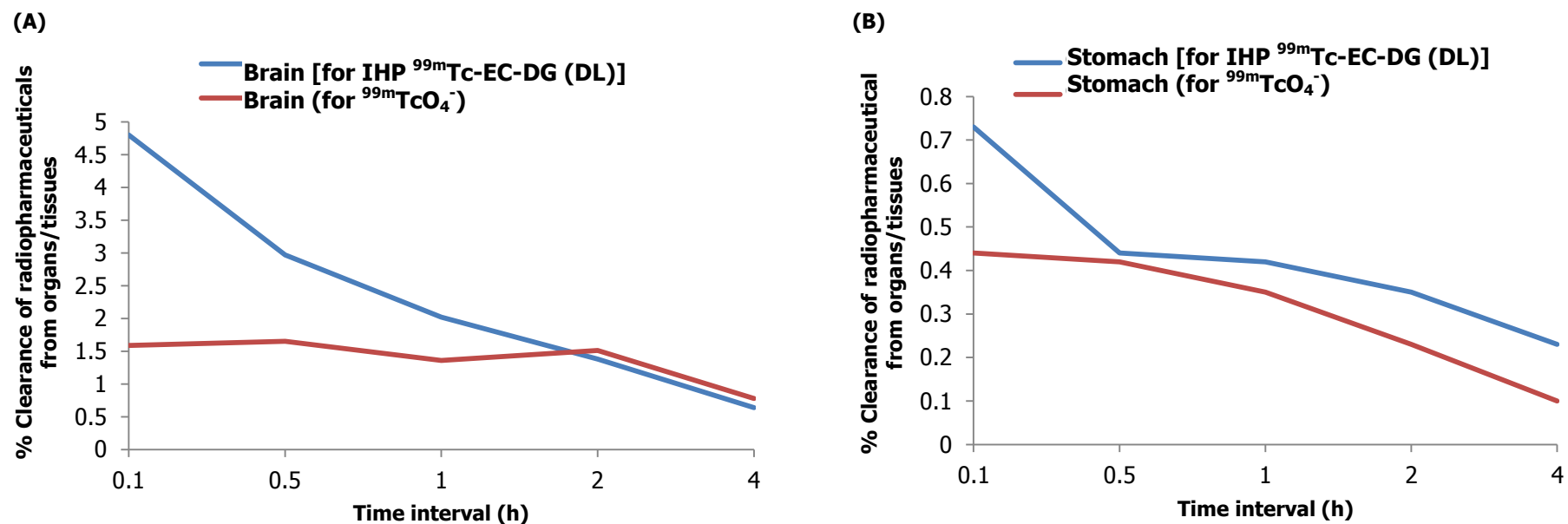


FIGURE 5.13: Comparison of clearance for the low biodistribution organs of IHP $^{99m}\text{Tc-EC-DG}$ and $^{99m}\text{TcO}_4^-$ in healthy rabbits. Mean % biodistribution values for the (A) brain (only low 1h to 4h) and (B) stomach are shown with time.

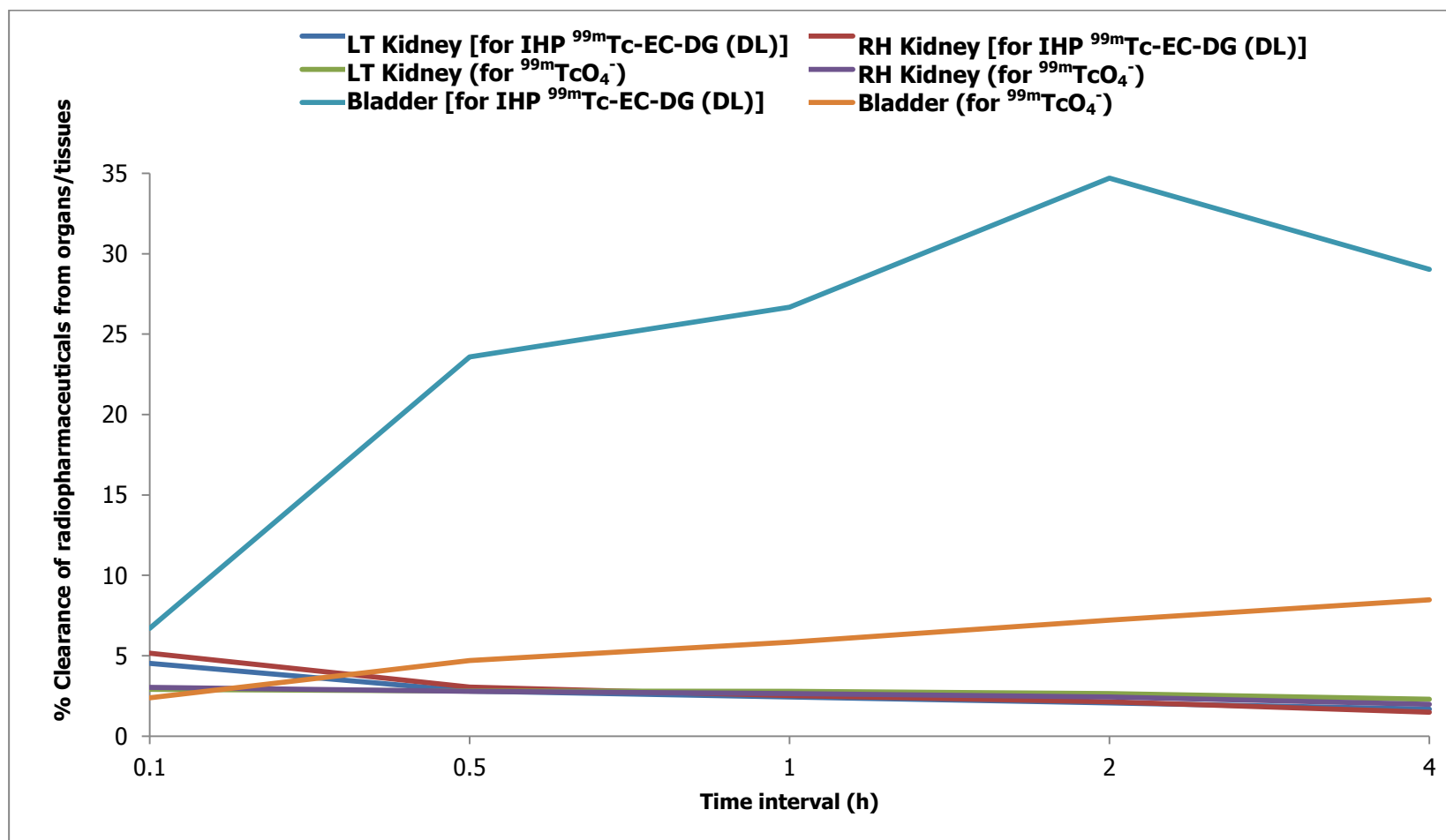


FIGURE 5.14: Clearance profile of IHP $^{99m}\text{Tc-EC-DG}$ and $^{99m}\text{TcO}_4^-$ excretion by kidneys into the bladder for healthy rabbits

Early uptake to the heart by IHP ^{99m}Tc -EC-DG (DL) and $^{99m}\text{TcO}_4^-$ was also present with all the result evaluation techniques. The lowest uptake was confirmed to the brain, stomach, muscles, joints and skin. Biodistribution differences of IHP ^{99m}Tc -EC-DG (DL) and $^{99m}\text{TcO}_4^-$ were reported on of the static and SPECT/CT images. The thyroid and salivary glands showed mild to high uptake of $^{99m}\text{TcO}_4^-$, with no uptake of IHP ^{99m}Tc -EC-DG to these areas.

5.3.3 Septic IFI/IF rabbit model

A comparison was made between the biodistribution of the IHP ^{99m}Tc -EC-DG (DL) and ^{67}Ga -citrate in septic IFI/IF induced in healthy rabbits. The septic IFI/IF was induced with *E. coli* in the right gluteus muscle.

5.3.3.1 Radiosynthesis of IHP ^{99m}Tc -EC-DG (DL)

The complexation of the EC-DG with freshly eluted $^{99m}\text{TcO}_4^-$ (1480 MBq in 0.5 ml) was carried out at pH 5.5 in a laminar flow cabinet in a Type B hot laboratory. The radiochemical purity of the IHP ^{99m}Tc -EC-DG (DL) complex was assessed with ITLC chromatography using ITLC-SC strips developed in saline and Whatman No. 1 developed in acetone. QC was performed directly after the completion of the ^{99m}Tc -EC-DG (DL). The IHP ^{99m}Tc -EC-DG complex evaluated on the Whatman No. 1 paper remained at the origin, however on ITLC-SC it migrated to the front solvent. TLC analyses of purity of IHP ^{99m}Tc -EC-DG directly labelled complex was >92% (Whatman/acetone) and less than 3% $^{99m}\text{TcO}_4^-$ colloidal formation (ITLC-SC/saline). The final pH was 6.5 for the IHP ^{99m}Tc -EC-DG directly labelled complex. The radiopharmaceutical was within the specification for the use in an animal experiment.

5.3.3.2 *In vivo* biodistribution images

Five minutes after administration of IHP ^{99m}Tc -EC-DG (DL) static acquisitions of both thighs in focus was done, for five minute acquiring times. This was followed by static images at 1-, 2-, 3-, 4-, 6 h and SPECT/CT at 2- and 4 h

post radiopharmaceutical administration. After the IHP ^{99m}Tc -EC-DG imaging was completed ^{67}Ga -citrate was administered to the same five rabbits and static and SPECT/CT was performed at 24- and 48 h post administration. The static images obtained from the septic IFI/IF rabbits injected with IHP ^{99m}Tc -EC-DG (A-F) and ^{67}Ga -citrate (G-H) is presented in Figure 5.15 and -5.16 for the different time intervals.

^{67}Ga -citrate imaging was not performed earlier than 24 hours as at 48 h 75 % of the administered dose of ^{67}Ga -citrate is still present in different organs in the body (Hughes 2003:198). The background of ^{67}Ga -citrate is high for images acquired before 24 h post administration and this may lead to false-negative reporting of small IFI/IF areas. In clinical practice, scintigraphic imaging for IFI/IF is performed on 24-, 48- and sometimes at 72 h. By acquiring ^{67}Ga -citrate images after 24 h, a good target-to-background ratio was obtained.

Well-defined intense increased IHP ^{99m}Tc -EC-DG (DL) uptake was noted in the septic IFI/IF area at the 0.1 h acquired static images which decreased to moderate increased uptake at 1 h (Figure 5.15A and -B). Mild accumulation of IHP ^{99m}Tc -EC-DG was observed on the 2- and 3 h static images at sites of IFI/IF (Figure 5.15C and -D). Poor-defined areas of increased uptake were noted on the 4- and 6 h views to the area of septic IFI/IF (Figure 5.13E and -F). The bladder increased in size (before masking) from 0.1-4 h indicating radiopharmaceutical excretion through the urinary system, from the kidneys into the bladder. Figure 5.16A and Figure 5.16B showed an intense increased accumulation of ^{67}Ga -citrate at the site of septic IFI/IF on the static acquired images at 24- and 48 h.

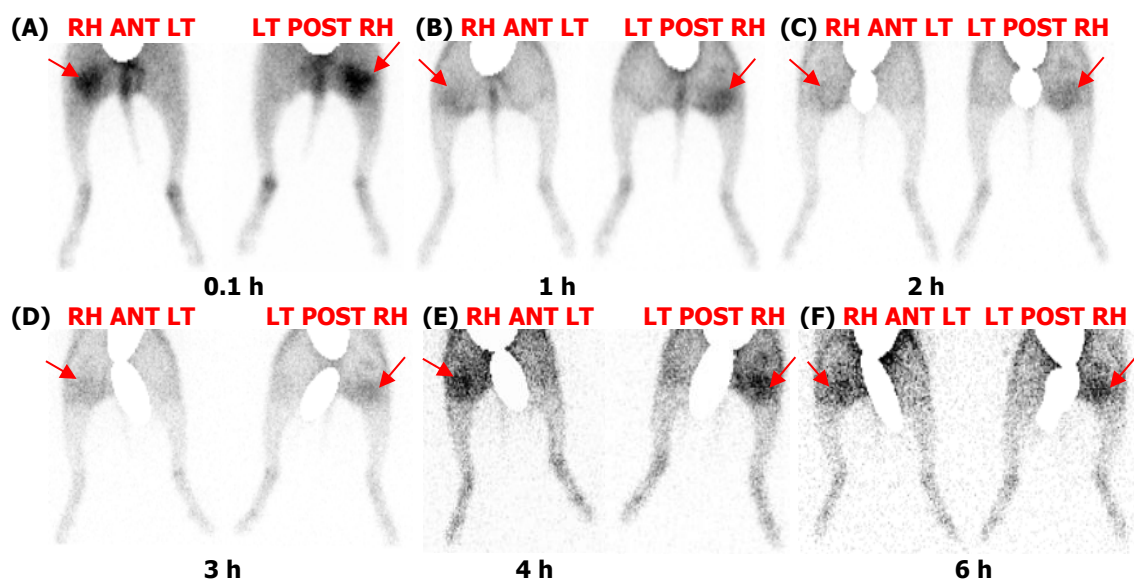


FIGURE 5.15: ANT septic IFI/IF static images of IHP ^{99m}Tc -EC-DG (A-F) was obtained at (A) 0.1-, (B) 1-, (C) 2-, (D) 3-, (E) 4- and (F) 6 hour post administration. Arrow indicate increase radiopharmaceutical uptake in septic IFI/IF induced area.

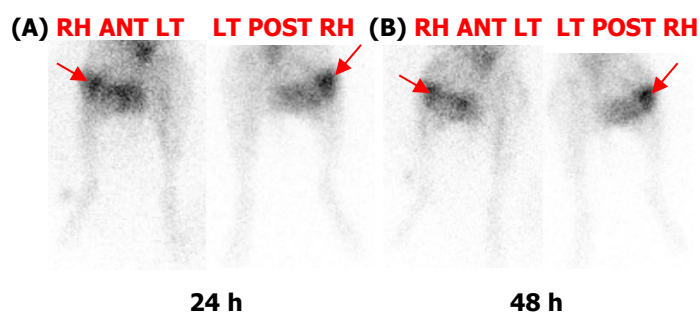


FIGURE 5.16: ^{67}Ga -citrate static images were obtained at (A) 24- and (B) 48 hour post radiopharmaceutical administration. Arrows indicate increased radiopharmaceutical uptake in septic IFI/IF induced area.

In Figure 5.17 the transverse (A), sagittal (B) and coronal (C) fused IHP ^{99m}Tc -EC-DG SPECT/CT images of the site of septic induced IFI/IF at 4 h post radiopharmaceutical administration are shown. Well-defined intense increased IHP ^{99m}Tc -EC-DG uptake was noted in the right thigh on the 2- and 4 h SPECT/CT images, correlating with the site of induced septic inflammation/infection.

In Figure 5.18 the transverse (A), sagittal (B) and coronal (C) fused ^{67}Ga -citrate SPECT/CT images of the site of septic induced IFI/IF at 48 h post radiopharmaceutical administration. Intense increased ^{67}Ga -citrate accumulation was noted on the 24- and 48 h (Figure 5.18) SPECT/CT images in the region of septic IFI/IF. The ^{67}Ga -citrate (static and SPECT/CT) images confirmed successful induction of the septic IFI/IF in the rabbit model.

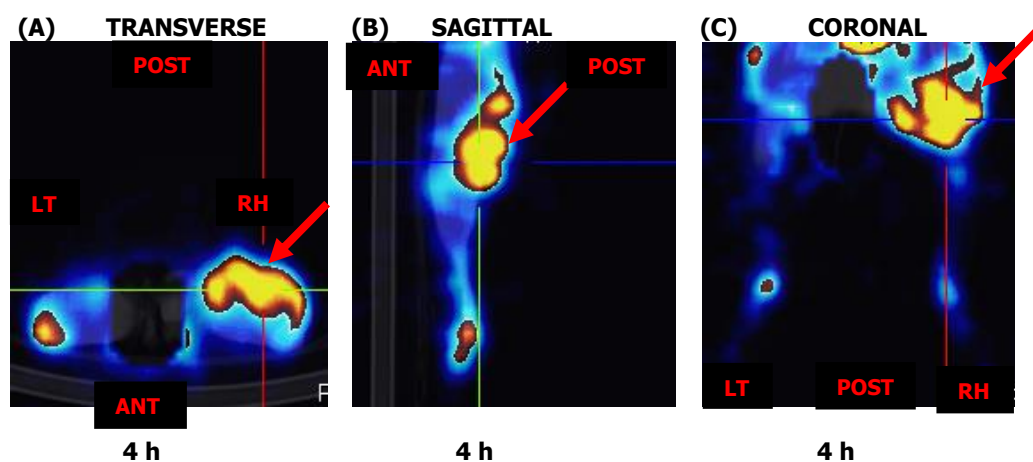


FIGURE 5.17: IHP $^{99\text{m}}\text{Tc}$ -EC-DG fused SPECT/CT (A) transverse, (B) sagittal and (C) coronal images with *E. coli* thigh muscle IFI/IF (arrow) 4 hour post radiopharmaceutical administration.

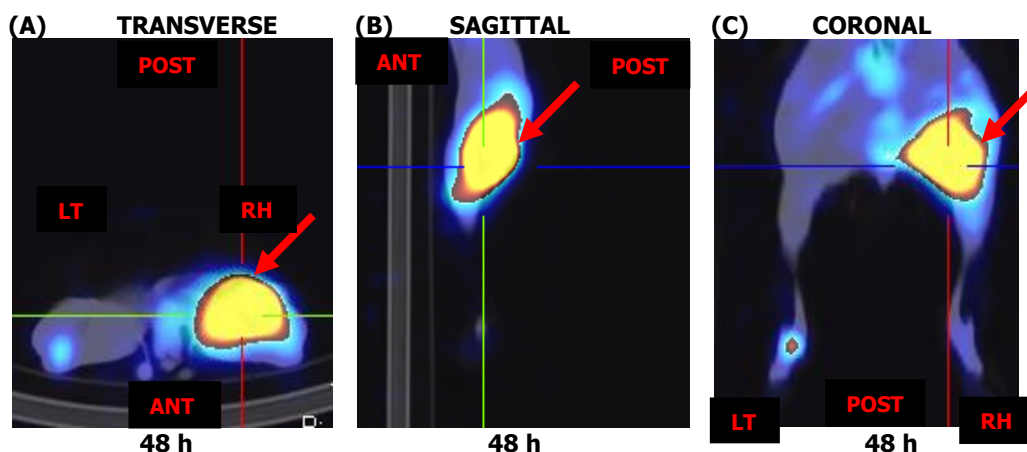


FIGURE 5.18: ^{67}Ga -citrate fused SPECT/CT (A) transverse, (B) sagittal and (C) coronal images with *E. coli* thigh muscle infection (arrow) 48 hour POST radiopharmaceutical administration.

5.3.3.3 SQ and SQUAL analysis

The four-point grading scale (0 to 3) of SQ and SQUAL indicative factors was used for the evaluation of the scintigraphic images. The SQ and SQUAL scale and reporting factors were used as a reporting index to visually interpret and determine if IHP $^{99\text{m}}\text{Tc}$ -EC-DG (DL) biodistributed to the area of sterile IFI/IF.

The SQ and SQUAL results of the static and SPECT/CT images of the biodistribution of the IHP ^{99m}Tc -EC-DG (DL) and ^{67}Ga -citrate to the site of septic induced IFI/IF, is summarised in Table 5.7. The SQ results reported septic IFI/IF biodistribution at 0.1 h was 3, for 1-4 h reported as 2 and at 6 h as 1 for the static images. The SPECT/CT SQ for IHP ^{99m}Tc -EC-DG for the SPECT/CT images acquired at 2- and 4 h was reported as 2, indicating moderate biodistribution to the area of induced IFI/IF (Table 5.7). The ^{67}Ga -citrate SQUAL results reported on the area of induced septic IFI/IF at 24- and 48 h as positive for the static and SPECT/CT images. The SQ results rated the biodistribution to the septic IFI/IF area as 3 (severely increased uptake) for both imaging time intervals and for the static and SPECT/CT images of ^{67}Ga -citrate. The SQUAL reporting of the static and SPECT/CT images confirmed biodistribution of IHP ^{99m}Tc -EC-DG and ^{67}Ga -citrate as positive to the area of septic IFI/IF. The SQ results were rated as severely increased to the IFI/IF site for ^{67}Ga -citrate for the static and SPECT/CT images, whereas IHP ^{99m}Tc -EC-DG (DL) was only reported as severe at 0.1 h static acquired image (Table 5.7). The SQ and SQUAL confirmed successful biodistribution of IHP ^{99m}Tc -EC-DG (DL) to the induced septic IFI/IF in rabbits and though lower, compared good with ^{67}Ga -citrate.

The reporting results visually identified IHP ^{99m}Tc -EC-DG biodistribution to the area of septic IFI/IF as early as 0.1 h post administration and the optimal IFI/IF detection time point at 0.1 h post RP administration (Table 5.7). The ^{67}Ga -citrate images confirmed that septic IFI/IF were positively induced and when compared to the IHP ^{99m}Tc -EC-DG images confirmed biodistribution as the test radiopharmaceutical to the site of IFI/IF. The septic IFI/IF detection of ^{67}Ga -citrate at 24- and 48 h were superior to the IFI/IF of the IHP ^{99m}Tc -EC-DG (DL) at 0.1-1 h post administration for the static and SPECT/CT images (Figure 5.15, -5.16, -5.17 & 5.18). A non-significant difference between the T/NT ratio for the different time intervals was indicated for IHP ^{99m}Tc -EC-DG and ^{67}Ga -citrate in rabbits with septic IF/IF. The SQ and SQUAL reporting results for ^{67}Ga -citrate compared to fall in line with the quantitative results obtained, but there were differences obtained with IHP ^{99m}Tc -EC-DG relating to the optimal imaging time point. The SQ results found the IHP ^{99m}Tc -EC-DG to be at 0.1 h and the quantitative results at 6 h post radiopharmaceutical administration.

TABLE 5.7: Comparison of the SQ and SQUAL static and SPECT/CT results of the biodistribution to the septic IFI/IF of IHP ^{99m}Tc -EC-DG (DL) and ^{67}Ga -citrate in rabbits

Radiopharmaceutical	Time intervals (h)	Static			SPECT/CT		
		<i>n</i>	SQUAL	SQ	<i>n</i>	SQUAL	SQ
IHP ^{99m}Tc -EC-DG (DL)	0.1	5	Post	3	*	*	*
	1	5	Post	2	*	*	*
	2	5	Post	2	1	Post	2
	3	5	Post	2	*	*	*
	4	5	Post	2	1	Post	2
	6	5	Post	1	*	*	*
^{67}Ga -citrate	24	5	Post	3	1	Post	3
	48	5	Post	3	1	Post	3

5.3.3.4 Quantitative analysis

To determine the IHP ^{99m}Tc -EC-DG or ^{67}Ga -citrate accumulation in the IFI/IF thigh, reference images were selected. On all the reference images, an automatically adjusted ROI was drawn over the right thigh region (T) and a mirror image region was created over the contralateral normal thigh area (NT). Accumulation of the tracer (radionuclide or radiopharmaceutical) at the site of septic IFI/IF was expressed as the ratio of counts in the target muscle to the counts in the non-target muscle (T/NT ration). Statistical calculations were done on all the data and also included of the namely mean and *SEM* was calculated. A *P* value of <0.05 was considered statistically significant. The ROIs were drawn over IFI/IF RH gluteus area indicated as the target (T) and the healthy LT gluteus area indicated as non-target (NT). Differences between the groups were calculated using the Signed Rank Test for paired data and the Wilcoxon Wallis Test for unpaired data.

Table 5.8 indicates the NT (%LT) and T (%RH) uptake of the IHP ^{99m}Tc -EC-DG for each of the six rabbits induced with septic IFI/IF at 0.1-, 1-, 2-, 3-, 4- and 6 h post administration. The data for the IHP ^{99m}Tc -EC-DG uptake in the septic IFI/IF is expressed as the mean \pm *SEM*. Table 5.9 indicates target-to-non-target (T/NT) ratios for the IHP ^{99m}Tc -EC-DG (DL) (0.1-6 h) and ^{67}Ga -citrate (24- and 48 h) that represents the median of the T uptake divided by the median of the NT uptake.

TABLE 5.8: Percentage target and non-target biodistribution of IHP ^{99m}Tc -EC-DG (DL) and ^{67}Ga -citrate in rabbits induced ($n=5$) with septic IFI/IF

Radiopharmaceutical	Time intervals (h)	P-value	% Biodistribution			
			Non-target		Target	
			Median	Mean \pm SEM	Median	Mean \pm SEM
IHP ^{99m}Tc -EC-DG (DL)	0.1	0.06	33.00	32.34 \pm 1.01	67.82	67.82 \pm 0.99
	1	0.06	33.51	34.79 \pm 1.49	66.49	65.21 \pm 1.49
	2	0.06	35.27	34.75 \pm 1.04	64.73	65.24 \pm 1.04
	3	0.06	34.83	34.22 \pm 1.37	65.17	65.78 \pm 1.37
	4	0.06	32.90	32.67 \pm 1.27	67.10	67.33 \pm 1.27
	6	0.06	33.47	32.85 \pm 0.81	66.53	67.15 \pm 0.81
^{67}Ga -citrate	24	0.06	20.05	19.37 \pm 1.39	79.95	80.63 \pm 1.39
	48	0.06	17.74	16.43 \pm 1.83	82.26	83.57 \pm 1.83

In Table 5.8 the ^{99m}Tc -EC-DG target-to-non-target (T/NT) % uptake at 0.1-, 1-, 2-, 3-, 4- and 6 h post administration is given, as well as the target-to-non-target (T/NT) ratios of ^{67}Ga -citrate at 24- and 48 h post administration. Mean \pm SEM of the T/NT ratios of the IHP ^{99m}Tc -EC-DG and ^{67}Ga -citrate were compared. The highest mean % uptake for IHP ^{99m}Tc -EC-DG (DL) was 67.82% at 0.1 h, followed by 67.33% at 4 h. The highest % uptake of ^{67}Ga -citrate was 83% at 48 h post administration. More than 10 % mean difference was noted between the uptakes of IHP ^{99m}Tc -EC-DG with ^{67}Ga -citrate in septic IFI/IF area in rabbits.

The statistical significance ($P < 0.05$) of the T/NT ^{67}Ga -citrate and IHP ^{99m}Tc -EC-DG (KF) for each time interval is also provided in Table 5.8. The Wilcoxon test was used to calculate the P -value of the T with the NT percentage biodistribution at 0.1-, 1-, 2-, 3-, 4- and 6 h post administration for the IHP ^{99m}Tc -EC-DG and for ^{67}Ga -citrate at 24- and 48 h post administration for ^{67}Ga -citrate. A P value < 0.05 (red values) was considered statistically significant. In The differences between the T and the NT uptake of IHP ^{99m}Tc -EC-DG (KF) and ^{67}Ga -citrate in septic IFI/IF in rabbits (Table 5.8) could not be indicated with a 95% certainty ($P = 0.06$). ^{67}Ga -citrate is used in clinical practice for the diagnosis of IFI/IF, even though there might not be a statistical significant difference between the T and NT area, the diagnosis of septic IFI/IF can still be made visually. IHP ^{99m}Tc -EC-DG like ^{67}Ga -citrate, did not have a statistical significant difference of the T with the NT, but can also be interpreted as an area of accumulation in septic IFI/IF. ^{99m}Tc -EC-DG should therefore be

investigated as possible diagnostic radiopharmaceutical in humans as it could identify induced septic IFI/IF in rabbits.

Table 5.9 indicates the target-to-non-target (T/NT) ratios that represent the mean of the T uptake divided by the mean of the NT uptake. The T/NT ratios at 0.1-, 1-, 2-, 3-, 4- and 6 h post administration is given, as well as the target-to-non-target (T/NT) ratios of ^{67}Ga -citrate at 24- and 48 h post administration. The mean values of the T/NT ratios of the IHP $^{99\text{m}}\text{Tc}$ -EC-DG (0.1-6 h) and ^{67}Ga -citrate from (24- and 48 h) are calculated as follows: 2.11 ± 0.10 , 1.90 ± 0.13 , 1.89 ± 0.09 , 1.94 ± 0.13 , 2.08 ± 0.12 and 2.05 ± 0.08 at 0.1-, 1-, 2-, 3-, 4- and 6 h after IHP $^{99\text{m}}\text{Tc}$ -EC-DG administration. At 24- and 48 h the T/NT ratio of ^{67}Ga -citrate T/NT was 4.28 ± 0.42 and 5.45 ± 0.81 . The highest T/NT for IHP $^{99\text{m}}\text{Tc}$ -EC-DG (DL) to the area of septic IFI/IF was at 0.1 h and for ^{67}Ga -citrate was found at 48 h in rabbits respectively.

TABLE 5.9: Target-to-non-target ratios of IHP $^{99\text{m}}\text{Tc}$ -EC-DG (DL) and ^{67}Ga -citrate of septic IFI/IF thigh muscles in rabbits ($n=5$) at different time intervals

Rabbit no.	IHP $^{99\text{m}}\text{Tc}$ -EC-DG (DL)						^{67}Ga -citrate	
	Target-to-non-target ratio						Target-to-non-target ratio	
	0.1 h	1 h	2 h	3 h	4 h	6 h	24 h	48 h
1	1.93	1.58	1.69	1.66	1.76	1.91	3.53	3.81
2	2.35	2.18	1.84	1.95	1.89	1.89	5.77	8.20
3	1.89	1.63	1.80	1.82	2.04	2.22	4.60	6.35
4	2.32	2.08	2.23	2.41	2.37	2.25	3.53	4.63
5	2.05	1.98	1.88	1.87	2.34	1.99	3.99	4.22
Mean \pm SEM	2.11 ± 0.10	1.90 ± 0.13	1.89 ± 0.09	1.94 ± 0.13	2.08 ± 0.12	2.05 ± 0.08	4.28 ± 0.42	5.45 ± 0.81

The highest T/N ratio was 2.11 ± 0.10 for IHP $^{99\text{m}}\text{Tc}$ -EC-DG at 0.1 h post administration. It is emphasized that there is no large difference of the mean value at 0.1- and 4 h T/NT ratio. ^{67}Ga -citrate overall had the highest ratio of 5.45 ± 0.81 of the two RP at 48 h post administration (Table 5.9).

5.3.4 Sterile IFI/IF rabbit model

The uptake of IHP $^{99\text{m}}\text{Tc}$ -EC-DG (KF) in an induced infection/inflammation area (sterile IFI/IF) in rabbits was studied in comparison with ^{67}Ga -citrate, that is worldwide used for the detection of IFI/IF and tumours (Hughes 2003:196). During the study the uptake in IFI/IF areas (target) relative to non IFI/IF (non-target) areas was evaluated. The statistical analysis was performed using the Wilcoxon test to calculate the

differences between the target (focal area of sterile IFI/IF) and non-target areas (healthy opposite non-infected area) of the unpaired groups.

5.3.4.1 Radiosynthesis of IHP ^{99m}Tc -EC-DG (KF)

The radiolabelling of IHP ^{99m}Tc -EC-DG was achieved by using the kit formulation procedure (section 3.3.5.4) by adding $^{99m}\text{TcO}_4^-$ (1480 MBq) into lyophilized EC-DG and tin/buffer vials. The complexation was carried out at a pH of 5.5 in a laminar flow cabinet situated in a Type B radiological controlled laboratory. The TLC analyses of the radiochemical purity of ^{99m}Tc -EC-DG were >93% with less than 1% colloidal formation present. The labelled compound was therefore within specification (radiochemical purity and pH) for use in the animal model. The final pH measured after the labelling procedure was 7.

5.3.4.2 *In vivo* biodistribution images

Static images of the abdomen and lower limbs were taken at 0.1-, 1-, 2-, 3-, 4- and 6 h after administration of the IHP ^{99m}Tc -EC-DG (KF) and at 24- and 48 h for ^{67}Ga -citrate in the rabbits in which sterile IFI/IF was induced with zymosan in the thigh muscle 7 days before (marked with arrow). Optimal images with good target-to-background ratio were obtained. The ANT and POST static images obtained from the sterile IFI/IF rabbits administered with IHP ^{99m}Tc -EC-DG and ^{67}Ga -citrate is presented Figure 5.19 and Figure 5.20. The site of induced IF/IFI demonstrates well-defined increased IHP ^{99m}Tc -EC-DG (KF) uptake at the 0.1 h static view, decreasing uptake on the 1- to 6 h views, slightly more compared to background. Significant increase in IHP ^{99m}Tc -EC-DG (KF) uptake is observed in the bladder from the 0.1 h images, increasing in size towards the 6 h images. This increase in bladder size indicates radiopharmaceutical excretion through the kidneys into the bladder. Background activity decreased significantly compared to the first static image.

Well-defined intense increased IHP ^{99m}Tc -EC-DG (KF) uptake was noted on the static image at 0.1 h which decreased to mild increased uptake with the 1 h imaging time interval (Figure 5.19B). Mild increased IHP ^{99m}Tc -EC-DG (KF) uptake was noted on the 2-, 3- and 4 h static images. A poor-defined area of

very little increased uptake is noted on the 6 h view. Marked increased accumulation was seen on the static images in the area of sterile IFI/IF at 24- and 48 h post administration of ^{67}Ga -citrate (Figure 5.20).

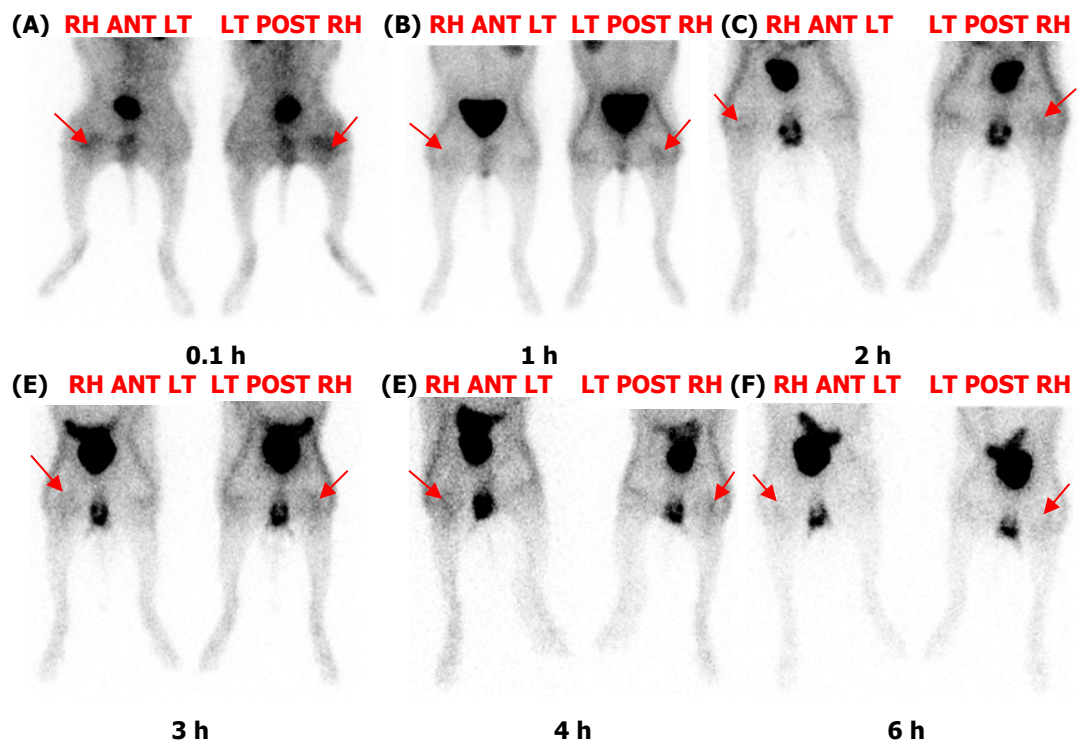


FIGURE 5.19: ANT sterile IFI/IF static images of IHP $^{99\text{m}}\text{Tc}$ -EC-DG (KF) (A-F) at (A) 0.1-, (B) 1-, (C) 2-, (D) 3-, (E) 4- and (F) 6 hour POST administration. Arrows indicate increased radiopharmaceutical uptake in sterile IFI/IF induced area.

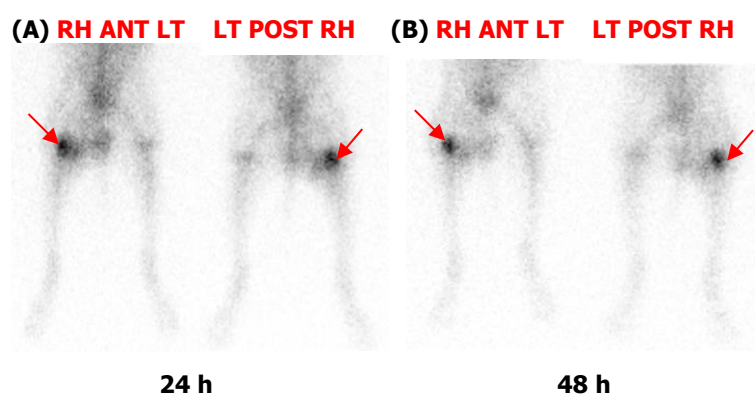


FIGURE 5.20: ANT sterile IFI/IF static images of ^{67}Ga -citrate (A) 24- and (B) 48 hour POST administration. Arrows indicate increased radionuclide uptake in sterile IFI/IF induced area.

In Figure 5.21 the coronal (A) fused IHP $^{99\text{m}}\text{Tc}$ -EC-DG SPECT/CT image of the site of sterile induced IFI/IF at 4 h post RP administration and the coronal (B)

fused ^{67}Ga -citrate SPECT/CT images of the site of sterile induced IFI/IF at 48 h post RP administration are shown. The bladder was masked out on the IHP $^{99\text{m}}\text{Tc}$ -EC-DG (KF) SPECT/CT images. Intense increased ^{67}Ga -citrate uptake was noted on the 24 h and the 48 h static images in the region of sterile IFI/IF.

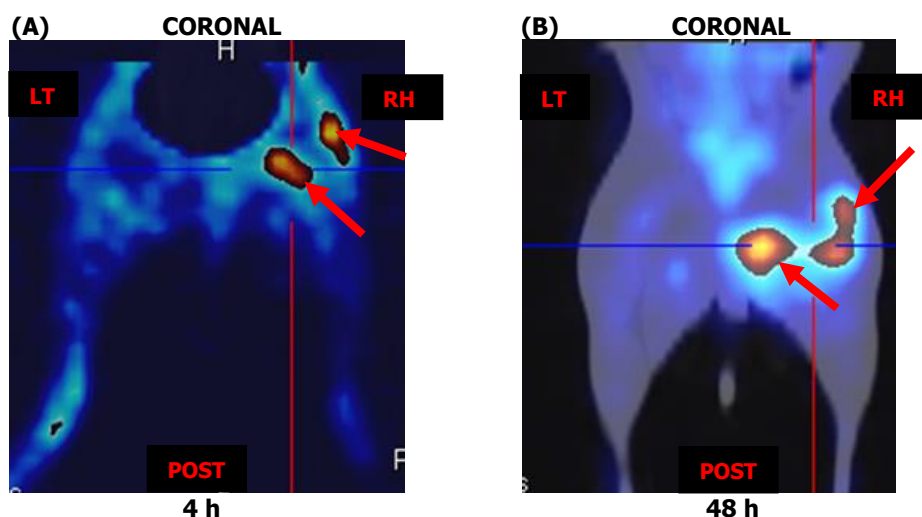


FIGURE 5.21: (A) 4 hour IHP $^{99\text{m}}\text{Tc}$ -EC-DG fused SPECT/CT coronal images and (B) 48 hour ^{67}Ga -citrate fused SPECT/CT coronal images of the zymosan induced IFI/IF in the thigh muscle (arrow).

Two focal areas of well-defined increased IHP $^{99\text{m}}\text{Tc}$ -EC-DG (KF) uptake were noted in the right thigh, correlating with the site of induced sterile IFI/IF on the SPECT/CT images (Figure 5.21A). Intense increased ^{67}Ga -citrate uptake was noted on the 48 h SPECT/CT images in the region of sterile IFI/IF (Figure 5.21B); however the site of increased ^{67}Ga -citrate uptake appears bigger than that of the site of increased $^{99\text{m}}\text{Tc}$ -EC-DG uptake.

5.3.4.3 SQ and SQUAL analysis

The SQ and SQUAL results allocated reporting biodistribution intensities (positive, negative or background) and index values (0-3) to the static and SPECT/CT images of the biodistribution of the IHP $^{99\text{m}}\text{Tc}$ -EC-DG (KF) and ^{67}Ga -citrate in the area of sterile induced IFI/IF are tabulated in Table 5.10. The SQ results reported sterile IFI/IF uptake at 0.1 h as 3, for 1-4 h as 2 and at 6 h as 1 for the static images. The SPECT/CT SQ for IHP $^{99\text{m}}\text{Tc}$ -EC-DG grading of 2 were higher than the static images at 4 h grading 1 post RP administration (Table 5.10). The ^{67}Ga -citrate SQUAL results reported on the area of induced sterile IFI/IF at 24- and 48 h as positive for the static and

SPECT/CT images. The SQ results rated the uptake to the sterile IFI/IF area as 3 for both imaging time intervals and the static and SPECT/CT images of ^{67}Ga -citrate. The SQUAL confirmed uptake of IHP $^{99\text{m}}\text{Tc}$ -EC-DG (KF) and ^{67}Ga -citrate to the area of sterile IFI/IF. The SQ results of ^{67}Ga -citrate were reported for the 24- and 48 h as 3, whereas the IHP $^{99\text{m}}\text{Tc}$ -EC-DG was only reported on the early image at 0.1 h as 3.

IHP $^{99\text{m}}\text{Tc}$ -EC-DG uptake to the area of sterile IFI/IF was visually identified as early was visually identified as 0.1 h post administration and the optimal IFI/IF detection was at 0.1 h post RP administration (Table 5.10). A diverse number of mechanisms is involved with the biodistribution of ^{67}Ga -citrate to IFI/IF, these include forming complexes with transferrin and which can bind to lactoferrin, bacterial siderophores, inflammatory proteins and cell walls (Mettler & Guiberteau 2012:406). The ^{67}Ga -citrate images confirmed that sterile IFI/IF was successfully induced with biodistribution of this test radiopharmaceutical to the site of IFI/IF.

TABLE 5.10: Comparison of the SQ and SQUAL static and SPECT/CT results of the biodistribution to the sterile IFI/IF of IHP $^{99\text{m}}\text{Tc}$ -EC-DG (KF) and ^{67}Ga -citrate in rabbits

Radiopharmaceutical	Time intervals (h)	Static			SPECT/CT		
		<i>n</i>	SQUAL	SQ	<i>n</i>	SQUAL	SQ
IHP $^{99\text{m}}\text{Tc}$ -EC-DG KF	0.1	5	Post	3	*	*	*
	1	5	Post	2	*	*	*
	2	5	Post	2	1	Post	2
	3	5	Post	2	*	*	*
	4	5	Post	1	1	Post	2
	6	5	Post	1	*	*	*
^{67}Ga -citrate	24	5	Post	3	1	Post	3
	48	5	Post	3	1	Post	3

5.3.4.4 Quantitative analysis of images of sterile IFI/IF in rabbits

The ROIs which were drawn over IFI/IF RH gluteus area indicated the target (T) and the healthy LT gluteus area indicated the non-target (NT). Table 5.41 indicates the %T (%RH) and %NT (%LT) biodistribution results of the IHP $^{99\text{m}}\text{Tc}$ -EC-DG and ^{67}Ga -citrate of five rabbits induced with sterile IFI/IF. The data for the IHP $^{99\text{m}}\text{Tc}$ -EC-DG biodistribution in the sterile IFI/IF is expressed as the mean \pm SEM. The highest mean values are indicated in bold. In Table 5.11 the highest mean % uptake for IHP

^{99m}Tc -EC-DG was 69% at 6 h and for ^{67}Ga -citrate 79% at 48 h. A 10 % mean difference was noted between the uptakes of IHP ^{99m}Tc -EC-DG with ^{67}Ga -citrate in sterile IFI/IF in rabbits. ^{67}Ga -citrate had at 24- and 48 h higher uptake to the area of induced sterile IFI/IF compared to IHP ^{99m}Tc -EC-DG kit at 0.1-, 1-, 2-, 3-, 4- and 6 h (Table 5.11).

TABLE 5.11: %Non-target and %Target biodistribution of IHP ^{99m}Tc -EC-DG KF and ^{67}Ga -citrate in rabbits induced ($n=5$) with sterile IFI/IF

Radiopharmaceutical	Time intervals (h)	<i>P</i> -value	% Biodistribution			
			Non-target		Target	
			Median	Mean \pm SEM	Median	Mean \pm SEM
IHP ^{99m}Tc -EC-DG (KF)	0.1	0.06	36.58	35.77 \pm 1.25	63.42	64.18 \pm 1.23
IHP ^{99m}Tc -EC-DG (KF)	1	0.06	38.98	36.61 \pm 2.08	61.02	63.43 \pm 2.09
IHP ^{99m}Tc -EC-DG (KF)	2	0.06	32.66	33.35 \pm 1.47	67.34	66.65 \pm 1.47
IHP ^{99m}Tc -EC-DG (KF)	3	0.06	32.89	33.52 \pm 1.12	67.11	66.48 \pm 1.12
IHP ^{99m}Tc -EC-DG (KF)	4	0.06	32.47	33.45 \pm 1.36	67.53	66.55 \pm 1.36
IHP ^{99m}Tc -EC-DG (KF)	6	0.06	31.65	30.66 \pm 1.27	68.35	69.34 \pm 1.27
^{67}Ga -citrate	24	0.06	24.12	23.13 \pm 1.89	75.88	76.87 \pm 1.89
^{67}Ga -citrate	48	0.06	21.52	20.37 \pm 2.37	78.48	79.65 \pm 2.37

The statistical significance ($P < 0.05$) of the T with NT of ^{67}Ga -citrate and IHP ^{99m}Tc -EC-DG (KF) of each time interval is also provided in Table 5.11. The Wilcoxon test was used to calculate the P -value of the T with the NT % biodistribution at 0.1-, 1-, 2-, 3-, 4- and 6 h post administration for the IHP ^{99m}Tc -EC-DG and for ^{67}Ga -citrate at 24- and 48 h post administration. A P value < 0.05 (red values) was considered statistically significant. There was an insignificant ($P = 0.06$) difference between the biodistribution of the T (sterile IFI/IF) with the NT (healthy) for IHP ^{99m}Tc -EC-DG (KF) and ^{67}Ga -citrate in IFI/IF for five rabbits ($n=5$) at the different imaging time intervals (Table 5.11). ^{67}Ga -citrate is used in clinical practice for the diagnosis of IFI/IF in many countries, even though there might not be a statistical significant difference between the T and NT area, the diagnosis of sterile IFI/IF could still be made visually. IHP ^{99m}Tc -EC-DG like ^{67}Ga -citrate, did not have a statistical significant difference of the T with the NT, but can also be interpreted as an area of accumulation in sterile IFI/IF. IHP ^{99m}Tc -EC-DG as possible diagnostic radiopharmaceutical should be investigated in humans as it could identify induced sterile IFI/IF in rabbits.

Table 5.12 indicates the target-to-non-target (T/NT) ratios that represent the mean of the T uptake divided by the mean of the NT uptake. The T/NT ratios at 0.1-, 1-, 2-, 3-, 4- and 6 h post administration is given, as well as the target-to-non-target (T/NT) ratios of ^{67}Ga -citrate at 24- and 48 h post administration. The mean values of the T/NT ratios of the IHP $^{99\text{m}}\text{Tc}$ -EC-DG (0.1-6 h) and ^{67}Ga -citrate from (24- and 48 h) are calculated as follows: 1.81 ± 0.10 , 1.77 ± 0.17 , 2.02 ± 0.13 , 2.00 ± 0.10 , 2.01 ± 0.12 and 2.28 ± 0.14 at 0.1-, 1-, 2-, 3-, 4- and 6 h after IHP $^{99\text{m}}\text{Tc}$ -EC-DG administration.

At 24- and 48 h the T/NT ratio of ^{67}Ga -citrate T/NT was 3.47 ± 0.45 and 4.30 ± 0.86 . The highest T/NT for IHP $^{99\text{m}}\text{Tc}$ -EC-DG and ^{67}Ga -citrate was found at 6- and 48 h respectively.

TABLE 5.12: T/NT ratios of IHP $^{99\text{m}}\text{Tc}$ -EC-DG and ^{67}Ga -citrate of sterile IFI/IF thigh muscles in rabbits ($n=5$) at different time intervals

Rabbit no.	IHP $^{99\text{m}}\text{Tc}$ -EC-DG						^{67}Ga -citrate	
	T/NT ratio						T/NT ratio	
	0.1 h	1 h	2 h	3 h	4 h	6 h	24 h	48 h
1	1.61	1.45	1.86	1.73	1.81	1.94	3.00	3.01
2	1.62	1.57	2.12	2.04	2.25	2.44	5.22	7.68
3	2.13	2.37	2.44	2.33	2.25	2.75	3.32	3.21
4	1.73	1.53	1.64	1.84	1.66	2.14	2.67	3.65
5	1.95	1.94	2.06	2.04	2.08	2.16	3.15	3.98
Mean \pm SEM	1.81 ± 0.10	1.77 ± 0.17	2.02 ± 0.13	2.00 ± 0.10	2.01 ± 0.12	2.28 ± 0.14	3.47 ± 0.45	4.30 ± 0.86

The highest T/N ratio was 2.28 ± 0.14 for IHP $^{99\text{m}}\text{Tc}$ -EC-DG at 6 h post administration and 4.30 ± 0.86 for ^{67}Ga -citrate at 48 h post administration (Table 5.12). ^{67}Ga -citrate had the highest T/NT of the two RP at 48 h post administration (4.30 ± 0.86).

The SQ (3 – severely increased biodistribution) and SQUAL (positive) results for ^{67}Ga -citrate (Table 5.10) compared to the quantitative results (Table 5.11 and -5.12) obtained, but differences were obtained with IHP $^{99\text{m}}\text{Tc}$ -EC-DG relating to the optimal imaging time point. The SQ value of 3 obtained for IHP $^{99\text{m}}\text{Tc}$ -EC-DG biodistribution to the area of sterile IFI/IF was the highest at 0.1 h and the quantitative results found the 6 h post radiopharmaceutical administration as the highest biodistribution to sterile IFI/IF area. The bladder was fuller on the 6 h images (Figure 5.19F) than at 0.1 h (Figure 5.19A) and this could have influenced the visual reporting of the images. The

bladder was not masked out for the reporting of the scintigraphic images. There were also no significant differences between the biodistribution of the 0.1 h (64.18 ± 1.23) and the 6 h (69.34 ± 1.27) biodistribution of the IHP ^{99m}Tc -EC-DG (KF).

5.4 KEY FINDINGS – HEALTHY AND IFI/IF RABBIT MODELS

5.4.1 Healthy rabbit model

The normal areas of increased biodistribution of $^{99m}\text{TcO}_4^-$ in humans are the salivary glands, stomach and thyroid (Harper *et al.* 1965:101). The healthy rabbits administered with $^{99m}\text{TcO}_4^-$ showed low uptake to the stomach (Figure 5.13B) and high uptake to the liver (5.12A) due to interspecies differences. The normal uptake to thyroid and salivary glands of $^{99m}\text{TcO}_4^-$ in healthy rabbits show similar uptake to humans and baboons (Chapter 6). The biodistribution of IHP ^{99m}Tc -EC-DG in healthy rabbits was statistically different from $^{99m}\text{TcO}_4^-$ but showed similar high uptake to the liver (5.12A). The first $^{99m}\text{TcO}_4^-$ eluent of the day was used and no other radiopharmaceuticals were labelled during this research, thereby limiting biodistribution discrepancies.

5.4.2 IFI/IF rabbit models

Figure 5.22 shows a comparison of the two IFI/IF (septic and sterile) models of rabbits. It should be taken into account that two different formulations of IHP ^{99m}Tc -EC-DG were used and a direct comparison could not be made with *P*-values. Higher ratios were observed for IHP ^{99m}Tc -EC-DG in the septic IFI/IF before 1 hour after administration as compared to IHP ^{99m}Tc -EC-DG in sterile IFI/IF in rabbits. The highest T/NT ratio for the two IFI/IF models administered with IHP ^{99m}Tc -EC-DG was found at 6 hours in the sterile IFI/IF induced area. The T/NT ratio for IHP ^{99m}Tc -EC-DG (KF) did not show significant biodistribution differences between 1-4 hours to the septic and sterile IFI/IF areas. Overall ^{67}Ga -citrate had highest T/NT ratio (in septic IFI/IF model) compared with the two formulations of IHP ^{99m}Tc -EC-DG for the different IFI/IF models. The T/NT ratios were higher in the bacterial induced IFI/IF for ^{67}Ga -citrate compared to the IFI/IF induced with zymosan for both (Figure 5.19).

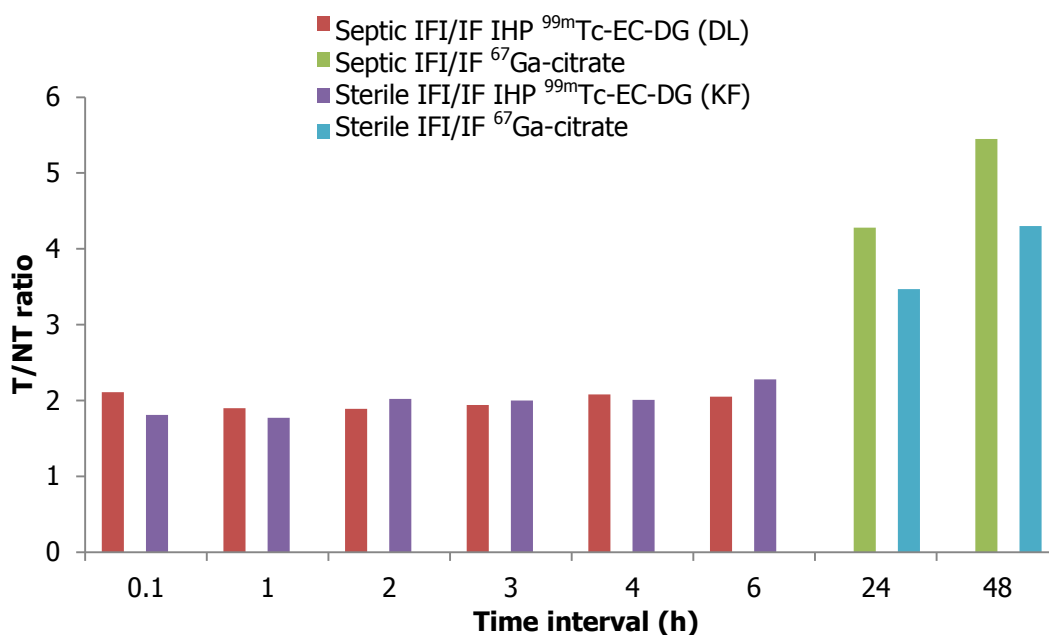


FIGURE 5.22: T/NT ratios of IHP ^{99m}Tc-EC-DG and ⁶⁷Ga-citrate of septic- and sterile IFI/IF thigh muscles in rabbits at different time intervals

Zymosan induces a granulocyte rich immune response (Oyen *et al.* 2001:153) by stimulation of dendritic cells that activates secretion of interleukin-10 (Rosenzwajg, Jourquin, Tailleux and Gluckman 2002:1186; Dillon *et al.* 2006:916). In this research zymosan was used as a representative of a basic fungi model (Rosenzwajg, Jourquin, Tailleux and Gluckman 2002:1181) of IFI/IF where interaction of IHP ^{99m}Tc-EC-DG and ⁶⁷Ga-citrate can be evaluated. There is a variety of mechanisms involved with the biodistribution of ⁶⁷Ga-citrate in IFI/IF, where these include forming complexes with transferrin and can bind to lactoferrin, bacterial siderophores, inflammatory proteins and cell walls (Mettler & Guiberteau 2012:406). This can be an explanation as to why the ⁶⁷Ga-citrate biodistribution indicated a higher biodistribution in septic (*E. coli*) compared to the sterile (zymosan – fungi) IFI/IF, because it not only binds to leucocytes but also to bacterial siderophores present in the septic IFI/IF area. The IHP ^{99m}Tc-EC-DG mainly binds to leucocytes as there was no significant difference between septic and sterile IFI/IF biodistribution thereof and this is evident as the sterile IFI/IF was mainly a granulocyte activating IFI/IF animal model.

5.5 SIDE-EFFECTS OF IHP ^{99m}Tc -EC-DG IN HEALTHY AND IFI/IF INDUCED RABBITS

No anaphylactic reactions were observed with IHP ^{99m}Tc -EC-DG (DL and KF) in all the rabbits studied for biodistribution and IFI/IF. No animals died during the acquisition protocol or during the 7 days after completion of the experiments.

5.6 DISCUSSION

According to literature $^{99m}\text{TcO}_4^-$ has been evaluated as a radionuclide marker of pulmonary aspiration of gastric contents of rabbits (Irwin *et al.* 1988:1270-1275) using only planar imaging. No literature could be found on the normal biodistribution of $^{99m}\text{TcO}_4^-$ in rabbits. The anatomy as provided by these authors (Figure 5.23) did not correlate with the CT topogram (Figure 2.16), the reason being that only planar imaging was performed. Irwin *et al.* (1988:1272) reported the stomach has high uptake which differs from our findings where the liver shows a very high uptake relative to minimal uptake in the stomach. The position of the stomach used in this research correlates to a PET image of New Zealand White rabbit (Figure 5.24) by Tsao *et al.* (2011:5).

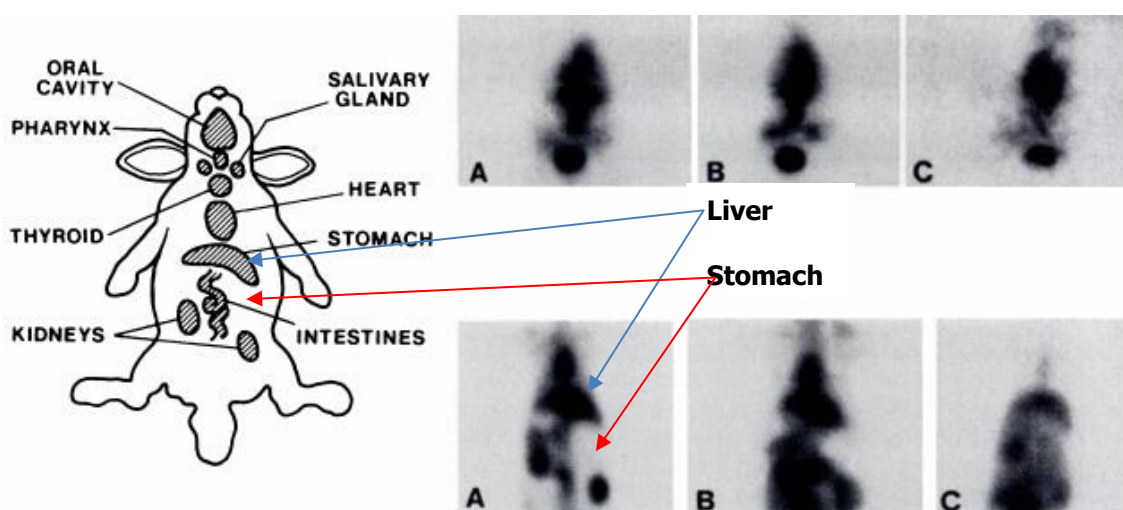


FIGURE 5.23: The schematic whole-body image of the anatomy and scintigraphic images provided by Irwin *et al.* (1988:1271) on the normal biodistribution of $^{99m}\text{TcO}_4^-$ in a New Zealand White rabbit. The images at various time points (A=1 h, B=4 h and C=24 h) demonstrate the head and neck regions (top panel) and the thoracic and abdominal regions (bottom panel).

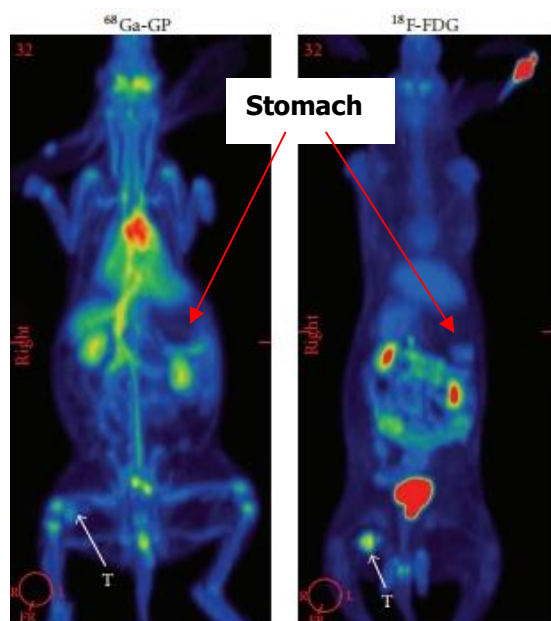


FIGURE 5.24: PET whole-body image of a New Zealand White Rabbit (Tsao *et al.* 2011:5)

5.7 CONCLUSION

Differences were observed in the normal biodistribution of $^{99m}\text{TcO}_4^-$ in rabbits compared to the normal biodistribution described in the literature of humans (Harper *et al.* 1965:101 and baboons (Chapter 6). The areas of increased normal uptake of IHP $^{99m}\text{Tc-EC-DG}$ was observed to the myocardium (early), liver, intestines (late), with relatively fast radiopharmaceutical excretion from the kidneys into the bladder. No significantly increased uptake of IHP $^{99m}\text{Tc-EC-DG}$ was found to the brain and the stomach. $^{67}\text{Ga-citrate}$ gave better results than IHP $^{99m}\text{Tc-EC-DG}$ to visualise IFI/IF, yet the latter compared favourably in both the sterile and septic IFI/IF rabbit model. The IHP $^{99m}\text{Tc-EC-DG}$ may not be as sensitive to IFI/IF as $^{67}\text{Ga-citrate}$, since uptake was mainly dependent on cell infiltration. It could be used to localise IFI/IF especially when the latter has high cellular response e.g. abscess formation.

CHAPTER 6

RESEARCH PHASE THREE: THE BABOON MODEL

6.1 INTRODUCTION

The normal biodistribution pattern of IHP ^{99m}Tc -EC-DG in healthy animals at various scintigraphic imaging time intervals had to be evaluated as part of the aim. The IHP ^{99m}Tc -EC-DG had to be compared with $^{99m}\text{TcO}_4^-$ to confirm also the *in vivo* biodistribution stability. Two labelling techniques was also used during this research and it needed to be determined if any biodistribution differences could be noted when scintigraphic imaging was performed. The baboon model was ideal for this, as it resemblances the human physiology and the same scintigraphic equipment used for human could be used for baboons (Dormehl, Hugo & Beverley 1992:109).

The research design was two-fold (Figure 6.1 for the research design). A complete literature review (Chapter 2) was carried out relating to ^{99m}Tc -EC-DG, $^{99m}\text{TcO}_4^-$, animal models for radiopharmaceutical toxicity testing and the baboon model. The prospective *in vivo* study was done on seven (12-15 kg) baboons (*Papio ursinus*) obtained from the Animal Research Centre (UFS) and were imaged at the DNM at UAH. Male and female baboons were used. Research phase three was divided into three different groups (illustrated in Figure 6.1) in order to answer the research questions.

The uptake of IHP ^{99m}Tc -EC-DG (KF), IHP ^{99m}Tc -EC-DG (DL) and $^{99m}\text{TcO}_4^-$ (control group) was determined in different organs at specific time points. The radionuclide and radiopharmaceutical dosages for the $^{99m}\text{TcO}_4^-$, (DL) and (KF) of IHP ^{99m}Tc -EC-DG for the healthy baboons are summarized in Table 6.1. The protocol that was designed, tried to limit the imaging time intervals to a minimum without losing statistical data in order to ensure as little as possible discomfort to baboons by reducing anesthetic time.

6.2 MATERIALS AND METHODS

6.2.1 Sample size

The statistical and economic considerations were taken into account to determine the sample size of phase three. The sample included six male and one female baboons (Figure 6.1 and Figure 6.2). As there were only a limited amount of baboons at the UFS Animal Research Centre available for research purposes, the baboons were used twice for the different sections of phase three.

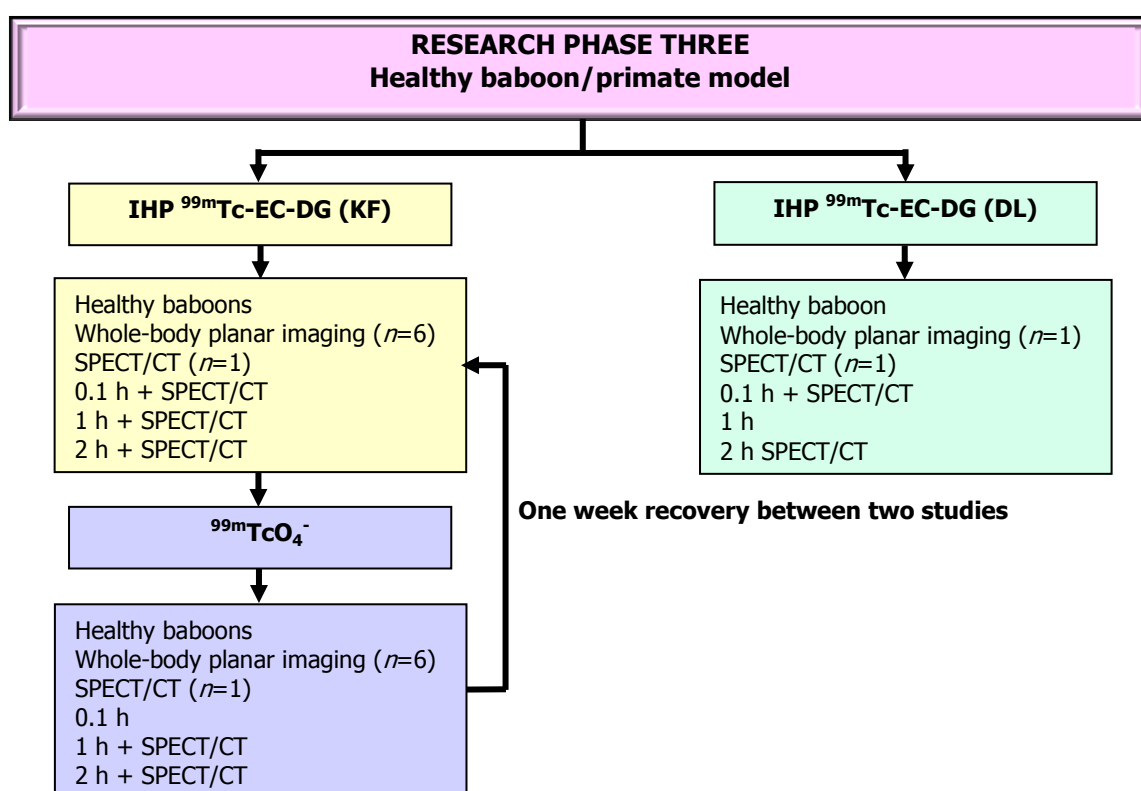


FIGURE 6.1: Research design for phase three with healthy baboons as animal model



FIGURE 6.2: One of the baboons used for phase three with two of the research personnel

6.2.2 Radiosynthesis of ^{99m}Tc -EC-DG (DL) and -(KF)

The radiolabelling of IHP ^{99m}Tc -EC-DG (DL) was achieved for administration to the healthy baboons according to the procedure described in section 3.3.5.3 (Chapter 3). The IHP ^{99m}Tc -EC-DG (KF) was radiolabelled as described in section 3.3.5.4.

6.2.3 Gamma scintigraphy studies

6.2.3.1 Normal biodistribution

Each of the healthy baboons were injected intravenously with either IHP ^{99m}Tc -EC-DG, prepared according to the direct labelling ($n=1$) or kit formulation procedure ($n=6$), or $^{99m}\text{TcO}_4^-$ ($n=6$). The dose administered was 296 MBq per animal in 0.2 cm^3 (Table 6.1).

TABLE 6.1: Summary of radionuclide and radiopharmaceutical dosages administered to the healthy baboons in phase three

Study group	Radionuclide/RP administered	Number of baboons (n)	Injected dose (MBq/baboon)
Healthy baboons	IHP ^{99m}Tc -EC-DG (KF)	6	265.46 ± 27.82
Healthy baboons	$^{99m}\text{TcO}_4^-$	6	343.07 ± 59.80
Healthy baboon	IHP ^{99m}Tc -EC-DG (DL)	1	276.3

The baboons were sedated using ketamine (15 mg/kg) intramuscular as needed. Only males were catheterised with a Foley catheter No.8 passed through the urethra into the bladder. The imaging was performed with the Siemens Symbia T SPECT/CT dual head gamma camera equipped with a LEHR parallel-hole collimator using parameters listed in Table 6.2. The baboon groups were immobilised in the supine position on the camera bed. Whole-body scanning (ANT and POST) at 15 cm per minute with scintigraphic images acquired at 0.1-, 1- and 2 h post administration of ^{99m}Tc -EC-DG [both (DL) and (KF)] and $^{99m}\text{TcO}_4^-$. One baboon of each group also received a low dose whole-body SPECT/CT (Figure 6.3) for IHP ^{99m}Tc -EC-DG (KF) at 0.1-, 1- and 2 h, the IHP ^{99m}Tc -EC-DG (DL) at 0.1- and 2 h and for $^{99m}\text{TcO}_4^-$ at 1- and 2 h.

TABLE 6.2: Siemens SYMBIA camera parameters for the two-bed SPECT imaging

SPECT camera parameter	Setting
Window settings - $^{99m}\text{TcO}_4^-$	140 keV (15%)
Matrix size	128 x 128
Zoom	1
Degrees of Rotation per detector	180
Time per views in seconds	7
Number of views per detector	90
Orbit	Noncircular
Mode	Continuous
Number of scans	2
Scan 1 Label	Chest Bed 1
Scan 2 Label	Abdomen Bed 2
Pause between Scans	No
Scan Direction	Scan out

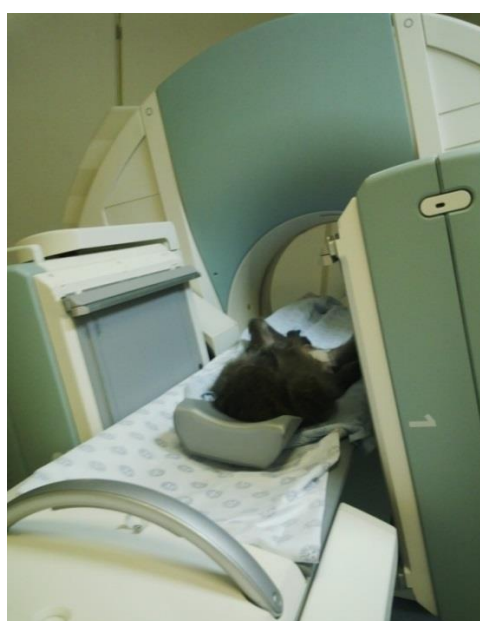


FIGURE 6.3: One of the baboons that received a SPECT/CT during phase three

The normal biodistribution of $^{99m}\text{TcO}_4^-$ ($n=6$) in healthy baboons had to be determined as no literature could be found about the normal scintigraphic imaging biodistribution of $^{99m}\text{TcO}_4^-$ in healthy baboons (control group).

6.2.4 Data analysis

6.2.4.1 *Quantitative analysis of the image of healthy baboons*

The Department of Medical Physics were consulted for recommendations regarding the management of data and the processing of results. The Department of Biostatistics performed the statistical data analysis. Biodistribution of the IHP $^{99m}\text{Tc-EC-DG}$ (KF), $^{99m}\text{TcO}_4^-$ and IHP $^{99m}\text{Tc-EC-DG}$ (DL) were determined in the same way, firstly the total body counts were determined by drawing the ROIs over the image of the entire baboon. To determine the uptake (counts) of the different radiopharmaceuticals in the organs, ROIs were drawn over the organs including the brain, heart, both kidneys (RH and LT separate ROIs), both lungs (RH and LT separate ROIs), skin, muscle, stomach, left knee joint, urinary bladder and the injection site in the images taken at 0-, 1- and 2 h. At the time when adjacent organs were examined, the maximum display range was firstly set at low and was increased gradually until the organs could be well visualized and yet remain distinct. The percentage uptake of the injected activity by these organs at various time intervals was calculated as: organ counts at a specific time per total body counts at that time. All values were expressed as the mean \pm SEM.

6.2.4.2 *SQ and SQUAL analysis*

The same SQ and SQUAL data interpretation form design was used to rate the biodistribution to specific major organs of research phase three (section 5.2.4.3). The biodistribution of $^{99m}\text{TcO}_4^-$, IHP $^{99m}\text{Tc-EC-DG}$ (DL) and IHP $^{99m}\text{Tc-EC-DG}$ (KF) in the main organs of healthy baboons were evaluated by using the information obtained for the image interpretation form and used to confirm observations made from other quantitative results. The statistical analysis of research phase three was performed by the Department of

Biostatistics of the UFS. The Sign Ranked test for paired data was calculated for the differences between variables.

6.3 RESULTS AND DISCUSSION

6.3.1 Healthy Baboon Model

6.3.1.1 Radiosynthesis of $^{99m}\text{Tc-EC-DG (KF)}$ and $^{99m}\text{Tc-EC-DG (DL)}$

$^{99m}\text{TcO}_4^-$ was used to label EC-DG with the direct labelling technique and for the kit formulation as described in Chapter 3 (section 3.3.5.3 & 3.3.5.4) to achieve different labelling formulations of IHP $^{99m}\text{Tc-EC-DG}$. The QC results for the IHP $^{99m}\text{Tc-EC-DG (KF)}$ and the IHP $^{99m}\text{Tc-EC-DG (DL)}$ of research phase three are reported in this section.

The labelling of the IHP $^{99m}\text{Tc-EC-DG}$ with the direct labelling method and the IHP $^{99m}\text{Tc-EC-DG (KF)}$ were performed in a laminar flow cabinet in Type B hot laboratory. The complexation of the EC-DG with freshly eluted $^{99m}\text{TcO}_4^-$ (1480 MBq in 0.5 ml) was carried out at a pH 4. The radiochemical purity of the IHP $^{99m}\text{Tc-EC-DG (KF)}$ and IHP $^{99m}\text{Tc-EC-DG (DL)}$ complex were assessed with ITLC chromatography as described in chapter 3 (section 3.3.3.5). QC was performed directly after completion of the labelling of the $^{99m}\text{Tc-EC-DG (KF)}$ and the $^{99m}\text{Tc-EC-DG (DL)}$. TLC analyses of radiochemical purity of IHP $^{99m}\text{Tc-EC-DG (KF)}$ and (DL) was more than 90% (Whatman/acetone) with less than 1% colloidal formation (ITLC-SC/saline). The final pH was 7 for the both IHP $^{99m}\text{Tc-EC-DG}$ labelling techniques. The HPLC-QC could not be performed on the IHP $^{99m}\text{Tc-EC-DG}$ used for research phase three, as the equipment necessary was not available at the DNM at UAH.

6.3.1.2 *In vivo normal biodistribution images*

In this section the biodistribution results of IHP $^{99m}\text{Tc-EC-DG (KF)}$ in healthy baboons for research phase three is given for 0.1-, 1- and 2 h post radiopharmaceutical administration. Anterior (ANT) and posterior (POST)

whole-body planar images of the normal biodistribution of IHP ^{99m}Tc -EC-DG (KF) in a healthy baboon at 0.1-, 1- and 2 h post administration were obtained (Figure 6.4). Specific organs of interest are indicated with the different types and colour arrows.

Optimal whole-body images were obtained immediately (0.1 h) after IHP ^{99m}Tc -EC-DG (KF) administration, followed by delayed imaging at 1- and 2 h. Good target-to-background ratio was noted on all three imaging time intervals. The 0.1 h images of the baboons demonstrated increased IHP ^{99m}Tc -EC-DG biodistribution in the peri-nasal (snout) area which decreased over time to only background activity on the 2 h delayed images, this corresponds to blood pool activity. The long snout area of the baboons is vascular (Swindler & Wood 1982:60) and could explain the intense increase of IHP ^{99m}Tc -EC-DG activity at 0.1 h. Well-defined intense increased excretion of IHP ^{99m}Tc -EC-DG was observed in the kidneys on all the whole-body imaging time points. The bladder demonstrated intense increased IHP ^{99m}Tc -EC-DG (KF) activity on all three whole-body images acquired at different time intervals. The activity in the bladder is due to excretion by the kidneys, this was already evident early on the 0.1 whole-body images (Figure 6.4). The carbonylglycine present in IHP ^{99m}Tc -EC-DG interacts with the renal tubular transport proteins increasing radiopharmaceutical excretion by the kidneys (Vanbilloen, Cleynhens & Verbruggen 2000:207). No obvious biodistribution was observed in the skin areas (ears) this fall in line with background activity in the rest of the whole-body of the baboons. The 0.1 h whole-body images demonstrated no RP biodistribution to the area of the intestines. An area of increasing activity could be seen in the area of the intestines from the 1 h to the 2 h whole-body. Mild increased radiopharmaceutical uptake was noted in the joints, specifically the hand- and knee joints. These uptakes are only mildly increased in comparison to the background activity. Background radiopharmaceutical activity was noted in the region of the muscles with no well-defined increased uptake. The baboons were passive the day before the experiment. Muscle and brown fat uptake can be seen in other glucose metabolic imaging agents like ^{18}F -FDG due to the increased glucose consumption of muscles during exercise or exposure to cold temperatures.

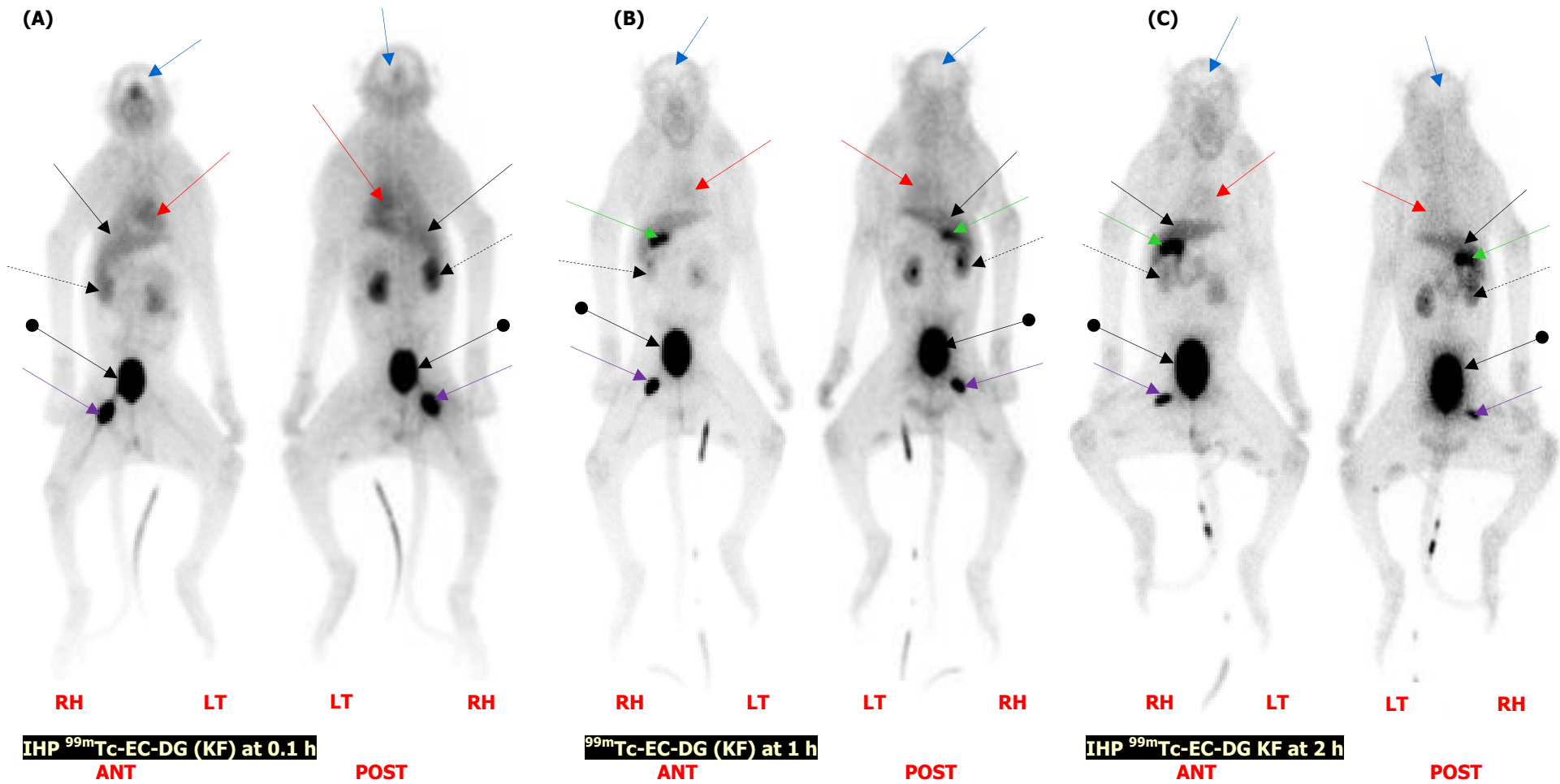


FIGURE 6.4: Biodistribution of IHP ^{99m}Tc -EC-DG (KF) in healthy baboons at (A) 0.1-, (B) 1- and (C) 2 hour post administration

Liver	←	Gallbladder	←	Injection site	←	Brain	←
Kidney	←	Urinary bladder	←	Stomach	←	Heart	←

There was no IHP ^{99m}Tc -EC-DG uptake in the region of the stomach. No early bloodpool activity was observed in the lungs on the whole-body at 0.1 h and uptake of IHP ^{99m}Tc -EC-DG (KF) was also absent on images acquired later. There was no RP uptake noted in the region of the brain, even less compared to that of background. No IHP ^{99m}Tc -EC-DG (KF) uptake was noted on the 0.1 to 2 h images in the region of the neck area where the thyroid and salivary glands (parotid glands) can be found, indicating limited amount of free $^{99m}\text{TcO}_4^-$. Intense increased blood pool activity was noted in the heart on the 0.1 h whole-body images and was still evident on the 2 h images confirming biodistribution of IHP ^{99m}Tc -EC-DG to the heart. Notable intense increased IHP ^{99m}Tc -EC-DG (KF) uptake was present in the liver at 0.1 h, correlating with bloodpool activity that decreased slightly towards the 2 h whole-body image. No radiopharmaceutical uptake was observed in the region of the spleen and region of the stomach on all the whole-body images acquired at different time intervals. A well-defined gallbladder was observed on the 1 h whole-body images (Figure 6.4B), increasing in visibility on the 2 h whole-body image. Clear excretion from the gallbladder into the intestines was visible on the 2 h whole-body images of all the baboons administered with IHP ^{99m}Tc -EC-DG (KF). A focal area of intense increased radiopharmaceutical activity was noted in the RH inguinal fossa, decreasing significantly over time. This correlates with the site of IHP ^{99m}Tc -EC-DG (KF) administration.

Figure 6.5, Figure 6.6 and Figure 6.7 show the co-registered SPECT/CT (transverse, sagittal and coronal) images of healthy baboons acquired at 0.1-, 1- and 2 h post administered of the IHP ^{99m}Tc -EC-DG (KF) SPECT/CT images. The SPECT/CT provided additional anatomical and physiological information about exact biodistribution of the IHP ^{99m}Tc -EC-DG (KF) to the different organs and tissue in healthy baboons. Excretion through the kidneys to the bladder was evident by the intense IHP ^{99m}Tc -EC-DG (KF) activity present in the bladder on the 0.1-, 1- and 2 h SPECT/CT images. No IHP ^{99m}Tc -EC-DG uptake was observed in the region of the skeleton. Mild increased IHP ^{99m}Tc -EC-DG uptake was noted in the joints, specifically the hand- and knee joints. This radiopharmaceutical uptake are only mildly more than that of background activity and was also seen on the whole-body images.

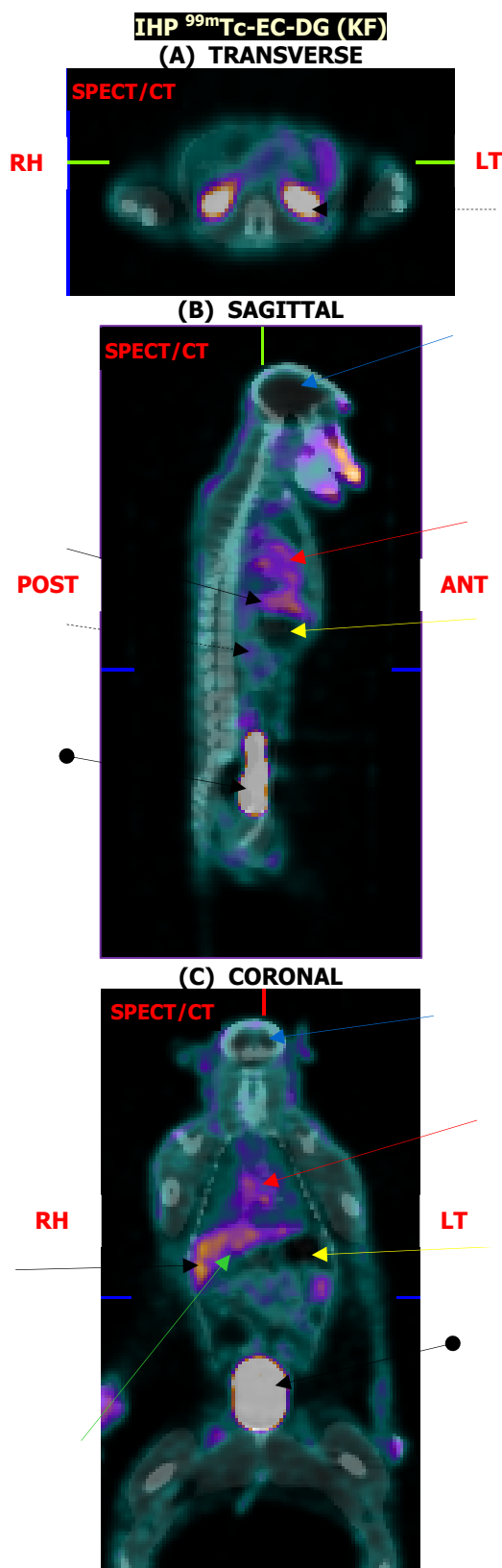


FIGURE 6.5: SPECT/CT (A) transverse, (B) sagittal and (C) coronal images post IHP ^{99m}Tc -EC-DG (KF) administration acquired at 0.1 hour post radiopharmaceutical administration. Liver (solid arrow), kidney (dashed arrow), urinary bladder (ball arrow), stomach (yellow arrow), heart (red arrow) and gallbladder (green arrow) are well outlined. The injection site (purple arrow) is also visible and no brain uptake (blue arrow).

Liver	←	Gallbladder	←	Injection site	←	Brain	←
Kidney	←	Urinary bladder	←	Stomach	←	Heart	←

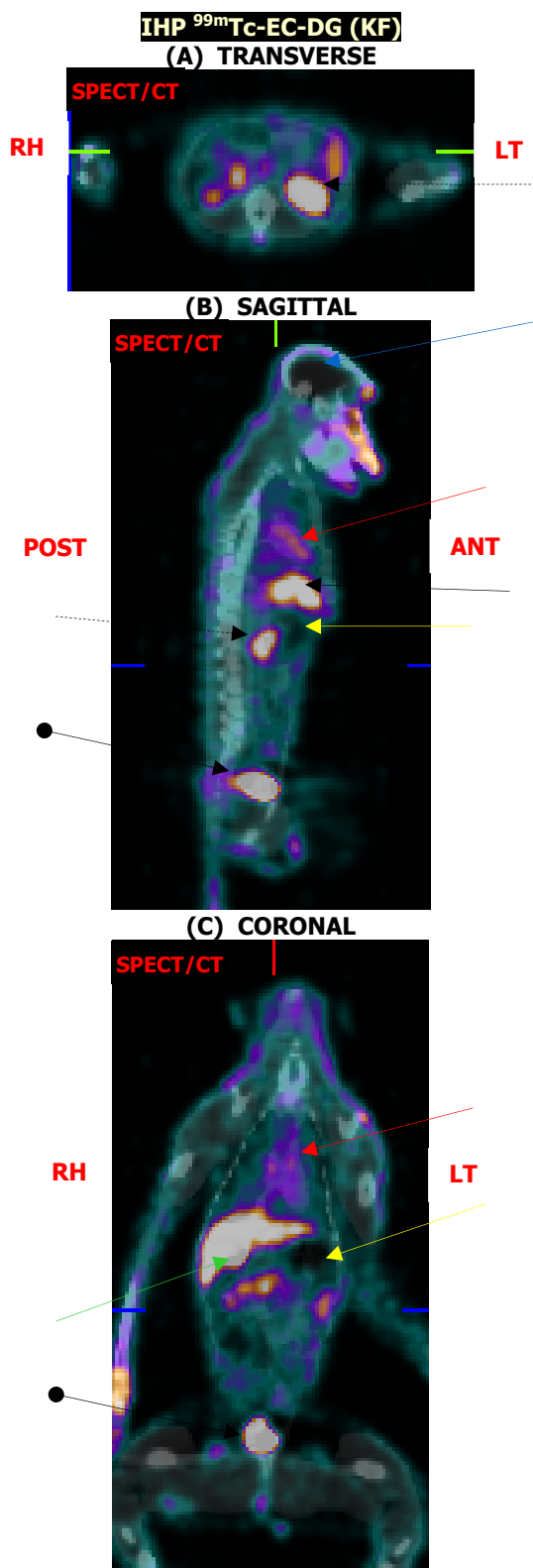


FIGURE 6.6: Co-registered SPECT/CT at 1 hour (A) transverse, (B) sagittal and (C) coronal images of healthy baboons acquired post IHP ^{99m}Tc -EC-DG (KF) administration

Liver	←	Gallbladder	←	Injection site	←	Brain	←
Kidney	←	Urinary bladder	←	Stomach	←	Heart	←

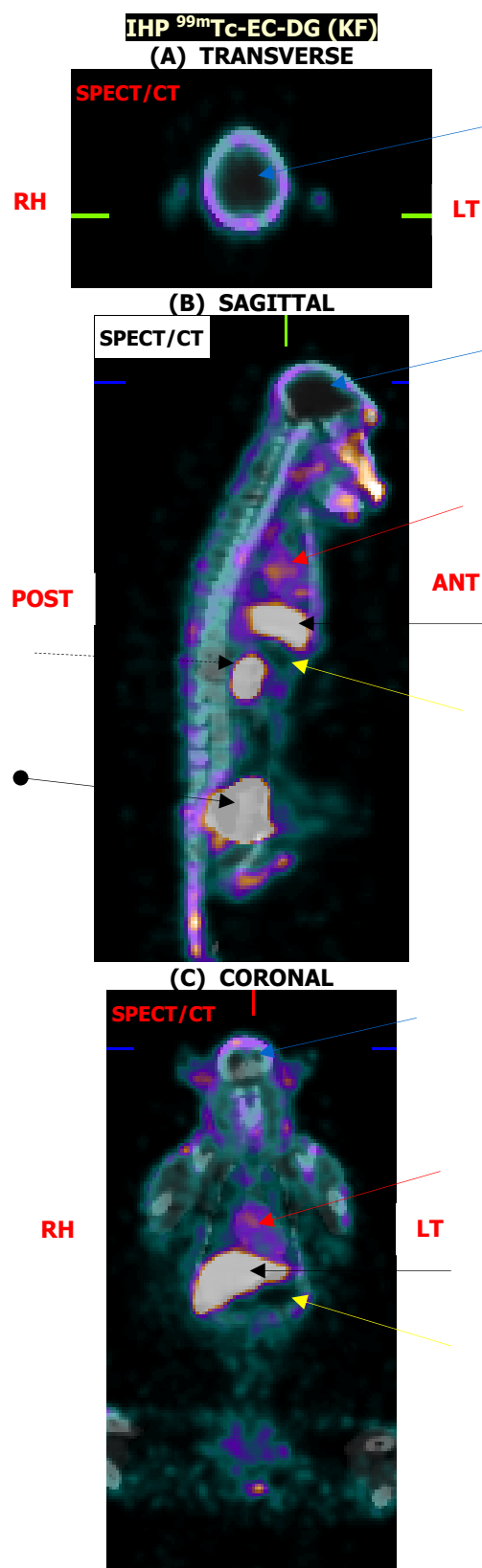


FIGURE 6.7: SPECT/CT (A) transverse, (B) sagittal and (C) coronal images acquired at 2 hour post administration of IHP ^{99m}Tc -EC-DG (KF)

Liver	←	Gallbladder	←	Injection site	←	Brain	←
Kidney	←	Urinary bladder	←	Stomach	←	Heart	←

The 0.1-, 1- and 2 h SPECT/CT images of IHP ^{99m}Tc -EC-DG (KF) demonstrated no uptake in the lungs. No radiopharmaceutical uptake in the brain was observed on any of the three SPECT/CT scans. Increased IHP ^{99m}Tc -EC-DG (KF) bloodpool activity in the heart was observed on the 0.1 h SPECT/CT, and biodistribution was evident on the 1- and 2 h SPECT/CT scans, confirming biodistribution of IHP ^{99m}Tc -EC-DG (KF) to the heart. Well-defined increased uptake was noted in the liver on the 0.1 h SPECT/CT; decreasing slightly towards 2 hours.

No RP uptake could be seen in the area of the spleen on all three SPECT/CT scans performed on different time intervals. Intense increased IHP ^{99m}Tc -EC-DG (KF) uptake was noted early on in the kidneys and was still present at 2 h post RP administration. No increased uptake was seen in the region of the stomach on the 0.1-, 1- and 2 h SPECT/CT scans. No uptake was observed in muscles, only background activity was visible on all SPECT/CT acquired scans at different time intervals. IHP ^{99m}Tc -EC-DG (KF) uptake in the gallbladder was observed on the 0.1 h SPECT/CT (not on the 0.1 h planar whole-body) and increased intensity on the 1-2 h SPECT/CT view. Excretion of IHP ^{99m}Tc -EC-DG (KF) from the gallbladder into the intestines was present on the 1- and 2 h SPECT/CT images. Biodistribution of IHP ^{99m}Tc -EC-DG (KF) to the snout (nasal area) of the baboons was observed on the 0.1-, 1- and 2 h SPECT/CT scans. The snout area is vascular and has a complex drainage pattern (Swindler & Wood 1982:60).

6.3.1.3 SQ and SQUAL analysis

The planar whole-body and SPECT/CT images were reported on, by the same nuclear medicine physician as used for research phase two. The same data interpretation form with the four-point grading scale (0 to 4) was used. SQ and SQUAL indicative factors were also reported on for biodistribution of IHP ^{99m}Tc -EC-DG (KF) to the different organs at specific time intervals. The SQ and SQUAL results of the normal biodistribution of the IHP ^{99m}Tc -EC-DG (KF) to the different organs in healthy baboons, as reported by the nuclear medicine physician for the planar whole-body and SPECT/CT images is summarised in Table 6.3.

TABLE 6.3: The SQ and SQUAL planar whole-body- and SPECT/CT results of the biodistribution IHP ^{99m}Tc-EC-DG (KF) to the organs of healthy baboons

Organ/ tissue	Time interval (h)	IHP ^{99m} Tc-EC-DG (KF)					
		Static			SPECT/CT		
		<i>n</i>	SQUAL	SQ	<i>n</i>	SQUAL	SQ
Lungs	0.1	6	Bkg	0	1	Bkg	0
	1	6	Bkg	0	1	Bkg	0
	2	6	Bkg	0	1	Bkg	0
Liver	0.1	6	Post	2	1	Post	2
	1	6	Post	2	1	Post	2
	2	6	Post	2	1	Post	2
Stomach	0.1	6	Neg	0	1	Neg	0
	1	6	Neg	0	1	Neg	0
	2	6	Neg	0	1	Neg	0
Spleen	0.1	6	Neg	0	1	Neg	0
	1	6	Neg	0	1	Neg	0
	2	6	Neg	0	1	Neg	0
Kidneys	0.1	6	Post	3	1	Post	3
	1	6	Post	2	1	Post	3
	2	6	Post	2	1	Post	3
Thyroid	0.1	6	Neg	0	1	Neg	0
	1	6	Neg	0	1	Neg	0
	2	6	Neg	0	1	Neg	0
Muscle	0.1	6	Neg	0	1	Neg	0
	1	6	Neg	0	1	Neg	0
	2	6	Neg	0	1	Neg	0
Intestines	0.1	6	Bkg	1	1	Post	1
	1	6	Post	1	1	Post	1
	2	6	Post	2	1	Post	2
Brain	0.1	6	Neg	0	1	Neg	0
	1	6	Neg	0	1	Neg	0
	2	6	Neg	0	1	Neg	0
Bladder	0.1	6	Post	3	1	Post	3
	1	6	Post	3	1	Post	3
	2	6	Post	3	1	Post	3
Skin	0.1	6	Neg	0	1	Neg	0
	1	6	Neg	0	1	Neg	0
	2	6	Neg	0	1	Neg	0
Gallbladder	0.1	6	Post	2	1	Post	3
	1	6	Post	3	1	Post	3
	2	6	Post	3	1	Post	3
Heart	0.1	6	Post	2	1	Post	2
	1	6	Post	1	1	Post	1
	2	6	Post	1	1	Post	1
Skeleton	0.1	6	Neg	0	1	Neg	0
	1	6	Neg	0	1	Neg	0
	2	6	Neg	0	1	Neg	0
Joints	0.1	6	Post	1	1	Post	1
	1	6	Post	1	1	Post	1
	2	6	Post	1	1	Post	1
Salivary glands	0.1	6	Neg	0	1	Neg	0
	1	6	Neg	0	1	Neg	0
	2	6	Neg	0	1	Neg	0

The SQUAL results indicated background activity of IHP ^{99m}Tc-EC-DG (KF) to the lungs and muscles at the different time intervals. Positive SQUAL results were obtained for the gallbladder, joints, intestines, kidneys and the heart. The stomach, spleen, thyroid, skin, brain, skeleton and salivary glands gave negative SQUAL results. SQ values of 2-3 were allocated to the liver, kidneys and gallbladder. A SQ value of 1-2 was assigned to the intestines, heart and joints. A SQ value of 0 was allocated to the lungs, stomach, spleen, thyroid, muscle, brain, skin, skeleton and salivary glands.

6.3.1.4 Quantitative analysis of IHP ^{99m}Tc -EC-DG (KF) images

The activity in all organs and tissues was expressed as the percentage of the total body activity per organ and presented as the mean \pm SEM (for values obtained in $n=6$ baboons), at 0.1-, 1- and 2 h post IHP ^{99m}Tc -EC-DG (KF) administration. All the data was decay corrected to the time of IHP ^{99m}Tc -EC-DG (KF) administration. Table 6.4 gives the results of the normal biodistribution of the IHP ^{99m}Tc -EC-DG (KF) in healthy baboons with the statistical calculations performed. The median of the data for IHP ^{99m}Tc -EC-DG (KF) is also provided in Table 6.4. The median is not directly addressed in the data analysis, but only to provide a complete summary of the data obtained. The four organs with the highest uptake were highlighted in bold and the lowest uptake organs in blue.

The mean uptake values of the IHP ^{99m}Tc -EC-DG (KF) were the highest to the liver (5.14 ± 0.36), heart (4.41 ± 0.35), LT kidney (2.38 ± 0.30), RH kidney (2.30 ± 0.22) with excretion into the bladder (30.07 ± 5.83) of the healthy baboons (Table 6.4). The brain (0.17 ± 0.02), stomach (0.07 ± 0.01), skin (0.01 ± 0.00) and muscle (0.03 ± 0.00) demonstrated the lowest IHP ^{99m}Tc -EC-DG (KF) uptake in the healthy baboon at 2 h.

Analysis of the results primarily indicated that the biodistribution in the healthy baboons administered with IHP ^{99m}Tc -EC-DG (KF) for all the time intervals was the highest to the kidneys with excretion into the bladder, liver and the heart (Table 6.4). The uptake in the heart was probably due to the glucose uptake by the myocytes.

TABLE 6.4: Biodistribution of IHP ^{99m}Tc -EC-DG (KF) in healthy baboons

Organ/Tissue	Time interval h	Median	Mean \pm SEM
LT Lung	0.1	1.76	1.71 \pm 0.16
	1	0.80	0.82 \pm 0.07
	2	0.40	0.40 \pm 0.02
RT Lung	0.1	2.12	2.07 \pm 0.12
	1	1.03	1.07 \pm 0.06
	2	0.52	0.51 \pm 0.03
Liver	0.1	5.31	5.14 \pm 0.36
	1	3.50	3.36 \pm 0.40
	2	2.24	2.33 \pm 0.26
Stomach	0.1	0.20	0.23 \pm 0.05
	1	0.13	0.14 \pm 0.02
	2	0.07	0.07 \pm 0.01
LT Kidney	0.1	2.03	2.38 \pm 0.30
	1	1.02	1.08 \pm 0.11
	2	0.63	0.67 \pm 0.05
RH Kidney	0.1	2.18	2.30 \pm 0.22
	1	1.25	1.32 \pm 0.21
	2	0.74	0.71 \pm 0.05
Spleen	0.1	0.31	0.30 \pm 0.04
	1	0.16	0.18 \pm 0.03
	2	0.07	0.09 \pm 0.02
Large intestines	0.1	0.25	0.23 \pm 0.05
	1	0.19	0.17 \pm 0.02
	2	0.07	0.08 \pm 0.01
Small intestines	0.1	0.38	0.35 \pm 0.03
	1	0.21	0.21 \pm 0.03
	2	0.10	0.12 \pm 0.01
Brain	0.1	0.44	0.45 \pm 0.05
	1	0.27	0.29 \pm 0.03
	2	0.16	0.17 \pm 0.02
Heart	0.1	4.43	4.41 \pm 0.35
	1	1.74	1.75 \pm 0.17
	2	0.89	0.95 \pm 0.06
Nose	0.1	0.81	0.80 \pm 0.07
	1	0.38	0.38 \pm 0.02
	2	0.19	0.19 \pm 0.01
Mouth	0.1	1.54	1.65 \pm 0.20
	1	0.87	0.85 \pm 0.08
	2	0.45	0.47 \pm 0.05
Gallbladder	0.1	0.99	1.11 \pm 0.17
	1	1.18	1.19 \pm 0.12
	2	1.12	1.14 \pm 0.17
Skin	0.1	0.02	0.02 \pm 0.00
	1	0.02	0.02 \pm 0.00
	2	0.01	0.01 \pm 0.00
Muscle	0.1	0.10	0.11 \pm 0.01
	1	0.06	0.06 \pm 0.01
	2	0.03	0.03 \pm 0.00
Testes	0.1	0.21	0.21 \pm 0.05
	1	0.15	0.16 \pm 0.04
	2	0.08	0.08 \pm 0.02
Joint	0.1	0.29	0.31 \pm 0.02
	1	0.21	0.21 \pm 0.02
	2	0.15	0.15 \pm 0.01
Bladder	0.1	15.13	14.74 \pm 1.07
	1	29.20	28.45 \pm 4.26
	2	32.83	30.07 \pm 5.83

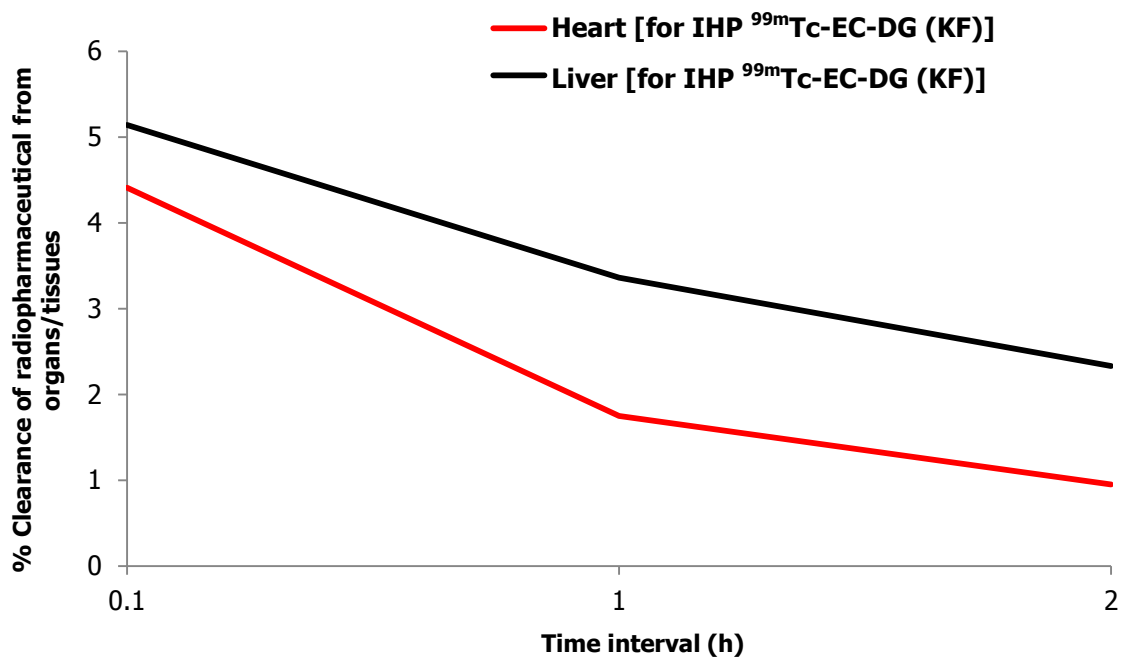


FIGURE 6.8: Clearance of highest uptake organs from *in vivo* results of IHP ^{99m}Tc -EC-DG (KF) in healthy baboons. Mean % biodistribution values for the liver and heart are shown with time.

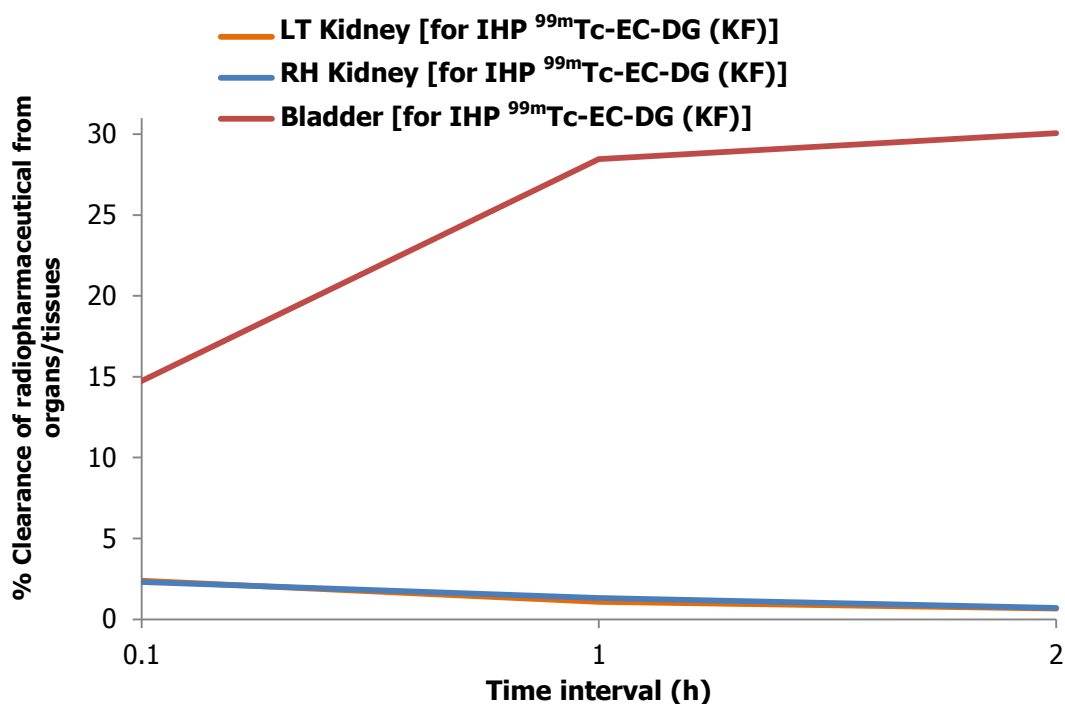


FIGURE 6.9: Clearance profile of IHP ^{99m}Tc -EC-DG (KF) excretion by kidneys into the bladder for healthy baboons

The highest rate of excretion of IHP ^{99m}Tc -EC-DG (KF) was obtained from the heart and the liver between 0.1 h and 1 h after administration (Figure 6.8). The high uptake of the IHP ^{99m}Tc -EC-DG by the kidneys (Figure 6.9) was

expected because the EC and EC-conjugates interact with renal tubules in the kidney (Zhang *et al.* 2012:6). Liver uptake decreased over time (Figure 6.8).

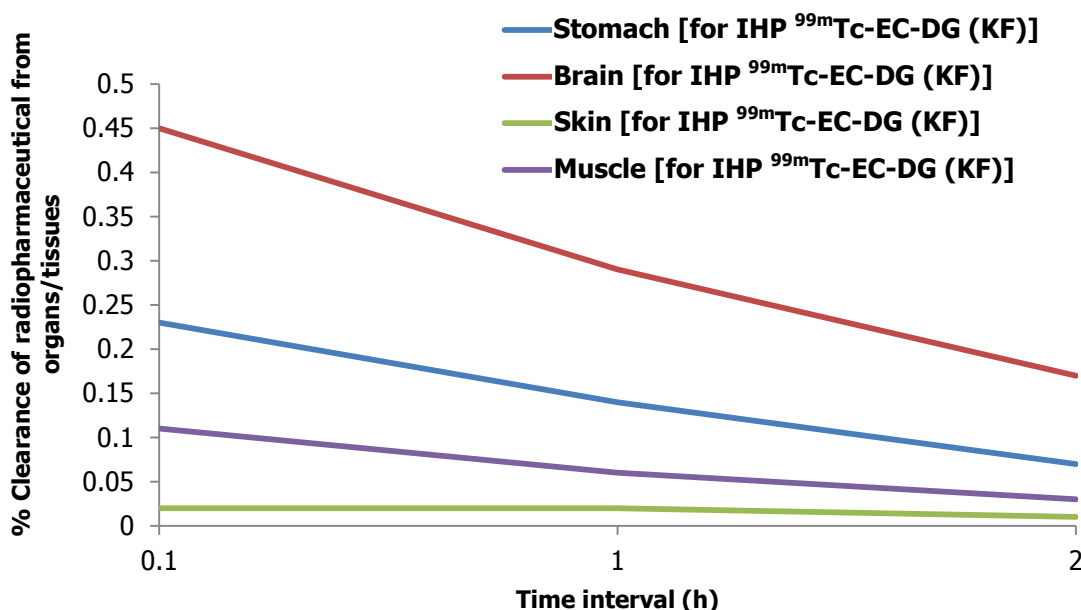


FIGURE 6.10: Clearance of lowest uptake organs from *in vivo* results of IHP ^{99m}Tc -EC-DG (KF) in healthy baboons. Mean % biodistribution values for the stomach, brain and skin are shown with time.

The brain, skin, stomach and muscle have the lowest IHP ^{99m}Tc -EC-DG (KF) uptake and a constant decrease in uptake was seen in the brain, stomach and muscle from 0.1-2 h (Figure 6.10). A minimal, slow decrease was seen in the skin only from 1-2 h (Figure 6.10). The low brain uptake of IHP ^{99m}Tc -EC-DG can be attributed to its hydrophilic characteristic that prevents it to cross the blood-brain barrier (Schechter *et al.* 2009:1590), as well as relatively larger molecular weight/size.

6.3.1.5 Comparison of IHP ^{99m}Tc -EC-DG (KF) with $^{99m}\text{TcO}_4^-$

The biodistribution-, statistical- and SQ and the SQUAL static and SPECT/CT image results of the normal biodistribution of $^{99m}\text{TcO}_4^-$ with the results of the IHP ^{99m}Tc -EC-DG (KF) at specific time intervals in healthy baboons are given in this section.

6.3.1.5.1 *In vivo normal biodistribution images*

Figure 6.11 and Figure 6.12 show an image comparison of the ANT and POST scintigraphic images of the biodistribution of $^{99m}\text{TcO}_4^-$ with IHP $^{99m}\text{Tc-EC-DG}$ (KF) in healthy baboons at 0.1-, 1- and 2 h post radiopharmaceutical administration. Figure 6.13 and Figure 6.14 show the SPECT/CT (transverse, sagittal and coronal) image comparison of the $^{99m}\text{TcO}_4^-$ with IHP $^{99m}\text{Tc-EC-DG}$ (KF) SPECT/CT at 1- and 2 h post administration. Radiopharmaceutical excretion of IHP $^{99m}\text{Tc-EC-DG}$ (KF) biodistribution and $^{99m}\text{TcO}_4^-$ was found to be via the kidneys into the bladder for all the baboons. The primary elimination path of $^{99m}\text{TcO}_4^-$ for the first three days after administration in humans is by the excretion from the kidneys into the bladder and this was similar for the baboons (Beasley *et al.* 1977:522). As with humans it was found that $^{99m}\text{TcO}_4^-$ localisation in the kidneys is low (Beasley 1966:1435). The localisation (visibility) of $^{99m}\text{TcO}_4^-$ to the kidneys were less than for the IHP $^{99m}\text{Tc-EC-DG}$ (KF) and the differences can be attributed to the EC complexes present in IHP $^{99m}\text{Tc-EC-DG}$ (KF) (Vanbilloen *et al.* 2000:213). The bladder size increased from the 0.1-2 h whole-body images, but the bladder filled slower in size with $^{99m}\text{TcO}_4^-$ than with the IHP $^{99m}\text{Tc-EC-DG}$ (KF). The kidneys were observed on the 0.5-2 h whole-body and SPECT/CT images and were less in intensity compared with the IHP $^{99m}\text{Tc-EC-DG}$ (KF) kidney uptake. The bladder size was quantified with ROI also drawn around catheters that contained urine.

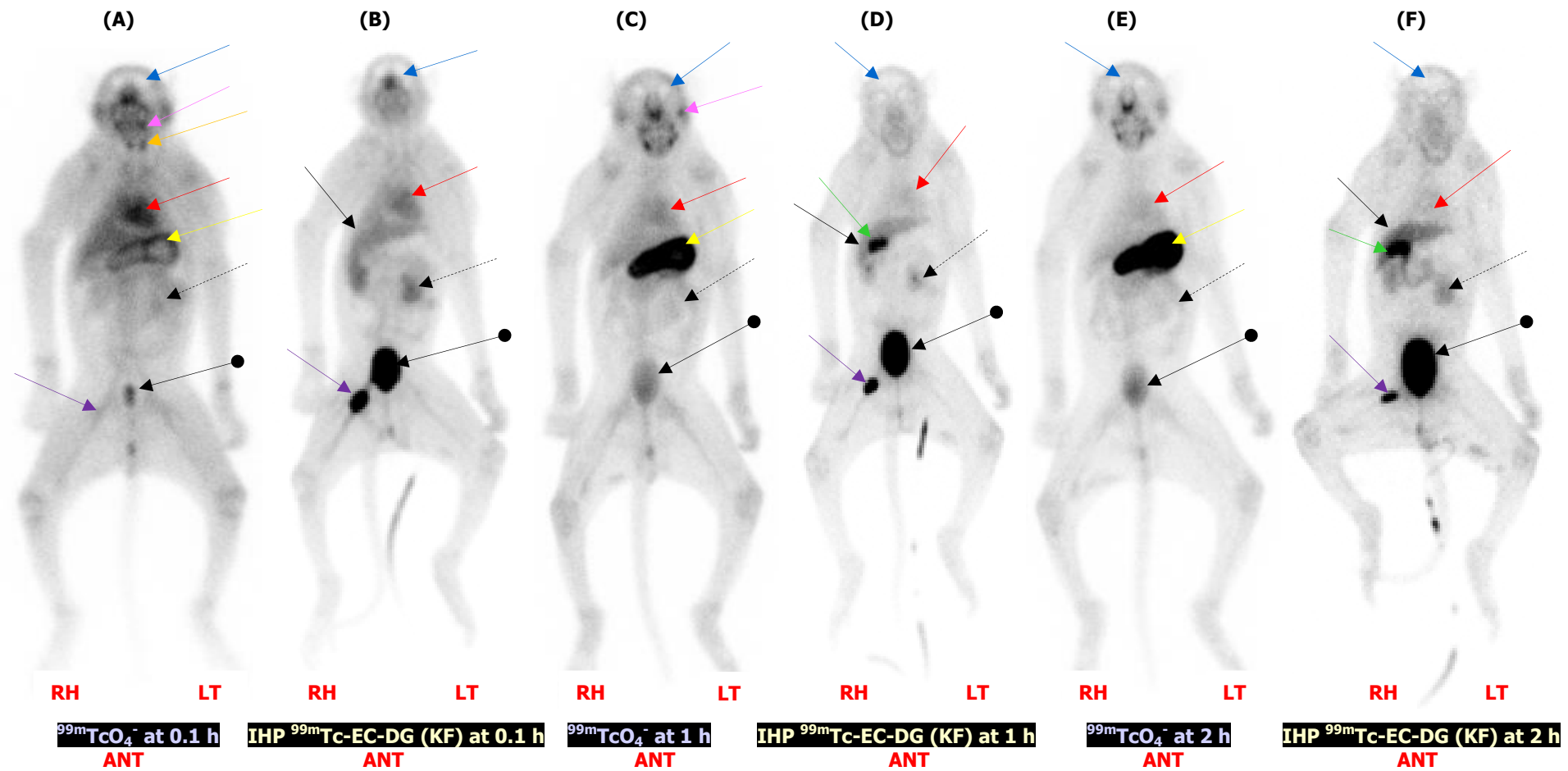


FIGURE 6.11: ANT biodistribution whole-body images of $^{99m}\text{TcO}_4^-$ (A, C & E) and IHP $^{99m}\text{Tc-EC-DG (KF)}$ (B, D & F) in healthy baboons at (A & B) 0.1-, (C & D) 1- and (E & F) 2 hour post administration. Liver (solid arrow), kidney (dashed arrow), urinary bladder (ball arrow), stomach (yellow arrow), salivary glands (pink arrow), gallbladder (green arrow), thyroid (orange arrow) and heart (red arrow) are well outlined. The injection site (purple arrow) is also visible and no brain uptake (blue arrow).

Liver	←	Gallbladder	←	Injection site	←	Brain	←
Kidney	←	Urinary bladder	←	Stomach	←	Heart	←

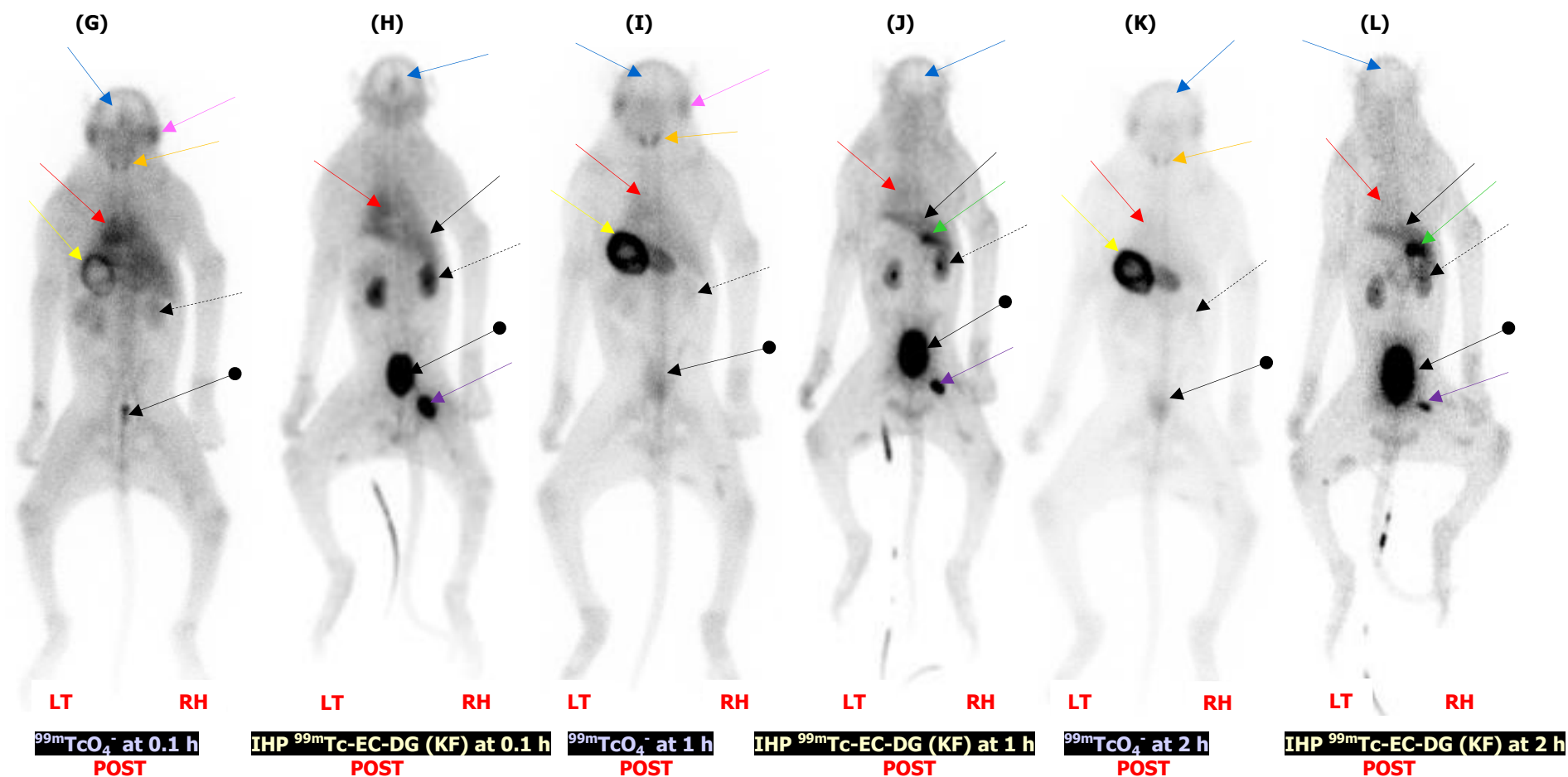


FIGURE 6.12: POST biodistribution images of $^{99m}\text{TcO}_4^-$ (G, I & K) and IHP $^{99m}\text{Tc-EC-DG (KF)}$ (H, J & L) in healthy baboons at (G & H) 0.1-, (I & J) 1- AND (K & L) 2 hour post administration. Liver (solid arrow), kidney (dashed arrow), urinary bladder (ball arrow), stomach (yellow arrow), salivary glands (pink arrow), gallbladder (green arrow), thyroid (orange arrow) and heart (red arrow) are well outlined. The injection site (purple arrow) is also visible and no brain uptake (blue arrow).

Liver ←—— Gallbladder ←—— Injection site ←—— Brain ←——
 Kidney ←----- Urinary bladder ←● Stomach ←—— Heart ←——

No out-of-the-ordinary-high uptake of $^{99m}\text{TcO}_4^-$ was observed to the skin of the baboons on the whole-body and SPECT/CT scans acquired at the different time intervals. The background activity of $^{99m}\text{TcO}_4^-$ and IHP $^{99m}\text{Tc-EC-DG}$ (KF) to the skin was comparable low. Increased $^{99m}\text{TcO}_4^-$ uptake (higher than background activity) was noted on the 1- and 2 h whole-body and SPECT/CT scans for the intestines. This can be explained as activity passed on from the gastric mucosa into the intestines (small bowel and colon) as in humans (Beasley *et al.* 1966:1435; Harbert & Da Rocha 1984:244). The IHP $^{99m}\text{Tc-EC-DG}$ showed increased activity in the colon of the healthy baboons at 1-2 h and was attributed to hepato-biliary excretion. Leucocytes are present in the gastro-intestinal tract mucosa of humans (Ming *et al.* 1989:297) and IHP $^{99m}\text{Tc-EC-DG}$ was confirmed to be taken up by leucocytes (section 5.4.2). Thus the intestinal IHP $^{99m}\text{Tc-EC-DG}$ uptake in the baboon is probably due to the presence of leucocytes in the mucosa of the colon. Mild increased $^{99m}\text{TcO}_4^-$ uptake was noted in the region of the spine, pelvis and long bones on the 1- and 2 h whole-body images and on the 1 h SPECT/CT scan. Low uptake of $^{99m}\text{TcO}_4^-$ to the femurs of rats has been found in studies where they have been used as normal healthy control groups (Meneses do Rêgo *et al.* 2010:11). Only $^{99m}\text{TcO}_4^-$ background activity was noted in the region of the lungs at 0.1 h, decreasing to 2 h. No uptake of $^{99m}\text{TcO}_4^-$ was observed to the brain of the baboons. This was expected since $^{99m}\text{TcO}_4^-$ cannot cross the blood-brain barrier in humans unless damaged (Wagner *et al.* 1995:214). $^{99m}\text{TcO}_4^-$ was also initially developed for brain tumour localisation (Harper *et al.* 1965:104). Two small well-defined focal areas of increased $^{99m}\text{TcO}_4^-$ uptake were observed in the neck area of the baboons on the ANT and POST whole-body images at 0.1-2, this matches the thyroid activity found in humans (Beasley *et al.* 1966:1430). Symmetrical focal areas of increased $^{99m}\text{TcO}_4^-$ accumulation in the lateral aspects of the face was observed on all the acquired whole-body images and SPECT/CT scan acquired at different time intervals. This increased $^{99m}\text{TcO}_4^-$ uptake matches the anatomical localisation of the parotid glands (largest of the salivary glands) in the baboons (Swindler & Wood 1982:66). Normal uptake of $^{99m}\text{TcO}_4^-$ is also found in the salivary glands in humans (Beasley *et al.* 1966:1430).

Intense increased uptake of $^{99m}\text{TcO}_4^-$ to the stomach of the baboons was noted on all the whole-body and SPECT/CT images acquired at the different time intervals. High concentrations of $^{99m}\text{TcO}_4^-$ in the stomach were well described in previous studies in humans (Beasley *et al.* 1966:1435). The IHP $^{99m}\text{Tc-EC-DG}$ (KF) showed no uptake in the salivary glands, thyroid and stomach when compared to the $^{99m}\text{TcO}_4^-$ whole-body

and SPECT/CT scans acquired at the different time intervals. The 0.1 h images of the baboons demonstrated increased focal $^{99m}\text{TcO}_4^-$ uptake in the peri-nasal (snout) area of the baboons on the 0.1 h whole-body images and were still clearly present on the 2 h delayed images. $^{99m}\text{TcO}_4^-$ normal uptake to the nasal mucosa has been reported in humans (Beasley *et al.* 1966:1430). The long snout area of the baboons is vascular (Swindler & Wood 1982:60) and could explain the intense increased IHP $^{99m}\text{Tc-EC-DG}$ activity at 0.1 h.

The heart demonstrated intense increased $^{99m}\text{TcO}_4^-$ accumulation on the 0.1 h whole-body images due to blood pool activity. The $^{99m}\text{TcO}_4^-$ activity was still present on the 2 h whole-body and SPECT/CT scans in the myocardium and this slow disappearance of $^{99m}\text{TcO}_4^-$ from the heart has also been reported in nude mice (Razzak *et al.* 1967:58-59). Initial bloodpool activity was also seen with IHP $^{99m}\text{Tc-EC-DG}$, but the 0.1 h bloodpool activity of $^{99m}\text{TcO}_4^-$ was higher. The 2 h concentration of $^{99m}\text{TcO}_4^-$ and IHP $^{99m}\text{Tc-EC-DG}$ (KF) was similar in intensity on the whole-body and SPECT/CT scans in the baboons.

Intense increased $^{99m}\text{TcO}_4^-$ uptake was noted in the liver on the 0.1 h whole-body images corresponding with bloodpool activity. The $^{99m}\text{TcO}_4^-$ activity in the liver decreased fast and at 2 h post radionuclide administration it is visible on the whole-body images as slightly higher than background activity. Low to minimal similar uptake of $^{99m}\text{TcO}_4^-$ to the liver was also observed in humans (Beasley *et al.* 1966:1435). IHP $^{99m}\text{Tc-EC-DG}$ (KF) uptake was significant in the liver, but did not decrease as fast in intensity compared to $^{99m}\text{TcO}_4^-$, even though the gallbladder was clearly visualised and hepato-biliary excretion from the gallbladder into the intestines took place.

No $^{99m}\text{TcO}_4^-$ was observed in the region of the spleen on the whole-body and SPECT/CT images of the baboons. $^{99m}\text{TcO}_4^-$ uptake, slightly higher than background activity, was noted in the joints at different time intervals on the whole-body and SPECT/CT images. No $^{99m}\text{TcO}_4^-$ uptake was found in the region of the muscles. The gallbladder could not be observed in the region of the liver on the whole-body and SPECT/CT scans acquired at different time intervals after $^{99m}\text{TcO}_4^-$ administration.

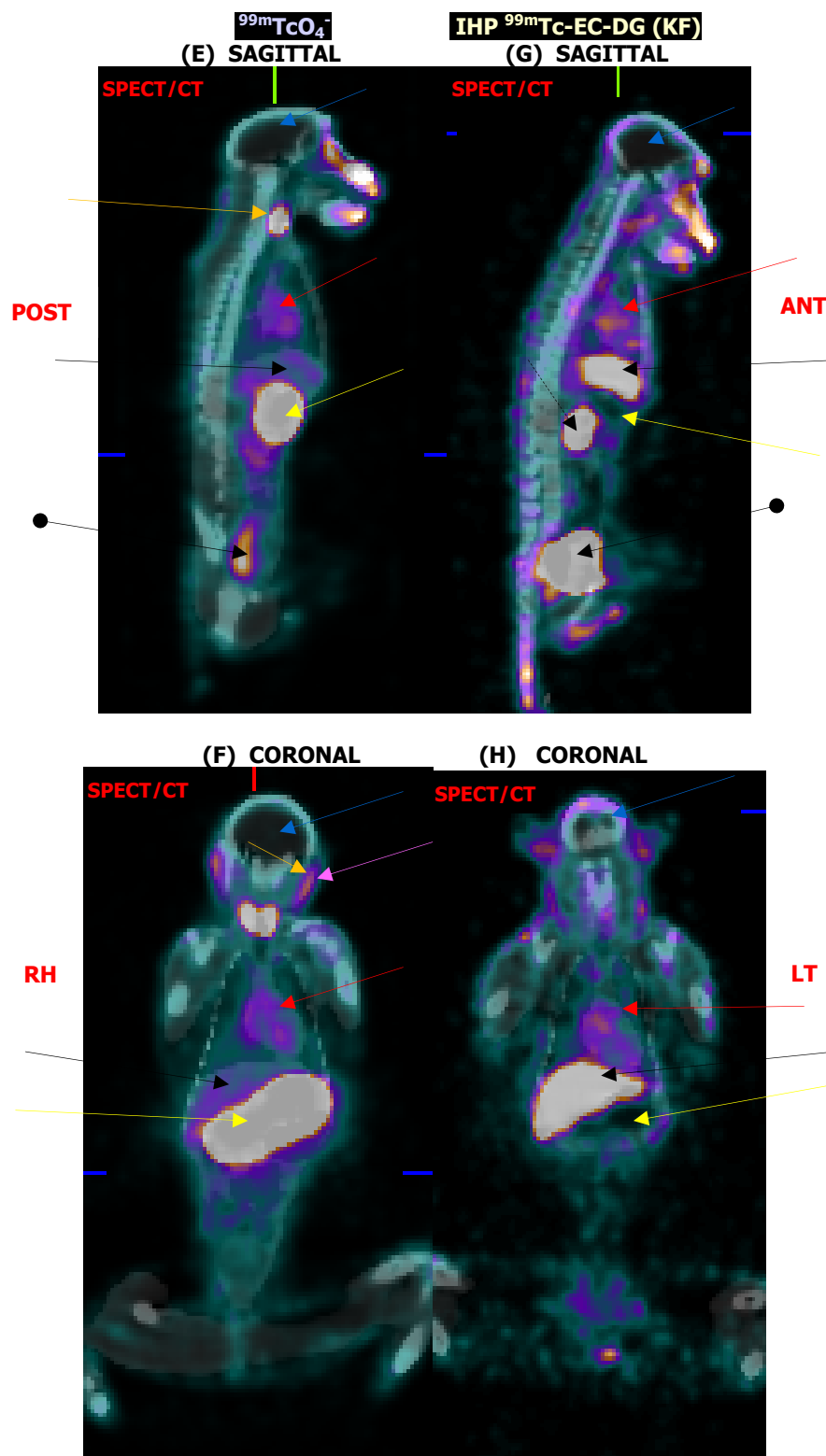


FIGURE 6.14: $^{99m}\text{TcO}_4^-$ co-registered SPECT/CT (E) sagittal and (F) coronal images and IHP $^{99m}\text{Tc-EC-DG (KF)}$ SPECT/CT (G) sagittal and (H) coronal images at 2 hour post radiopharmaceutical administration.

Liver ← Gallbladder ← Injection site ← Brain ←
 Kidney ← Urinary bladder ← Stomach ← Heart ←

6.3.1.5.2 SQ and SQUAL analysis

The comparison of the SQ and SQUAL normal biodistribution results of $^{99m}\text{TcO}_4^-$ with IHP $^{99m}\text{Tc-EC-DG}$ (KF) to the different organs in healthy baboons and the results of the organs for the planar whole-body and SPECT/CT images are summarised in Table 6.5.

TABLE 6.5: Comparison of the SQ and SQUAL planar whole-body- and SPECT/CT results of $^{99m}\text{TcO}_4^-$ and IHP $^{99m}\text{Tc-EC-DG}$ (KF) biodistribution to organs of healthy baboons

Organ/ tissue	Time interval (h)	IHP $^{99m}\text{Tc-EC-DG}$ (KF)						$^{99m}\text{TcO}_4^-$					
		Static			SPECT/CT			Static			SPECT/CT		
		<i>n</i>	SQUAL	SQ	<i>n</i>	SQUAL	SQ	<i>n</i>	SQUAL	SQ	<i>n</i>	SQUAL	SQ
Lungs	0.1	6	Bkg	0	*	*	*	6	Bkg	1	*	*	*
	1	6	Bkg	0	1	Bkg	0	6	Bkg	0	1	Bkg	0
	2	6	Bkg	0	1	Bkg	0	6	Bkg	0	1	Bkg	0
Liver	0.1	6	Post	2	*	*	*	6	Post	2	*	*	*
	1	6	Post	2	1	Post	2	6	Post	1	1	Post	1
	2	6	Post	2	1	Post	2	6	Post	1	1	Post	1
Stomach	0.1	6	Neg	0	*	*	*	6	Post	3	*	*	*
	1	6	Neg	0	1	Neg	0	6	Post	3	1	Post	3
	2	6	Neg	0	1	Neg	0	6	Post	3	1	Post	3
Spleen	0.1	6	Neg	0	*	*	*	6	Neg	0	*	*	*
	1	6	Neg	0	1	Neg	0	6	Neg	0	1	Neg	0
	2	6	Neg	0	1	Neg	0	6	Neg	0	1	Neg	0
Kidneys	0.1	6	Post	3	*	*	*	6	Post	3	*	*	*
	1	6	Post	2	1	Post	3	6	Post	3	1	Post	1
	2	6	Neg	2	1	Post	3	6	Post	3	1	Neg	0
Thyroid	0.1	6	Neg	0	*	*	*	6	Post	2	*	*	*
	1	6	Neg	0	1	Neg	0	6	Post	3	1	Post	3
	2	6	Neg	0	1	Neg	0	6	Post	3	1	Post	3
Muscle	0.1	6	Neg	0	*	*	*	6	Neg	0	*	*	*
	1	6	Neg	0	1	Neg	0	6	Neg	0	1	Neg	0
	2	6	Neg	0	1	Neg	0	6	Neg	0	1	Neg	0
Intestines	0.1	6	Bkg	1	*	*	*	6	Neg	0	*	*	*
	1	6	Post	1	1	Post	1	6	Post	1	1	Post	1
	2	6	Post	2	1	Post	2	6	Post	2	1	Post	1
Brain	0.1	6	Neg	0	*	*	*	6	Neg	0	*	*	*
	1	6	Neg	0	1	Neg	0	6	Neg	0	1	Neg	0
	2	6	Neg	0	1	Neg	0	6	Neg	0	1	Neg	0
Bladder	0.1	6	Post	3	*	*	*	6	Post	2	*	*	*
	1	6	Post	3	1	Post	3	6	Post	2	1	Post	2
	2	6	Post	3	1	Post	3	6	Post	2	1	Post	2
Skin	0.1	6	Neg	0	*	*	*	6	Neg	0	*	*	*
	1	6	Neg	0	1	Neg	0	6	Neg	0	1	Neg	0
	2	6	Neg	0	1	Neg	0	6	Neg	0	1	Neg	0
Gallbladder	0.1	6	Post	2	*	*	*	6	Neg	0	*	*	*
	1	6	Post	3	1	Post	3	6	Neg	0	1	Neg	0
	2	6	Post	3	1	Post	3	6	Neg	0	1	Neg	0
Heart	0.05	6	Post	2	*	*	*	6	Post	3	*	*	*
	1	6	Post	1	1	Post	1	6	Post	2	1	Post	2
	2	6	Post	1	1	Post	1	6	Post	1	1	Post	2
Bone	0.1	6	Neg	0	*	*	*	6	Neg	0	*	*	*
	1	6	Neg	0	1	Neg	0	6	Bkg	1	1	Bkg	1
	2	6	Neg	0	1	Neg	0	6	Bkg	1	1	Bkg	1
Joints	0.1	6	Post	1	*	*	*	6	Post	1	*	*	*
	1	6	Post	1	1	Post	1	6	Post	1	1	Post	1
	2	6	Post	1	1	Post	1	6	Post	1	1	Post	1
Salivary glands	0.1	6	Neg	0	*	*	*	6	Post	3	*	*	*
	1	6	Neg	0	1	Neg	0	6	Post	3	1	Post	2
	2	6	Neg	0	1	Neg	0	6	Post	3	1	Post	3

According to the SQUAL results, background activity was mainly present in the skeleton and lungs for the $^{99m}\text{TcO}_4^-$, similar results were found for the IHP $^{99m}\text{Tc-EC-DG}$ (KF) administered to the

baboons. Positive SQUAL results were reported for biodistribution $^{99m}\text{TcO}_4^-$ to the bladder, intestines, liver, kidneys and the early images of the heart. Similar SQUAL results were observed for the IHP $^{99m}\text{Tc-EC-DG}$ (KF) in these organs. Negative *in vivo* uptake was reported in the brain and spleen for both RPs. Positive *in vivo* activity was reported to the salivary glands, thyroid and stomach for the static and SPECT/CT images of the $^{99m}\text{TcO}_4^-$, but negative for the IHP $^{99m}\text{Tc-EC-DG}$ (KF). The SQ values for $^{99m}\text{TcO}_4^-$ between 2 and 3 were allocated to the stomach, salivary glands, thyroid, heart, kidneys and bladder. A zero SQ value was assigned to the spleen, brain, skin, gallbladder and muscles for the $^{99m}\text{TcO}_4^-$ biodistribution. Similarly a zero value was assigned to the muscle, spleen, brain and skin for the IHP $^{99m}\text{Tc-EC-DG}$ (KF) biodistribution.

6.3.1.5.3 Comparison of the quantitative analysis

In Table 6.6 the IHP $^{99m}\text{Tc-EC-DG}$ (KF) biodistribution results are compared with the results of $^{99m}\text{TcO}_4^-$ for different organs/tissues of healthy baboons. The activity in all organs and tissue samples was expressed as the percentage of the total body activity per organ and presented as the mean \pm SEM, at 0.1-, 1- and 2 h post radiopharmaceutical administration. Statistical calculations of the data for IHP $^{99m}\text{Tc-EC-DG}$ (KF) and $^{99m}\text{TcO}_4^-$ in healthy baboons are presented in Table 6.6. A *P* value <0.05 was considered statistically significant (highlighted in red).

Corresponding mean biodistribution values of IHP $^{99m}\text{Tc-EC-DG}$ (KF) and $^{99m}\text{TcO}_4^-$ were high to the liver, heart and bladder for the different imaging time intervals in the healthy baboons (Table 6.6). The heart also demonstrated high increased uptake results on the 0.1 h imaging time interval. The skeleton, joint, brain, testes and skin demonstrated the corresponding low uptake for the IHP $^{99m}\text{Tc-EC-DG}$ (KF) and $^{99m}\text{TcO}_4^-$ uptake in the healthy baboons for the different time intervals (Table 6.6). Opposite high uptake was found with $^{99m}\text{TcO}_4^-$ in the stomach of baboons with low uptake of IHP $^{99m}\text{Tc-EC-DG}$ (KF) in the same organ.

TABLE 6.6: Comparison of the biodistribution of IHP ^{99m}Tc -EC-DG (KF) with $^{99m}\text{TcO}_4^-$ in healthy baboons

Organ or Tissue	Time interval (h)	Median		Mean \pm SEM		P-value
		IHP ^{99m}Tc -EC-DG (KF)	$^{99m}\text{TcO}_4^-$	IHP ^{99m}Tc -EC-DG (KF)	$^{99m}\text{TcO}_4^-$	
LT Lung	0.1	1.76	2.20	1.71 ± 0.16	2.10 ± 0.13	0.16
	1	0.80	1.43	0.82 ± 0.07	1.46 ± 0.16	0.03
	2	0.40	1.12	0.40 ± 0.02	1.02 ± 0.09	0.03
RT Lung	0.1	2.12	2.21	2.07 ± 0.12	2.34 ± 0.29	0.56
	1	1.03	1.54	1.07 ± 0.06	1.50 ± 0.15	0.09
	2	0.52	1.10	0.51 ± 0.03	1.08 ± 0.23	0.09
Liver	0.1	5.31	3.99	5.14 ± 0.36	3.95 ± 0.24	0.06
	1	3.50	2.55	3.36 ± 0.40	2.74 ± 0.20	0.31
	2	2.24	2.16	2.33 ± 0.26	2.12 ± 0.18	0.84
Stomach	0.1	0.20	8.52	0.23 ± 0.05	8.36 ± 0.67	0.03
	1	0.13	13.88	0.14 ± 0.02	13.91 ± 1.35	0.03
	2	0.07	18.78	0.07 ± 0.01	18.23 ± 0.68	0.03
LT Kidney	0.1	2.03	∞	2.38 ± 0.30	∞	∞
	1	1.02	∞	1.08 ± 0.11	∞	∞
	2	0.63	∞	0.67 ± 0.05	∞	∞
RH Kidney	0.1	2.18	∞	2.30 ± 0.22	∞	∞
	1	1.25	∞	1.32 ± 0.21	∞	∞
	2	0.74	∞	0.71 ± 0.05	∞	∞
Spleen	0.1	0.31	∞	0.30 ± 0.04	∞	∞
	1	0.16	∞	0.18 ± 0.03	∞	∞
	2	0.07	∞	0.09 ± 0.02	∞	∞
Large intestines	0.1	0.25	∞	0.23 ± 0.05	∞	∞
	1	0.19	∞	0.17 ± 0.02	∞	∞
	2	0.07	∞	0.08 ± 0.01	∞	∞
Small intestines	0.1	0.38	∞	0.35 ± 0.03	∞	∞
	1	0.21	∞	0.21 ± 0.03	∞	∞
	2	0.10	∞	0.12 ± 0.01	∞	∞
Brain	0.1	0.44	0.68	0.45 ± 0.05	0.69 ± 0.04	0.03
	1	0.27	0.61	0.29 ± 0.03	0.55 ± 0.10	0.06
	2	0.16	0.54	0.17 ± 0.02	0.53 ± 0.01	0.03
Heart	0.1	4.43	6.00	4.41 ± 0.35	5.91 ± 0.37	0.09
	1	1.74	3.60	1.75 ± 0.17	3.77 ± 0.26	0.03
	2	0.89	2.85	0.95 ± 0.06	2.88 ± 0.25	0.03
Nose	0.1	0.81	1.28	0.80 ± 0.07	1.25 ± 0.10	0.03
	1	0.38	1.00	0.38 ± 0.02	1.05 ± 0.07	0.03
	2	0.19	0.83	0.19 ± 0.01	0.85 ± 0.07	0.03
Mouth	0.1	1.54	0.54	1.65 ± 0.20	0.54 ± 0.04	0.03
	1	0.87	0.41	0.85 ± 0.08	0.43 ± 0.05	0.03
	2	0.45	0.32	0.47 ± 0.05	0.41 ± 0.10	0.31
Gallbladder	0.1	0.99	∞	1.11 ± 0.17	∞	∞
	1	1.18	∞	1.19 ± 0.12	∞	∞
	2	1.12	∞	1.14 ± 0.17	∞	∞
Skin	0.1	0.02	0.02	0.02 ± 0.00	0.02 ± 0.00	0.84
	1	0.02	0.02	0.02 ± 0.00	0.02 ± 0.00	1.00
	2	0.01	0.01	0.01 ± 0.00	0.01 ± 0.00	0.84
Muscle	0.1	0.10	0.12	0.11 ± 0.01	0.12 ± 0.01	0.56
	1	0.06	0.09	0.06 ± 0.01	0.09 ± 0.01	0.03
	2	0.03	0.06	0.03 ± 0.00	0.08 ± 0.02	0.03
Testes	0.1	0.21	0.71	0.21 ± 0.05	0.68 ± 0.05	0.03
	1	0.15	0.53	0.16 ± 0.04	0.55 ± 0.05	0.03
	2	0.08	0.47	0.08 ± 0.02	0.47 ± 0.07	0.03
Joint	0.1	0.29	0.93	0.31 ± 0.02	0.94 ± 0.05	0.03
	1	0.21	0.82	0.21 ± 0.02	0.84 ± 0.04	0.03
	2	0.15	0.62	0.15 ± 0.01	0.65 ± 0.04	0.03
Bladder	0.1	15.13	1.51	14.74 ± 1.07	1.57 ± 0.15	0.03
	1	29.20	2.38	28.45 ± 4.26	2.69 ± 0.73	0.03
	2	32.83	3.05	30.07 ± 5.83	3.16 ± 0.66	0.03

∞ Statistical calculation could not be performed as ROIs could not be drawn on IHP ^{99m}Tc -EC-DG (KF) or $^{99m}\text{TcO}_4^-$ biodistribution images

Almost no uptake of IHP ^{99m}Tc -EC-DG (KF) was observed in the stomach, compared to the high uptake of $^{99m}\text{TcO}_4^-$ to the stomach (Figure 6.15). The uptake of $^{99m}\text{TcO}_4^-$ increased from the 0.1 to the 2 h whole-body images.

In Figure 6.16 the *in vivo* clearance of the (A) liver and (B) heart with high uptake of $^{99m}\text{TcO}_4^-$ and IHP ^{99m}Tc -EC-DG (KF) are depicted. IHP ^{99m}Tc -EC-DG and $^{99m}\text{TcO}_4^-$ had the highest uptake in the liver at 0.1 h and constant clearance was seen from 0.1-2 h post administration (Figure 6.16A). The IHP ^{99m}Tc -EC-DG (KF) and $^{99m}\text{TcO}_4^-$ uptake in the heart was a maximum at 0.1 h and decreased constantly over time (Figure 6.16B). $^{99m}\text{TcO}_4^-$ had the highest uptake in the heart for all the whole-body imaging time intervals in the baboons. In Figure 6.17 the *in vivo* clearance of the (A) brain and (B) skin with low uptake of $^{99m}\text{TcO}_4^-$ and IHP ^{99m}Tc -EC-DG (KF) are depicted. ^{99m}Tc -EC-DG (KF) had lower brain uptake than $^{99m}\text{TcO}_4^-$ and the IHP ^{99m}Tc -EC-DG (KF) cleared faster than $^{99m}\text{TcO}_4^-$ (Figure 6.17A). The low skin uptake of IHP ^{99m}Tc -EC-DG and $^{99m}\text{TcO}_4^-$ was found to be the same and decreased after 1 h of administration (Figure 6.17B).

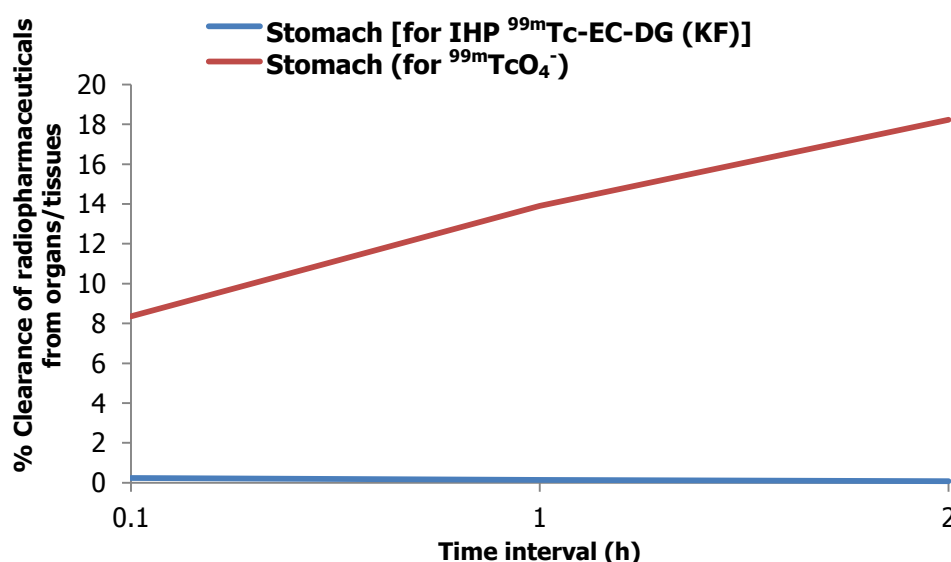
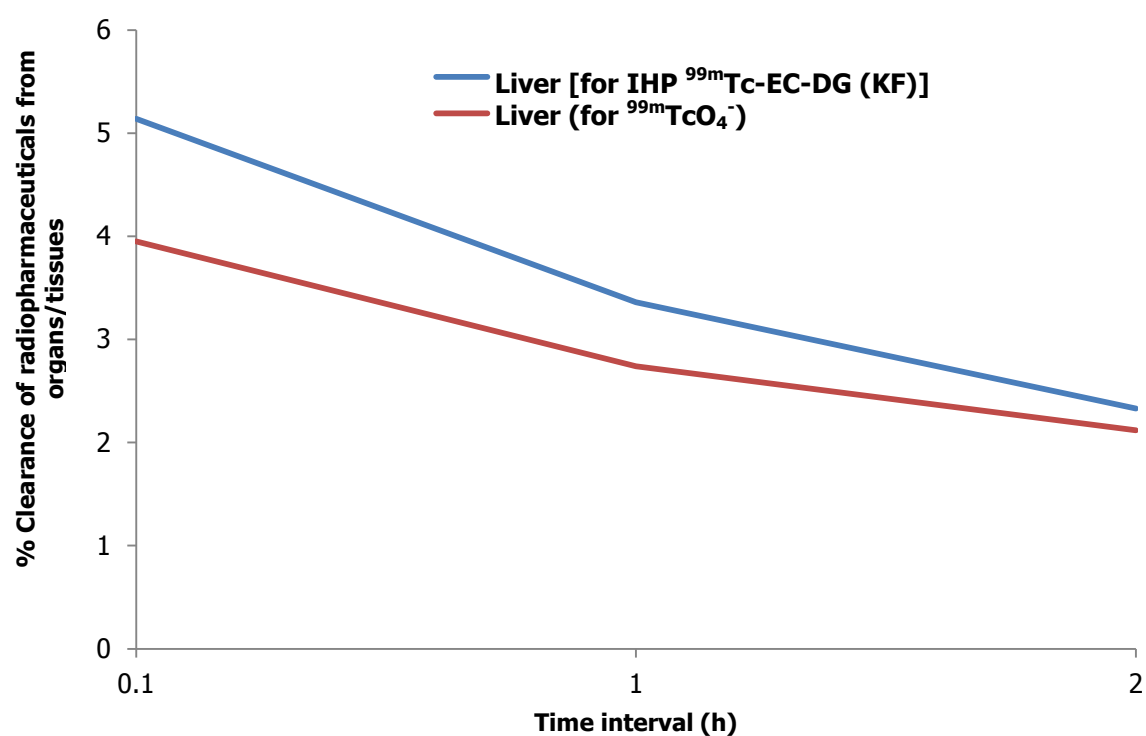


FIGURE 6.15: Comparison of clearance from the stomach for IHP ^{99m}Tc -EC-DG (KF) and $^{99m}\text{TcO}_4^-$ in healthy baboons. Mean % uptake values for the stomach are shown with time.

(A)



(B)

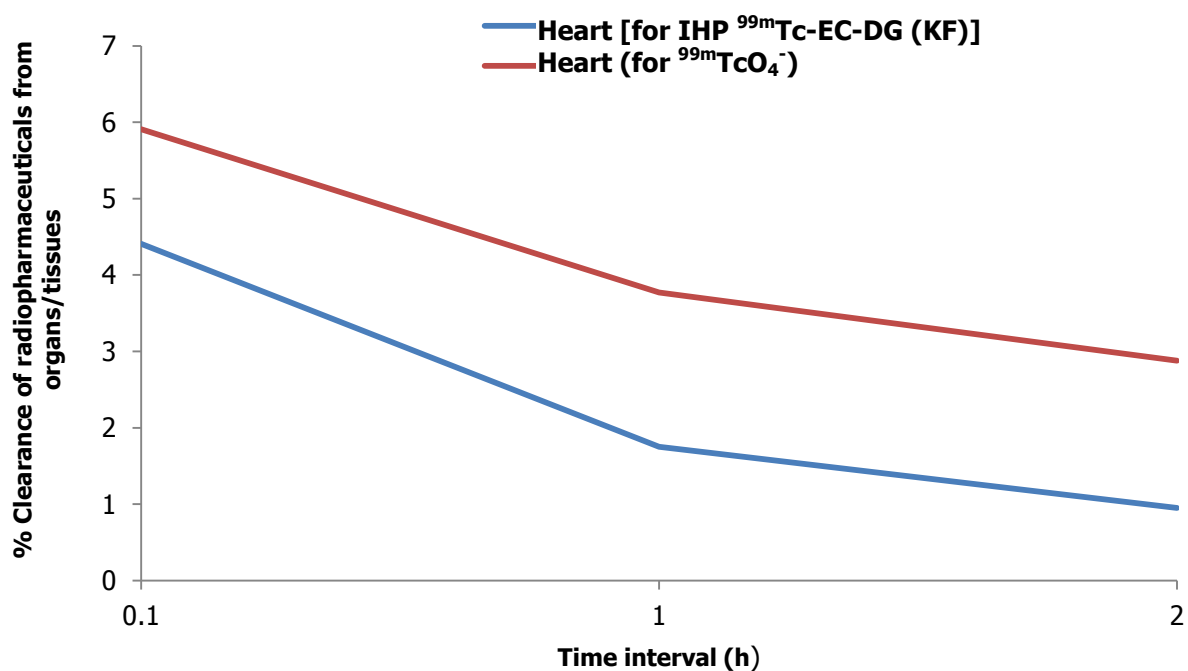
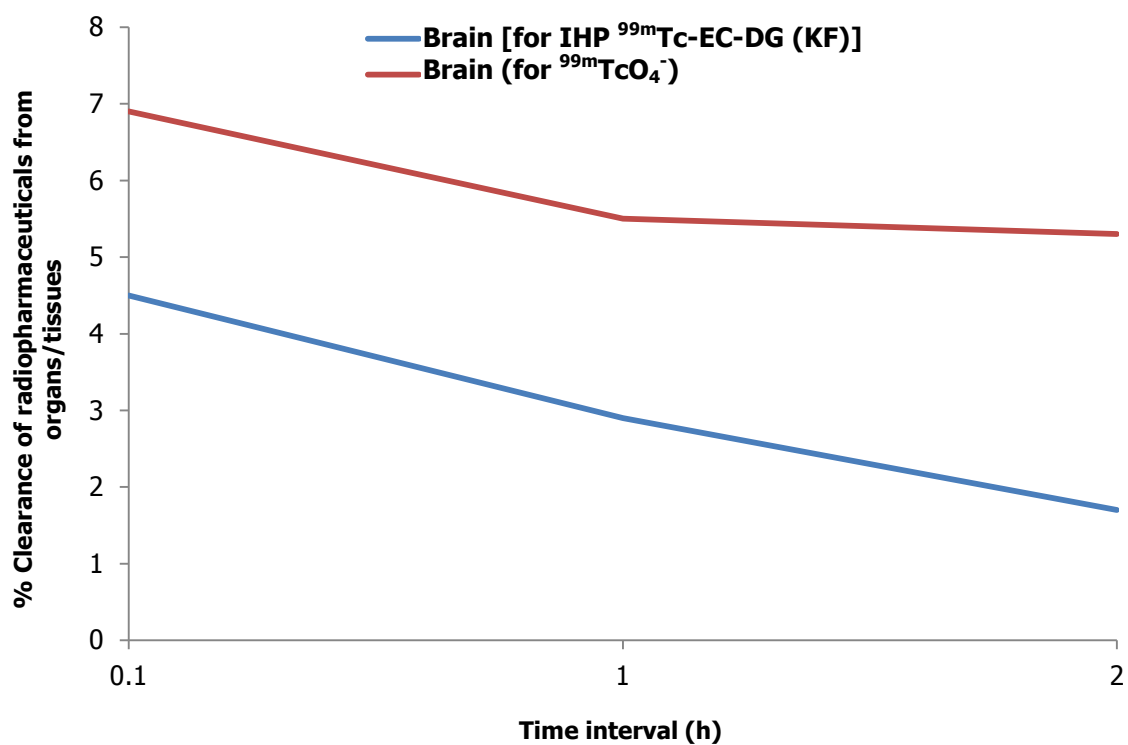


FIGURE 6.16: Comparison of clearance from the highest uptake organs of IHP ^{99m}Tc -EC-DG (KF) and $^{99m}\text{TcO}_4^-$ in healthy baboons. Mean % uptake values for the (A) liver and (B) heart are shown with time.

(A)



(B)

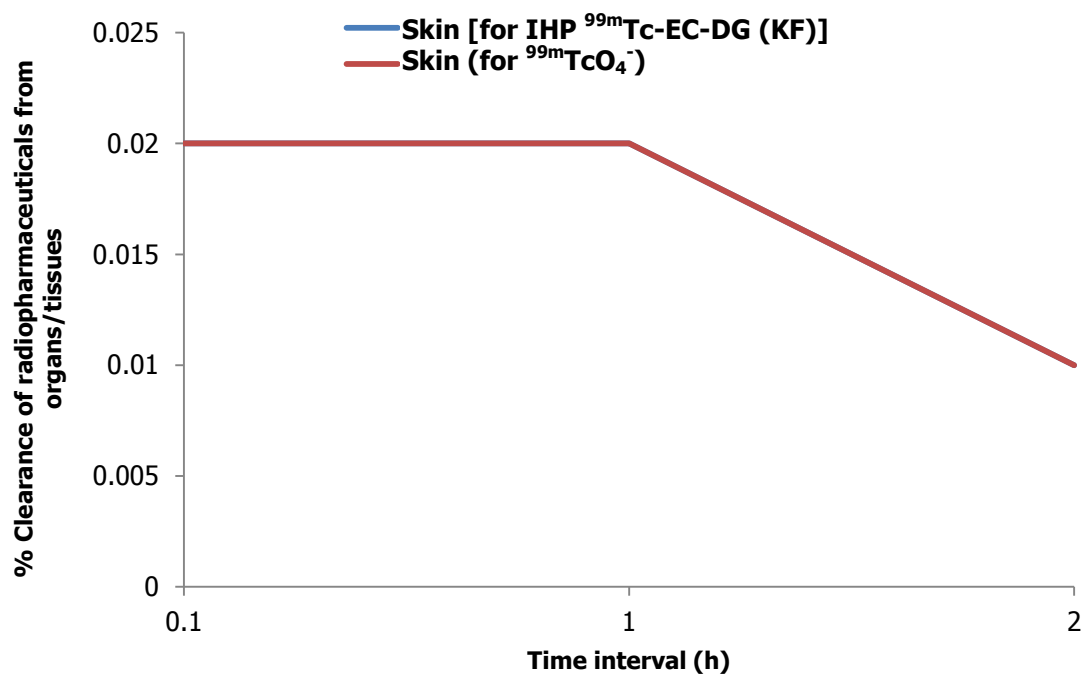


FIGURE 6.17: Comparison from the lowest uptake organs of IHP ^{99m}Tc -EC-DG (KF) and $^{99m}\text{TcO}_4^-$ in healthy baboons. Mean % uptake values for the (A) brain and (B) skin are shown with time.

Characteristic uptake of $^{99m}\text{TcO}_4^-$ in healthy baboons was present in the salivary glands, thyroid and stomach, similar to humans (Beasley *et al.* 1966:1435). By visual evaluation indicated that the thyroid, salivary glands and stomach showed high uptake of $^{99m}\text{TcO}_4^-$, with no uptake of IHP $^{99m}\text{Tc-EC-DG}$ (KF) to these areas. Good labelling efficiency of IHP $^{99m}\text{Tc-EC-DG}$ (KF) could be confirmed when compared to $^{99m}\text{TcO}_4^-$ whole-body and SPECT/CT images as no salivary glands, or thyroid was visible, indicating no $^{99m}\text{TcO}_4^-$. The normal excretory route of $^{99m}\text{TcO}_4^-$ in humans is by the urinary tract into the bladder and this is also the case for baboons. The SQ, SQUAL and quantitative results of the SPECT/CT and whole-body images, confirmed excretion from the kidneys into the urinary tract for the IHP $^{99m}\text{Tc-EC-DG}$ (KF) and $^{99m}\text{TcO}_4^-$ in the healthy baboons. Early uptake in the heart by IHP $^{99m}\text{Tc-EC-DG}$ (KF) and $^{99m}\text{TcO}_4^-$ was also present with all the result evaluation techniques. The lowest uptake was confirmed to the brain, muscles, joints and skin. Biodistribution differences of IHP $^{99m}\text{Tc-EC-DG}$ (KF) and $^{99m}\text{TcO}_4^-$ were reported on for the whole-body and SPECT/CT images.

6.3.1.6 Comparison of IHP $^{99m}\text{Tc-EC-DG}$ (KF) with IHP $^{99m}\text{Tc-EC-DG}$ (DL)

In this section a comparison is made between the biodistribution-, statistical-, SQ and the SQUAL static and SPECT/CT image results of the normal biodistribution of IHP $^{99m}\text{Tc-EC-DG}$ (DL) with the results of the IHP $^{99m}\text{Tc-EC-DG}$ (KF) at specific time intervals in healthy baboons.

6.3.1.6.1 *In vivo* normal biodistribution images

Figure 6.18 and Figure 6.19 show an image comparison between the ANT and POST scintigraphic images of the biodistribution of IHP $^{99m}\text{Tc-EC-DG}$ (DL) and the IHP $^{99m}\text{Tc-EC-DG}$ (KF) in healthy baboons at 0.1-, 1- and 2 h post radiopharmaceutical administration. Specific

organs of interest are indicated with the different types and colour arrows in Figures 6.18-6.19.

The 0.1 h whole-body images of the baboons administered IHP ^{99m}Tc -EC-DG (KF) and IHP ^{99m}Tc -EC-DG (DL) demonstrated increased uptake in the snout (peri-nasal) area. The activity in the snout area decreased over time to only background activity on the 2 h delayed images, this corresponded to blood pool activity. The long snout areas of the baboons are vascular (Swindler & Wood 1982:60) and could explain the intense increase IHP ^{99m}Tc -EC-DG activity at 0.1 h. Well-defined intense increased excretion of IHP ^{99m}Tc -EC-DG (KF) and (–DL) was observed in the kidneys on all the whole-body imaging time points. The bladder demonstrated similar intense increased IHP ^{99m}Tc -EC-DG (KF) and (–DL) activity on all three whole-body images acquired at different time intervals. The activity in the bladder was due to excretion by the kidneys, this was already evident on the 0.1 h whole-body images (Figure 6.18). The carbonylglycine present in IHP ^{99m}Tc -EC-DG (KF) and (–DF) interacts with the renal tubular transport proteins increasing radiopharmaceutical excretion by the kidneys (Vanbilloen *et al.* 2000:207).

No obvious uptake was observed in the skin areas (ears) for both test formulations. The 0.1 h whole-body images demonstrated no RP uptake to the area of the intestines for IHP ^{99m}Tc -EC-DG (KF) and (–DL). An area of increasing activity could be seen in the area of the intestines from the 1 h to the 2 h whole-body for both formulations. Mild increased RP uptake was noted in the joints, specifically the hand- and knee joints for IHP ^{99m}Tc -EC-DG (KF) and (–DL). These uptakes are only mildly higher than that of background activity. Background radiopharmaceutical activity was noted in the region of the muscles with no well-defined increased uptake. The baboons were passive the day before both experiments. Muscle and brown fat uptake was reported in other glucose metabolic imaging agents like ^{18}F -FDG due to the increased

glucose consumption of muscles during exercise of exposure to cold temperatures.

There was no IHP ^{99m}Tc -EC-DG (KF) and (-DL) uptake in the region of the stomach, confirming good labelling with no free $^{99m}\text{TcO}_4^-$ for the different test formulations. No early bloodpool activity was observed in the lungs on the whole-body at 0.1 h and uptake of IHP ^{99m}Tc -EC-DG (KF) and (-DL) was also absent on images acquired later. There was no uptake of IHP ^{99m}Tc -EC-DG (KF) and (-DF) in the region of the brain, even less compared to that of background. No IHP ^{99m}Tc -EC-DG (KF) and (-DL) uptake was observed on the 0.1-2 h images in the region of the neck area, where the thyroid and salivary glands (parotid glands) can be found, indicating limited amount of free $^{99m}\text{TcO}_4^-$. Intense increased blood pool activity was noted in the heart on the 0.1 h whole-body images for both test formulations and was still evident on the 2 h images confirming uptake of IHP ^{99m}Tc -EC-DG (KF) and (-DL) in the heart. Notable intense increased IHP ^{99m}Tc -EC-DG (KF) and (-DL) uptake was present in the liver at 0.1 h, correlating with bloodpool activity that decreased slightly towards the 2 h whole-body image. A well-defined gallbladder was observed on the 1 h whole-body images (Figure 6.18C and D), the IHP ^{99m}Tc -EC-DG (KF) uptake in gallbladder appeared to be higher than with the IHP ^{99m}Tc -EC-DG (DL). The baboon used for the IHP ^{99m}Tc -EC-DG (DL) was slightly smaller than the one used for the IHP ^{99m}Tc -EC-DG (KF) and could have played a role as the gallbladder could be smaller and influenced visibility. Only one baboon was imaged with IHP ^{99m}Tc -EC-DG (DL), these variances between the formulations should be investigated in a larger animal sample. The IHP ^{99m}Tc -EC-DG (KF) also showed increased gallbladder uptake on the 2 h whole-body image compared to low visibility of the gallbladder with IHP ^{99m}Tc -EC-DG (DL). Clear excretion from the gallbladder into the intestines was visible on the 2 h whole-body images of all the baboons administered with IHP ^{99m}Tc -EC-DG (KF).

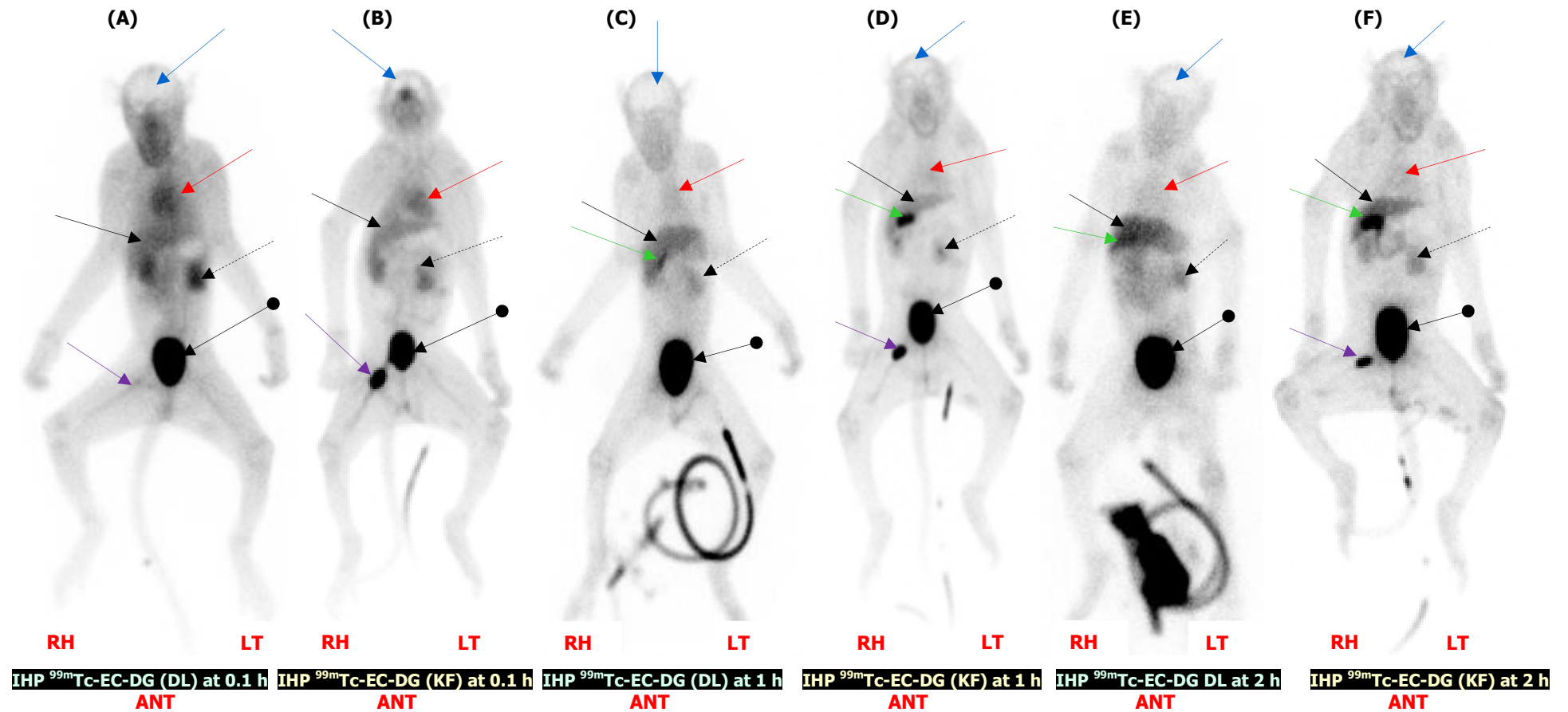


FIGURE 6.18: ANT whole-body biodistribution images IHP ^{99m}Tc-EC-DG (DL) (A, C & E) and IHP ^{99m}Tc-EC-DG (KF) (B, D & F) in healthy baboons at (A & B) 0.1-, (C & D) 1- and (E & F) 2 hour post administration. Liver (solid arrow), kidney (dashed arrow), urinary bladder (ball arrow), gallbladder (green arrow) and heart (red arrow) are well outlined. The injection site (purple arrow) is also visible and no brain uptake (blue arrow).

Liver	←	Gallbladder	←	Injection site	←	Brain	←
Kidney	←	Urinary bladder	←	Stomach	←	Heart	←

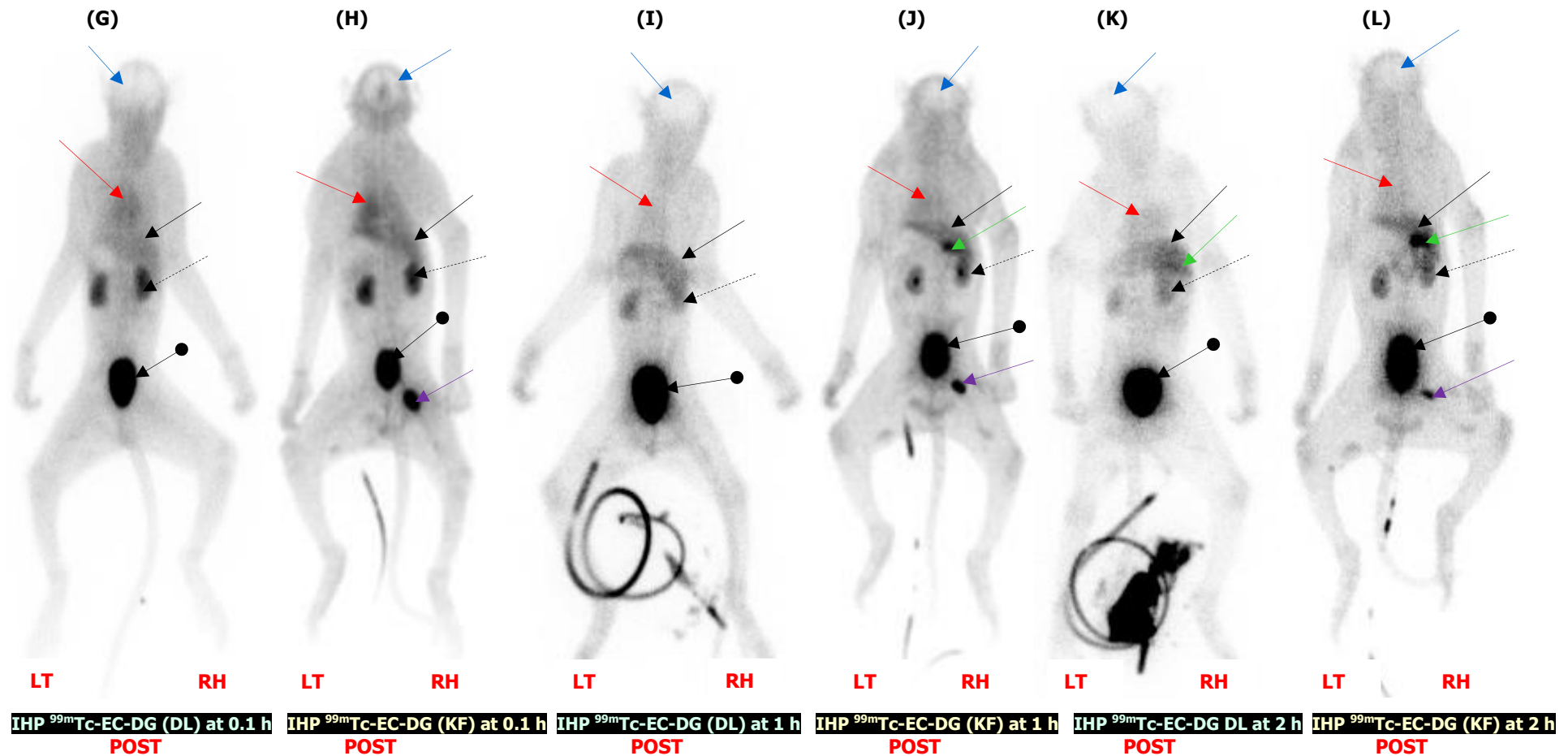


FIGURE 6.19: POST biodistribution images IHP ^{99m}Tc -EC-DG (DL) (G, I & K) and IHP ^{99m}Tc -EC-DG (KF) (H, J & L) in healthy baboons at (G & H) 0.1-, (I & J) 1- and (K & L) 2 hour post administration. Liver (solid arrow), kidney (dashed arrow), urinary bladder (ball arrow), gallbladder (green arrow) and heart (red arrow) are well outlined. The injection site (purple arrow) is also visible and no brain uptake (blue arrow).

Figure 6.20 and Figure 6.21 show the SPECT/CT (transverse, sagittal and coronal) image comparison of the IHP ^{99m}Tc -EC-DG (DL) with the IHP ^{99m}Tc -EC-DG (KF) SPECT/CT at 0.1- and 2 h post administration. Excretion through the kidneys to the bladder was evident by the intense IHP ^{99m}Tc -EC-DG (KF) and (–DL) activity present in the bladder on the 0.1- and 2 h SPECT/CT images. No IHP ^{99m}Tc -EC-DG uptake was observed in the region of the skeleton. Mild increased IHP ^{99m}Tc -EC-DG (DL) and (–KF) uptake was noted in the joints, specifically the hand- and knee joints. This radiopharmaceutical test formulation uptake is only mildly higher than that of background activity and was also seen on the whole-body images.

The 0.1- and 2 h SPECT/CT images of IHP ^{99m}Tc -EC-DG (KF) and (–DL) demonstrated no uptake in the lungs. No radiopharmaceutical uptake in the brain was observed on any of the three SPECT/CT scans for the different formulation of IHP ^{99m}Tc -EC-DG (KF). Increased IHP ^{99m}Tc -EC-DG (KF) and (–DL) bloodpool activity in the heart was observed on the 0.1 h SPECT/CT and on the 2 h SPECT/CT scans, confirming uptake of IHP ^{99m}Tc -EC-DG (KF) and (–DL) in the heart. Well-defined increased uptake was noted in the liver on the 0.1 h SPECT/CT and slightly decreased on the 2 h SPECT/CT scans for both RP test formulations.

No IHP ^{99m}Tc -EC-DG (KF) and (–DL) uptake was observed to the area of the spleen on the SPECT/CT scans performed on 0.1- and 2 h. Intense increased IHP ^{99m}Tc -EC-DG (KF) and (–DL) uptake was noted early on in the kidneys and were still present at 2 h post RP administration. No increased uptake was seen in the region of the stomach on the 0.1- and 2 h SPECT/CT scans for IHP ^{99m}Tc -EC-DG (KF) and (–DL). No uptake was observed in muscles, only background activity on all SPECT/CT acquired scans at different time intervals.

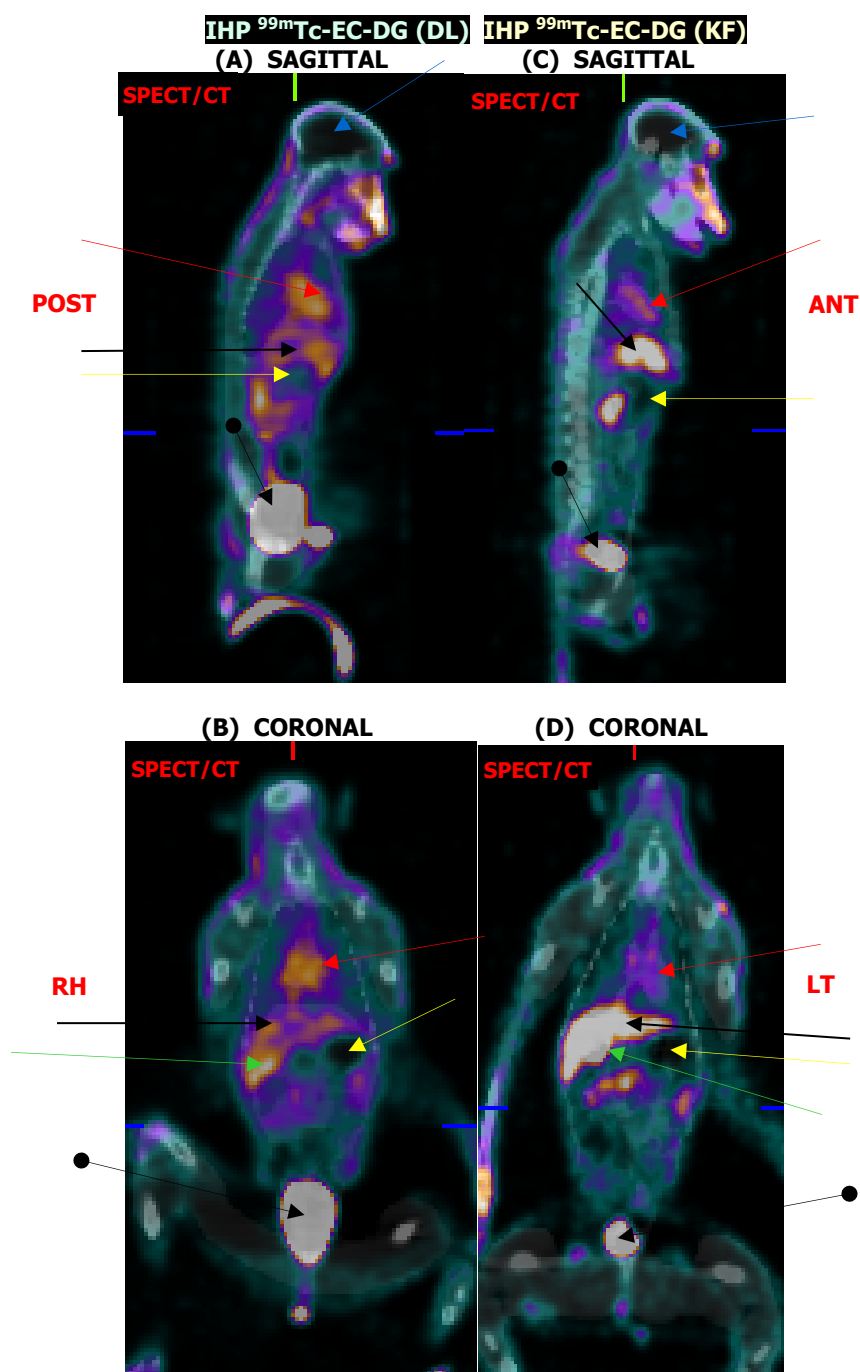


FIGURE 6.20: IHP ^{99m}Tc -EC-DG (DL) co-registered SPECT/CT (A) sagittal and (B) coronal images and IHP ^{99m}Tc -EC-DG (KF) SPECT/CT (C) sagittal and (D) coronal images at 0.1 hour post radiopharmaceutical administration. Liver (solid arrow), urinary bladder (ball arrow), stomach (yellow arrow) and heart (red arrow) are well outlined. The injection site (purple arrow) is also visible and no brain uptake (blue arrow).

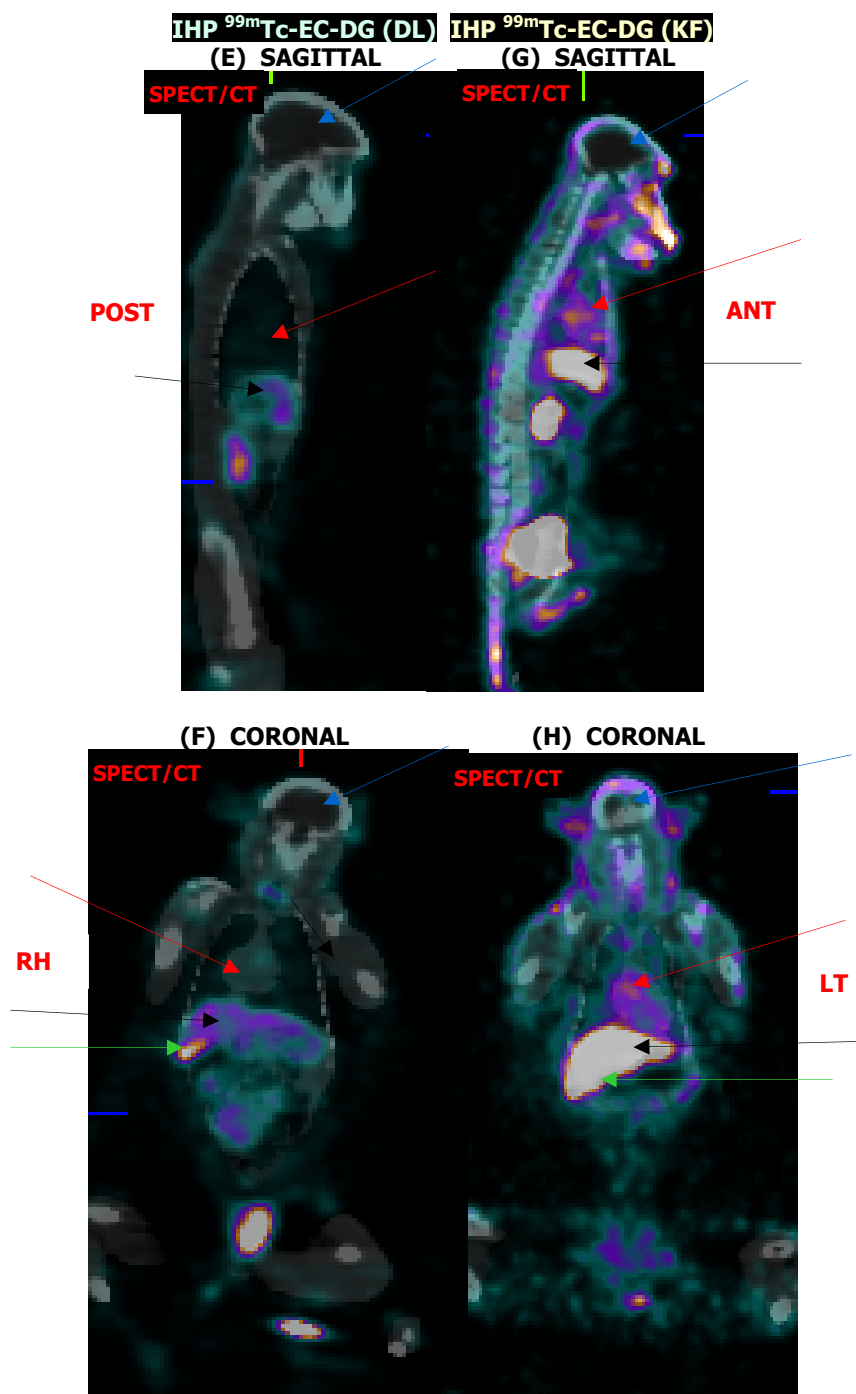


FIGURE 6.21: IHP ^{99m}Tc -EC-DG (DL) co-registered SPECT/CT (E) sagittal and (F) coronal images and IHP ^{99m}Tc -EC-DG (KF) SPECT/CT (G) sagittal and (H) coronal images at 2 hour post radiopharmaceutical administration.

Liver	←	Gallbladder	←	Injection site	←	Brain	←	
Kidney	←	Urinary bladder	←	●	Stomach	←	Heart	←

IHP ^{99m}Tc -EC-DG (KF) and (–DL) uptake in the gallbladder was observed on the 0.1 h SPECT/CT (not on the 0.1 h planar whole-body) and increased in intensity on the 2 h SPECT/CT scans. The IHP ^{99m}Tc -EC-DG (KF) uptake in the gallbladder was slightly higher than that of the of IHP ^{99m}Tc -EC-DG (DL) on the SPECT/CT scan acquired at 0.1- and 2 h. Uptake of IHP ^{99m}Tc -EC-DG (KF) and (–DL) to the snout (nasal area) of the baboons was similar and was observed on the 0.1- and 2 h SPECT/CT scans. The snout area is vascular and has a complex drainage pattern (Swindler & Wood 1982:60).

6.3.1.6.2 *SQ and SQUAL analysis*

The comparison of the SQ and SQUAL normal biodistribution results of IHP ^{99m}Tc -EC-DG (DL) with IHP ^{99m}Tc -EC-DG (KF) to the different organs in healthy baboons, is summarised in Table 6.7. The results of the organs as reported by the nuclear medicine physician for the planar whole-body and SPECT/CT images are summarised.

The SQUAL indicated no differences between the IHP ^{99m}Tc -EC-DG (DL) and IHP ^{99m}Tc -EC-DG (KF), except for the gallbladder and intestines. The 1 h whole-body images for IHP ^{99m}Tc -EC-DG (KF) was allocated positive for the intestines, but for IHP ^{99m}Tc -EC-DG (DL) background was allocated. No differences were allocated by the SQUAL to the intestines for the SPECT/CT scans. The 0.1 h whole-body images for IHP ^{99m}Tc -EC-DG (KF) was allocated positive for the gallbladder, but for IHP ^{99m}Tc -EC-DG (DL) negative was allocated. No differences were allocated by the SQUAL to the gallbladder for the SPECT/CT scans. Negative SQUAL was reported for the stomach, thyroid, spleen, brain, muscle, skin, skeleton and salivary glands for the IHP ^{99m}Tc -EC-DG (DL) and (–KF). Positive SQUAL was indicated for the liver, kidneys, bladder, heart and joints for both test formulations.

TABLE 6.7: Comparison of the SQ and SQUAL planar whole-body- and SPECT/CT results of the biodistribution to the organs of IHP ^{99m}Tc -EC-DG (DL) and IHP ^{99m}Tc -EC-DG (KF) in healthy baboons

Organ/ tissue	Time interval (h)	IHP ^{99m}Tc -EC-DG (KF)						IHP ^{99m}Tc -EC-DG (DL)					
		Static			SPECT/CT			Static			SPECT/CT		
		n	SQUAL	SQ	n	SQUAL	SQ	n	SQUAL	SQ	n	SQUAL	SQ
Lungs	0.1	6	Bkg	0	1	Bkg	0	1	Bkg	1	1	Bkg	1
	1	6	Bkg	0	*	*	*	1	Bkg	1	*	*	*
	2	6	Bkg	0	1	Bkg	0	1	Bkg	0	1	Bkg	0
Liver	0.1	6	Post	2	1	Post	2	1	Post	2	1	Post	2
	1	6	Post	2	*	*	*	1	Post	3	*	*	*
	2	6	Post	2	1	Post	2	1	Post	2	1	Post	2
Stomach	0.1	6	Neg	0	1	Neg	0	1	Neg	0	1	Neg	0
	1	6	Neg	0	*	*	*	1	Neg	0	*	*	*
	2	6	Neg	0	1	Neg	0	1	Neg	0	1	Neg	0
Spleen	0.1	6	Neg	0	1	Neg	0	1	Neg	0	1	Neg	0
	1	6	Neg	0	*	*	*	1	Neg	0	*	*	*
	2	6	Neg	0	1	Neg	0	1	Neg	0	1	Neg	0
Kidneys	0.1	6	Post	3	1	Post	3	1	Post	3	1	Post	3
	1	6	Post	2	*	*	*	1	Post	2	*	*	*
	2	6	Post	2	1	Post	3	1	Post	2	1	Post	2
Thyroid	0.1	6	Neg	0	1	Neg	0	1	Neg	0	1	Neg	0
	1	6	Neg	0	*	*	*	1	Neg	0	*	*	*
	2	6	Neg	0	1	Neg	0	1	Neg	0	1	Neg	0
Muscle	0.1	6	Neg	0	1	Neg	0	1	Neg	0	1	Neg	0
	1	6	Neg	0	*	*	*	1	Neg	0	*	*	*
	2	6	Neg	0	1	Neg	0	1	Neg	0	1	Neg	0
Intestines	0.1	6	Bkg	1	1	Post	1	1	Bkg	1	1	Post	1
	1	6	Post	1	*	*	*	1	Bkg	1	*	*	*
	2	6	Post	2	1	Post	2	1	Post	2	1	Post	2
Brain	0.1	6	Neg	0	1	Neg	0	1	Neg	0	1	Neg	0
	1	6	Neg	0	*	*	*	1	Neg	0	*	*	*
	2	6	Neg	0	1	Neg	0	1	Neg	0	1	Neg	0
Bladder	0.1	6	Post	3	1	Post	3	1	Post	3	1	Post	3
	1	6	Post	3	*	*	*	1	Post	3	*	*	*
	2	6	Post	3	1	Post	3	1	Post	3	1	Post	3
Skin	0.1	6	Neg	0	1	Neg	0	1	Neg	0	1	Neg	0
	1	6	Neg	0	*	*	*	1	Neg	0	*	*	*
	2	6	Neg	0	1	Neg	0	1	Neg	0	1	Neg	0
Gallbladder	0.1	6	Post	2	1	Post	3	1	Neg	0	1	Post	1
	1	6	Post	3	*	*	*	1	Post	2	*	*	*
	2	6	Post	3	1	Post	3	1	Post	2	1	Post	2
Heart	0.1	6	Post	2	1	Post	2	1	Post	2	1	Post	2
	1	6	Post	1	*	*	*	1	Post	1	*	*	*
	2	6	Post	1	1	Post	1	1	Post	1	1	Post	1
Skeleton	0.1	6	Neg	0	1	Neg	0	1	Neg	0	1	Neg	0
	1	6	Neg	0	*	*	*	1	Neg	0	*	*	*
	2	6	Neg	0	1	Neg	0	1	Neg	0	1	Neg	0
Joints	0.1	6	Post	1	1	Post	1	1	Post	1	1	Post	1
	1	6	Post	1	*	*	*	1	Post	1	*	*	*
	2	6	Post	1	1	Post	1	1	Post	1	1	Post	1
Salivary glands	0.1	6	Neg	0	1	Neg	0	1	Neg	0	1	Neg	0
	1	6	Neg	0	*	*	*	1	Neg	0	*	*	*
	2	6	Neg	0	1	Neg	0	1	Neg	0	1	Neg	0

* No SPECT/CT acquired at time interval

The lungs was the only organ that was allocated as background by the SQUAL indicator. The SQ for the lungs at 0.1- and 1 h was 0 for the IHP ^{99m}Tc -EC-DG (KF), but 1 for IHP ^{99m}Tc -EC-DG (DL) for the whole-body images. The SQ of the lungs at 0.1 h for the SPECT/CT scans was 0 for the IHP ^{99m}Tc -EC-DG (KF), but 1 for the IHP ^{99m}Tc -EC-DG (DL). At 1 h the SQ was 2 for the IHP ^{99m}Tc -EC-DG (KF), but 3 for the IHP ^{99m}Tc -EC-DG (DL). No SQ differences were observed for the SPECT/CT scans of the livers at 0.1- and 2 h. The gallbladder for the baboons administered with IHP ^{99m}Tc -EC-DG (KF) received a higher SQ score for the whole-body and SPECT/CT

images acquired at the different time intervals compared to the one baboon administered with IHP ^{99m}Tc -EC-DG (DL). The largest differences were seen at the 0.1 h time interval for the whole-body and SPECT/CT, where IHP ^{99m}Tc -EC-DG (KF) was allocated 2 and IHP ^{99m}Tc -EC-DG (DL) was allocated 0. The SQ for the SPECT/CT images of the gallbladder for IHP ^{99m}Tc -EC-DG (KF) was 3, but for the IHP ^{99m}Tc -EC-DG (DL) was 1.

6.3.1.6.3 *Comparison of the quantitative analysis*

In Table 6.8 the IHP ^{99m}Tc -EC-DG (DL) biodistribution results is compared with the results of IHP ^{99m}Tc -EC-DG (KF) for different organs/tissues of healthy baboons. The activity in all organs and tissue samples was expressed as the percentage of the total body activity per organ and presented as the mean \pm SEM, at 0.1-, 1- and 2 h post radiopharmaceutical administration. Statistical calculations also included in Table 6.8 are the median and the mean \pm SEM of the data for the IHP ^{99m}Tc -EC-DG (KF) in healthy baboons. A mean \pm SEM could not be calculated for the IHP ^{99m}Tc -EC-DG (DL) as only one baboon was used in Table 6.8.

The highest value between the IHP ^{99m}Tc -EC-DG (DL) and IHP ^{99m}Tc -EC-DG (KF) for a specific time interval indicated in bold. A statistical significance (P -value) could not be calculated between the IHP ^{99m}Tc -EC-DG (KF) and IHP ^{99m}Tc -EC-DG (DL) as there was a difference in the number of animals used for this experiment (Table 6.8). No noteworthy differences between the mean values of IHP ^{99m}Tc -EC-DG (KF) and (–DF) for the lungs, liver, stomach, spleen, large intestines, small intestines, brain, nose, mouth, gallbladder, skin and testes were observed (Table 6.8).

TABLE 6.8: Comparison of the biodistribution of IHP ^{99m}Tc -EC-DG (DL) with IHP ^{99m}Tc -EC-DG (KF) in healthy baboons

Organ/ Tissue	Time interval (h)	Median	% Biodistribution	Mean \pm SEM
		IHP ^{99m}Tc -EC-DG (KF)	IHP ^{99m}Tc -EC-DG (DL)	IHP ^{99m}Tc -EC-DG (KF)
LT Lung	0.1	1.76	2.49*	1.71 \pm 0.16
	1	0.80	0.71*	0.82 \pm 0.07
	2	0.40	0.28*	0.40 \pm 0.02
RT Lung	0.1	2.12	2.76*	2.07 \pm 0.12
	1	1.03	0.76*	1.07 \pm 0.06
	2	0.52	0.35*	0.51 \pm 0.03
Liver	0.1	5.31	5.79*	5.14 \pm 0.36
	1	3.50	2.92*	3.36 \pm 0.40
	2	2.24	2.36*	2.33 \pm 0.26
Stomach	0.1	0.20	0.50*	0.23 \pm 0.05
	1	0.13	0.21*	0.14 \pm 0.02
	2	0.07	0.10*	0.07 \pm 0.01
LT Kidney	0.1	2.03	3.48*	2.38 \pm 0.30
	1	1.02	1.41*	1.08 \pm 0.11
	2	0.63	0.68*	0.67 \pm 0.05
RH Kidney	0.1	2.18	3.51*	2.30 \pm 0.22
	1	1.25	1.36*	1.32 \pm 0.21
	2	0.74	0.90*	0.71 \pm 0.05
Spleen	0.1	0.31	0.26*	0.30 \pm 0.04
	1	0.16	0.14	0.18 \pm 0.03
	2	0.07	0.08*	0.09 \pm 0.02
Large intestines	0.1	0.25	0.37*	0.23 \pm 0.05
	1	0.19	0.14*	0.17 \pm 0.02
	2	0.07	0.10*	0.08 \pm 0.01
Small intestines	0.1	0.38	0.33*	0.35 \pm 0.03
	1	0.21	0.14*	0.21 \pm 0.03
	2	0.10	0.09*	0.12 \pm 0.01
Brain	0.1	0.44	0.41*	0.45 \pm 0.05
	1	0.27	0.15*	0.29 \pm 0.03
	2	0.16	0.08*	0.17 \pm 0.02
Heart	0.1	4.43	2.77*	4.41 \pm 0.35
	1	1.74	0.99*	1.75 \pm 0.17
	2	0.89	1.06*	0.95 \pm 0.06
Nose	0.1	0.81	1.15*	0.80 \pm 0.07
	1	0.38	0.36*	0.38 \pm 0.02
	2	0.19	0.17*	0.19 \pm 0.01
Mouth	0.1	1.54	1.98*	1.65 \pm 0.20
	1	0.87	0.72*	0.85 \pm 0.08
	2	0.45	0.37*	0.47 \pm 0.05
Gallbladder	0.1	0.99	1.03*	1.11 \pm 0.17
	1	1.18	0.53*	1.19 \pm 0.12
	2	1.12	0.46*	1.14 \pm 0.17
Skin	0.1	0.02	0.03*	0.02 \pm 0.00
	1	0.02	0.02*	0.02 \pm 0.00
	2	0.01	0.01*	0.01 \pm 0.00
Muscle	0.1	0.10	0.23*	0.11 \pm 0.01
	1	0.06	0.09*	0.06 \pm 0.01
	2	0.03	0.05*	0.03 \pm 0.00
Testes	0.1	0.21	0.20*	0.21 \pm 0.05
	1	0.15	0.24*	0.16 \pm 0.04
	2	0.08	0.16*	0.08 \pm 0.02
Joint	0.1	0.29	0.40*	0.31 \pm 0.02
	1	0.21	0.25*	0.21 \pm 0.02
	2	0.15	0.16*	0.15 \pm 0.01
Bladder	0.1	15.13	20.98*	14.74 \pm 1.07
	1	29.20	57.85*	28.45 \pm 4.26
	2	32.83	58.36*	30.07 \pm 5.83

All data are the mean % biodistribution to specific organs of the IHP ^{99m}Tc -EC-DG (DL) ($n=1$ baboon), \pm the SEM, and the mean % biodistribution of the IHP ^{99m}Tc -EC-DG (KF) ($n=6$ baboons) at 0.1-, 1- and 2 h post administration.

*No Mean \pm SEM could be calculated

Mean differences worth mentioning was found at 0.1 h where the IHP ^{99m}Tc -EC-DG (DL) (3.48 and 3.51) mean value for the kidneys were higher compared to the IHP ^{99m}Tc -EC-DG (KF) (2.38 and 2.30). Differences at 0.1- and 1 h was observed for the heart, where IHP ^{99m}Tc -EC-DG (KF) (4.41; 1.75) was higher than IHP ^{99m}Tc -EC-DG (DL) (2.77 ; 0.99) for both time intervals. At all three imaging time intervals of the bladder very high mean differences were observed between the IHP ^{99m}Tc -EC-DG (KF) (14.74; 28.45; 30.07) and the IHP ^{99m}Tc -EC-DG (DL) (20.98; 57.85; 58.36). The IHP ^{99m}Tc -EC-DG (DL) therefore indicated a higher localisation in the kidneys and higher excretion of IHP ^{99m}Tc -EC-DG (DL) into the bladder compared to the IHP ^{99m}Tc -EC-DG (KF). As only one baboon was imaged with IHP ^{99m}Tc -EC-DG (DL) the exact reasons for this difference in renal excretion function cannot be determined and could be investigated in a larger animal sample.

SQUAL differences were indicated between the IHP ^{99m}Tc -EC-DG (DL) and IHP ^{99m}Tc -EC-DG (KF) for the intestines at 1 h and for the gallbladder at 0.1 h (Table 6.7). SQ differences were observed for the lungs at 0.1 h and liver at 0.1- and 2 h between the two formulations of IHP ^{99m}Tc -EC-DG (Table 6.7). Quantitative differences were indicated for the heart at 0.1- and 1 h, for the kidneys at 0.1 h and for the bladder at all three imaging time intervals between IHP ^{99m}Tc -EC-DG (DL) and IHP ^{99m}Tc -EC-DG (KF) (Table 6.8). The *in vivo* clearance of the organs in which differences between IHP ^{99m}Tc -EC-DG (DL) and IHP ^{99m}Tc -EC-DG (KF) were found with the SQUAL, SQ and quantitative method were depicted in Figures 6.21-6.23.

In Figure 6.21A the *in vivo* clearance of the intestines of IHP ^{99m}Tc -EC-DG (DL) and IHP ^{99m}Tc -EC-DG (KF) indicates high clearance between 0.1- and 1 h for the small- and the large intestines. The large intestines of the baboons administered with IHP ^{99m}Tc -EC-DG (KF) overall showed the slowest clearance over the 2 h after administration. Clearance difference of the gallbladders of IHP ^{99m}Tc -EC-DG (DL) and IHP ^{99m}Tc -EC-DG (KF) was observed between 0.1-1 h, where IHP ^{99m}Tc -EC-DG (DL) showed intense clearance and IHP ^{99m}Tc -EC-DG (KF) a slight increase in uptake (Figure 6.22B). These significant clearance changes are only observed between 0.1-1 h for IHP ^{99m}Tc -EC-DG (DL) and IHP ^{99m}Tc -EC-DG (KF) and similar slow clearance for both formulations was found from 1 h up to 2 h. The highest

clearance from the lungs for IHP ^{99m}Tc -EC-DG (DL) and IHP ^{99m}Tc -EC-DG (KF) was observed before 1 h (Figure 6.23A). Very similar clearance was found between 1 and 2 h for IHP ^{99m}Tc -EC-DG (DL) and IHP ^{99m}Tc -EC-DG (KF). Minimal insignificant clearance differences were found in the liver of the baboons administered with IHP ^{99m}Tc -EC-DG (DL) and IHP ^{99m}Tc -EC-DG (KF) (Figure 6.23B). Faster clearance of IHP ^{99m}Tc -EC-DG (KF) compared to IHP ^{99m}Tc -EC-DG DL was observed in the heart before 1 h (Figure 6.22C). The greatest clearance differences were observed in the heart between 1-2 h, where uptake with IHP ^{99m}Tc -EC-DG (DL) increased and IHP ^{99m}Tc -EC-DG (KF) decreased between these two formulations. IHP ^{99m}Tc -EC-DG (DL) had the highest localisation in the kidneys and the fastest clearance before 1 h compared to IHP ^{99m}Tc -EC-DG (KF) (Figure 6.24A). After 1 h IHP ^{99m}Tc -EC-DG (KF) and IHP ^{99m}Tc -EC-DG (DL) showed very similar clearance in the kidneys of the baboons. IHP ^{99m}Tc -EC-DG (KF) and IHP ^{99m}Tc -EC-DG (DL) (highest) showed increased accumulation in the bladder before 1 h. Similarities were observed between 1-2 h as there was almost no clearance or accumulation for both RP formulations, staying constant.

The differences found between the IHP ^{99m}Tc -EC-DG (KF) and IHP ^{99m}Tc -EC-DG (DL) for the lungs, liver and intestines in baboons with the different evaluation techniques indicated that these differences were small and should be considered as not significant. The variances found between the IHP ^{99m}Tc -EC-DG (KF) and IHP ^{99m}Tc -EC-DG (DL) in the heart, gallbladder, kidneys and bladder were higher and could indicate possible implications of the minimal differences between these two formulations of IHP ^{99m}Tc -EC-DG. A larger animal sample with IHP ^{99m}Tc -EC-DG (DL) should be investigated to confirm that these differences in organ biodistribution and clearance can be attributed not to a specific baboon, but to the labelling techniques.

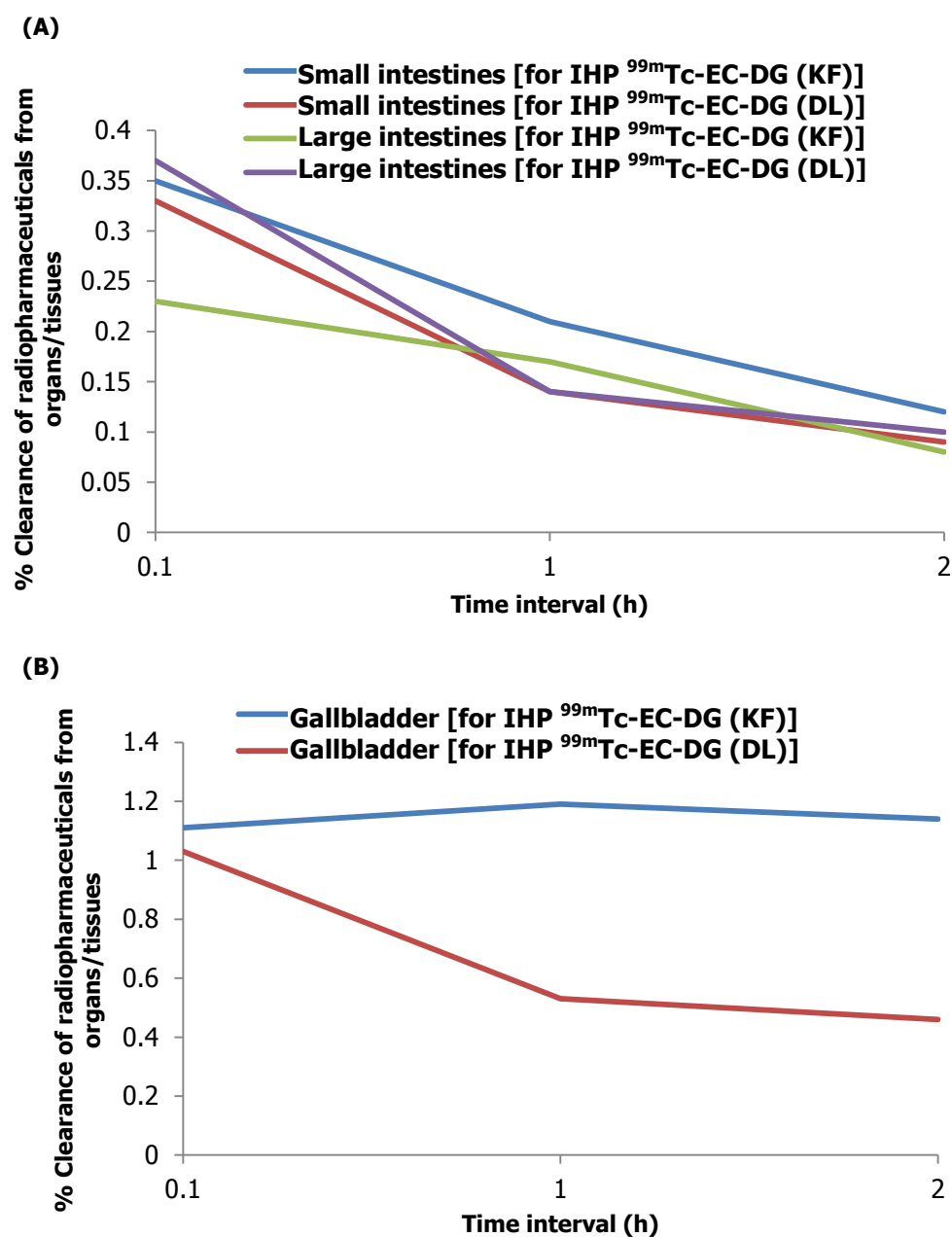


FIGURE 6.22: Comparison of clearance of the high uptake organs from the IHP $^{99m}\text{Tc-EC-DG}$ (KF) and IHP $^{99m}\text{Tc-EC-DG}$ (DL) in healthy baboons. Mean % uptake values for the (A) intestines and the (B) gallbladder are shown with time.

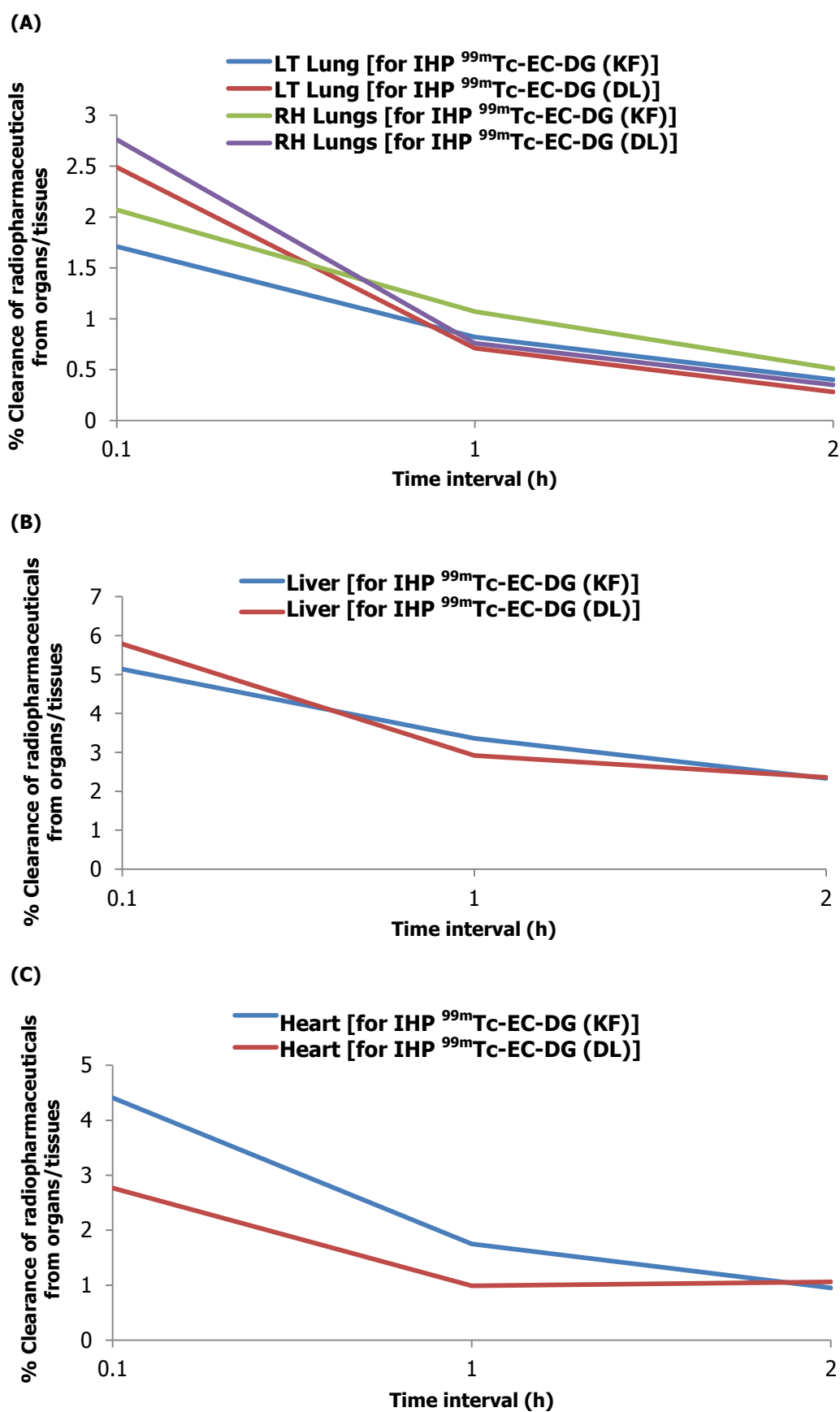


FIGURE 6.23: Comparison of clearance of high uptake organs for IHP ^{99m}Tc -EC-DG (KF) and IHP ^{99m}Tc -EC-DG (DL) in healthy baboons. Mean % uptake values for the (A) lungs, (B) liver and (C) heart are shown with time.

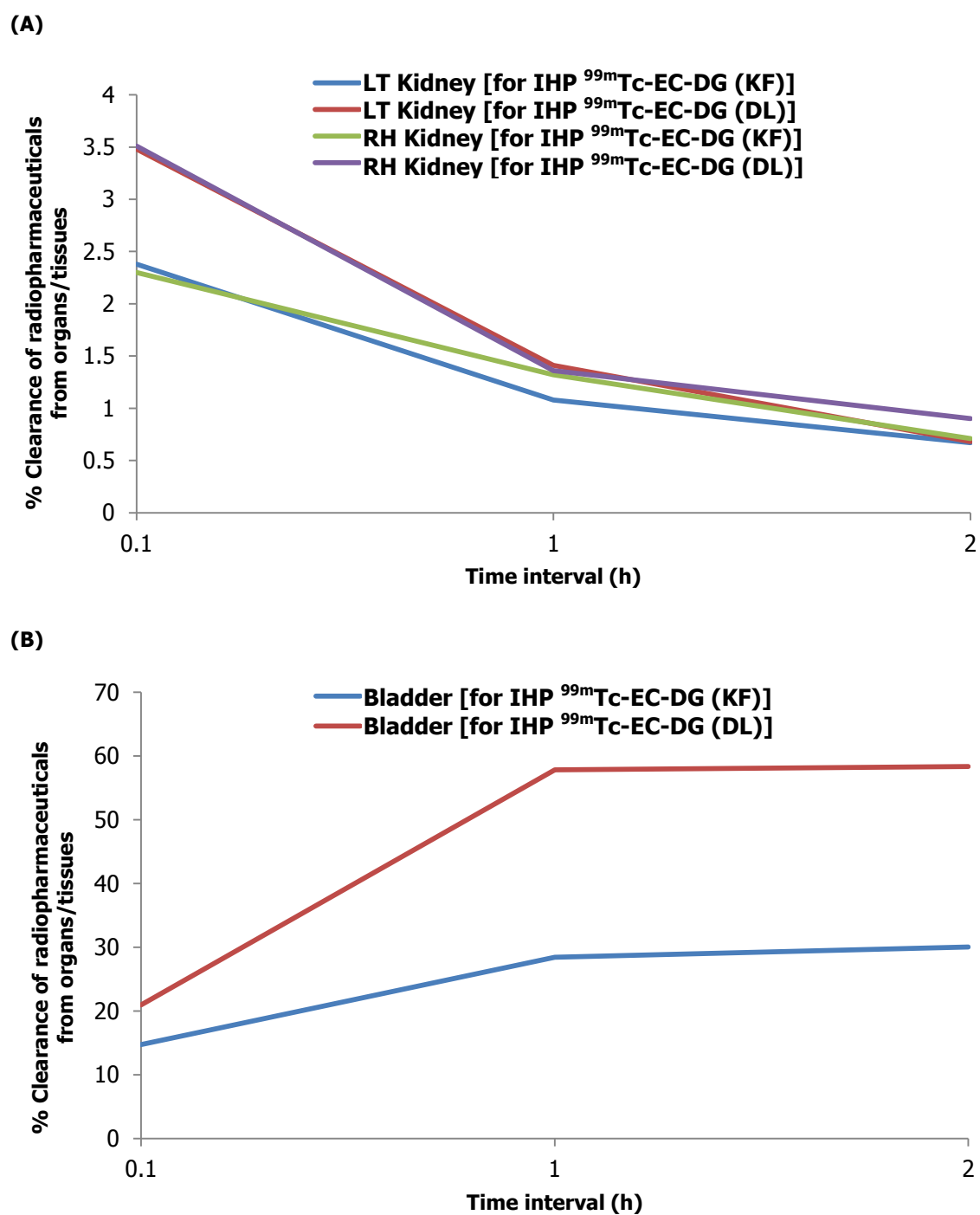


FIGURE 6.24: Clearance profile of IHP ^{99m}Tc -EC-DG (KF) and IHP ^{99m}Tc -EC-DG (DL) excretion by (A) kidneys into the (B) bladder for healthy baboons

6.4 KEY FINDINGS – HEALTHY BABOON MODELS

The uptake of IHP ^{99m}Tc -EC-DG (KF) in the healthy baboons was the highest in the kidneys with excretion into the bladder, followed by the liver and the heart. IHP ^{99m}Tc -EC-DG had no uptake in the brain and the assumption can be made that it cannot cross the blood-brain barrier (Schechter *et al.* 2009:1590). A possible explanation for IHP ^{99m}Tc -EC-DG not being able to cross the blood-brain barrier can be attributed to its hydrophilic characteristic and the relatively large molecular weight/size of $^{99m}\text{TcO}_4^-$ that it is labelled with.

The uptake of $^{99m}\text{TcO}_4^-$ in the healthy baboons were found to be the salivary glands, thyroid and stomach analogous to that found humans (Beasley *et al.* 1966:1435). The thyroid, salivary glands and stomach showed high uptake of $^{99m}\text{TcO}_4^-$, with no uptake of IHP ^{99m}Tc -EC-DG (KF) to these areas. The normal excretory route of $^{99m}\text{TcO}_4^-$ in humans is by the urinary tract into the bladder and this is also the case for baboons. $^{99m}\text{TcO}_4^-$ showed a kidney clearance into the bladder than IHP ^{99m}Tc -EC-DG (KF). Early uptake in the heart by IHP ^{99m}Tc -EC-DG (DL) and $^{99m}\text{TcO}_4^-$ was also present with all the result evaluation techniques. IHP ^{99m}Tc -EC-DG and $^{99m}\text{TcO}_4^-$ had low uptake in the brain, muscles, joints and skin.

The differences found between the IHP ^{99m}Tc -EC-DG (KF) and IHP ^{99m}Tc -EC-DG (DL) for the lungs, liver and intestines in baboons with the different evaluation techniques indicated that these differences were small and should be considered as not significant. The variances found between the IHP ^{99m}Tc -EC-DG (KF) and IHP ^{99m}Tc -EC-DG (DL) in the heart, gallbladder, kidneys and bladder were higher and could indicate possible implications of the minimal differences between these two formulations of IHP ^{99m}Tc -EC-DG. A larger animal sample with IHP ^{99m}Tc -EC-DG (DL) should be investigated to confirm that these differences in organ biodistribution and clearance can be attributed not to a specific baboon, but to the labelling techniques.

6.5 SIDE-EFFECTS OF IHP ^{99m}Tc -EC-DG IN HEALTHY BABOONS

The utilisation of a baboon model before the future research and testing of the IHP ^{99m}Tc -EC-DG in human trials was a good quality assurance safety option. The healthy baboons administered with IHP ^{99m}Tc -EC-DG (DL) and (-KF) showed no anaphylactic

reactions. None of the baboons died during these experiments and safety of IHP ^{99m}Tc -EC-DG (DL) and (-KF) was also established with this pre-clinical healthy baboon study.

6.6 INTERSPECIES DIFFERENCES BETWEEN HEALTHY BABOONS AND RABBITS

The greatest biodistribution differences with IHP ^{99m}Tc -EC-DG in the healthy baboons and rabbits were observed in the gallbladder. The gallbladders of the rabbits could not be visualised even after 4 h after administration with SPECT/CT imaging (Figure 5.11), whereas it could clearly be observed on 0.1 h SPECT/CT in baboons (Figure 6.5). Interspecies biodistribution differences between rabbits and baboons were also found with $^{99m}\text{TcO}_4^-$. The $^{99m}\text{TcO}_4^-$ uptake in the livers of rabbits was very high (Figure 5.11) and were visually comparable to the uptake of $^{99m}\text{TcO}_4^-$ to the stomach of baboons (Figure 6.13). The rabbit study showed very low $^{99m}\text{TcO}_4^-$ uptake in the stomach (Figure 5.11). These organ biodistribution differences were only clearly observed on the SPECT/CT images as the rabbit is a very small animal.

In the area of the brain increased uptake could be seen up to 1 hour after IHP ^{99m}Tc -EC-DG administration of the radiopharmaceutical, this was not seen with the baboons. The ear was used as injection site with the rabbits and the femoral vein for the baboons. The slow clearance of the IHP ^{99m}Tc -EC-DG from the veins close to the brain could give the wrong impression that there is brain uptake in the early images of the rabbits. The slow clearance of activity from the ear vein also influenced the count statistics for the brain.

6.7 CONCLUSION

$^{99m}\text{TcO}_4^-$ uptake in healthy baboons showed coinciding results with that found in clinical studies in humans (Beasley *et al.* 1966:1435). Certain biodistribution similarities were found in IHP ^{99m}Tc -EC-DG and $^{99m}\text{TcO}_4^-$ to the skin, muscle, brain, heart, lungs and liver in non-fasting, passive healthy baboons. The greatest biodistribution differences between by visual interpretation (SQ and SQUAL) between the IHP ^{99m}Tc -EC-DG and $^{99m}\text{TcO}_4^-$ was found to be the thyroid, salivary glands and stomach of baboons. These

differences also confirmed the good labelling efficiency of IHP $^{99m}\text{Tc-EC-DG}$ as organs in which free $^{99m}\text{TcO}_4^-$ is indicated showed no RP uptake with IHP $^{99m}\text{Tc-EC-DG}$. Biodistribution and clearance differences were found between IHP $^{99m}\text{Tc-EC-DG}$ (KF) and IHP $^{99m}\text{Tc-EC-DG}$ (DL) in the heart, gallbladder, kidneys and bladder. The gallbladder was not clearly visualized on the 0.1 h whole-body images, but could be clearly observed on the 0.1 h SPECT/CT scans for both test formulations. This finding again emphasised the value of SPECT/CT imaging in pre-clinical studies to confirm anatomical and physiological organ localisation. Biodistribution differences were found with IHP $^{99m}\text{Tc-EC-DG}$ and $^{99m}\text{TcO}_4^-$ of healthy baboons compared to the healthy rabbits to specific organs. The biodistribution of $^{99m}\text{TcO}_4^-$ was similar to that found in humans confirming the baboon as an excellent model for pre-clinical biodistribution studies.

CHAPTER 7

CONCLUSION AND RECOMMENDATIONS

7.1 INTRODUCTION

The field of Nuclear Medicine can be divided into molecular imaging (diagnostic) and therapeutic treatment. The development of radiolabelled biochemical compounds and imaging devices to detect radioactivity by external imaging has expanded the use of nuclear medicine studies in drug developmental research. In the RSA context, the burden of disease on the RSA economy has increased due to high levels of human immunodeficiency virus (HIV) and TB. The ideal would be to provide high quality health care services to all government patients and therefore, research should be done in different areas like low-priced effective drugs and low-cost diagnostic imaging techniques. Research on new development radiopharmaceuticals for the diagnosis of cancer, infection and other disease can be a viable option in the area of nuclear medicine diagnostic imaging. The search for the novel radiopharmaceutical that has all the ideal characteristics e.g. safe, low cost, low radiation to patient and staff (short-half-life), and distinguishing between infection and a variety of tumours has not yet been found (Figure 1.1). An in-depth study was done with the IHP ^{99m}Tc -EC-DG as a metabolic, diagnostic imaging agent for the detection of tumours and IFI/IF utilising animal models. In this chapter, the conclusions made from each of the three phases of this research evaluating the IHP ^{99m}Tc -EC-DG in different animal models are given. Recommendations on future research projects to be performed with the IHP ^{99m}Tc -EC-DG are also given, as well as an overall conclusion for this research.

7.2 OVERVIEW OF THE STUDY

7.2.1 Research problem

^{18}F -FDG is currently the gold standard in glucose metabolism imaging agents for tumours, but is not used by all nuclear medicine private practices and government nuclear medicine departments due to the following reasons:

- ^{18}F is cyclotron produced thus expensive for consumers that do not have their own cyclotron for production. Transport cost charges further increase the price if it has to be transported over long distances.
- Special motivations have to support ^{18}F -FDG PET/CT diagnostic studies to be performed in private practice, if the government department does not have their own PET camera.
- Not all medical aids provide funding for ^{18}F -FDG studies due to their high cost and patients cannot always afford to pay R25 000 for a diagnostic study.
- PET (with CT) cameras are expensive and not all government or private practices can afford this equipment.

There is also other limitations to ^{18}F -FDG e.g. short physical half-life (no late imaging can be performed) and high brain uptake (difficult to evaluate low grade tumours even with SUV). Since these impacts the use of ^{18}F -FDG negatively there is a need for a glucose metabolism imaging agent overcoming these challenges.

7.2.2 Methods of investigation

In this thesis different animal models were studied with *ex vivo* and *in vivo* biodistribution analysis. These models included:

- nude mice model to evaluate IHP $^{99\text{m}}\text{Tc}$ -EC-DG for normal and tumour biodistribution compared to ^{18}F -FDG,
- the rabbit model for IHP $^{99\text{m}}\text{Tc}$ -EC-DG biodistribution in normal, septic- and sterile IFI/IF compared to $^{99\text{m}}\text{TcO}_4^-$ and ^{67}Ga -citrate,
- the baboon model to evaluate the normal biodistribution of IHP $^{99\text{m}}\text{Tc}$ -EC-DG (KF and DL) compared to $^{99\text{m}}\text{TcO}_4^-$.

7.2.3 Results and findings

7.2.3.1 Normal biodistribution

7.2.3.1.1 Excretion routes

IHP $^{99\text{m}}\text{Tc}$ -EC-DG has two main excretion routes namely the hepatobiliary and renal system. Factors that can influence the biliary excretion of radiopharmaceuticals are molecular size, -weight,

polarity (lipid solubility), molecular structure, possibly the protein binding and animal species (Wistow *et al.* 1977:459). Increased molecular weight (300 to 1000 g/mol) and lipid polarity of compounds tend to elevate biliary excretion and this could contribute to the early excretion of ^{99m}Tc -EC-DG (molecular weight 685.54 g/mol) in the non-fasting baboon (Wistow *et al.* 1977:455; Yang *et al.* 2003:466).

7.2.3.1.2 *Organ biodistribution*

All three animal species showed increased biodistribution of the IHP ^{99m}Tc -EC-DG to the liver. IHP ^{99m}Tc -EC-DG demonstrated rapid clearance by the kidneys and a decrease in background activity on the scintigraphic images could also be noted. In the rabbits high activity in the region of the brain could be seen up to 1 hour after the administration of the IHP ^{99m}Tc -EC-DG. The test radiopharmaceutical was administered into the ear vein and slow clearance of the radioactivity from the veins close to the brain could give the wrong impression that there is brain uptake and influence count statistics. No biodistribution to the brain was found in the different animal models on the SPECT/CT images despite the fact that glucose is the essential fuel for the human brain metabolism. This is in contrast with ^{18}F -FDG which shows high levels of uptake in the brain. The conclusion can be made that the IHP ^{99m}Tc -EC-DG does not pass over the BBB in accordance with earlier literature findings. The lower heart uptake with IHP ^{99m}Tc -EC-DG, is most likely due to the fact that the healthy baboons were not fasting which reduces blood clearance of a glucose metabolism imaging agent. The influence of fasting on biodistribution to the myocardium can further be investigated.

7.2.3.1.3 *Interspecies differences*

Similar biodistribution results were obtained between the different healthy animal species with the IHP ^{99m}Tc -EC-DG, but differences

were found between the animal species of the control groups with $^{99m}\text{TcO}_4^-$. The $^{99m}\text{TcO}_4^-$ biodistribution to the stomach and liver of the New Zealand White rabbits differed from the Southern African baboons. The liver uptake of the rabbits was similar to that of the stomach of the baboons. Physiological differences exist between different animal species and the assumption should not be made that similar biodistribution results will be obtained with the same radiopharmaceutical in the different animal species. The biodistribution differences of $^{99m}\text{TcO}_4^-$ to the same organs of rabbits and baboons were not clear on planar imaging, but improved on SPECT/CT images, because of the improved resolution of SPECT and 3-Dimensional display. Biodistribution to the gallbladder of the healthy baboon on the whole-body planar imaging increased with time and was confirmed with SPECT/CT imaging.

The healthy rabbits administered with IHP $^{99m}\text{Tc-EC-DG}$ showed increased uptake in the area close to the brain up to 1 hour after radiopharmaceutical administration. This increased IHP $^{99m}\text{Tc-EC-DG}$ uptake in the area of the brain could not be seen with the baboons. The rabbits were injected into the ear vein and the slow clearance of IHP $^{99m}\text{Tc-EC-DG}$ out of the veins close to the brain from the ear gave the impression that there is brain uptake. The uptake IHP $^{99m}\text{Tc-EC-DG}$ in the region of the brain at 1 hour was not visible on the SPECT/CT and it could be confirmed that there was no brain uptake in the rabbits. Thus, there are no interspecies differences in the brain uptake of the rabbits compared to the baboons. The administration site for radiopharmaceuticals in different animal studies should therefore be carefully be chosen, as it give the impression that interspecies difference exist when it is not present.

7.2.3.2 Tumour biodistribution

IHP $^{99m}\text{Tc-EC-DG}$ and $^{18}\text{F-FDG}$ showed similar uptake results in lung tumours induced in nude mice. These similarities were also found for lung tumours,

liver and heart uptake as well as excretion by the kidneys as described in the literature by Yang *et al.* (2003:465-473). Differences between IHP ^{99m}Tc -EC-DG values and values reported by Yang *et al.* (2003:465-473) for tumour uptake and blood clearance could be due to differences in the formulation and amounts of EC-DG administered.

7.2.3.3 IFI/IF biodistribution

Zymosan, used in this research, induced a low grade cellular IFI/IF response while *E. coli* induced a bacterial IFI/IF. IHP ^{99m}Tc -EC-DG had similar uptake in the zymosan and *E.coli* IFI/IF, whereas ^{67}Ga -citrate had an increased uptake in *E. coli* compared to zymosan IFI/IF. ^{67}Ga -citrate uses a variety of uptake mechanisms as mentioned earlier (section 2.5.3.2). Bacterial siderophores are present were not seen with zymosan induced IFI/IF and can provide a possible explanation for the higher uptake of ^{67}Ga -citrate in *E. coli*. It was therefore concluded that IHP ^{99m}Tc -EC-DG is mainly dependent on a cellular response while ^{67}Ga -citrate utilised multiple mechanisms. IHP ^{99m}Tc -EC-DG can be taken up in low grade cellular IFI/IF since the zymosan dosage used induced a low grade IFI/IF. Yet early diagnosis of IFI/IF is possible with IHP ^{99m}Tc -EC-DG, as uptake in septic and sterile IFI/IF could be localised on early images (1 h after administration).

7.2.3.4 Synthesis

Labelling efficiency of 90% could be achieved for the IHP ^{99m}Tc -EC-DG, with a pH ranging from 6-7 suitable for human administration. The IHP ^{99m}Tc -EC-DG labelling techniques proved to be accurate and valid, with no significant biodistribution differences. The labelling efficiency of the IHP ^{99m}Tc -EC-DG was satisfactory for future clinical purposes in humans although improvement of the labelling protocol is desirable to achieve 95% radiochemical purity. This will most likely be achieved through kit formulation.

7.2.3.5 Safety

IHP ^{99m}Tc -EC-DG's compliance with non-toxicity and pyrogenicity was confirmed with no anaphylactic reactions noted in the animals. None of the animals administered with the IHP ^{99m}Tc -EC-DG in this research showed any adverse reactions or decay in health during the seven days of monitoring post imaging. The safe administration of IHP ^{99m}Tc -EC-DG in different animal species (rabbits, mice and baboons) was established (yet previously reported in literature as well).

7.3 RECOMMENDATIONS FROM THIS RESEARCH

The following recommendations relating to the use of animal models for radiopharmaceutical research are made:

- IHP ^{99m}Tc -EC-DG has been shown to be safe in three animal models and should be pursued in human clinical trials, firstly as a lung cancer imaging agent and later its ability to image other types of tumours. Furthermore, its ability as infection imaging agent should also be pursued.
- The rabbit model should ideally not be used for developmental radiopharmaceuticals in gallbladder studies due to its anatomical position deep within the abdominal cavity. The baboon model would be a better option, because the evaluation of IHP ^{99m}Tc -EC-DG demonstrated clearly visible uptake in the gallbladder on the images.
- When visually evaluating the labelling efficiency of ^{99m}Tc in rabbits, increased biodistribution to the salivary glands and thyroid would indicate poor labelling and not the stomach necessarily. No $^{99m}\text{TcO}_4^-$ uptake was evident in the stomach when normal biodistribution images of rabbits were evaluated. The stomach biodistribution of $^{99m}\text{TcO}_4^-$ differs from that observed in humans (literature) and baboons. Interspecies differences relating to radiopharmaceutical biodistribution does exist and should be considered when designing a pre-clinical study.
- Researchers should be aware of the physiological differences in uptake of radiopharmaceuticals in different organs of animal species, especially when choosing an animal model to evaluate the normal biodistribution of a radiopharmaceutical. The baboon model may be best model for normal radiopharmaceutical biodistribution studies.

7.4 CONTRIBUTION AND SIGNIFICANCE OF THE RESEARCH

Low cost and availability are only some of the very important characteristics needed for optimal application of a radiopharmaceutical for clinical purposes. IHP ^{99m}Tc -EC-DG may prove a very attractive radiopharmaceutical as a glucose metabolism imaging agent, since it has several advantages including good *in vivo* stability after administration up to six hours (no thyroid visible on late scintigraphic imaging), low gamma ray emissions (140.5 keV), early infection/inflammation- and tumour detection in animals and readily availability of a generator which permits on site radionuclide availability. IHP ^{99m}Tc -ECDG imaging can also be performed with a standard gamma camera and collimator. No special additional imaging equipment to gamma camera necessary for example a PET camera or medium- or high energy collimators (very expensive). The newly developed EC-technology technique enables the labelling of radioisotopes for various imaging applications, e.g. ^{99m}Tc -EC-DG (for non-small cell lung cancer imaging), ^{99m}Tc -EC-Annexin (cell apoptosis) and ^{99m}Tc -EC-Metronidazole to image tumour cell hypoxia. Cold metallic treatment products in the developmental stages, labelled with the aid of EC-technology include Platinum-EC-G and $^{187}\text{Rhenium}$ -EC-G. The IHP ^{99m}Tc -EC-DG as a newly developed radiopharmaceutical, pose advantages such as low-cost imaging with basic gamma camera equipment and standard collimator. Third World Countries can reap the benefits of research in radiopharmaceuticals like ^{99m}Tc -EC-DG, where cost-effectiveness is of critical importance.

7.4.1 Advantages of IHP ^{99m}Tc -EC-DG

The IHP ^{99m}Tc -EC-DG has a number of advantages which include the following:

- Labelling of EC-DG with $^{99m}\text{TcO}_4^-$ is fairly easy, efficiently and high radiochemical purity and stability can be achieved.
- IHP ^{99m}Tc -EC-DG (pure gamma-emitter) has a lower radiation burden compared to ^{18}F -FDG (beta-emitter) and can be especially of value when paediatric patients are in need of diagnostic imaging.
- Faster detection of focal IFI/IF compared to ^{67}Ga -citrate (24-78 hours post administration images) and ^{99m}Tc -HMPAO (early imaging only performed 6 hours post administration) used in most nuclear medicine departments for imaging of IFI/IF. Since IHP ^{99m}Tc -EC-DG has shorter investigation times it provides an alternative to evaluate IFI/IF.

- Imaging does not require special equipment like ^{67}Ga -citrate (a medium energy collimator) and ^{18}F -FDG (PET camera).
- No white blood cell labelling (with its associated health risks) is required for IFI/IF imaging and can be directly injected into the patient.
- $^{99\text{m}}\text{Tc}$ physical half-life of 6 h can facilitate late imaging if needed.
- $^{99\text{m}}\text{Tc}$ is freely available in nuclear medicine departments and labelling with EC-DG can be immediately performed.
- IHP $^{99\text{m}}\text{Tc}$ -EC-DG can be cost effective: With this research five dosages for baboons were obtained from one labelled kit formulation which indicates that two human doses is achievable from each kit. ^{18}F -FDG is sold per single patient dose.
- IHP $^{99\text{m}}\text{Tc}$ -EC-DG biodistribution images demonstrated no significant interfering bowel activity indicating its usefulness for abdominal IFI/IF.
- A variety of IFI/IF (sterile and septic) could be detected with IHP $^{99\text{m}}\text{Tc}$ -EC-DG (possible opportunistic).
- Less likeliness of inducing an immunogenic response (adverse effects) than radiopharmaceuticals that contain artificially produced blood elements and humanised murine antibodies.

7.5 FUTURE RESEARCH

Future potential ground-breaking research projects to be performed with $^{99\text{m}}\text{Tc}$ -EC-DG include:

- The clinical pilot study, "Molecular Imaging of in-house prepared $^{99\text{m}}\text{Tc}$ -EC-DG and ^{18}F -FDG in Breast and Non-small-cell lung cancer," was approved by the Medicines Control Council of the Department of Health (RSA) and UFS Faculty of Health Sciences Research Ethical Committee approved to be conducted at UAH in Bloemfontein. This study is the first of its kind in the world that will be performed with $^{99\text{m}}\text{Tc}$ -EC-DG to evaluate of breast cancer.
- Future clinical studies can focus on gathering human whole-body biodistribution and dosimetry studies to provide radiation dose estimates for adult human males and females and validate the baboon as a substitute to human research subjects. The research participants should however void their bladder to reduce the absorbed radiation dose to the urinary bladder and to improve imaging to structures around pelvic area.

- The evaluation of ^{99m}Tc -EC-DG in the detection of brain tumours (BBB damaged) which would be unique as no publications could be found for human studies.
- The diagnostic evaluation of ^{99m}Tc -EC-DG in neurological diseases, for example Alzheimer's disease.
- Evaluation of ^{99m}Tc -EC-DG as an IFI/IF imaging tool in humans still needs to be explored and compared with other known IFI/IF imaging radionuclides and radiopharmaceuticals like ^{99m}Tc -HMPAO, ^{18}F -FDG and ^{67}Ga -citrate. ^{99m}Tc -EC-DG can play a possible role as a cost-effective imaging radiopharmaceutical to detect and assess TB and the response to newly developed drugs.
- Comparative studies of ^{99m}Tc -EC-DG with newly developmental radionuclides and radiopharmaceuticals like ^{68}Ga -citrate, $^{68}\text{Ga}(3+)$, ^{68}Ga -DOTA-VAP-P, ^{68}Ga -TAFC-, ^{68}Ga -NOTA-UBI and ^{18}F -FDG for diagnostic infection imaging.
- As ^{99m}Tc -EC-DG is a glucose analogue similar to ^{18}F -FDG but with low brain uptake. Bunevicius *et al.* (2013:1-11) indicated that ^{18}F -FDG can be an alternative, non-invasive tool to magnetic resonance imaging (MRI) and computed tomography (CT) for the management of acute stroke patients. ^{99m}Tc -EC-DG may have additional advantages over ^{18}F -FDG, for example imaging can be performed with no special equipment; only a gamma camera, low cost, non-invasive imaging and a low radiation dose (^{99m}Tc $t_{1/2}$ is 6 hours). Early and delayed (24 hour post injection) radiopharmaceutical imaging can provide important information on the central nervous system abnormalities. ^{99m}Tc -EC-DG imaging properties in acute stroke patients have not been researched yet, but need to be evaluated and compared to ^{18}F -FDG.
- The influence of fasting and sedation on ^{99m}Tc -EC-DG uptake in IFI/IF and tumours compared to similar influences on ^{18}F -FDG studies.
- A comparison in the sensitivity and specification between ^{99m}Tc -EC-DG and ^{18}F -FDG should be included in future research work. Since the imaging characteristics of a PET system seem to be superior to that of SPECT it is important to show that similar or improved sensitivity and specificity can be obtained.
- In order to make differential diagnosis between tumours and predict early treatment response a glucose metabolism imaging agent must also be able to evaluate cell nuclei activity (Yang *et al.* 2004:252). ^{99m}Tc -EC-DG is able to transport through the nuclei membrane, but ^{18}F -FDG is not able to perform this action due to "metabolic trapping". IHP ^{99m}Tc -EC-DG due to structural and chemical similarities to ^{99m}Tc -EC-DG in the literature should be further evaluated

in humans for its role in differential diagnosis of tumour and in the prediction of early treatment response.

7.6 CONCLUSIONS

IHP ^{99m}Tc -EC-DG's feasibility for the detection and diagnosis of IFI/IF and tumours in animals was confirmed in this research. It can therefore be an alternative to ^{18}F -FDG as glucose metabolism imaging agent for IFI/IF and tumour as well as for ^{67}Ga -citrate since earlier IFI/IF detection is possible. IHP ^{99m}Tc -EC-DG may be a superior agent to ^{18}F -FDG for brain - (BBB damaged) and lung tumour imaging due to the lower background (check blood background). IHP ^{99m}Tc -EC-DG with SPECT/CT can therefore provide cellular target and anatomical information about IFI/IF and specific tumours (only lung tumours were evaluated in this research). The evaluation of the biodistribution of the IHP ^{99m}Tc -EC-DG in animals confirmed its IFI/IF and tumour imaging potential as well as safety prior to possible use in humans.

The findings in research phase one supports the initial hypothesis that the IHP ^{99m}Tc -EC-DG has the potential to be used as a functional metabolic diagnostic imaging radiopharmaceutical. In addition comparable results were found with the gold standard, ^{18}F -FDG in lung tumour cell line inoculated into nude mice and may be in future a cheaper and more readily available alternative for lung tumour imaging than ^{18}F -FDG.

Human studies with IHP ^{99m}Tc -EC-DG should be pursued in order to increase current knowledge of ^{99m}Tc -EC-DG for future use in clinical practice, for example how variable factors like fasting or non-fasting affect tumour uptake in humans. The specific and high uptake (biodistribution) of the IHP ^{99m}Tc -EC-DG in infection/inflammation and non-small cell lung tumours, may have a diagnostic application.

7.7 CONCLUDING REMARK

From the research covered in this thesis there is no doubt that IHP ^{99m}Tc -EC-DG exhibits promising detection characteristics for IFI/IF and specific tumours. Furthermore, IHP ^{99m}Tc -EC-DG has a future potential to improve diagnosis and

prognosis, planning and monitoring of cancer treatment in humans and should be investigated further.

REFERENCES

- Alberts, B., Johnson, A., Lewis, J., Raff, M., Roberts, K. & Walter, P. 2002. *Molecular Biology*. Fourth Edition. New York: Garland Science.
- Almeida, C.A. & Barry, S.A. 2010. *Cancer basic science and clinical aspects*. First Edition. Oxford: Wiley-Blackwell.
- Aly, N. & El-Gendy, K. 2015. Impact of parathion exposure on some biochemical parameters in rabbit as a non target organism. *Alexandria Journal of Medicine* 51:11-17.
- Ando, A., Nitta, K., Ando, I., Sanada, S., Katsuda, S., Tonami, N., Hiraki, T., Hisada, K. & Ogawa, H. 1990. Mechanism of gallium 67 accumulation in inflammatory tissue. *European Journal of Nuclear Medicine* 17:21-27.
- Andros, G., Harper, P.V., Lathrop, K.A. & Robert, J.M. 1965. Pertechnetate-99m Localization in Man with Applications to Thyroid Scanning and the Study of Thyroid Physiology. *The journal of clinical endocrinology and metabolism* 25:1067-1076.
- Angelides, S., El-Mashaleh, M., Anagnostou, M., Howe, G., Spencer, D., Kumar, V. & Manolios, N. 2014. The role of ^{99m}Tc-labelled glucosamine (^{99m}Tc-ECDG) in the evaluation of rheumatic joint disease: a screening experience. *Nuclear Medicine Communications* 35:655-665.
- Babich, J.W. & Fischman, A.J. 1999. Target imaging of infection. *Advanced Drug Delivery Reviews* 37:237-252.
- Beasley, T.M., Palmer, H.E. & Nelps, W.B. 1966. Distribution and excretion of Technetium in Humans*. *Health Physics* 12:1425-1435.
- Bleeker-Rovers, C.P., Boerman, O.C., Rennen, H.J.J.M., Corstens, F.H.M. & Oyen, W.J.G. 2004. Radiolabeled compounds in diagnosis of infectious and inflammatory disease. *Current Pharmaceutical Design* 10:2935-2950.

Boellaard, R., O'Doherty, M.J., Weber, W.A., Mottaghy, F.M., Lonsdale, M.N., Stroobants, S.G., Oyen, W.J.G., Kotzerke, J., Hoekstra, O.S., Pruim, J., Marsden, P.K., Tatsch, K., Hoekstra, C.J., Visser, E.P., Arends, B., Verzijlbergen, F.J., Zijlstra, J.M., Comans, E.F.I., Lammertsma, A.A., Paans, A.M., Willemsen, A.T., Beyer, T., Bockisch, A., Schaefer-Prokop, C., Delbeke, D., Baum, R.P., Chiti, A. & Krause, B.J. 2009. FDG PET and PET/CT: EANM procedure guidelines for tumour PET imaging: version 1.0. *European Journal of Nuclear Medicine and Molecular Imaging* 37:181-200.

Bowen, M.L. & Orvig, C. 2008. 99m-Techetium carbohydrate conjugates as potential agents in molecular imaging. *Chemical Communications* 41:5077-5079.

Bradshaw, D., Pillay-Van Wyk, V., Laubscher, R., Nojilana, B., Groenewald, P., Nannan, N. & Metcalf, C. 2010. *Cause of death statistic for South Africa: Challenges and possibilities for improvement*. [Online]. Cape Town: Medical Research Council. [Accessed 10 December 2014]. Available from: <www.mrc.ac.za/bod/cause_death_statsSA.pdf> Retrieved on 7 June 2013.

Brown, G.K. 2000. Glucose transporters: Structure, function and consequences of deficiency. *Journal of Inherited Metabolic Disease* 23:237-247.

Bryant, J., Yang, D., Schechter, N. 2007. Evaluation of Tc-99m-EC-DG in lung cancer patients. *Journal of Nuclear Medicine* 48:354.

Buck, A.K., Nekolla, S., Ziegler, S., Beer, A., Krause, B.J., Herrmann, K., Scheidhauer, K., Wester, H.J., Rummeny, E.J., Schwaiger, M. & Drzezga, A. 2008. SPECT/CT. *Journal of Nuclear Medicine* 49:1305-1319.

Bushberg, J.T., Seibert, J.A., Leidholdt, E.M. & Boone, J.M. 2002. *The Essential Physics of Medical Imaging*. Second Edition. Philadelphia: Lippincott Williams and Wilkins.

Buscombe, J. 2013. Guidelines for the use of ^{18}F -FDG in infection and inflammation: a new step in cooperation between the EANM and SNMMI. *European Journal of Nuclear Medicine and Molecular Imaging* 40:1120-1121.

Case, J.A., Bateman, T.M., Cullom, J.S., Siegmund, M., Robison, K. & Rollo, D. 2012. Myocardial Uptake of a Novel Tc-99m Labeled Glucose Analog (Tc-99m EC-DG) in Normal and Ischemic Subjects during Rest and Exercise Stress Testing. Poster session presented at: *Seventeenth Annual Scientific Session of the American Society of Nuclear Cardiology*; September 6-9, 2012; Baltimore, United States of America.

Cell>Point. 2015. Patents. [Online]. [Accessed 2 January 2015]. Available from: <<http://cellpointweb.com/patents/>>

Chen, W., Silverman, D.H.S., Delaloye, S., Czernin, J., Kamdar, N., Pope, W., Satyamurthy, N, Schiepers, C & Cloughesy, T. 2006. ^{18}F -FDOPA PET Imaging of Brain Tumors: Comparison Study with ^{18}F -FDG PET and Evaluation of Diagnostic Accuracy. *Journal of Nuclear Medicine* 47:904-911.

Chen, Y., Huang, Z.W., He, L., Zheng, S.L., Li, J.L. & Qin, D.L. 2006. Synthesis and evaluation of a technetium-99m-labeled diethylene-triaminepentaacetate-deoxyglucose complex ($^{99\text{m}}\text{Tc}$]-DTPA-DG as a potential imaging modality for tumors. *Applied Radiation Isotopes* 64:342-347.

Dillon, S., Agrawal, S., Banerjee, K., Letterio, J., Denning, T.L., Oswald-Richter, K., Kasprovicz, D.J., Kellar, K., Pare, J., van Dyke, T., Ziegler, S., Unutmaz, D. & Pulendran, B. 2006. Yeast zymosan, a stimulus for TLR2 and dectin-1, induces regulatory antigen-presenting cells and immunological tolerance. *The Journal of Clinical Investigation* 116:916-928.

Diniz, S.O.F., Siqueira, C.F., Nelson, D.L., Martin-Comin, J. & Cardoso, V.N. 2005. Technetium-99m Ceftizoxime Kit Preparation. *Brazilian Archivers of Biology and Technology* 48:89-96.

Dippenaar, H., Joubert, G. & Van Rooyen, C. 2005. How cheap is primary health care? Cost per script at the Heidedal Community Health Centre and National District Hospital in Bloemfontein. *South African Family Practice* 47:37-39.

Dormehl, I.C., Hugo, N. & Beverley, G. 1992. The Baboon: An Ideal Model in Biomedical Research. *Anesthesia & Pain Control in Dentistry* 1:109-279.

Eckelman, W.C. 2009. Unparalleled Contribution of Technetium-99m to Medicine Over 5 Decades. *JACC: Cardiovascular Imaging* 2:364.

Edwards, C.L. & Hayes, R.L. 1969. Tumor Scanning with ^{67}Ga Citrate. *Journal of Nuclear Medicine* 10:103-105.

Elgazzar, A.H. 2012. *A Concise Guide to Nuclear Medicine*. First Edition. Heidelberg: Springer.

Elsinga, P., Todde, S., Penuelas, I., Meyer, G., Farstad, B., Faivre-Chauvet, A., Mikolajczak, R., Westera, G., Gmeiner-Stopar, T., Decristoforo, C. & The Radiopharmacy Committee of the EANM. 2010. Guidance on current good radiopharmacy practice (cGRPP) for small-scale preparation of radiopharmaceuticals. *European Journal of Nuclear Medicine Molecular Imaging* 37:1049-1062.

Erdő, F., Török, K., Arányi, P. & Székely, J.I. 1993. A new assay for antiphlogistic activity: Zymosan-induced mouse ear inflammation. *Agents Actions* 39:137-142.

Eubank, W.B. & Mankoff, D.A. 2005. Evolving Role of Positron Emission Tomography in Breast Cancer Imaging. *Seminars in Nuclear Medicine* 35:84-99.

European Association of Nuclear Medicine (EANM) Radiopharmacy Committee. 2007. Guidelines on current good radiopharmacy practice (cGRPP) in the preparation of radiopharmaceuticals. [Online]. [Accessed 18 July 2014]. Available from: www.eanm.org/publications/guidelines/gl_radioph_cgrpp.pdf?PHPSESSID=e8r7fer3i65c20t463hsjbb8t5

Fanti, S., Mohsen, F. & Mansi, L. 2009. *Atlas of PET/CT A Quick Guide to Image Interpretation*. Heidelberg: Springer.

Festing, M.F.W. & Altman, D.G. 2002. Guidelines for the Design and Statistical Analysis of Experiments Using Laboratory Animals. *Institute for Laboratory Animal Research Journal* 43 244-258.

Franken, P.R., Guglielmi, J., Vanhove, C., Koulibaly, M., Defrise, M., Darcourt, J. & Pourcher, T. 2010. Distribution and Dynamics of $^{99\text{m}}\text{Tc}$ -Pertechnetate Uptake in the

Thyroid and Other Organs Assessed by Single-Photon Emission Computed Tomography in Living Mice. *Thyroid* 20:519-526.

Fueger, B.J., Czernin, J., Hildebrandt, I., Tran, C., Halpern, B.S., Stout, D., Phelps, M.E. & Weber, W.A. 2006. Impact of Animal Handling on the Results of ^{18}F -FDG PET studies in Mice. *Journal of Nuclear Medicine* 47:999-1006.

Fukuda, H., Kubota, K. & Matsuzawa, T. 2013. Pioneering and Fundamental Achievements on the Development of Positron Emission Tomography (PET) in Oncology. *The Tohoku Journal of Experimental Medicine* 230:155-169.

Gatley, S.J. 2003. Labeled Glucose Analogs in the Genomic Era. *The Journal of Nuclear Medicine* 44(7):1082-1086.

Gilles, R.J., Schomack, P.A., Secomb, T.W., Raghunand, N. 1999. Cause and Effects of Heterogeneous Perfusion in Tumors. *Neoplasia* 1(3):197-207.

Giovanella, B.C., Yim, S.O., Stehlin, J.S., Williams, L.J. 1972. Development of Invasive Tumors in the "Nude" Mouse After Injection of Cultured Human Melanoma Cells. *Journal of the National Cancer Institute* 48:1531-1533.

Gonzaleza, J., Hidalgo, F., Esteller, A. & Lopez, M.A. 1983. Effect of biliverdin and bilirubin on the hepatic excretion of bile pigments in the rabbit. *Comparative Biochemistry and Physiology* 74:67-70.

Govender, R.D. 2005. The barriers and challenges to Health Promotion in Africa. *The South African Family Practice* 47:39-42.

Groch, M.W. & Erwin, W.D. 2000. SPECT in the Year 2000: Basic Principles. *Journal of Nuclear Medicine Technology* 28:233-244.

Hamazawa, Y., Koyama, K., Okamura, T., Wada, Y., Wakasa, T., Okuma, T., Yasuyoshi, W. & Inoue, Y. 2007. Comparison of dynamic FDG-microPET study in a rabbit turpentine-induced inflammatory model and in a rabbit VX2 tumor model. *Annals of Nuclear Medicine* 21:47-55.

Hammersley, P.A.G. & Taylor, D.M. 1979. The Mechanism of the Localization of ^{67}Ga Citrate in Experimental Abscesses. *European Journal of Nuclear Medicine* 4:271-275.

Hammersley, P.A.G., Taylor, D.M. & Cronshaw, S. 1980. The Mechanism of ^{67}Ga Uptake in Animal and Human Tumours. *European Journal of Nuclear Medicine* 5:411-415.

Handel, T.M. & Hamel, D.J eds. 2009. *Methods in Enzymology, Volume 461, Chemokines, Part B*. First Edition. United States of America: Academic Press.

Hara, N., Onoguchi, M., Takenaka, K., Matsubara, K., Ujita, H. and Kenko, Y. 2010. Assessment of Patient Exposure to X-Radiation from SPECT/CT Scanners. *Journal of Nuclear Medicine Technology* 38:138-147.

Harapanhalli, R.S. 2010. Food and Drug Administration Requirements for Testing and Approval of New Radiopharmaceuticals. *Seminars in Nuclear Medicine* 40:364-384.

Harbert, J. & Da Rocha, A.F.G. 1984. *Textbook of Nuclear Medicine Volume I: Basic Science*. Second Edition. Philadelphia: Lea & Febiger.

Harper, P.V., Lathrop, K.A., Jiminez, F., Fink, R. & Gottschalk, A. 1965. Technetium $^{99\text{m}}$ as a Scanning Agent. *Radiology* 85:101-109.

Harris, B., Goudge, J., Ataguba, J.E., McIntyre, D., Nxumalo, N, Jikwana, S. & Matthew, C. 2011. Inequities in access to health care in South Africa. *Journal of Public Health Policy* 32:102-123.

Helal, N. 2015. Patient organs dose calculations in nuclear medicine. *International Journal of Research and Reviews in Applied Sciences* 11:153-161.

Hughes, D.K. 2003. Nuclear Medicine and Infection Detection: The Relative Effectiveness of Imaging with ^{111}In -Oxine-, $^{99\text{m}}\text{Tc}$ -HMPAO-, and $^{99\text{m}}\text{Tc}$ -Stannous Fluoride Colloid-Labeled Leukocytes and with ^{67}Ga -citrate. *Journal of Nuclear Medicine Technology* 31:196-201.

Hung, J.C., Ponto, J.A. & Hammes, R.J. 1996. Radiopharmaceutical-Related Pitfalls and Artifacts. *Seminars in Nuclear Medicine* 26:208-255.

Hunter, P.A., Darby, G.K. & Russell, N.J. eds. 1995. *Symbiotic Associations*. Cambridge: Cambridge University Press.

International Atomic Energy Agency (IAEA). 2008a. *Clinical Applications of SPECT/CT: New Hybrid Nuclear Medicine Imaging System*. Vienna: IAEA.

International Atomic Energy Agency (IAEA). 2008b. *Technetium-99m Radiopharmaceuticals: Manufacture of kits*. Vienna: IAEA.

International Atomic Energy Agency (IAEA). 2009. *Technetium-99m Radiopharmaceuticals: Status and trends*. Vienna: IAEA.

Imam, S.K. 2005. Molecular Nuclear Imaging: The Radiopharmaceuticals (Review). *Cancer Biotherapy & Radiopharmaceuticals* 20:163-170.

Irwin, R.S., Doherty, P.W., Bartter, T., Gionet, M.M. & Collins, J.A. 1988. Evaluation of Technetium Pertechnetate as a Radionuclide Marker of Pulmonary Aspiration of Gastric Contents in Rabbits*. *Chest* 93:1270-1275.

Jacene, H.A., Goetze, S., Patel, H., Wahl, R.L. & Ziessman, H.A. 2008. Advantages of Hybrid SPECT/CT vs SPECT Alone. *The Open Medical Imaging Journal* 2:67-79.

Jalilian, A.R., Novinrooz, A., Motamedi-Sedeh, F., Moradkhani, Rajamand, A.A. & Solati, J. 2009. Evaluation of [^{67}Ga]Citrate in The Detection of Various Microorganism Infection in Animal Models. *Iranian Journal of Nuclear Medicine* 17:34-41.

Kim, E.E., Lee, D.S., Tateishi, U & Baum, R.P. 2012. *Handbook of Nuclear Medicine and Molecular Imaging: Principles and Clinical Applications*. Singapore: World Scientific Publishing.

Kim, E.E. & Yang, D.J. 2001. *Targeted Molecular Imaging in Oncology*. First Edition. New York: Springer.

Koba, W., Jelicks, L.A. & Fine, E.J. 2013. MicroPET/SPECT/CT Imaging of Small Animal Models of Disease. *The American Journal of Pathology* 182:319-323.

Kobayashi, T., Taniquchi, S., Ye, Y., Niekrasz, M., Nour, B. & Cooper, D.K. 1998. Comparison of bile chemistry between humans, baboons, and pigs: implications for clinical and experimental liver xenotransplantation. *Laboratory Animal Sciences* 48:197-200.

Koivula, T. 2011. *Development of radiosynthesis methods for ^{18}F -labelled radiopharmaceuticals*. Ph.D. thesis, University of Helsinki, Helsinki, Finland.

Kowalsky, R.J. & Perry, J.R. 2011. *Radiopharmaceuticals in Nuclear Pharmacy and Nuclear Medicine*. Third Edition. Washington: American Pharmacists Association.

Kumar, R., Nadig, M.R., Balakrishnan, V., Bal, C. & Malhotra, A. 2006. FDG-PET Imaging in Infection and Inflammation. *Indian Journal of Nuclear Medicine* 21:104-113.

Kumar, V., Ali, M., Angelides, S. & Manolios, N. 2007. Synthesis and characterization of $^{99\text{m}}\text{Tc}$ -Glucosamine & $^{99\text{m}}\text{Tc}$ -His-CP and evaluation of their utility in imaging inflammatory arthritis. *ANZ Nuclear Medicine* 38:10-13.

Lambrecht, F.Y., Durkan, K. & Unak, P. 2008. Preparation, quality control and stability of $^{99\text{m}}\text{Tc}$ -cefuroxime axetil. *Journal of Radioanalytical and Nuclear Chemistry* 275:161-164.

Lee, A.L., Kim, J.I., Lee, J.W., Cho, Y.J., Lee, B.H., Chung, H.W., Park, K.K. & Han, J.S. 2012. Effects of Various Anesthetic Protocols on ^{18}F -Fluorodeoxyglucose Uptake into the Brains and Hearts of Normal Miniature Pigs. *Journal of the American Association for Laboratory Animal Science* 51:246-252.

Lee, K.H., Ko, B.H., Paik, J.Y., Jung, K.H., Choe, Y.S., Choi, Y. & Kim, B.T. 2005. Effects of Anesthetic Agents and Fasting Duration of ^{18}F -FDG Biodistribution and Insulin Levels in Tumor-Bearing Mice. *Journal of Nuclear Medicine* 46:1531-1536.

National Center for Biotechnology. *PubChem Compound Database CID=45100585*. [Online]. [Accessed 30 August 2014]. Available from:
<<http://pubchem.ncbi.nlm.nih.gov/summary/summary.cgi?cid=45100585>>

Levy, O.M., Gittelman, M.C., Strashun, A.M., Cohen E.L. & Fine, E.J. 1983. Diagnosis of acute testicular torsion using radionuclide scanning. *Journal Urology* 129:957-958.

Medicines Control Council. 2003. *Registration of Medicines. Clinical (2.09)*. [Online]. [Accessed 13 December 2014]. Available from:
<<http://www.mccza.com>>

Medicines Control Council. 2010. *Inspectorate and Law Enforcement. Guide to good manufacturing practice for medicines in South Africa (4.01)*. [Online]. [Accessed 13 December 2014]. Available from:
<<http://www.mccza.com>>

Medicines Control Council. 2012. *Registration of Medicines. General Information (2.01)*. [Online]. [Accessed 13 December 2014]. Available from:
<<http://www.mccza.com>>

Meneses do Rêgo, A.C., Araújo-Filho, I., Medeiros Azevedo, Í., Jácome, D.T., de Alcântara, R., Ramalho, O., Medeiros, A.C. 2010. Biodistribution of technetium-99m pertechnetate after Roux-en-Y gastric bypass (Capella technique) in rats. *Acta Cirúrgica Brasileira* 25:9-12.

Mettler, F.A. & Guiberteau, M.J. 2012. *Essentials of Nuclear Medicine Imaging*. Sixth Edition. Philadelphia: Elsevier.

Ming, R.H., Strickland, R.G., Listrom, M. & Fenoglio-Preiser, C. 1989. The CD4 Leu 8⁺ T helper cell in colonic mucosa: a quantitative and functional analysis. *Clinical and Experimental Immunology* 75:297-300.

Mochizuki, T., Tsukamoto, E., Kuge, Y., Kanegae, K., Zhao, S., Hikosaka, K., Hosokawa, M., Kohanawa, M. & Tamaki, N. 2001. FDG Uptake and Glucose Transporter Subtype Expressions in Experimental Tumor and Inflammation Models. *Journal of Nuclear Medicine* 42:1551-1555.

Moore, D.M. 2000. *Laboratory Animal Medicine and Science Series II. Rats and Mice: Biology*. Washington: University of Washington.

Mrabet, Y. 2009. *Glycolysis*. [Online]. [Accessed 3 January 2015]. Available from: <http://en.wikibooks.org/wiki/Structural_Biochemistry/Volume_2#/media/File:Glycolysis.svg>

National Cancer Institute. 2012. *NCI Drug Dictionary*. [Online]. [Accessed 13 May 2012]. Available from: <<http://www.cancer.gov/drugdictionary?CdrID=640261>>

Naudé, H. 1998. *Scatter and attenuation correction techniques for absolute quantification of radionuclide distributions with SPECT*. Ph.D. thesis, University of the Free State, Bloemfontein, RSA.

Nelson, D.L. & Cox, M.M. 2004. *Lehninger Principles of Biochemistry*. Fourth Edition. New York: Freeman and Company.

Oyen, W.J.G., Boerman, O.C. & Corstens. 2001. Animal models of infection and inflammation and their role in experimental nuclear medicine. *Journal of Microbiological Methods* 47:151-157.

Oxford Concise Medical Dictionary. 2003. Sixth Edition. Oxford: Oxford University Press.

Oxford Dictionary of Chemistry. 2004. Fourth Edition. Oxford: Oxford University Press.

Pauwels, E.K.J, McCready, V.R., Stoot, J.H.M.B & van Deurzen, D.F.P. 1998(a). The mechanism of accumulation of tumour-localising radiopharmaceuticals. *European Journal of Nuclear Medicine* 25:277-305.

Pauwels, E.K.J., Ribeiro, M.J., Stoot, J.H.M.B., McCready, V.R., Bourguignon, M. & Mazière, B. 1998(b). FDG Accumulation and Tumor Biology. *Nuclear Medicine & Biology* 25:317-322.

Petruzzi, N., Shanthly, N. & Thakur, M. 2009. Recent trends in Soft-tissue infection imaging. *Seminars in Nuclear Medicine* 39:115-123.

Pomper, M.G. & Lee, J.S. 2005. Small Animal Imaging in Drug Development. *Current Pharmaceutical Design* 11:3247-3272.

Quesenberry, K. & Carpenter, J.W. 2011. *Ferrets, Rabbits and Rodents: Clinical Medicine and Surgery*. Missouri: Elsevier Saunders.

Rahmim, A. & Zaidi, H. 2008. PET versus SPECT: strengths, limitations and challenges. *Nuclear Medicine Communications* 29:193-207.

Razzak, M.A., Naguib, M. & El-Garhy, M. 1967. Fate of Sodium Pertechnetate-Techetium-99m. *Journal of Nuclear Medicine* 8:50-59.

Rennen, H.J.J.M, Boerman, O.C., Oyen, W.J.G. & Corstens, F.H.M. 2001. Imaging infection/inflammation in the new millennium. *European Journal of Nuclear Medicine* 28:241-252.

Richmond, A. & Su, Y. 2008. Mouse xenograft models vs GEM models for human cancer therapeutics. *Disease Models & Mechanisms* 1:78-82.

Rosenzwajg, M., Jourquin, F., Tailleux, L. & Gluckman, J.C. 2002. CD40 ligation and phagocytosis differently affect the differentiation of monocytes into dendritic cells. *Journal of Leukocyte Biology* 72:1180-1189.

Rossouw, D.D., Lötter, M.G., Du Raan, H., Jansen, S.E., Höhn, A. & Burger, B.V. 2005. Radiosynthesis and evaluation of two novel ¹²³I-labeled 2-methyl-4-nitroimidazole derivatives as potential infection imaging agents. *Nuclear Medicine and Biology* 32:385-394.

Russell, P., Hertz, P. & McMillan, B. 2011. *Biology: The Dynamic Science*. Second Edition. Belmont: Brooks/Cole.

Russell, W.M.S. & Burch. R.L. 1959. *The Principles of Humane Experimental Technique*. London: Methuen.

Rygaard, J. & Povlsen, C.O. 1969. Heterotransplantation of a human malignant tumor to 'nude' mice. *Acta Pathologica et Microbiologica Scandinavica* 77:758-760.

Saha, G.B. 1996. *The Chemistry of Tc-99m-Labeled Radiopharmaceuticals*. New Mexico: University of New Mexico Pharmacy Continuing Education.

Saha, G.B. 2003. *Fundamentals of Nuclear Pharmacy*. Fifth Edition. New York: Springer.

Saha, G.B. 2006. *Physics and Radiobiology of Nuclear Medicine*. Third Edition. New York: Springer.

Sathekge, M.M., Maes, A. Pottel, H. Stoltz, A. & Wiele, C. 2010. Dual time-point FDG PET/CT for differentiating benign from malignant solitary pulmonary nodules in a TB endemic area. *South African Medical Journal* 100:598-601.

Schechter, N.R., Erwin, W.D., Yang, D.J., Kim, E.E., Munden, R.F., Forster, K., Taing, L.C., Cox, J.D., Macapinlac, H.A. & Podoloff, D.A. 2009. Radiation dosimetry and biodistribution of ^{99m}Tc -ethylenedicysteine-deoxyglucose in patients with non-small-cell lung cancer. *European Journal of Nuclear Medical Molecular Imaging* 36:1583-1591.

Schechter, N.R., Yang, D.J., Azhdarinia, A. & Chanda, M. 2007. Technologies for Translational Imaging Using Generators in Oncology. *Anti-Cancer Drug Discovery* 2:251-258.

Sharkey, F.E. & Fogh, J. 1984. Considerations in the use of nude mice for cancer research. *Cancer Metastasis Reviews* 3:341-360.

Shukla, S.K., Manni, G.B. & Cipriani, C. 1977. Behaviour of pertechnetate ion in humans. *Journal of Chromatography* 143:522-526.

Signore, A., Alessandria, D. Lazzeri, E. & Dierckx, R. 2008. Can we produce an image of bacteria with radiopharmaceuticals? *European Journal of Nuclear Medicine Molecular Imaging* 35:1051-1055.

Silindir, M & Özer, A.Y. 2008. Adverse Reactions to Radiopharmaceuticals (ARRP): Particular To Technetium Radiopharmaceuticals. *FABAD Journal Pharmaceutical Sciences* 33:109-117.

Som, P., Atkins, H.L., Bandoypadhyay, D., Fowler, J.S., MacGregor, R.R., Matsui, K., Oster, Z.H., Sacker, D.F., Shiue, C.Y., Turner, H., Wolf, A.P. & Zabinski, S.V. 1980. A Fluorinated Glucose Analog, 2-fluoro-2-deoxy-D-glucose (F-18): Nontoxic Tracer for Rapid Tumor Detection. *The Journal of Nuclear Medicine* 21:670-675.

Southworth, R., Parry, C.R., Parkes, H.G., Medina, R.A. & Garlick, P.B. 2003. Tissue-specific differences in 2-fluoro-2-deoxyglucose metabolism beyond FDG-6-P: a ^{19}F NMR spectroscopy study in the rat. *NMR in Biomedicine* 16:494-502.

Swindler, D.R. & Wood, C.D. 1982. *An atlas of Primate Gross Anatomy*. Florida: Robert E. Krieger Publishing Company.

Sykes, T.R., Noujaim, A.A., Stephens-Newsham, L.G., Lentle, B.C., Ng, P.K. & Hooper, H.R. 1987. Biological behavior of ^{67}Ga -citrate in New Zealand White rabbits. *European Journal of Nuclear Medicine* 13:95-99.

Taylor, B. & Burns, D. 2005. Can medical scheme reform lead to fairer distribution of limited resources? A funding perspective. *South African Medical Journal* 95:175-179.

Theodorakis, M.C., Groutas, W.C., Bermudez, A.J., Magnin, D. & Stefankou, S.V.A. 1980. Localization of Technetium 99m-Ethylenediamine-N,N'bis(alpha-2-hydroxy-5-bromophenyl)acetic acid and technetium 99m-N-(2-mercapto-1-oxopropyl)glycine in Hepatobiliary System. *Journal of Pharmaceutical Sciences* 69:581-584.

Toutain, P.L., Ferran, A. & Bousquet-Mélou, A. 2010. *Handbook of Experimental Pharmacology*. Heidelberg: Springer-Verlag.

Tsao, N., Wang, C.H., Her, L.J., Tzen, K.Y., Chen, J.Y., Yu D.F. & Yang D.J. 2011. Development of ^{68}Ga -Glycopeptide as an Imaging Probe for Tumor Angiogenesis. *Journal of Biomedicine and Biotechnology* 2011:1-9.

Tsopelas, C. 2015. Radiotracers used for the scintigraphic detection of infection and inflammation. *The Scientific World Journal* 2015:1-33.

Uthamanthil, R.K., Hachem, R.Y., Gagea, M., Reitzel, R.A., Borne, A.T. & Tinkey, P.T. 2013. Urinary Catheterization of Male Rabbits: A New Technique and a Review of Urogenital Anatomy. *Journal of the American Association for Laboratory Animal Science* 52:180-185.

Uz ZaMan, M. 2007. ^{99m}Tc -EC-deoxyglucose – a poor man's ^{18}F -FDG: what will be the future of PET in molecular imaging? *European Journal of Nuclear Medicine Molecular Imaging* 34:429.

Vanbilloen, H.P., Cleynhens, B.J. & Verbruggen A.M. 2000. Technetium-99m Labeled Ethylenecysteamine Cysteine (^{99m}Tc -ECC), the Mono-acid Derivative of ^{99m}Tc -L,L-ethylenedicysteine. *Nuclear Medicine and Biology* 27:207-214.

VandeBerg, J.L., Williams-Blangero, S & Tardif, S.D. eds. 2009. *The Baboon in Biomedical Research*. First Edition. New York: Springer Science and Business Media.

Van der Laken, C.J., Boerman, O.C., Oyen, W.J.G., Van de Ven, M.T.P., Ven Der Meer, J.W.M. & Corstens, F.H.M. 1998. The kinetics of radiolabelled interleukin-8 in infection and sterile inflammation. *Nuclear Medicine Communications* 19:271-281.

Varga, M. 2013. *Textbook of Rabbit Medicine*. Second Edition. China: Elsevier.

Velikyan, I. 2014. Prospective of ^{68}Ga -Radiopharmaceutical Development. *Theranostics* 4:47-79.

Wagner, H.N. 2006. *A Personal History of Nuclear Medicine*. First Edition. London: Springer Science & Business.

Wagner, H. N. 1995. *Principles of Nuclear Medicine*. Second Edition. Philadelphia: W.B. Saunders Company.

Warburg, O. 1956. On the Origin of Cancer Cells. *Science* 123:309-314.

Weissleder, R., Ross, B.D., Rehemtulla, A., Gambhir, S.S. 2010. *Molecular Imaging Principles and Practice*. First Edition. Connecticut: People's Medical Publishing House.

Williams, L.E. 2011. *Radiopharmaceuticals: Introduction to Drug Evaluation and Dose Estimation*. First Edition. Florida: Taylor & Francis Group.

Wistow, B.W., Subramanian, G., Van Heertum, R.L., Henderson, R.W., Gagne, G.M., Hall, R.C. & McAfee, J.G. 1977. An Evaluation of ^{99m}Tc -Labeled Hepatobiliary Agents. *Journal of Nuclear Medicine* 18:455-461.

Workman, P., Aboagye, E.O., Balkwill, F., Balmain, A., Bruder, G., Chaplin, D.J., Double, J.A., Everitt, J., Farningham, D.A.H., Glennie, M.J., Kelland, L.R., Robinson, V., Stratford, I.J., Tozer, G.M., Watson, S., Wedge, S.R. & Eccles, S.A. 2010. Guidelines for the welfare and use of animals in cancer research. *British Journal of Cancer* 102:1555-1577.

Xiong, Q.F. & Chen, Y. 2008. Deoxyglucose Compounds Labeled with Isotopes Different from 18-Fluoride: Is There a Future in Clinical Practice? *Cancer Biotherapy & Radiopharmaceuticals* 23:376-381.

Yang, D.J., Azhdarinia, A & Edmund K.E. 2005. Tumor Specific Imaging Using Tc-99m and Ga-68 Labeled Radiopharmaceuticals. *Current Medical Imaging Reviews* 1:25-34.

Yang, D.J., Azhdarinia, A., Yu, D.F., Kim, E.E. & Podoloff, D.A. 2001. ^{99m}Tc -EC-Deoxyglucose: Synthesis, Cellular uptake, Biodistribution and Scintigraphic imaging. *Journal of Labelled Compounds and Radiopharmaceuticals* 44:513-514.

Yang, D.J., Kim, C.G., Schechter, N.R., Azhdarinia, A., Yu, D.F., Oh, C.S., Bryant, J.L., Won, J.J., Kim, E.E. & Podoloff, D.A. 2003. Imaging with ^{99m}Tc ECDG Targeted at the Multifunctional Glucose Transport System: Feasibility Study with Rodents. *Radiology* 226:465-473.

Yang, D.J., Kim, C.G. & Inoue, T. 2006. Targeted molecular imaging in oncology. *Annals of Nuclear Medicine* 20:1-11.

Yang, D.J., Liu, C.W., Yu, D.F. & Kim, E. 2004. *Ethylenedicysteine (EC)-drug conjugates compositions and methods for tissue specific disease imaging*. US 6,692,724 B1.

Yang, D., Yukihiro, M., Yu, D.F., Ito, M., Oh, C.S., Kohanim, S., Azhdarinia, A., Kim, C.G., Bryant, J., Kim, E.E. & Podoloff, D. 2004. Assessment of Therapeutic Response Using ^{99m}Tc -Ethylenedicysteine-Glucosamine. *Cancer Biotherapy & Radiopharmaceuticals* 19:443-455.

Zanzonico, P. 2004. Positron Emission Tomography: A Review of Basic Principles, Scanner Design and Performance, and Current Systems. *Seminars in Nuclear Medicine* 34:87-111.

Zanzonico, P. 2008. Routine Quality Control of Clinical Nuclear Medicine Instrumentation: A Brief Review. *Journal of Nuclear Medicine* 49:1114-1131.

Zhang, Y.H., Bryant, J., Kong, F.L., Yu, D.F., Mendez, R., Kim, E.E. & Yang, D. 2012. Molecular Imaging of Mesothelioma with ^{99m}Tc -ECG and ^{68}Ga -ECG. *Journal of Biomedicine and Biotechnology* 2012:1-9.

Zhang, Y., Oh, C.S., Yang, D., Yu, D.F., Kohanim, S., Mendez, R., Chanda, J.B. and Kim, E. 2010. EC-DG: A molecule suitable in theranostic in cancers. *Journal of Nuclear Medicine* 51:1529.

Ziegler, S.I. 2005. Positron Emission Tomography: Principles, Technology, and Recent Developments. *Nuclear Physics A* 752:679-678.

Ziessman, H.A., O'Malley, J.P., Thrall, J.H. & Fahey, F.H. 2014. *The Requisites Nuclear Medicine*. Fourth Edition. Philadelphia: Elsevier Saunders.

LIST OF APPENICES

**APPENDIX A: Ionising Radiation Control Commission Committee
approval letter**

APPENDIX B: Universitas Academic Hospital approval letter

APPENDIX C: North-West University approval letter

APPENDIX D: University of the Free State Ethics Committee approval letter

APPENDIX E: Animal welfare score sheet - rabbits

APPENDIX F: Animal welfare score sheet - baboons

APPENDIX A

Ionising Radiation Control Commission Committee approval letter

APPROVAL FOR USE OF IONISING RADIATION

RADIATION CONTROL COMMITTEE

UNIVERSITAS/PELONOMI HOSPITALS

Project title: In-House Manufactured ^{99m}Tc -Ethylenedicysteine-deoxyglucose in Rabbits, Mice and Baboons: normal, Infection and Tumour Biodistribution.

Principle Investigator: J Horn-Lodewyk

Department: Nuclear Medicine

Laboratories: Nuclear Medicine Department, Universitas Hospital

Number of Patients: None (Animal Study: Mice, Baboons and Rabbits)

Radionuclide: ^{99m}Tc , ^{67}Ga , ^{18}F .

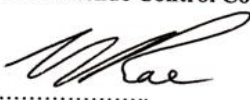
Activity MBq (mCi)	Dose per subject (mSv)	Annual limit Radiation worker	Annual limit Public
74 (2) ^{99m}Tc	?	20 mSv	1 mSv
74 (2) ^{67}Ga	?	20 mSv	1 mSv

Comments:

The investigator intends to use the above isotopes for development of a novel tracer in nuclear medicine. The only doses delivered during the study will be delivered to animals and ethics approval will be sought for that. It seems to me that although the number of animals involved is rather large, the doses per animal are small, and the radiation workers giving the isotopes to the animals should therefore not be exposed to excessive doses of radiation. The estimated doses to the injecting and imaging personnel (? the student) are not detailed in the document, but all isotope doses are lower than those routinely used in human imaging. No adverse effects are expected for the personnel conducting the study.


CHAIRPERSON
Radionuclide Control Committee

8/10/12
DATE


SECRETARY

29/9/2012
DATE

APPENDIX B

Universitas Academic Hospital approval letter

11 September 2012

Me. J. Horn-Lodewyk
Chief Nuclear Medicine Radiographer
Department of Nuclear Medicine
Universitas of Free State
(051) 405 3487



health

Department of
Health
FREE STATE PROVINCE

Dear Me. Horn-Lodewyk

RESEARCH PROJECT: IN-HOUSE MANUFACTURED ^{99m}Tc-ETHYLENEDICYSSTEINE-DEOXYGLUCOSE IN RABBITS, MICE AND BABOONS: NORMAL INFECTION AND TUMOUR BIODISTRIBUTION.

Herewith permission for the mentioned project to be done at Universitas Academic Hospital on the following conditions:

1. The research should not expose the users and the Department to any avoidable harm.
2. Annual progress reports should be submitted and also a research report at the end of the research process.
3. Reporting of Adverse Events related to the research process must be done within 48 hours of discovery.
4. There shall be provision for obtaining informed consent from all patients/staff where appropriate.
5. Briefing sessions should be conducted with all stakeholders prior to commencement and at the end of the study to provide feedback where appropriate.
6. That approval is obtained from the Ethics Committee.

The Chief Executive Officer must be notified if the findings of the project will be published and a research report needs to be sent to the Head Clinical Services as soon as the study is completed.

Yours sincerely

DR NIC R J VAN ZYL
HEAD: CLINICAL SERVICES
UNIVERSITAS ACADEMIC HOSPITAL

DR NRJ VAN ZYL

2012-09-12

HEAD: CLINICAL SERVICES
UNIVERSITAS ACADEMIC HOSPITAL

HEAD: CLINICAL SERVICES: DR NRJ VAN ZYL
Private Bag X20660, Bloemfontein, 9300. Tel. No.: 051-4052866,
Fax: 051-4053500, Room 1077, First Floor, Universitas Academic Hospital
Email: vanzylnr@universitas.fs.gov.za

APPENDIX C

North-West University approval letter



NORTH-WEST UNIVERSITY
YUNIBESITHI YA BOKONE-BOPHIRIMA
NOORDWES-UNIVERSITEIT

Private Bag X6001, Potchefstroom
South Africa 2520

Tel: (018) 299-4900
Faks: (018) 299-4910
Web: <http://www.nwu.ac.za>

Ethics Committee

Tel +27 18 299 4850
Fax +27 18 293 5329
Email Ethics@nwu.ac.za

Prof J-R Zeevaert & A Grobler

1 August 2012

ETHICS APPROVAL OF PROJECT

The North-West University Ethics Committee (NWU-EC) hereby approves your project as indicated below. This implies that the NWU-EC grants its permission that, provided the special conditions specified below are met and pending any other authorisation that may be necessary, the project may be initiated, using the ethics number below.

Project title : Evaluation of in-house manufactured [99mTc]-ECDG in xenografted mice: Biodistribution and effectiveness of tumour detection

Project Leader Prof J-R Zeevaert en A Grobler:

N	W	U	-	0	0	0	4	2	-	1	2	-	A	5
Institution			Project Number						Year			Status		

Status: S = Submission; R = Re-Submission; P = Provisional Authorisation; A = Authorisation

Approval date: 2012/06/26

Expiry date: 2017/06/25

Special conditions of the approval (if any): None

General conditions:

While this ethics approval is subject to all declarations, undertakings and agreements incorporated and signed in the application form, please note the following:

- The project leader (principle investigator) must report in the prescribed format to the NWU-EC:
 - annually (or as otherwise requested) on the progress of the project;
 - without any delay in case of any adverse event (or any matter that interrupts sound ethical principles) during the course of the project.
- The approval applies strictly to the protocol as stipulated in the application form. Would any changes to the protocol be deemed necessary during the course of the project, the project leader must apply for approval of these changes at the NWU-EC. Would there be deviation from the project protocol without the necessary approval of such changes, the ethics approval is immediately and automatically forfeited.
- The date of approval indicates the first date that the project may be started. Would the project have to continue after the expiry date, a new application must be made to the NWU-EC and new approval received before or on the expiry date.
- In the interest of ethical responsibility the NWU-EC retains the right to:
 - request access to any information or data at any time during the course or after completion of the project;
 - withdraw or postpone approval if:
 - any unethical principles or practices of the project are revealed or suspected,
 - it becomes apparent that any relevant information was withheld from the NWU-EC or that information has been false or misrepresented,
 - the required annual report and reporting of adverse events was not done timely and accurately,
 - new institutional rules, national legislation or international conventions deem it necessary.

The Ethics Committee would like to remain at your service as scientist and researcher, and wishes you well with your project. Please do not hesitate to contact the Ethics Committee for any further enquiries or requests for assistance.


Yours sincerely

Prof Amanda Lourens
(chair NWU Ethics Committee)

APPENDIX D

University of the Free State Ethics Committee approval letter

UNIVERSITY OF THE
FREE STATE
UNIVERSITEIT VAN DIE
VRYSTAAT
YUNIBESITHI YA
FRISTATA

 UFS
UV

Internal Post Box / Interne Posbus G40
Faks / Fax (051) 4444359

E-mail address: StraussHS@ufs.ac.za

Me / Ms H Strauss 2013-01-18

MS J HORN-LODEWYK
DEPT OF NUCLEAR MEDICINE
FACULTY OF HEALTH SCIENCES
UFS

Dear Ms Horn

ANIMAL EXPERIMENT NR 20/2012
RESEARCHER: MS J HORN-LODEWYK, DEPT OF NUCLEAR MEDICINE
PROJECT TITLE: IN-HOUSE MANUFACTURED ^{99m}Tc -ETHYLENEDICYSSTEINE-DEOXYGLUCOSE
IN RABBITS, MICE AND BABOONS: NORMAL, INFECTION AND TUMOUR BIODISTRIBUTION


You are hereby kindly informed that the Interfaculty Animal Ethics Committee approved the following and it will be condoned at the meeting scheduled for 28 February 2013:

ANIMAL	NUMBER	EXPIRY DATE
Rabbits	30	Jan 2014
Mice	45	Jan 2014
Baboons	06	Jan 2014

Kindly take note of the following:

5. Fully completed and signed applications have to be submitted electronically to StraussHS@ufs.ac.za and a hard copy has to be submitted too.
6. A signed progress report with regard to the above study has to be submitted electronically to StraussHS@ufs.ac.za while a hard copy has to be submitted to Ms H Strauss, Room D115, Francois Retief building, Faculty of Health Sciences. A report has to be submitted when animals are physically involved and after completion of the study. Guidelines with regard to progress reports are available from the secretary and on the Faculty Intranet.
7. Researchers that plan to make use of the Animal Experimentation Unit must request a quotation from the Head, Mr Seb Lamprecht
8. Contract research: Fifty (50%) of the quoted amount is payable when you receive the letter of approval.

Regards



CHAIR:
INTERFACULTY ANIMAL ETHICS COMMITTEE

APPENDIX E

Animal welfare score sheet - rabbits

IN-HOUSE MANUFACTURED ^{99m}Tc-ETHYLENEDICYSSTEINE-DEOXYGLUCOSE IN RABBITS, MICE AND BABOONS: NORMAL, INFECTION AND TUMOUR BIODISTRIBUTION

ANIMAL MONITORING SHEET IHM ^{99m}Tc-ECDG- NORMAL BIODISTRIBUTION

UFS AENR. Project No. 20/2012 Investigator: J. Horn-Lodewyk
Animal ID No. 1 Species /Strain/ **White New Zealand Rabbits**
Animal Details (sex, age etc) Male

- Each animal is examined and observed for abnormalities at each time point (weekly or daily as appropriate)
- Observations are recorded in the table
- Normal clinical signs are recorded as "N"
- Abnormalities are recorded as "A" and severity is scored in brackets eg Breathing: A (3)
- Comments concerning abnormalities are recorded in the comments section of the table
- Additional observations tailored to the monitoring requirements for each animal experiment are to be added at "Other"

CLINICAL OBSERVATION (N or A)	DATE							
	30-01-13	31-01-13	01-02-13	02-02-13	03-02-13	04-02-13	05-02-13	06-02-13
UNDISTURBED								
Coat	N	N	N	N	N	N	N	N
Activity	N	N	N	N	N	N	N	N
Breathing	N	N	N	N	N	N	N	N
Movement/gait	N	N	N	N	N	N	N	N
Eating	N	N	N	N	N	N	N	N
Drinking	N	N	N	N	N	N	N	N
Alert/Sleeping	N	N	N	N	N	N	N	N
ON HANDLING								
Alert	N	N	N	N	N	N	N	N
Body condition	N	N	N	N	N	N	N	N
Bodyweight (g)	4200	4200	4200	4200	4250	4300	4300	4300
Body temperature (°C)	39.8	39.8	39.8	39.8	39.8	39.8	39.8	39.8
Dehydration	N	N	N	N	N	N	N	N
Eyes	N	N	N	N	N	N	N	N
Faeces	N	N	N	N	N	N	N	N
Nose	N	N	N	N	N	N	N	N
Breathing	N	N	N	N	N	N	N	N
Urine	N	N	N	N	N	N	N	N
Vocalisation	N	N	N	N	N	N	N	N
OTHER (specify)								
COMMENTS								
INITIALS:	<i>JHL</i>	<i>JHL</i>	<i>JHL</i>	<i>JHL</i>	<i>JHL</i>	<i>JHL</i>	<i>JHL</i>	<i>JHL</i>


Signature of Chief Investigator

2013-02-06
Date

**IN-HOUSE MANUFACTURED ^{99m}Tc-ETHYLENEDICYSSTEINE-DEOXYGLUCOSE
IN RABBITS, MICE AND BABOONS: NORMAL, INFECTION AND TUMOUR
BIODISTRIBUTION**

**ANIMAL MONITORING SHEET
IHM ^{99m}Tc-ECDG- NORMAL BIODISTRIBUTION**

UFS AENR. Project No. 20/2012 Investigator: J. Horn-Lodewyk
Animal ID No. 2 Species /Strain/ White New Zealand Rabbits
Animal Details (sex, age etc) Male

- Each animal is examined and observed for abnormalities at each time point (weekly or daily as appropriate)
- Observations are recorded in the table
- Normal clinical signs are recorded as "N"
- Abnormalities are recorded as "A" and severity is scored in brackets eg Breathing: A (3)
- Comments concerning abnormalities are recorded in the comments section of the table
- Additional observations tailored to the monitoring requirements for each animal experiment are to be added at "Other"

CLINICAL OBSERVATION (N or A)	DATE							
	30-01-13	31-01-13	01-02-13	02-02-13	03-02-13	04-02-13	05-02-13	06-02-13
UNDISTURBED								
Coat	N	N	N	N	N	N	N	N
Activity	N	N	N	N	N	N	N	N
Breathing	N	N	N	N	N	N	N	N
Movement/gait	N	N	N	N	N	N	N	N
Eating	N	N	N	N	N	N	N	N
Drinking	N	N	N	N	N	N	N	N
Alert/Sleeping	N	N	N	N	N	N	N	N
ON HANDLING								
Alert	N	N	N	N	N	N	N	N
Body condition	N	N	N	N	N	N	N	N
Bodyweight (g)	5200	5200	5200	5250	5250	5250	5300	5300
Body temperature (°C)	40.1	40.1	40.0	39.9	39.9	39.8	39.8	39.8
Dehydration	N	N	N	N	N	N	N	N
Eyes	N	N	N	N	N	N	N	N
Faeces	N	N	N	N	N	N	N	N
Nose	N	N	N	N	N	N	N	N
Breathing	N	N	N	N	N	N	N	N
Urine	N	N	N	N	N	N	N	N
Vocalisation	N	N	N	N	N	N	N	N
OTHER (specify)								
COMMENTS								
INITIALS:	<i>[Signature]</i>	<i>[Signature]</i>	<i>[Signature]</i>	<i>[Signature]</i>	<i>[Signature]</i>	<i>[Signature]</i>	<i>[Signature]</i>	<i>[Signature]</i>


 Signature of Chief Investigator

2013-02-06
 Date

**IN-HOUSE MANUFACTURED ^{99m}Tc-ETHYLENEDICYSSTEINE-DEOXYGLUCOSE
IN RABBITS, MICE AND BABOONS: NORMAL, INFECTION AND TUMOUR
BIODISTRIBUTION**

**ANIMAL MONITORING SHEET
IHM ^{99m}Tc-EC DG- NORMAL BIODISTRIBUTION**

UFS AENR. Project No. 20/2012 Investigator: J. Horn-Lodewyk
Animal ID No. 3 Species /Strain/ White New Zealand Rabbits
Animal Details (sex, age etc) Male

- Each animal is examined and observed for abnormalities at each time point (weekly or daily as appropriate)
- Observations are recorded in the table
- Normal clinical signs are recorded as "N"
- Abnormalities are recorded as "A" and severity is scored in brackets eg Breathing: A (3)
- Comments concerning abnormalities are recorded in the comments section of the table
- Additional observations tailored to the monitoring requirements for each animal experiment are to be added at "Other"

CLINICAL OBSERVATION (N or A)	DATE							
	30-01-13	31-01-13	01-02-13	02-02-13	03-02-13	04-02-13	05-02-13	06-02-13
UNDISTURBED								
Coat	A ₁	A ₁	A ₁	A ₁	A ₁	A ₁	A ₁	A ₁
Activity	N	N	N	N	N	N	N	N
Breathing	N	N	N	N	N	N	N	N
Movement/gait	N	N	N	N	N	N	N	N
Eating	N	N	N	N	N	N	N	N
Drinking	N	N	N	N	N	N	N	N
Alert/Sleeping	N	N	N	N	N	N	N	N
ON HANDLING								
Alert	N	N	N	N	N	N	N	N
Body condition	N	N	N	N	N	N	N	N
Bodyweight (g)	4600	4600	4600	4600	4650	4700	4700	4700
Body temperature (°C)	39.3	39.3	39.5	39.5	39.6	39.7	39.7	39.7
Dehydration	N	N	N	N	N	N	N	N
Eyes	N	N	N	N	N	N	N	N
Faeces	N	N	N	N	N	N	N	N
Nose	N	N	N	N	N	N	N	N
Breathing	N	N	N	N	N	N	N	N
Urine	N	N	N	N	N	N	N	N
Vocalisation	N	N	N	N	N	N	N	N
OTHER (specify)								
COMMENTS								
INITIALS:	<i>[Signature]</i>	<i>[Signature]</i>	<i>[Signature]</i>	<i>[Signature]</i>	<i>[Signature]</i>	<i>[Signature]</i>	<i>[Signature]</i>	<i>[Signature]</i>


 Signature of Chief Investigator

2013-02-06
 Date

**IN-HOUSE MANUFACTURED ^{99m}Tc-ETHYLENEDICYSSTEINE-DEOXYGLUCOSE
IN RABBITS, MICE AND BABOONS: NORMAL, INFECTION AND TUMOUR
BIODISTRIBUTION**

**ANIMAL MONITORING SHEET
IHM ^{99m}Tc-EC DG- NORMAL BIODISTRIBUTION**

UFS AENR. Project No. 20/2012 Investigator: J. Horn-Lodewyk
Animal ID No. 4 Species /Strain/ White New Zealand Rabbits
Animal Details (sex, age etc) Male

- Each animal is examined and observed for abnormalities at each time point (weekly or daily as appropriate)
- Observations are recorded in the table
- Normal clinical signs are recorded as "N"
- Abnormalities are recorded as "A" and severity is scored in brackets eg Breathing: A (3)
- Comments concerning abnormalities are recorded in the comments section of the table
- Additional observations tailored to the monitoring requirements for each animal experiment are to be added at "Other"

CLINICAL OBSERVATION (N or A)	DATE							
	30-01-13	31-01-13	01-02-13	02-02-13	03-02-13	04-02-13	05-02-13	06-02-13
UNDISTURBED								
Coat	N	N	N	N	N	N	N	N
Activity	N	N	N	N	N	N	N	N
Breathing	N	N	N	N	N	N	N	N
Movement/gait	N	N	N	N	N	N	N	N
Eating	N	N	N	N	N	N	N	N
Drinking	N	N	N	N	N	N	N	N
Alert/Sleeping	N	N	N	N	N	N	N	N
ON HANDLING								
Alert	N	N	N	N	N	N	N	N
Body condition	N	N	N	N	N	N	N	N
Bodyweight (g)	4700	4700	4700	4700	4750	4750	4800	4800
Body temperature (°C)	39.7	39.7	39.7	39.6	39.6	39.6	39.6	39.6
Dehydration	N	N	N	N	N	N	N	N
Eyes	N	N	N	N	N	N	N	N
Faeces	N	N	N	N	N	N	N	N
Nose	N	N	N	N	N	N	N	N
Breathing	N	N	N	N	N	N	N	N
Urine	N	N	N	N	N	N	N	N
Vocalisation	N	N	N	N	N	N	N	N
OTHER (specify)								
COMMENTS								
INITIALS:	<i>[Signature]</i>	<i>[Signature]</i>	<i>[Signature]</i>	<i>[Signature]</i>	<i>[Signature]</i>	<i>[Signature]</i>	<i>[Signature]</i>	<i>[Signature]</i>


 Signature of Chief Investigator

2013-02-06
 Date

**IN-HOUSE MANUFACTURED ^{99m}Tc-ETHYLENEDICYSSTEINE-DEOXYGLUCOSE
IN RABBITS, MICE AND BABOONS: NORMAL, INFECTION AND TUMOUR
BIODISTRIBUTION**

**ANIMAL MONITORING SHEET
IHM ^{99m}Tc-ECDG- NORMAL BIODISTRIBUTION**

UFS AENR. Project No. 20/2012 Investigator: J. Horn-Lodewyk
Animal ID No. 5 Species /Strain/ **White New Zealand Rabbits**
Animal Details (sex, age etc) Male

- Each animal is examined and observed for abnormalities at each time point (weekly or daily as appropriate)
- Observations are recorded in the table
- Normal clinical signs are recorded as "N"
- Abnormalities are recorded as "A" and severity is scored in brackets eg Breathing: A (3)
- Comments concerning abnormalities are recorded in the comments section of the table
- Additional observations tailored to the monitoring requirements for each animal experiment are to be added at "Other"

CLINICAL OBSERVATION (N or A)	DATE							
	30-01-13	31-01-13	01-02-13	02-02-13	03-02-13	04-02-13	05-02-13	06-02-13
UNDISTURBED								
Coat	A ₁	A ₁	A ₁	A ₁	A ₁	A ₁	A ₁	A ₁
Activity	N	N	N	N	N	N	N	N
Breathing	N	N	N	N	N	N	N	N
Movement/gait	N	N	N	N	N	N	N	N
Eating	N	N	N	N	N	N	N	N
Drinking	N	N	N	N	N	N	N	N
Alert/Sleeping	N	N	N	N	N	N	N	N
ON HANDLING								
Alert	N	N	N	N	N	N	N	N
Body condition	N	N	N	N	N	N	N	N
Bodyweight (g)	5150	5150	5150	5200	5200	5200	5200	5200
Body temperature (°C)	39.3	39.3	39.4	39.6	39.6	39.8	39.8	39.8
Dehydration	N	N	N	N	N	N	N	N
Eyes	N	N	N	N	N	N	N	N
Faeces	N	N	N	N	N	N	N	N
Nose	N	N	N	N	N	N	N	N
Breathing	N	N	N	N	N	N	N	N
Urine	N	N	N	N	N	N	N	N
Vocalisation	N	N	N	N	N	N	N	N
OTHER (specify)								
COMMENTS								
INITIALS:	<i>[Signature]</i>	<i>[Signature]</i>	<i>[Signature]</i>	<i>[Signature]</i>	<i>[Signature]</i>	<i>[Signature]</i>	<i>[Signature]</i>	<i>[Signature]</i>


Signature of Chief Investigator

2013-02-06
Date

**IN-HOUSE MANUFACTURED ^{99m}Tc-ETHYLENEDICYSSTEINE-DEOXYGLUCOSE
IN RABBITS, MICE AND BABOONS: NORMAL, INFECTION AND TUMOUR
BIODISTRIBUTION**

**ANIMAL MONITORING SHEET
IHM ^{99m}Tc-ECDG- NORMAL BIODISTRIBUTION**

UFS AENR. Project No. 20/2012 Investigator: J. Horn-Lodewyk
Animal ID No. 6 Species /Strain/ **White New Zealand Rabbits**
Animal Details (sex, age etc) Male

- Each animal is examined and observed for abnormalities at each time point (weekly or daily as appropriate)
- Observations are recorded in the table
- Normal clinical signs are recorded as "N"
- Abnormalities are recorded as "A" and severity is scored in brackets eg Breathing: A (3)
- Comments concerning abnormalities are recorded in the comments section of the table
- Additional observations tailored to the monitoring requirements for each animal experiment are to be added at "Other"

CLINICAL OBSERVATION (N or A)	DATE							
	06-02-13	07-02-13	08-02-13	09-02-13	10-02-13	11-02-13	12-02-13	13-02-13
UNDISTURBED								
Coat	N	N	N	N	N	N	N	N
Activity	N	N	N	N	N	N	N	N
Breathing	N	N	N	N	N	N	N	N
Movement/gait	N	N	N	N	N	N	N	N
Eating	N	N	N	N	N	N	N	N
Drinking	N	N	N	N	N	N	N	N
Alert/Sleeping	N	N	N	N	N	N	N	N
ON HANDLING								
Alert	N	N	N	N	N	N	N	N
Body condition	N	N	N	N	N	N	N	N
Bodyweight (g)	4400		4250			4400		4400
Body temperature (°C)	39.8		39.8			39.5		39.0
Dehydration	N	N	N	N	N	N	N	N
Eyes	N	N	N	N	N	N	N	N
Faeces	N	N	N	N	N	N	N	N
Nose	N	N	N	N	N	N	N	N
Breathing	N	N	N	N	N	N	N	N
Urine	N	N	N	N	N	N	N	N
Vocalisation	N	N	N	N	N	N	N	N
OTHER (specify)								
COMMENTS								
INITIALS:	<i>[Signature]</i>	<i>[Signature]</i>	<i>[Signature]</i>	<i>[Signature]</i>	<i>[Signature]</i>	<i>[Signature]</i>	<i>[Signature]</i>	<i>[Signature]</i>


Signature of Chief Investigator



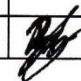





2013-02-13
Date

**IN-HOUSE MANUFACTURED ^{99m}Tc-ETHYLENEDICYSSTEINE-DEOXYGLUCOSE
IN RABBITS, MICE AND BABOONS: NORMAL, INFECTION AND TUMOUR
BIODISTRIBUTION**

**ANIMAL MONITORING SHEET
IHM ^{99m}Tc-ECDG- NORMAL BIODISTRIBUTION**

UFS AENR. Project No. 20/2012 Investigator: J. Horn-Lodewyk
Animal ID No. 87 Species /Strain/ **White New Zealand Rabbits**
Animal Details (sex, age etc) Male

- Each animal is examined and observed for abnormalities at each time point (weekly or daily as appropriate)
- Observations are recorded in the table
- Normal clinical signs are recorded as "N"
- Abnormalities are recorded as "A" and severity is scored in brackets eg Breathing: A (3)
- Comments concerning abnormalities are recorded in the comments section of the table
- Additional observations tailored to the monitoring requirements for each animal experiment are to be added at "Other"

CLINICAL OBSERVATION (N or A)	DATE							
	06-02-13	07-02-13	08-02-13	09-02-13	10-02-13	11-02-13	12-02-13	13-02-13
UNDISTURBED								
Coat	N	N	N	N	N	N	N	N
Activity	N	N	N	N	N	N	N	N
Breathing	N	N	N	N	N	N	N	N
Movement/gait	N	N	N	N	N	N	N	N
Eating	N	N	N	N	N	N	N	N
Drinking	N	N	N	N	N	N	N	N
Alert/Sleeping	N	N	N	N	N	N	N	N
ON HANDLING								
Alert	N	N	N	N	N	N	N	N
Body condition	N	N	N	N	N	N	N	N
Bodyweight (g)	4100	4100	4100			4300		4300
Body temperature (°C)	40.2		39.8			39.5		39.5
Dehydration	N	N	N	N	N	N	N	N
Eyes	N	N	N	N	N	N	N	N
Faeces	N	N	N	N	N	N	N	N
Nose	N	N	N	N	N	N	N	N
Breathing	N	N	N	N	N	N	N	N
Urine	N	N	N	N	N	N	N	N
Vocalisation	N	N	N	N	N	N	N	N
OTHER (specify)	N							
COMMENTS								
INITIALS:								


Signature of Chief Investigator

2013-02-13
Date

**IN-HOUSE MANUFACTURED ^{99m}Tc-ETHYLENEDICYSSTEINE-DEOXYGLUCOSE
IN RABBITS, MICE AND BABOONS: NORMAL, INFECTION AND TUMOUR
BIODISTRIBUTION**

**ANIMAL MONITORING SHEET
IHM ^{99m}Tc-ECDG- NORMAL BIODISTRIBUTION**

UFS AENR. Project No. 20/2012 Investigator: J. Horn-Lodewyk
Animal ID No. 90 Species /Strain/ **White New Zealand Rabbits**
Animal Details (sex, age etc) Male

- Each animal is examined and observed for abnormalities at each time point (weekly or daily as appropriate)
- Observations are recorded in the table
- Normal clinical signs are recorded as "N"
- Abnormalities are recorded as "A" and severity is scored in brackets eg Breathing: A (3)
- Comments concerning abnormalities are recorded in the comments section of the table
- Additional observations tailored to the monitoring requirements for each animal experiment are to be added at "Other"

CLINICAL OBSERVATION (N or A)	DATE							
	06-02-13	07-02-13	08-02-13	09-02-13	10-02-13	11-02-13	12-02-13	13-02-13
UNDISTURBED								
Coat	N	N	N	N	N	N	N	N
Activity	N	N	N	N	N	N	N	N
Breathing	N	N	N	N	N	N	N	N
Movement/gait	N	N	N	N	N	N	N	N
Eating	N	N	N	N	N	N	N	N
Drinking	N	N	N	N	N	N	N	N
Alert/Sleeping	N	N	N	N	N	N	N	N
ON HANDLING								
Alert	N	N	N	N	N	N	N	N
Body condition	N	N	N	N	N	N	N	N
Bodyweight (g)	3900		3900			4000		4000
Body temperature (°C)	39.8		39.8			39.3		39.5
Dehydration	N	N	N	N	N	N	N	N
Eyes	N	N	N	N	N	N	N	N
Faeces	N	N	N	N	N	N	N	N
Nose	N	N	N	N	N	N	N	N
Breathing	N	N	N	N	N	N	N	N
Urine	N	N	N	N	N	N	N	N
Vocalisation	N	N	N	N	N	N	N	N
OTHER (specify)	N							
COMMENTS								
INITIALS:	<i>[Signature]</i>	<i>[Signature]</i>	<i>[Signature]</i>	<i>[Signature]</i>	<i>[Signature]</i>	<i>[Signature]</i>	<i>[Signature]</i>	<i>[Signature]</i>

[Signature]
Signature of Chief Investigator








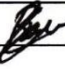
2013-02-13
Date

**IN-HOUSE MANUFACTURED ^{99m}Tc-ETHYLENEDICYSSTEINE-DEOXYGLUCOSE
IN RABBITS, MICE AND BABOONS: NORMAL, INFECTION AND TUMOUR
BIODISTRIBUTION**

**ANIMAL MONITORING SHEET
IHM ^{99m}Tc-ECDG- NORMAL BIODISTRIBUTION**

UFS AENR. Project No. 20/2012 Investigator: J. Horn-Lodewyk
Animal ID No. 10 Species /Strain/ White New Zealand Rabbits
Animal Details (sex, age etc) Male

- Each animal is examined and observed for abnormalities at each time point (weekly or daily as appropriate)
- Observations are recorded in the table
- Normal clinical signs are recorded as "N"
- Abnormalities are recorded as "A" and severity is scored in brackets eg Breathing: A (3)
- Comments concerning abnormalities are recorded in the comments section of the table
- Additional observations tailored to the monitoring requirements for each animal experiment are to be added at "Other"

CLINICAL OBSERVATION (N or A)	DATE							
	02-07-13	03-07-13	04-07-13	05-07-13	06-07-13	07-07-13	08-07-13	09-07-13
UNDISTURBED								
Coat	-	N	N	N	N	N	N	N
Activity	-	N	N	N	N	N	N	N
Breathing	-	N	N	N	N	N	N	N
Movement/gait	-	N	N	N	N	N	N	N
Eating	-	N	N	N	N	N	N	N
Drinking	-	N	N	N	N	N	N	N
Alert/Sleeping	-	N	N	N	N	N	N	N
ON HANDLING								
Alert	-	N	N	N	N	N	N	N
Body condition	-	N	N	N	N	N	N	N
Bodyweight (g)	4000	4000	-	-	4200	-	4200	4200
Body temperature (°C)	-	39.2	-	-	39.1	-	39.3	39.0
Dehydration	-	N	N	N	N	N	N	N
Eyes	-	N	N	N	N	N	N	N
Faeces	-	N	N	N	N	N	N	N
Nose	-	N	N	N	N	N	N	N
Breathing	-	N	N	N	N	N	N	N
Urine	-	N	N	N	N	N	N	N
Vocalisation	-	N	N	N	N	N	N	N
OTHER (specify)								
COMMENTS								
INITIALS:								


 Signature of Chief Investigator

2013-07-10
 Date

APPENDIX F

Animal welfare score sheet - baboons

IN-HOUSE MANUFACTURED ^{99m}Tc -ETHYLENEDICYSSTEINE-DEOXYGLUCOSE IN RABBITS, MICE AND BABOONS: NORMAL, INFECTION AND TUMOUR BIODISTRIBUTION

ANIMAL MONITORING SHEET IHM ^{99m}Tc -ECDG- NORMAL BIODISTRIBUTION PRIMATA

UFS AENR. Project No. 20/2012 Investigator: J. Horn-Lodewyk

Animal ID No. 1 / **PRIMATA PAPIO URSINUS** Species /Strain

Animal Details (sex, age etc) Male

- Each animal is examined and observed for abnormalities at each time point (weekly or daily as appropriate)
- Observations are recorded in the table
- Normal clinical signs are recorded as "N"
- Abnormalities are recorded as "A" and severity is scored in brackets eg Breathing: A (3)
- Comments concerning abnormalities are recorded in the comments section of the table
- Additional observations tailored to the monitoring requirements for each animal experiment are to be added at "Other"

CLINICAL OBSERVATION (N or A)	DATE							
	30-07-13	31-07-13	01-08-13	02-08-13	03-08-13	04-08-13	05-08-13	06-08-13
UNDISTURBED								
Coat	N	N	N	N	N	N	N	N
Activity	N	N	N	N	N	N	N	N
Breathing	N	N	N	N	N	N	N	N
Movement/gait	N	N	N	N	N	N	N	N
Eating	N	N	N	N	N	N	N	N
Drinking	N	N	N	N	N	N	N	N
Alert/Sleeping	N	N	N	N	N	N	N	N
ON HANDLING								
Alert	N	N	N	N	N	N	N	N
Body condition	N	N	N	N	N	N	N	N
Bodyweight(kg)	16.0	-	-	-	-	-	-	A
Body temperature (°C)	-	-	-	-	-	-	-	-
Dehydration	N	N	N	N	N	N	N	N
Eyes	N	N	N	N	N	N	N	N
Faeces	N	N	N	N	N	N	N	N
Nose	N	N	N	N	N	N	N	N
Breathing	N	N	N	N	N	N	N	N
Urine	N	N	N	N	N	N	N	N
Vocalisation	N	N	N	N	N	N	N	N
OTHER (specify)								
COMMENTS								
INITIALS:								

Signature of Chief Investigator







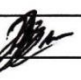

2013-08-07
Date

**IN-HOUSE MANUFACTURED ^{99m}Tc-ETHYLENEDICYSSTEINE-DEOXYGLUCOSE
IN RABBITS, MICE AND BABOONS: NORMAL, INFECTION AND TUMOUR
BIODISTRIBUTION**

**ANIMAL MONITORING SHEET
IHM ^{99m}Tc-ECDG- NORMAL BIODISTRIBUTION PRIMATA**

UFS AENR. Project No. 20/2012 Investigator: J. Horn-Lodewyk
Animal ID No. 2 / **PRIMATA PAPIO URSINUS** Species /Strain
Animal Details (sex, age etc) Male

- Each animal is examined and observed for abnormalities at each time point (weekly or daily as appropriate)
- Observations are recorded in the table
- Normal clinical signs are recorded as "N"
- Abnormalities are recorded as "A" and severity is scored in brackets eg Breathing: A (3)
- Comments concerning abnormalities are recorded in the comments section of the table
- Additional observations tailored to the monitoring requirements for each animal experiment are to be added at "Other"

CLINICAL OBSERVATION (N or A)	DATE							
	30-07-13	31-07-13	01-08-13	02-08-13	03-08-13	04-08-13	05-08-13	06-08-13
UNDISTURBED								
Coat	N	N	N	N	N	N	N	N
Activity	N	N	N	N	N	N	N	N
Breathing	N	N	N	N	N	N	N	N
Movement/gait	N	N	N	N	N	N	N	N
Eating	N	N	N	N	N	N	N	N
Drinking	N	N	N	N	N	N	N	N
Alert/Sleeping	N	N	N	N	N	N	N	N
ON HANDLING								
Alert	N	N	N	N	N	N	N	N
Body condition	N	N	N	N	N	N	N	N
Bodyweight(kg)	1/400	-	-	-	-	-	-	-
Body temperature (°C)	-	-	-	-	-	-	-	-
Dehydration	N	N	N	N	N	N	N	N
Eyes	N	N	N	N	N	N	N	N
Faeces	N	N	N	N	N	N	N	N
Nose	N	N	N	N	N	N	N	N
Breathing	N	N	N	N	N	N	N	N
Urine	N	N	N	N	N	N	N	N
Vocalisation	N	N	N	N	N	N	N	N
OTHER (specify)								
COMMENTS								
INITIALS:								


Signature of Chief Investigator








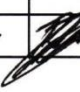
2013-08-07
Date

**IN-HOUSE MANUFACTURED ^{99m}Tc-ETHYLENEDICYSSTEINE-DEOXYGLUCOSE
IN RABBITS, MICE AND BABOONS: NORMAL, INFECTION AND TUMOUR
BIODISTRIBUTION**

**ANIMAL MONITORING SHEET
IHM ^{99m}Tc-ECDG- NORMAL BIODISTRIBUTION PRIMATA**

UFS AENR. Project No. 20/2012 Investigator: J. Horn-Lodewyk
Animal ID No. 3 / PRIMATA PAPIO URSINUS Species /Strain
Animal Details (sex, age etc) Female

- Each animal is examined and observed for abnormalities at each time point (weekly or daily as appropriate)
- Observations are recorded in the table
- Normal clinical signs are recorded as "N"
- Abnormalities are recorded as "A" and severity is scored in brackets eg Breathing: A (3)
- Comments concerning abnormalities are recorded in the comments section of the table
- Additional observations tailored to the monitoring requirements for each animal experiment are to be added at "Other"

CLINICAL OBSERVATION (N or A)	DATE							
	30-07-13	31-07-13	01-08-13	02-08-13	03-08-13	04-08-13	05-08-13	06-08-13
UNDISTURBED								
Coat	N	N	N	N	N	N	N	N
Activity	N	N	N	N	N	N	N	N
Breathing	N	N	N	N	N	N	N	N
Movement/gait	N	N	N	N	N	N	N	N
Eating	N	N	N	N	N	N	N	N
Drinking	N	N	N	N	N	N	N	N
Alert/Sleeping	N	N	N	N	N	N	N	N
ON HANDLING								
Alert	N	N	N	N	N	N	N	N
Body condition	N	N	N	N	N	N	N	N
Bodyweight(kg)	10.8	—	—	—	—	—	—	—
Body temperature (°C)	—	—	—	—	—	—	—	—
Dehydration	N	N	N	N	N	N	N	N
Eyes	N	N	N	N	N	N	N	N
Faeces	N	N	N	N	N	N	N	N
Nose	N	N	N	N	N	N	N	N
Breathing	N	N	N	N	N	N	N	N
Urine	N	N	N	N	N	N	N	N
Vocalisation	N	N	N	N	N	N	N	N
OTHER (specify)								
COMMENTS								
INITIALS:								


 Signature of Chief Investigator







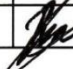

2013-08-07
 Date

**IN-HOUSE MANUFACTURED ^{99m}Tc-ETHYLENEDICYSSTEINE-DEOXYGLUCOSE
IN RABBITS, MICE AND BABOONS: NORMAL, INFECTION AND TUMOUR
BIODISTRIBUTION**


ANIMAL MONITORING SHEET
IHM ^{99m}Tc-ECDG (KIT) - NORMAL BIODISTRIBUTION PRIMATA

UFS AENR. Project No. 20/2012 Investigator: J. Horn-Lodewyk
Animal ID No. 4 / PRIMATA PAPIO URSINUS Species /Strain
Animal Details (sex, age etc) Male

- Each animal is examined and observed for abnormalities at each time point (weekly or daily as appropriate)
- Observations are recorded in the table
- Normal clinical signs are recorded as "N"
- Abnormalities are recorded as "A" and severity is scored in brackets eg Breathing: A (3)
- Comments concerning abnormalities are recorded in the comments section of the table
- Additional observations tailored to the monitoring requirements for each animal experiment are to be added at "Other"

CLINICAL OBSERVATION (N or A)	DATE							
	13-09-13	14-09-13	15-09-13	16-09-13	17-09-13	18-09-13	19-09-13	20-09-13
UNDISTURBED								
Coat	N	N	N	N	N	N	N	N
Activity	N	N	N	N	N	N	N	N
Breathing	N	N	N	N	N	N	N	N
Movement/gait	N	N	N	N	N	N	N	N
Eating	N	N	N	N	N	N	N	N
Drinking	N	N	N	N	N	N	N	N
Alert/Sleeping	N	N	N	N	N	N	N	N
ON HANDLING								
Alert	N	N	N	N	N	N	N	N
Body condition	N	N	N	N	N	N	N	N
Bodyweight (g) kg	1.70	1	1	1	1	1	1	1
Body temperature (°C)	1	1	1	1	1	1	1	1
Dehydration	N	N	N	N	N	N	N	N
Eyes	N	N	N	N	N	N	N	N
Faeces	N	N	N	N	N	N	N	N
Nose	N	N	N	N	N	N	N	N
Breathing	N	N	N	N	N	N	N	N
Urine	N	N	N	N	N	N	N	N
Vocalisation	N	N	N	N	N	N	N	N
OTHER (specify)								
COMMENTS								
INITIALS:								

2013-09-21
Signature of Chief Investigator







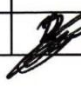


Date

**IN-HOUSE MANUFACTURED ^{99m}Tc-ETHYLENEDICYSSTEINE-DEOXYGLUCOSE
IN RABBITS, MICE AND BABOONS: NORMAL, INFECTION AND TUMOUR
BIODISTRIBUTION**

ANIMAL MONITORING SHEET
IHM ^{99m}Tc-ECDG (KIT) - NORMAL BIODISTRIBUTION PRIMATA

UFS AENR. Project No. 20/2012 Investigator: J. Horn-Lodewyk
Animal ID No. 5 / **PRIMATA PAPIO URSINUS** Species /Strain
Animal Details (sex, age etc) Male

- Each animal is examined and observed for abnormalities at each time point (weekly or daily as appropriate)
- Observations are recorded in the table
- Normal clinical signs are recorded as "N"
- Abnormalities are recorded as "A" and severity is scored in brackets eg Breathing: A (3)
- Comments concerning abnormalities are recorded in the comments section of the table
- Additional observations tailored to the monitoring requirements for each animal experiment are to be added at "Other"

CLINICAL OBSERVATION (N or A)	DATE							
	13-09-13	14-09-13	15-09-13	16-09-13	17-09-13	18-09-13	19-09-13	20-09-13
UNDISTURBED								
Coat	N	N	N	N	N	N	N	N
Activity	N	N	N	N	N	N	N	N
Breathing	N	N	N	N	N	N	N	N
Movement/gait	N	N	N	N	N	N	N	N
Eating	N	N	N	N	N	N	N	N
Drinking	N	N	N	N	N	N	N	N
Alert/Sleeping	N	N	N	N	N	N	N	N
ON HANDLING								
Alert	N	N	N	N	N	N	N	N
Body condition	N	N	N	N	N	N	N	N
Bodyweight (g) kg	2.0	1	1	1	1	1	1	1
Body temperature (°C)	1	1	1	1	1	1	1	1
Dehydration	N	N	N	N	N	N	N	N
Eyes	N	N	N	N	N	N	N	N
Faeces	N	N	N	N	N	N	N	N
Nose	N	N	N	N	N	N	N	N
Breathing	N	N	N	N	N	N	N	N
Urine	N	N	N	N	N	N	N	N
Vocalisation	N	N	N	N	N	N	N	N
OTHER (specify)								
COMMENTS								
INITIALS:								

Signature of Chief Investigator

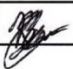

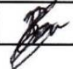



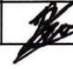

Date

**IN-HOUSE MANUFACTURED ^{99m}Tc-ETHYLENEDICYSSTEINE-DEOXYGLUCOSE
IN RABBITS, MICE AND BABOONS: NORMAL, INFECTION AND TUMOUR
BIODISTRIBUTION**

**ANIMAL MONITORING SHEET
IHM ^{99m}Tc-ECDD (KIT) - NORMAL BIODISTRIBUTION PRIMATA**

UFS AENR. Project No. 20/2012 Investigator: J. Horn-Lodewyk
Animal ID No. 6 / PRIMATA PAPIO URSINUS Species /Strain
Animal Details (sex, age etc) Male

- Each animal is examined and observed for abnormalities at each time point (weekly or daily as appropriate)
- Observations are recorded in the table
- Normal clinical signs are recorded as "N"
- Abnormalities are recorded as "A" and severity is scored in brackets eg Breathing: A (3)
- Comments concerning abnormalities are recorded in the comments section of the table
- Additional observations tailored to the monitoring requirements for each animal experiment are to be added at "Other"

CLINICAL OBSERVATION (N or A)	DATE							
	13-09-13	14-09-13	15-09-13	16-09-13	17-09-13	18-09-13	19-09-13	20-09-13
UNDISTURBED								
Coat	N	N	N	N	N	N	N	N
Activity	N	N	N	N	N	N	N	N
Breathing	N	N	N	N	N	N	N	N
Movement/gait	N	N	N	N	N	N	N	N
Eating	N	A 1	N	N	N	N	N	N
Drinking	N	N	N	N	N	N	N	N
Alert/Sleeping	N	N	N	N	N	N	N	N
ON HANDLING								
Alert	N	N	N	N	N	N	N	N
Body condition	N	N	N	N	N	N	N	N
Bodyweight (g) kg	250							
Body temperature (°C)								
Dehydration	N	N	N	N	N	N	N	N
Eyes	N	N	N	N	N	N	N	N
Faeces	N	N	N	N	N	N	N	N
Nose	N	N	N	N	N	N	N	N
Breathing	N	N	N	N	N	N	N	N
Urine	N	N	N	N	N	N	N	N
Vocalisation	N	N	N	N	N	N	N	N
OTHER (specify)								
COMMENTS		Not eating well						
INITIALS:								


 Signature of Chief Investigator









2013-09-21
 Date

**IN-HOUSE MANUFACTURED ^{99m}Tc-ETHYLENEDICYSSTEINE-DEOXYGLUCOSE
IN RABBITS, MICE AND BABOONS: NORMAL, INFECTION AND TUMOUR
BIODISTRIBUTION**

ANIMAL MONITORING SHEET
IHM ^{99m}Tc-EDCG (LL) - NORMAL BIODISTRIBUTION PRIMATA

UFS AENR. Project No. 20/2012 Investigator: J. Horn-Lodewyk
Animal ID No. _____ / PRIMATA PAPIO URSINUS Species /Strain
Animal Details (sex, age etc) _____

- Each animal is examined and observed for abnormalities at each time point (weekly or daily as appropriate)
- Observations are recorded in the table
- Normal clinical signs are recorded as "N"
- Abnormalities are recorded as "A" and severity is scored in brackets eg Breathing: A (3)
- Comments concerning abnormalities are recorded in the comments section of the table
- Additional observations tailored to the monitoring requirements for each animal experiment are to be added at "Other"

CLINICAL OBSERVATION (N or A)	DATE							
	13-09-13	14-09-13	15-09-13	16-09-13	17-09-13	18-09-13	19-09-13	20-09-13
UNDISTURBED								
Coat	N	N	N	N	N	N	N	N
Activity	N	N	N	N	N	N	N	N
Breathing	N	N	N	N	N	N	N	N
Movement/gait	N	N	N	N	N	N	N	N
Eating	N	N	N	N	N	N	N	N
Drinking	N	N	N	N	N	N	N	N
Alert/Sleeping	N	N	N	N	N	N	N	N
ON HANDLING								
Alert	N	N	N	N	N	N	N	N
Body condition	N	N	N	N	N	N	N	N
Bodyweight (g) kg	8.0	1	1	1	1	1	1	1
Body temperature (°C)	1	1	1	1	1	1	1	1
Dehydration	N	N	N	N	N	N	N	N
Eyes	N	N	N	N	N	N	N	N
Faeces	N	N	N	N	N	N	N	N
Nose	N	N	N	N	N	N	N	N
Breathing	N	N	N	N	N	N	N	N
Urine	N	N	N	N	N	N	N	N
Vocalisation	N	N	N	N	N	N	N	N
OTHER (specify)								
COMMENTS								
INITIALS:								


Signature of Chief Investigator

2013-09-21
Date